

Synthesis and evaluation of chromone derivatives as inhibitors of monoamine oxidase

AN Mpitimpiti
21253005

Dissertation submitted in fulfilment of the requirements for the degree *Magister Scientiae* in *Pharmaceutical Chemistry* at the Potchefstroom Campus of the North-West University

Supervisor: Dr ACU Lourens

Co-supervisors: Dr A Petzer
Prof JP Petzer

November 2014

The financial assistance of the National Research Foundation (NRF) and the Medical Research Council (MRC) towards this research is hereby acknowledged. Opinions expressed and conclusions arrived at are those of the author and are not necessarily to be attributed to the NRF or MRC.

Acknowledgements

- All glory be to God.
- I am deeply indebted to the following for their immense support and contribution:
 - My supervisor - Dr A.C.U Lourens (your guidance is truly boundless).
 - My co-supervisors, Prof J.P Petzer and Dr A. Petzer.
 - Dr J.Jordaan.
- My mother, Magret Chigeza (for your unconditional love and support).
- My family and friends.
- All those who knowingly and unknowingly supported me through out this journey.

Psalm 115 verse 1:

'Not to us, O Lord, not to us, but
to Your Name be the glory,
because of Your love and
faithfulness'

Table of Contents

Abstract	iv
Opsomming	vii
List of abbreviations	xi
CHAPTER 1	1
INTRODUCTION	1
1.1 BACKGROUND	1
1.1.1 Parkinson's disease	1
1.1.2 Monoamine oxidase	2
1.1.3 Chromones as MAO inhibitors	4
1.2 HYPOTHESIS OF THIS STUDY	7
1.3 AIMS AND OBJECTIVES	7
CHAPTER 2	10
LITERATURE REVIEW	10
2.1 INTRODUCTION	10
2.2 INCIDENCE	10
2.3 SYMPTOMS	11
2.4 PATHOLOGY	11
2.5 ETIOLOGY	13
2.5.1 Environmental Factors	13
2.5.2 Genetic Factors	15
2.6 MECHANISMS OF NEURODEGENERATION	15
2.6.1 Oxidative Stress	15
2.6.2 Altered mitochondrial function	18
2.6.3 Altered Proteolysis	18
2.6.4 Inflammatory Change	19
2.6.5 Excitotoxic Mechanisms	19
2.6.6 Apoptosis	19
2.7 TREATMENT	19
2.7.1 Symptomatic Treatment	19
2.7.2 Neuroprotective Drugs	24
2.8 MONOAMINE OXIDASE	27

2.8.1 General Background	27
2.8.2 Biological Function of MAO	28
2.8.3 Tissue Distribution	30
2.8.4 General Structure of MAO	30
2.8.5 Mechanism of Action of MAO	36
2.8.6 MAO-A in depression and Parkinson's disease	39
2.8.7 MAO-B in Parkinson's disease	39
2.8.8 Irreversible Inhibitors of MAO-B	40
2.8.9 Reversible Inhibitors of MAO-B	44
2.8.10 Reversible Inhibitors of MAO-A	44
2.8.11 Bifunctional Cholinesterase and MAO Inhibitors	45
2.9 ANIMAL MODELS OF PARKINSON'S DISEASE	45
2.9.1 MPTP mouse models	45
2.9.2 MPTP primate models	46
CHAPTER 3	48
SYNTHESIS AND CHEMISTRY	48
3.1 INTRODUCTION	48
3.2 CHEMISTRY	48
3.2.1 Results and Discussion	48
3.3 EXPERIMENTAL	59
3.3.1 Materials and Instrumentation	59
3.3.2 Synthetic Procedures	62
3.3.3 Physical and Spectroscopic data of synthesized compounds	63
3.4 SUMMARY	72
CHAPTER 4	73
BIOLOGICAL EVALUATION	73
4.1 INTRODUCTION	73
4.2 ENZYME KINETICS	73
4.2.1 Competitive Inhibition	75
4.2.2 Non-competitive Inhibition	76
4.2.3 K_i Determination	76
4.2.4 IC_{50} Determination and its relationship to K_i	77
4.3 IC_{50} VALUE DETERMINATION OF THE TEST INHIBITORS	78
4.3.1 Chemicals and Instrumentation	79
4.3.2 Method: IC_{50} value determination	79

4.3.3 Results and Discussion (IC ₅₀ determination)	80
4.4 MODE OF MAO INHIBITION	85
4.4.1 Construction of Lineweaver-Burk Plots	85
4.4.2 Results and Discussion (Mode of Inhibition).....	86
4.5 REVERSIBILITY STUDIES FOR MAO INHIBITION USING DIALYSIS	87
4.5.1 Dialysis	87
4.5.2 Results and Discussion (Reversibility Studies).....	88
4.6 SUMMARY	89
CHAPTER 5	90
CONCLUSION.....	90
BIBLIOGRAPHY	94
ADDENDUM.....	112
LIST OF ¹ H NMR AND ¹³ C NMR SPECTRA	113
LIST OF MASS SPECTROMETRY DATA	132
LIST OF INFRA-RED SPECTRA.....	140
LIST OF HPLC DATA.....	148
SUPPLEMENTARY DATA ON CRYSTAL STRUCTURE.....	155

ABSTRACT

TITLE

Synthesis and evaluation of chromone derivatives as inhibitors of monoamine oxidase

KEYWORDS

Chromones, monoamine oxidase inhibitors, Parkinson's disease

BACKGROUND AND RATIONALE

Parkinson's disease (PD) is a chronic, progressive neurodegenerative disorder affecting the central nervous system, primarily, the substantia nigra. It is characterized by loss of dopaminergic neurons in the nigro-striatal pathway, and ultimately patients with Parkinson's disease may lose up to 80% of their dopamine-producing cells in the brain. Symptoms include bradykinesia, muscle rigidity, resting tremor and impaired postural balance.

Symptomatic relief is obtained by using levodopa and various adjunct therapy including dopamine agonists, catechol-O-methyltransferase inhibitors and monoamine oxidase B inhibitors. Levodopa is used as the gold-standard for treatment of this disease. It effectively controls motor symptoms, however, motor complications that impair the quality of life develop with continued levodopa use. No treatments currently available can halt disease progression, therefore novel drugs that can slow down or stop disease progression are urgently required.

The monoamine oxidase (MAO) A and B enzymes are flavoenzymes that play an important role in the oxidative degradation of amine neurotransmitters such as dopamine, serotonin and epinephrine. Early attempts to block dopamine metabolism in the brain using non-selective MAO inhibitors was effective but led to side effects such as hypertensive crisis, thus they lost favor. The MAO-B enzyme is of particular importance in Parkinson's disease because it is more active than MAO-A in the basal ganglia, and is thus primarily responsible for the catabolism of dopamine in the brain. Selegiline and rasagiline, both irreversible, selective MAO-B inhibitors have proven efficacy in symptomatic treatment of Parkinson's disease, but due to the irreversible nature of their binding, it can take several weeks after treatment termination for the enzyme to recover. Use of reversible inhibitors such as lazabemide and safinamide do not have this disadvantage, and have safer side effect profiles. Unfortunately, clinical trials for lazabemide use in Parkinson's disease have been

discontinued. Therefore, due to the lack of disease modifying agents for Parkinson's disease, as well as safety concerns of current PD therapy, an urgent need exists for novel, safe and efficient MAO inhibitors. Current research is thus aimed at designing selective or non-selective reversible inhibitors that bind competitively to the enzyme.

The MAO inhibitory potential of chromone derivatives has been illustrated previously. Evaluation of C6- and C7-alkyloxy substituted chromones, for example revealed that these compounds were potent, selective and reversible MAO-B inhibitors. It has further been shown that chromone 3-carboxylic acid is a potent selective, irreversible MAO-B inhibitor. Phenylcarboxamide substitution in position 3 of chromone 3-carboxylic acid also results in potent, selective MAO-B inhibitory activity. Therefore, further evaluation of the effect of substitution with flexible side chains in the 3-position to evaluate MAO-B inhibition is of importance.

The chromone ring system is thus a privileged scaffold for the design of inhibitors that are selective for MAO-B and has the additional advantages of generally exhibiting low mammalian toxicity and ease of synthesis.

AIM

The aim of this study was to design, synthesize and evaluate novel chromone derivatives as inhibitors of monoamine oxidase.

RESULTS

Design and Synthesis

3-Aminomethylene-2,4-chromandiones and ester chromone derivatives were synthesized by coupling several aromatic and aliphatic amines and alcohols, to chromone 3-carboxylic acid, in the presence of CDI (carbonyldiimidazole). 15 Compounds were successfully synthesized and characterized by using NMR and IR spectroscopy, as well as mass spectrometry. X-ray crystallography was used to obtain a crystal structure for the 3-aminomethylene-2,4-chromandione derivative, **46**, in a bid to verify the structures of the synthesized compounds. Melting points of all compounds were determined, and the purity determined using HPLC techniques.

MAO inhibition studies

A fluorometric assay was employed using kynuramine as substrate, to determine the IC_{50} (50% inhibition concentration) values and SI (selectivity index) of the synthesized compounds. Generally, the esters exhibited weak MAO-A and MAO-B inhibition, while the 3-aminomethylene-2,4-chromandione derivatives showed promise as selective MAO-B inhibitors, with IC_{50} values in the micromolar range. Compound **38**, 3-[(benzylamino)methylidene]-3,4-dihydro-2*H*-1-benzopyran-2,4-dione, was the most potent MAO-B inhibitor with an IC_{50} value of 0.638 μ M and a SI of 122 for MAO-B inhibition. Interesting trends were revealed through analysis of the structure activity relationships, for example, for the 3-aminomethylene-2,4-chromandione derivatives, the presence of a chlorine moiety in the side chains of the compounds resulted in a decrease of MAO-B inhibition activity. Chain elongation further also resulted in weakening the MAO-B inhibition activity, while chain elongation in the ester derivatives led to a slight increase in MAO-B inhibition activity.

Reversibility studies

The reversibility of binding of the most potent compound in the 3-aminomethylene-2,4-chromandione series, **38**, was evaluated. None of the synthesized inhibitors were potent MAO-A inhibitors, therefore reversibility of MAO-A inhibition was not examined. Recovery of enzyme activity was determined after dialysis of the enzyme-inhibitor complexes. Analysis of the kinetic data obtained showed that MAO-B catalytic activity was recovered to 115% of the control value. This suggests that compound **38** is a reversible inhibitor of MAO-B.

Mode of inhibition

A set of Lineweaver-Burk plots were constructed to determine mode of inhibition of compound **38**. The results show linear lines that intersect at a single point just to the left on the y-axis. This indicates that compound **38** interacts competitively with the MAO-B enzyme.

In conclusion, chromone derivatives were synthesized and evaluated as inhibitors of MAO. Compound **38** was the most potent MAO-B inhibitor with an IC_{50} value of 0.638 μ M. The effect of chain elongation and introduction of flexible substituents in position 3 of the chromone 3-carboxylic acid nucleus was explored and the results showed that 3-aminomethylene-2,4-chromandione substitution is preferable over ester substitution.

OPSOMMING

TITEL

Sintese en evaluering van chromoonderivate as inhibeerders van monoamienoksidase

SLEUTELWOORDE

Chromone, monoamienoksidase-inhibeerders, Parkinson se siekte

AGTERGROND EN RASIONAAL

Parkinson se siekte is 'n chroniese, progressiewe neurodegeneratiewe siekte wat die sentrale senuweestelsel, en primêr, die substantia nigra, aantast. Dit word gekenmerk deur die verlies aan dopaminerge neurone in die nigrostriatale weg, en uiteindelik kan pasiënte met Parkinson's se siekte tot 80% van die dopamienproduserende selle in die brein verloor. Simptome sluit bradikinesie, spierstyfheid, rustende tremor en 'n verswakte posturale balans in.

Simptomatiesse verligting word verkry deur die gebruik van levodopa en verskeie addisionele middels soos die dopamienagoniste, katesjol-O-metieltransferase – en monoamienoksidase-inhibeerders. Levodopa word gebruik as die goudstandaard vir die behandeling van die siekte. Alhoewel die middel die motoriese simptome effektief beheer, ontwikkel motoriese komplikasies wat lei tot 'n verlies aan lewenskwaliteit met langdurige levodopa gebruik. Geen behandeling wat tans beskikbaar is kan die siekteverloop keer nie - nuwe geneesmiddels wat die siekteverloop kan vertraag of stop is dus dringend nodig.

Die monoamienoksidase (MAO) A en B ensieme is flavo-ensieme wat 'n belangrike rol speel in die oksidatiewe degradering van amienneuro-oordragstowwe soos dopamien, serotonien en epinefrien. Vroeë pogings om dopamienmetabolisme in die brein te blokkeer deur gebruik te maak van non-selektiewe MAO-inhibeerders was effektief, maar het gelei tot nuwe-effekte soos die ontstaan van 'n hipertensiewe krisis, en het in onguns verval. Die MAO-B ensiem is veral belangrik in Parkinson se siekte omdat dit meer aktief is as MAO-A in die basale ganglia, en dus primêr verantwoordelik is vir die katabolisme van dopamien in die brein. Selegilien and rasagilien, wat beide onomkeerbare, selektiewe MAO-B inhibeerders is, het bewese effektiwiteit in die simptomatiesse behandeling van Parkinson se siekte, maar weens die onomkeerbare aard van hulle binding, kan dit verskeie weke na staking van behandeling

neem vir die ensiem om te herstel. Die gebruik van omkeerbare inhibeerders soos lasabemied en safinamied het nie hierdie nadeel nie, en het dus beter veiligheidsprofiel. Ongelukkig is kliniese toetse vir lasebemied gestaak. Die tekort aan siektebeperkende middels vir Parkinson se siekte, sowel as die veiligheidsrisikos verbonde aan huidige behandeling, is aanduidend van die dringende behoefte aan nuwe, veilige en effektiewe MAO inhibeerders. Huidige navorsing is dus gemik op die ontwerp van selektiewe of non-selektiewe omkeerbare inhibeerders wat kompetierend aan die ensiem bind.

Die MAO inhiberende potensiaal van chromoonderivate is voorheen geïllustreer. Evaluering van C6- en C7-alkoksie gesubstitueerde chromone, het byvoorbeeld getoon dat hierdie chromone potente, selektiewe en omkeerbare MAO-B inhibeerders is. Daar is verder aangetoon dat chromoon-3-karboksielsuur 'n potente, selektiewe, onomkeerbare MAO-B inhibeerder is. Verder lei fenielkarboksamiedsubstitusie in posisie 3 van chromoon-3-karboksielsuur ook tot potente, selektiewe MAO-B inhiberende aktiwiteit. Verdere ondersoek na die effek van buigbare sykettings in posisie 3 op MAO-B inhibisie is dus van belang.

Die chromoonringsstelsel is dus 'n kern met potensiaal vir die ontwerp van selektiewe MAO-B inhibeerders en het verder in die algemeen lae soogdiertoksisiteit asook gemak van sintese, wat addisionele voordele is.

DOEL

Die doel van die studie was om nuwe chromoonderivate te ontwerp, te sintetiseer en te evalueer as inhibeerders van monoamienoksidase.

RESULTATE

Ontwerp en Sintese

Aminometileen-2,4-chromaandioon en ester chromoonderivate is gesintetiseer deur verskeie aromatiese en alifatiese amiene en alkohole in die teenwoordigheid van karboniëldiimidiasool (KDI) aan chromoon-3-karboksielsuur te koppel. 15 Verbindings is suksesvol gesintetiseer en gekarakteriseer deur gebruik te maak van KMR en IR spektroskopie, sowel as massaspektrometrie. X-straalkristallografie is gebruik om 'n kristalstruktuur van die aminometileenchromaandioon **46** te verkry, in 'n poging om die strukture van die gesintetiseerde verbindings te verifieer. Smeltpunte van alle verbindings is verder bepaal en suiwerheid vasgestel deur gebruik te maak van hoëdrukvlouistofchromatografie.

MAO inhibisiestudies

Die IC_{50} (50% inhibisiekonsentrasie) waardes en SI (selektiwiteitsindeks) van die gesintetiseerde verbindings is fluorometries bepaal deur kinuramien as substraat te gebruik. In die algemeen was die esters swak inhibeerders van MAO-A en MAO-B, terwyl sommige van die aminometileenchromaandioon derivate belowende aktiwiteit as selektiewe MAO-B inhibeerders getoon het, met IC_{50} waardes in die mikromolaar konsentrasiereeks. Verbinding **38**, 3-[(bensielamino)metilideen]-3,4-dihidro-2*H*-1-bensopiraan-2,4-dioon, was die mees potente MAO-B inhibeerder met 'n IC_{50} waarde van 0.638 μ M en 'n SI van 122 vir MAO-B inhibisie. Interessante tendense is waargeneem tydens die analise van die struktuuraktiwiteitsverwantskappe, vir die aminometileenchromaandioon derivate, byvoorbeeld, het die teenwoordigheid van 'n chloorgroep in die syketting van die verbindings tot 'n verlaging in MAO-B inhiberende aktiwiteit gelei. Kettingverlenging het verder ook 'n afname in MAO-B aktiwiteit in die reeks veroorsaak, terwyl kettingverlenging by die esterreeks tot 'n effense toename in aktiwiteit gelei het.

Omkeerbaarheidstudies

Die omkeerbaarheid van binding van die mees potente verbinding in die aminometileenchromaandioon reeks, naamlik verbinding **38**, is geëvalueer. Aangesien nie een van die gesintetiseerde verbindings noemenswaardige MAO-A inhiberende aktiwiteit getoon het nie, is omkeerbaarheid van binding vir MAO-A nie bepaal nie. Herstel van ensiemaktiwiteit na dialise van die ensiem-inhibeerderkomplekse is vasgestel. Analise van die kinetiese data het getoon dat MAO-B ensiemaktiwiteit tot 115% van die kontrole herstel het, waaruit afgelei kan word dat verbinding **38** 'n omkeerbare inhibeerder van MAO-B is.

Meganisme van inhibisie

'n Stel Lineweaver-Burk grafieke is opgestel om die meganisme van inhibisie wat verbinding **38** toon, vas te stel. Die resultate het aangetoon dat die lineêre lyne kruis by 'n enkele punt net regs van die y-as, wat aanduidend is dat verbinding **38** kompetierend aan die MAO-B ensiem bind.

Ter samevatting: Chromoonderivate is gesintetiseer en geëvalueer as MAO inhibeerders. Verbinding **38** was die mees potente MAO-B inhibeerder met 'n IC_{50} waarde van 0.638 μ M. Die effek van kettingverlenging en die teenwoordigheid van 'n buigbare ketting in posisie 3 van die chromoon-3-karboksielsuurkern is ondersoek en resultate het getoon dat die

aminometileen-2,4-chromaandione meer potente MAO-B inhibeerders as die esterchromone is.

List of abbreviations

3-MT	3-Methoxytyramine
3-OMD	3-O-Methyldopa
5-HT	Serotonin
6-OHDA	6-Hydroxydopamine
Å	Angstrom
AChE	Acetylcholinesterase
ATP	Adenosine triphosphate
ATP13A2	ATPase Type 13A2
CDCl₃	Deuteriochloroform
CDI	1,1'-Carbonyldiimidazole
CNS	Central nervous system
COMT	Catechol-O-methyltransferase
COX-2	Cyclooxygenase type 2
CSF	Cerebrospinal fluid
C-terminal	Carboxy terminal
Cys	Cysteine
D₁	Dopamine type 1 receptors
D₂	Dopamine type 2 receptors
D₃	Dopamine type 3 receptors
D₄	Dopamine type 4 receptors
DA	Dopamine

DATATOP	Deprenyl and tocopherol antioxidative therapy for parkinsonism
DDC	Dopa decarboxylase
DEPT	Distortionless enhancement by polarization transfer
DMF	Dimethylformamide
DMSO	Dimethyl sulfoxide
DMSO-<i>d</i>₆	Deuterodimethyl sulfoxide
DNA	Deoxyribonucleic acid
DOPAC	3,4-Dihydroxyphenylacetic acid
FAD	Flavin adenine dinucleotide
FADH₂	Reduced FAD
GAPDH	Glyceraldehyde-3-phosphate dehydrogenase
GBA	Glucocerebrosidase
Gly	Glycine
GPO	Glutathione peroxidase
GSH	Glutathione
GSSG	Glutathione disulfide
HMBC	Heteronuclear multiple bond correlation
HPLC	High performance liquid chromatography
HSQC	Heteronuclear single quantum correlation
HVA	Homovanillic acid
IC₅₀	Half maximal inhibitory concentration
Ile	Isoleucine

IR	Infra-red spectroscopy
KCl	Potassium chloride
L-dopa	Levodopa
LRRK-2	Leucine-rich-repeat-kinase-2
Lys	Lysine
MAO	Monoamine oxidase
MAO-A	Monoamine oxidase isoform A
MAO-B	Monoamine oxidase isoform B
mM	Millimolar
MPP	1-methyl-4-phenyl-4-propionoxypiperidine
MPP⁺	1-methyl-4-phenylpyridinium ion
MPTP	1-methyl-4-phenyl-1,2,5,6-tetrahydropyridine
MS	Mass spectrometry
N	Equivalence per liter
NA	Noradrenaline
NaOH	Sodium hydroxide
nM	Nanomolar
NMDA	N-methyl-D-aspartate
NMR	Nuclear magnetic resonance
N-terminus	Amino-terminus
OH⁻	Hydroxide ion
PD	Parkinson's disease

Phe	Phenylalanine
PINK1	PTEN-induced purative kinase 1
QSAR	Quantitative structure activity relationship
ROS	Reactive oxygen species
RT	Room temperature
SD	Standard deviation
Ser	Serine
SI	Selectivity index
SNpc	Substantia nigra pars compacta
TCH346	Omigapil
Thr	Threonine
TLC	Thin layer chromatography
Tyr	Tyrosine
Val	Valine
λ_{ex}	Excitation wavelength
λ_{em}	Emission wavelength
μl	Microliter
μM	Micromolar
A	Alpha
<	Less than

Kinetics:

E	Enzyme
[E]	Enzyme concentration
ES	Enzyme-substrate complex
[I]	Inhibitor concentration
[S]	Substrate concentration
K_d	Equilibrium dissociation constant
K_i	Inhibition constant
K_m	Michaelis-Menten constant
v_i	Initial reaction velocity
V_{max}	Maximum velocity

NMR:

Δ	Delta scale used to indicate chemical shift
J	Coupling constant
br d	Broad doublet
br s	Broad singlet
br t	Broad triplet
D	Doublet
Dd	Doublet of doublets
Ddd	Doublet of doublets of doublets
M	Multiplet

P	Pentet
Ppm	Parts per million
Q	Quartet
S	Singlet
T	Triplet

CHAPTER 1

INTRODUCTION

1.1 Background

1.1.1 Parkinson's disease

Parkinson's disease (PD) is the second most common neurodegenerative disorder affecting the brain (Brichta *et al.*, 2013) and is also the most common progressive neurodegenerative movement disorder (Chung *et al.*, 2003). The world-wide incidence of the disease is estimated at 315 per 100 000 for persons 40 years and older. This prevalence increases with age to 1 903 per 100 000 for persons 80 years and older (Ross & Abbott, 2014). PD is pathologically characterized by the death of the neurons in the substantia nigra and the presence of proteinaceous deposits, known as Lewy bodies, resulting in the characteristic motor symptoms. Motor symptoms include bradykinesia (slowness), muscle rigidity, resting tremor and an impairment of postural balance (Dauer & Przedborski, 2003; Schwarzschild *et al.*, 2006). It, however, not only affects brain regions associated with regulation of movement, but also various regions involved in regulatory pathways. These include, the putamen and the caudate nucleus for example. Pathological changes in PD thus do not only include dopaminergic systems, but involves non-dopaminergic neurotransmitter systems, which may also be further disrupted by long-term levodopa therapy. Neurotransmitter receptor- and transporter-expression levels further change as the disease progresses (Fox *et al.*, 2008).

Due to its distinctive pathology, PD is primarily characterized by motor symptoms, although non-motor symptoms frequently appear especially in later stages of the disease (Schwarzschild *et al.*, 2006). Non-motor symptoms can significantly impair the quality of life of a patient and, in advanced PD, are notoriously difficult to treat (Chaudhuri *et al.*, 2006; Adler, 2005). These symptoms are cognitive dysfunction, psychiatric disorders such as depression and anxiety, autonomic disturbances such as orthostatic hypotension, bladder disturbances and sexual dysfunction, and sensory disorders which include pain, fatigue and weight changes (Dexter & Jenner, 2013; Langston, 2006; Chaudhuri *et al.*, 2006).

The primary cause of PD is not fully understood, though genetic and environmental factors are believed to be linked to disease development (Dauer & Przedborski, 2003). Several

mechanisms and contributing factors have been implicated as leading to the characteristic neurodegeneration found in PD. These include, but are not limited to oxidative stress, mitochondrial dysfunction, gene mutations, excitotoxicity, altered proteolysis and apoptosis (Dauer & Przedborski, 2003, Schapira, 2006). PD is more prevalent in men than in women, possibly due to the protective effects of estrogen. Several other factors are also associated with a lowered incidence of the disease. Regular caffeine consumption (three or more cups of coffee per day) is associated with decreased PD risk in men. In women, regular coffee consumption is associated with a significantly lower incidence of PD among women who never used postmenopausal estrogens (Ascherio *et al.*, 2001; Ascherio *et al.*, 2004; Hu *et al.*, 2007; Ross *et al.*, 2000).

Current treatment strategies are mainly aimed at restoring striatal dopamine activity with levodopa as the gold-standard of therapy. Levodopa is given in combination with carbidopa, a DOPA decarboxylase (aromatic-L-amino acid decarboxylase) inhibitor which prevents peripheral levodopa metabolism. Other adjunct therapies include dopamine agonists, which stimulate dopamine receptors, MAO-B (monoamine oxidase-B) inhibitors and COMT (catechol-O-methyltransferase) inhibitors which prevent dopamine degradation (Lees, 2005). Several potential neuroprotective or disease modifying agents have shown the possibility of neuroprotection in clinical trials, but since it could not be ascertained whether the improvement in PD was due to neuroprotective effects and/or symptomatic relief none of the several candidate agents has been established as neuroprotective therapy for PD thus far (Stocchi, 2014).

1.1.2 Monoamine oxidase

Monoamine oxidase (MAO) is an enzyme distributed extensively in higher eukaryotes and in mammals, and is present in two isoforms, MAO-A and MAO-B. The MAOs are enzymes containing FAD (flavin adenine dinucleotide) as a cofactor and these enzymes are found bound to the outer mitochondrial membrane. The MAOs catalyze the oxidative deamination of various biogenic and dietary monoamines. Abnormal MAO levels in the human body are associated with several disease states such as schizophrenia, depression, Parkinson's disease, attention deficit disorder and abnormal sexual maturity (Haung & Faulkner, 1981; Singh & Sharma, 2014). MAO-A and MAO-B are different with respect to their amino acid sequence, three dimensional structure, tissue distribution as well as substrate and inhibitor specificities (Singh & Sharma, 2014; Pisani *et al.*, 2013; Wouters, 1998). MAO-A

preferentially deaminates serotonin whilst MAO-B shows a preference for phenethylamine as substrate. Both deaminate dopamine equally well (Youdim *et al.*, 2006).

Since inhibition of the MAOs can potentially modulate neurotransmitter levels (for example dopamine) in the brain that are actively involved in the pathogenesis of some neurodegenerative, age-related diseases (Henchcliffe *et al.*, 2005), MAO inhibitors have found particular application as potential therapeutic agents in disorders such as PD (Pisani *et al.*, 2013). Current therapeutic strategies are effective symptomatically by compensating for diminished striatal dopamine levels, however arresting disease progression is the ultimate goal to protect against continued neurotoxic processes (Foley & Riederer, 2000).

The MAO catalytic cycle produces hydrogen peroxide as a by-product. Hydrogen peroxide is a precursor of harmful reactive oxygen species (ROS), and can lead to oxidative stress through the Fenton reaction. Thus, inhibition of the MAO enzymes can decrease hydrogen peroxide and subsequent ROS formation, and limit oxidative stress (Zecca *et al.*, 2004). MAO-B levels furthermore increase with increasing age in humans, thus novel MAO-B inhibitors that bind non-covalently may serve as useful neuroprotective agents against PD (Edmondson *et al.*, 2007).

Efforts aimed at developing MAO inhibitors have previously been focused on the discovery of novel selective MAO-B or MAO-A inhibitors. MAO-A selective inhibitors have been found to be effective in treatment of depression whilst MAO-B selective inhibitors (such as rasagiline and selegiline) have been found useful in PD therapy, particularly as adjunct therapy to levodopa (Gaspar *et al.*, 2011a). These agents all bind to the enzyme irreversibly, resulting in slow enzyme recovery time, with the enzyme requiring more than a week to be restored completely (Timar, 1988). Numerous MAO inhibitors have fallen out of favor due to adverse effects such as hepatotoxicity, orthostatic hypotension and the “cheese reaction” which results in hypertensive crisis (Gaspar *et al.*, 2011a). Current research is therefore aimed at designing selective or non-selective reversible inhibitors that bind competitively to the enzyme. Such compounds have much better side effect profiles (Youdim & Bakhle, 2006).

The lack of disease modifying agents for PD as well as safety concerns of current PD therapy suggest that an urgent need exists for novel, safe, selective and efficient MAO inhibitors (Fiedorowicz & Swartz, 2004).

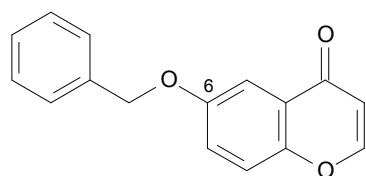
1.1.3 Chromones as MAO inhibitors

Several heterocyclic scaffolds have been investigated in a bid to discover novel MAO inhibitors. These include xanthenes, coumarins, chalcones as well as chromones (Gaspar *et al.*, 2011b).

Chromone is the chemical name used to describe 4*H*-1-benzopyran-4-one (**1**), which is a structural isomer of coumarin (**2**). Compounds that contain this benzopyrone scaffold are thus collectively known as chromones (Edwards & Howell, 2000). An abundance of chromone derivatives occurs in nature, and a vast range of pharmacological activities such as immune-stimulation (Gamal-Eldeen *et al.*, 2007, Djemgou *et al.*, 2006), anti-inflammatory (Gabor, 1986), anti-oxidant (Kuroda *et al.*, 2009), anti-HIV (Zhou *et al.*, 2010), anti-cancer (Martens & Mithöfer, 2005), anti-ulcer (Parmer *et al.*, 1987), biocidal (Binbuga *et al.*, 2008), wound healing (Sumiyoshi & Kimura, 2010), anti-bacterial and anti-fungal (Jovanovic *et al.*, 1994, Grindlay & Reynolds, 1986) have been reported for these compounds. Due to their plant origin, chromones are present in large amounts in the human diet and generally exhibit low mammalian toxicity (Ortwine, 2004). The chromone ring system (**1**) is therefore considered to be a privileged scaffold due to its range of pharmacological and biological effects as well as the low risk of toxicity associated with it (Machado & Marques, 2010).

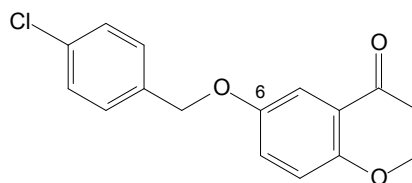


The MAO inhibitory potential of chromone derivatives has further been illustrated previously. Legoabe *et al.* (2012a), for example, synthesized a series of C6-alkyloxy substituted chromone derivatives and evaluated these compounds as inhibitors of MAO. These chromones were found to be potent, reversible MAO-B inhibitors with IC_{50} values ranging between 0.002 - 0.076 μ M. The structures, IC_{50} and selectivity index (SI) values of some of the MAO inhibitors synthesised in this study are given in Figure 1.1 (compounds **3** - **6**).



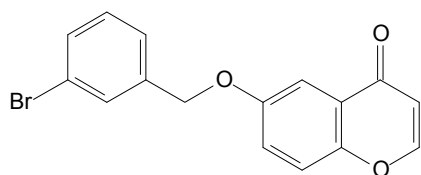
3

IC_{50} (MAO-A) = 3.3 μ M
 IC_{50} (MAO-B) = 0.053 μ M
 SI = 62



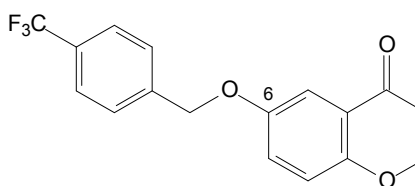
4

IC_{50} (MAO-A) = 0.106 μ M
 IC_{50} (MAO-B) = 0.002 μ M
 SI = 53



5

IC_{50} (MAO-A) = 0.386 μ M
 IC_{50} (MAO-B) = 0.002 μ M
 SI = 193

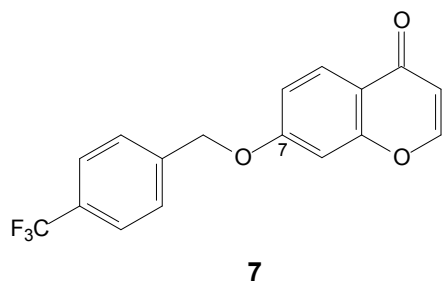


6

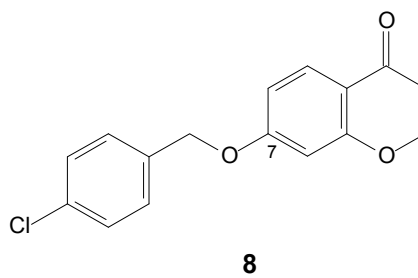
IC_{50} (MAO-A) = 0.879 μ M
 IC_{50} (MAO-B) = 0.002 μ M
 SI = 440

Figure 1.1 Structures of C6-substituted chromones synthesized by Leogoabe *et al.* (2012a).

It was noted that substitution with a halogen on the benzyloxy phenyl ring of chromone **3** in particular increased activity and the most potent MAO-B inhibitors in this series had IC_{50} values of 0.002 μ M (2 nM) (compounds **4** - **6**). Although nine of the fifteen synthesized chromones also exhibited IC_{50} values in the nM range for the inhibition of MAO-A, selectivity index values indicated that these compounds were selective for the MAO-B iso-enzyme. Similarly, a series of C7-substituted chromone derivatives (Figure 1.2) were also shown to be potent monoamine oxidase inhibitors (Legoabe *et al.*, 2012b). Compound **7** was identified as the most potent C7-substituted MAO-B inhibitor exhibiting, an IC_{50} value of 0.008 μ M for MAO-B and an IC_{50} of 1.97 μ M for MAO-A.



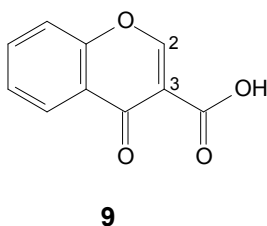
IC₅₀ (MAO-A) = 1.97 μM
 IC₅₀ (MAO-B) = 0.008 μM
 SI: 246



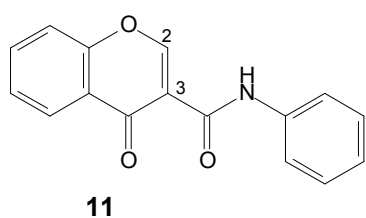
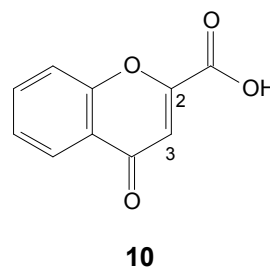
IC₅₀ (MAO-A) = 0.495 μM
 IC₅₀ (MAO-B) = 0.029 μM
 SI: 17

Figure 1.2 Structures of C7-substituted chromones (Legoabe *et al.*, 2012b).

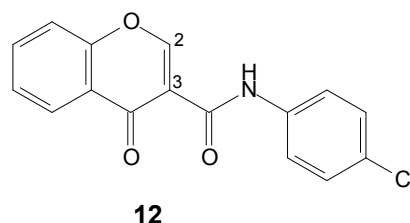
Interestingly, C5-benzyloxy substituted chromone analogues displayed poor MAO-B inhibition when compared to the C6- and C7-substituted analogues (Legoabe *et al.*, 2012c). It has further been shown that while chromone 3-carboxylic acid (**9**) is a potent selective, irreversible MAO-B inhibitor (IC₅₀: 0.048 μM), the presence of the carboxylic acid group in position 2 of the γ-pyrone nucleus (**10**) results in a loss of activity (Alcaro *et al.*, 2010; Gaspar *et al.*, 2011a,b; Helguera *et al.*, 2013). Similarly, phenylcarboxamide substitution in position 3 of the γ-pyrone nucleus results in potent, selective MAO-B inhibitory activity, for example compounds **11** and **12** with IC₅₀ values of 0.40 μM and 0.063 μM, respectively, while related 2-phenylcarboxamide substitution generally results in poor activity (Gaspar *et al.*, 2011a,b; Helguera *et al.*, 2013).



IC₅₀ (MAO-B) = 0.048 μM



IC₅₀ (MAO-B) = 0.40 μM
 SI = >250



IC₅₀ (MAO-B) = 0.063 μM
 SI = >1585

From the above discussion it is thus clear that the 4*H*-1-benzopyran-4-one scaffold is a privileged scaffold for the design of inhibitors that are selective for MAO-B and has the additional advantages of ease of synthesis and potential low toxicity (Ellis, 2009).

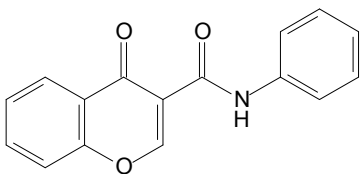
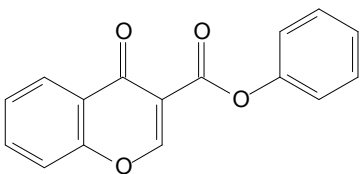
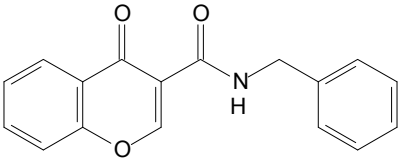
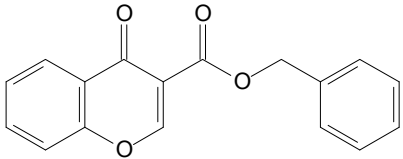
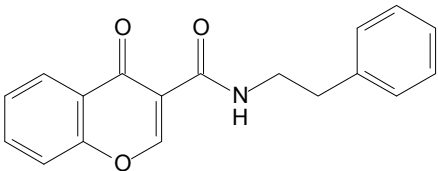
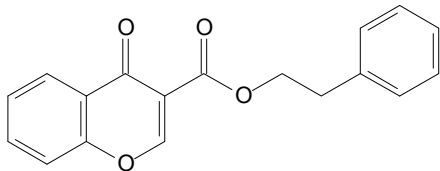
1.2 The hypothesis of this study

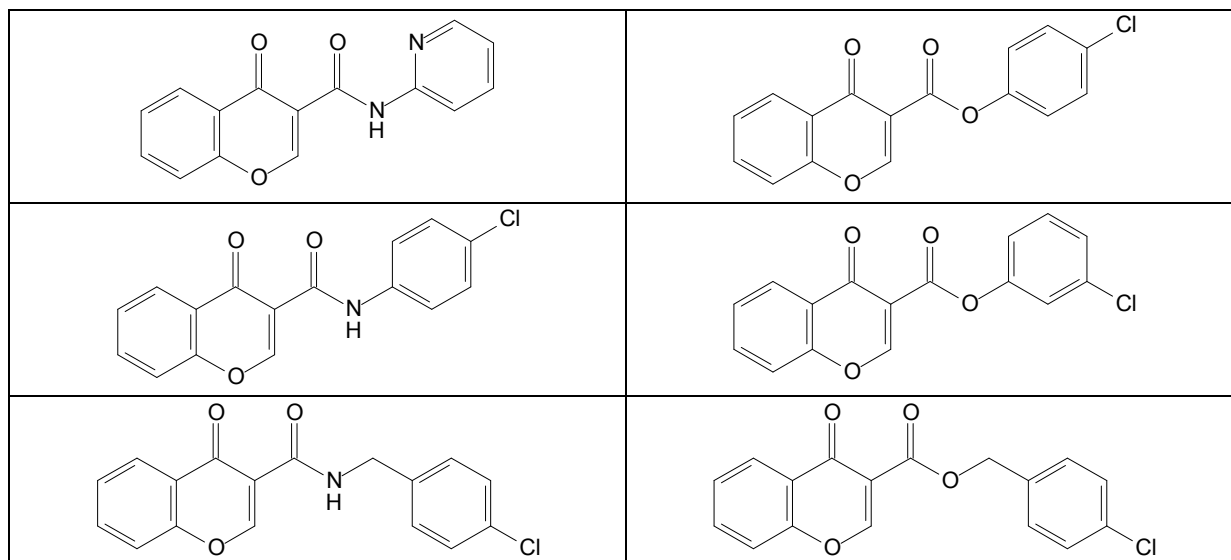
The MAO inhibitory activity of the chromone scaffold has been validated as discussed above. Chromone 3-carboxylic acid (**9**) will serve as lead compound in this study. Although the MAO inhibitory activity of rigid phenylcarboxamide derivatives of chromone 3-carboxylic acid have previously been investigated, the effect of chain elongation and the introduction of a more flexible substituent in this position has not been previously explored. Flexible substitution in position 6 and 7, and rigid amide groups in position 3 have resulted in potent MAO inhibitors. It is thus postulated that the introduction of a flexible ester or amide side chain in position 3 of the chromone nucleus will result in potent, selective MAO inhibition.

1.3 Aims and objectives

The aim of this study is to synthesize and evaluate chromone derivatives as potential MAO inhibitors and thus to contribute to the known structure-activity relationships of the MAO inhibitory activity of chromones. Different amide and ester substituents will be introduced on position 3 of the chromone scaffold to further investigate the effect of substitution in this position in particular. Compounds **11** and **12** will be re-synthesized and included for reference purposes. The structures of some of the proposed compounds are given in table 1.1 below.

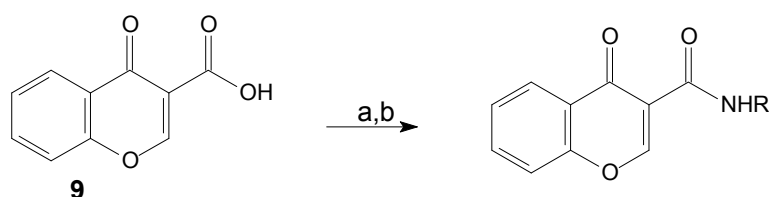
Table 1.1 Proposed compounds to be synthesized

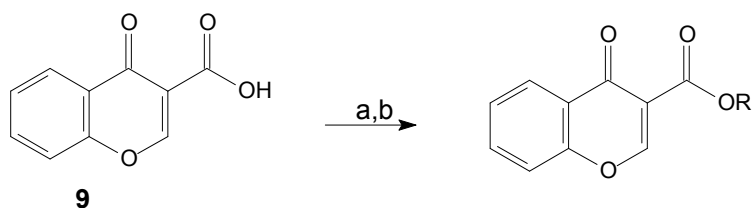


The objectives of the study can be summarized as follows:

- To synthesize novel 3-carboxychromones. The proposed synthetic route involves the coupling of different amines to chromone-3-carboxylic acid in the presence of carbonyldiimidazole (CDI), (Scheme 1.1), to yield the amide derivatives. Related ester derivatives will be synthesized using the same methodology (Scheme 1.2).



Scheme 1.1: Proposed synthesis of amide derivatives. Reagents and conditions (a) CDI, DMF, 60°C, 2 h. (b) R-NH₂, DMF, rt, overnight.



Scheme 1.2: Proposed synthesis of ester chromone derivatives. Reagents and conditions (a): CDI, DMF, 60°C, 2 h. (b) R-OH, DMF, rt, overnight.

- To screen synthesized chromones as inhibitors of recombinant human MAO-A and MAO-B. A fluorometric assay will be used with kynuramine as substrate.

3. To determine reversibility of binding to the MAO enzymes using dialysis studies for selected compounds, since both a reversible and irreversible mode of binding has previously been reported for chromone derivatives (Legoabe *et al.*, 2012b).
4. To determine the mode of binding, by constructing Lineweaver-Burk plots for selected compounds.

CHAPTER 2

LITERATURE STUDY

2.1 Introduction

Parkinson's disease (PD) is a neurodegenerative disorder characterized mainly by the loss of dopaminergic neurons found in the substantia nigra pars compacta (SNpc) in the mesencephalon (Dauer & Przedborski, 2003) (Figure 2.1). The disease was first described in 1800 by James Parkinson in his monograph entitled "An Essay on the Shaking Palsy", and in recognition of his work, Jean Martin Charcot proposed the syndrome be named *maladie de Parkinson* (Parkinson's disease) (Lees *et al.*, 2009).

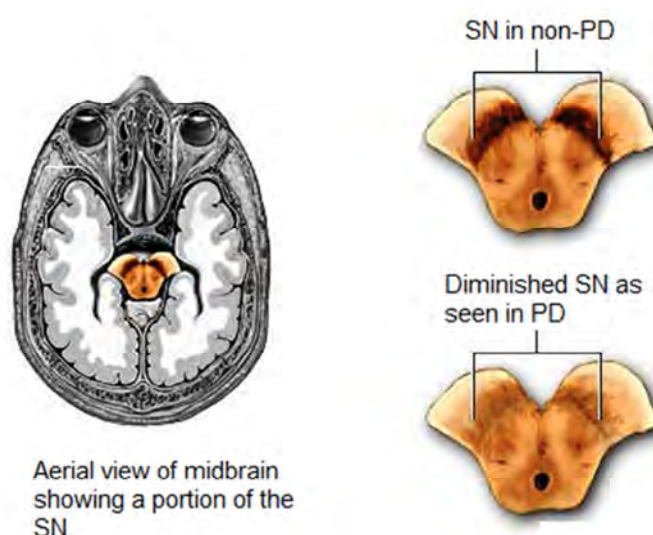


Figure 2.1 Brain section showing substantia nigra in Parkinson's disease and in a non-Parkinson's disease. SN: Substantia nigra, PD: Parkinson's disease (Barichella *et al.*, 2010).

2.2 Incidence

The average age of onset of PD is 60 years (Lees *et al.*, 2009; Olanow, 2004), but 10% of cases have been classified as young onset occurring between 20 - 50 years of age. The incidence of the disease rises with age, from 17.4 in 100 000 people aged between 50 and 59 years to 93.1 in 100 000 people aged between 70 - 79 years. The lifetime risk of developing PD is 1.5%. Ageing is a major risk factor for developing PD (Lees *et al.*, 2009). PD is more prevalent in men than in women, this may be because of the protective effects of

estrogen (Dexter & Jenner, 2013). With age, loss of estrogen in women may remove its protective effect, and there is evidence to suggest that early menopause, hysterectomy or the removal of ovaries increase the risk of PD in women, compared to that seen in men (Ragonese *et al.*, 2004; Popat *et al.*, 2005).

In Africa, with particular reference to Southern Africa, very little is known about PD (Heligman *et al.*, 2000). Okubadejo and colleagues (2006) conducted a study on PD in Africa and they found comparatively little PD-related research published from Africa, thus numerous research opportunities exist in this field. The only documented incidence study in Africa was done in Benghazi, North East Libya between 1982 and 1984 (Ashok *et al.*, 1986). It was determined that the crude incidence rate of PD was 4.5 per 100 000 people per year. Data did not however show any information concerning the sex, or age of the people involved in the study (Okubadejo *et al.*, 2006).

2.3 Symptoms

The clinical syndrome of PD is called parkinsonism and it reflects the earliest and most striking physical disabilities consisting of motor impairments (Wichmann & DeLong, 1993). These motor impairments include:

- Bradykinesia (movements are slow and poor).
- Rigidity of the muscles.
- Tremors at rest (these tremors do not impair activities of daily living and decrease when voluntary motion occurs (Dauer & Przedborski, 2003).
- Impaired postural balance that disrupts gait and causes falling (Standaert & Roberson, 2011).

PD is a complex illness that contains in addition to motor symptoms, non-motor symptoms such as sleep disturbances, depression, sensory abnormalities, autonomic dysfunction and cognitive decline (Dexter & Jenner, 2013; Langston, 2006).

2.4 Pathology

The striatum is the major target for dopaminergic neurons that originate from the SNpc and dopamine released into the striatum regulates normal coordinated body movements produced by stimulation of D₁ receptors and inhibition of D₂ receptors. Thus, degeneration of dopaminergic neurons in the basal ganglia will result in the characteristic disorderly movements associated with PD (Morelli *et al.*, 2007). Dopaminergic neuronal loss

associated with PD has a characteristic topology that can be distinguished from that observed in normal ageing. Cell loss in PD occurs mainly in the ventrolateral and caudal parts of the SNpc whilst in normal ageing the dorsomedial aspect of the SNpc is affected (Fearnly & Lees, 1991).

In order to diagnose PD, both Lewy bodies and SNpc dopaminergic neuronal loss has to be present (as shown in figure 2.2). The presence of Lewy bodies alone does not signify PD, as it can be found in Alzheimer's disease specifically in 'dementia with Lewy bodies disease' (Gibb & Lees, 1988). Lewy bodies are spherical eosinophilic inclusions that contain ubiquitinated proteins such as α -synuclein (Forno, 1996; Spillantini *et al.*, 1998).

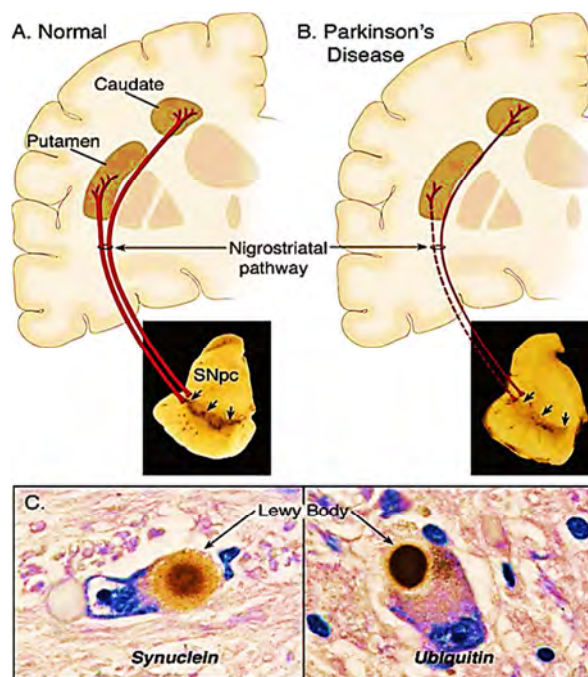


Figure 2.2 Part A shows the nigrostriatal pathway in red (thick solid lines) showing the projection of dopaminergic neurons from the SNpc (normal pigmentation shown) to the putamen and caudate nucleus found in the basal ganglia and synapse in the striatum. In part B the nigrostriatal pathway is shown in red as found in PD (the pathway degenerates) with depigmentation of the SNpc. The dashed red line shows marked loss of dopamine neurons to the putamen and the solid thin red line shows moderate loss to the caudate nucleus (Dauer & Przedborski, 2003).

Any disease that causes direct striatal damage or contributes towards striatal dopamine (DA) deficiency, can therefore clinically lead to parkinsonism (Dauer & Przedborski, 2003). PD can thus be produced by other disorders such as stroke, rare neurodegenerative disorders and intoxication with DA antagonists, and is thus not just idiopathic in nature (Standaert & Roberson, 2011).

Neurodegeneration in PD is found not only in dopaminergic neurons but also in the cerebral cortex, olfactory bulb, noradrenergic (locus coeruleus), serotonergic (raphe), and cholinergic (nucleus basalis of Meynert, dorsal motor nucleus of vagus) neuronal systems. Dementia that accompanies PD results mainly from degeneration in both the hippocampus and cholinergic cortical inputs (Dauer & Przedborski, 2003).

PD pathology does not start in the SNpc but rather in the olfactory bulb and lower brain stem where the presence of Lewy bodies and deposition of α -synuclein originate, from where it then spreads in stages to the midbrain and finally to the cortical regions (Dexter & Jenner, 2013).

2.5 Etiology

The specific causes of Parkinson's disease are not fully understood (Olanow & Tatton, 1999; Priyadarshi *et al.*, 2001). Age is the one factor that strongly relates to onset of PD, though very little has been done to understand how ageing is involved in PD. Most concepts involving cell death in PD do not consider the role that ageing plays, as in experimental studies, the animals employed are young animals used to show or hypothesize how the disease progresses (Schapira & Jenner, 2011).

The main factors thought to be involved in the etiology of PD are environmental factors and genetic factors. For most of the 20th century the environmental toxin hypothesis was more dominant due to evidence of post-encephalitic PD and the role of 1-methyl-4-phenyl-1,2,3,6-tetrahydropyridine (MPTP) in inducing parkinsonism. However, mutations in certain genes have been found to play a role as well (Dauer & Przedborski, 2003; Langston *et al.*, 1983).

2.5.1 Environmental Factors

Several environmental factors increase the risk of developing PD (Priyadarshi *et al.*, 2001; Tanner & Langston, 1990). These are exposure to well water, pesticides (paraquat, organophosphates, and rotenone), herbicides, industrial chemicals, wood pulp mills, farming and living in a rural environment (Olanow & Tatton, 1999). Rural environment living can increase the risk of PD as it may be related to potential exposure to neurotoxins present in pesticides, well water or spring water (Priyadarshi *et al.*, 2001).

The environmental hypothesis is based on the presence of environmental toxins such as MPTP, cyanide, carbon disulphide and toluene. MPTP, which is a by-product of the illicit manufacture of a synthetic meperidine derivative, was observed in the brains of drug addicts

who manufactured and ingested it unwittingly and presented with characteristics of a syndrome with the clinical and pathological features of PD (Langston *et al.*, 1983).

MPTP is a highly lipophilic substance that crosses the blood brain barrier easily. In a reaction catalyzed by monoamine oxidase B (MAO-B) in the astrocytes, MPTP is converted to the pyridinium ion (MPP⁺). MPP⁺, via active transport, moves into the extracellular space and enters the dopaminergic neurons through a dopamine transporter in the plasma membrane (Speciale, 2002). The presence of MPP⁺ in the dopaminergic cells causes damage to the mitochondrial electron transport chain, specifically complex 1 which results in lower ATP formation and production of ROS. This leads to neurodegeneration as shown in figure 2.3 (Nicklas *et al.*, 1985; Speciale, 2002).

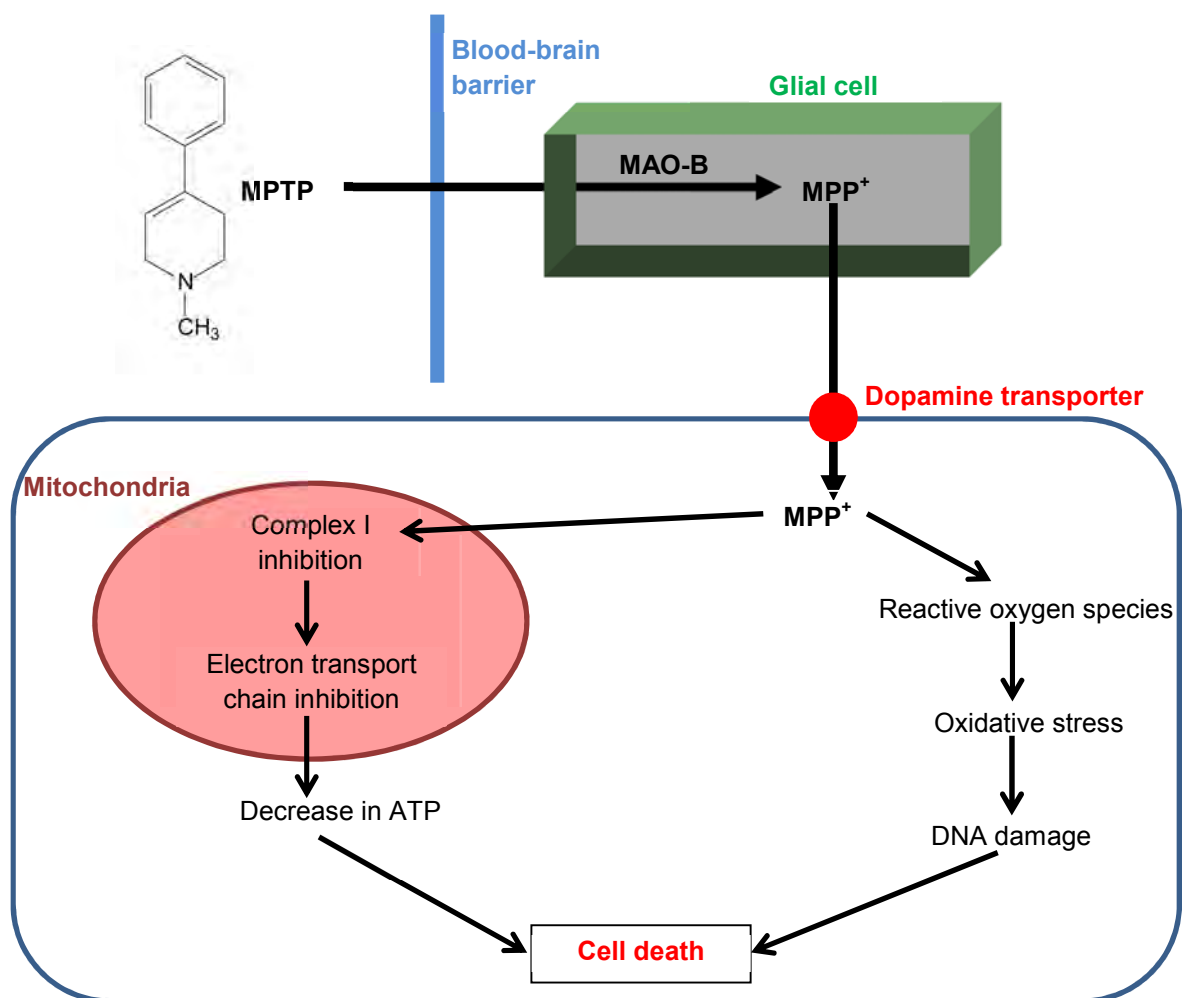


Figure 2.3 MPTP toxicity and subsequent cell death (Muramatsu & Araki, 2002).

2.5.2 Genetic Factors

Genetic studies have shown several mutations in seven genes that are linked with L-dopa responsive parkinsonism (Lees *et al.*, 2009). These genes are: Parkin, PINK1 (PTEN-induced putative kinase 1), DJ-1, ATP13A2, α -synuclein, LRRK-2 (leucine-rich-repeat-kinase-2) and GBA (glucocerebrosidase). In LRRK-2, a kinase coding for the protein dardarin, six pathogenic mutations have been reported, the most common mutation being Gly2019Ser. This mutation has a worldwide frequency of 1% in sporadic cases and 4% in patients with hereditary parkinsonism (Lees *et al.*, 2009). Mutations in DJ-1, PINK1 and ATP13A2 are rare but parkin mutations represent the second most common genetic cause of L-dopa responsive parkinsonism (Lees *et al.*, 2009). The majority of patients with PINK1 mutations have an onset of parkinsonism at an age younger than 40 years (Shapira & Jenner, 2011).

It was discovered in 1997 that mutations in the gene for α -synuclein cause an inherited form of PD (Dauer & Przedborski, 2003). Parkin is also the most common genetic link to young onset PD, while it is LRRK-2 for late onset PD. Mutations in α -synuclein are rarely encountered but through their discovery, α -synuclein was identified as the major component in Lewy bodies and Lewy neurites leading to the labeling of PD as a synucleinopathy (Dexter & Jenner, 2013). Many of the familial PD neurodegenerative mechanisms overlap with the pathogenic mechanisms present in sporadic PD such as mitochondrial dysfunction, oxidative stress and protein alteration (Dexter & Jenner, 2013). Figure 2.4 shows the various genetic components involved in the etiology of PD.

2.6 Mechanisms of Neurodegeneration (Pathogenesis)

2.6.1 Oxidative Stress

Since the 1980s there has been an increase in the number of publications that implicate formation of reactive oxygen species as a final step in neuronal death, resulting in PD of whatever origin (Dexter & Jenner, 2013). Catalase, superoxide dismutase and glutathione peroxidase all form part of the major antioxidant enzyme systems in the brain. Deficiencies in these enzymes as well as decreased levels of glutathione (present in PD) lead to oxidative damage to lipids, proteins and DNA, and indicate that oxidative stress plays a role in the pathogenesis of PD (Shapira & Jenner, 2011).

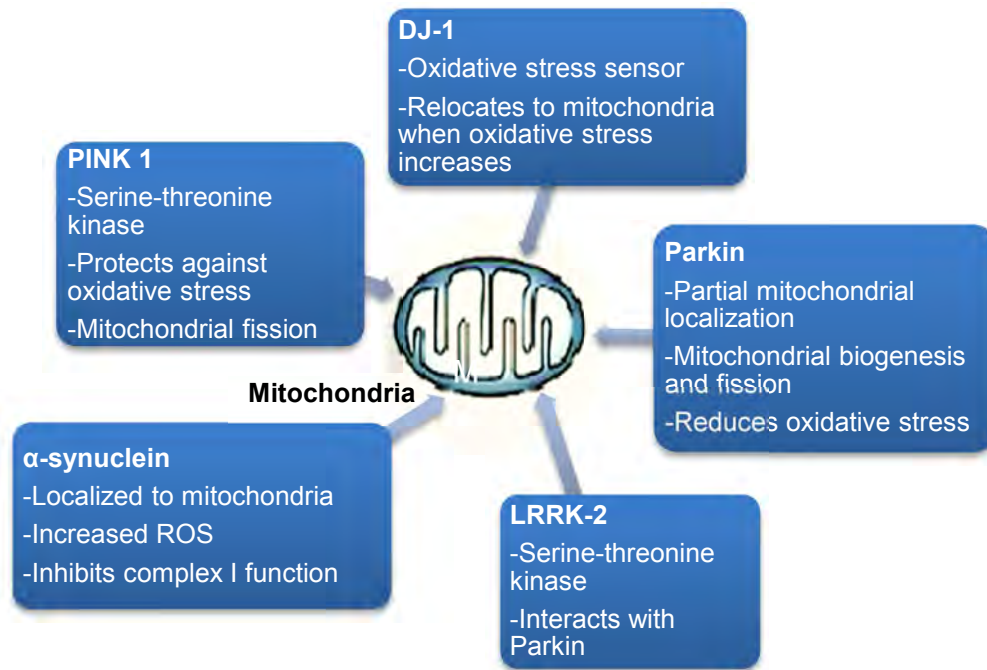


Figure 2.4 Important genes in PD and their corresponding functions (Henchcliffe & Beal, 2008).

It is normally inactivated in the brain by glutathione peroxidase making use of glutathione (GSH) as a cofactor (figure 2.5). A deficiency in glutathione, as seen in PD, can subsequently lead to a decrease in the brain's ability to clear hydrogen peroxide which can cause oxidative stress and cell death (Youdim & Bakhle, 2006).

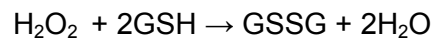


Figure 2.5 H_2O_2 clearance which, under normal circumstances, occurs in the presence of GSH.

MAO activity is further influenced by levels of iron in animals and humans. In many neurodegenerative diseases, for example PD, the sites of neuronal death in the brain are the sites where iron also accumulates (Zecca *et al.*, 2004; Youdim & Bakhle, 2006). Increased oxidative stress links MAO to iron and neuronal damage. In PD, low GSH levels and accumulated hydrogen peroxide and iron results in the Fenton reaction as shown in figure 2.6. In the Fenton reaction, iron in the ferrous ion form (Fe^{2+}) generates the hydroxyl radical from hydrogen peroxide, and this hydroxyl radical depletes cellular anti-oxidants, and reacts with and damages DNA, lipids and proteins. Furthermore, brain MAO and brain iron increase with increasing age thus increasing the likelihood of the Fenton reaction and generation of hydroxyl radicals (Youdim & Bakhle, 2006).

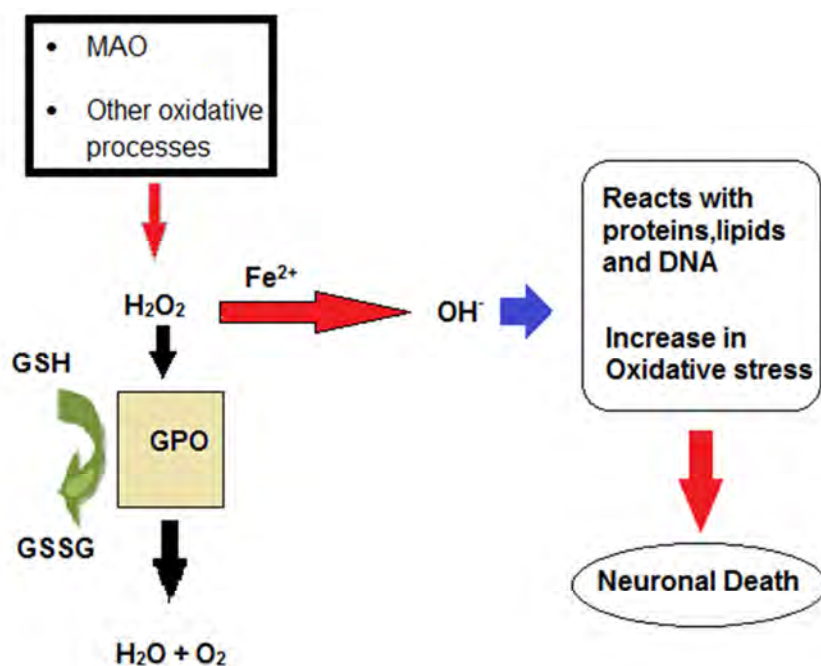
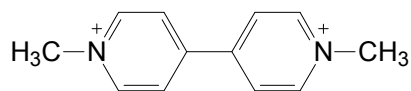


Figure 2.6 The mechanism of neurotoxicity induced by iron and hydrogen peroxide via the Fenton reaction (Youdim & Bakhle, 2006).

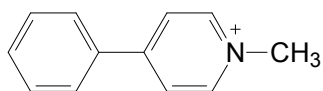
Proof of oxidative stress in the SNpc has been provided by post-mortem studies conducted in PD brains that showed increased iron, low levels of glutathione (GSH) and damage due to oxidation in lipids, proteins and nucleic acids (Olanow & Tatton, 1999). Neurotoxins such as 6-hydroxydopamine (6-OHDA), MPTP, paraquat and rotenone are known to induce dopaminergic neurodegeneration. The administration of these toxins also results in the formation of ROS, although MPTP is the only toxin that has been linked to human parkinsonism. MPTP shows similarities to rotenone in that they can both inhibit complex I resulting in an increase in the production of superoxide which subsequently form toxic hydroxyl radicals or react with nitric acid to form peroxynitrite. Both of these are powerful oxidizing agents. This can thus ultimately cause cellular damage by reacting with proteins, nucleic acids and lipids or even the electron transport chain causing mitochondrial damage (Dauer & Przedborski, 2003).

Paraquat (**13**), a herbicide which presents a risk for the development of PD on exposure, shows structural similarity to MPP^+ (**14**) as shown in figure 2.7. Paraquat does not penetrate the blood brain barrier easily, and its toxicity is possibly mediated by superoxide radical formation (Day *et al.*, 1999). When paraquat is administered systemically to mice, SNpc

dopaminergic neuron degeneration occurs with subsequent α -synuclein containing inclusions (Dauer & Przedborski, 2003).



13 Paraquat



14 MPP⁺

Figure 2.7 Structural similarities of paraquat (**13**) and MPP⁺ (**14**).

Rotenone, a potent rotenoid, is used extensively as an insecticide and fish poison. Its lipophilicity results in its ease of access to all organs in the human body (Dauer & Przedborski, 2003). The administration of low-dose intravenous rotenone to rats results in selective degeneration of nigrostriatal dopamine neurons with α -synuclein positive Lewy body inclusions as confirmed by Greenamyre *et al.*, (2001), suggesting preferential sensitivity to complex I inhibition (Dauer & Przedborski, 2003).

2.6.2 Altered Mitochondrial Function

Interest in the role of mitochondria in the development of PD pathogenesis arose from genetic investigations in familial PD (Dexter & Jenner, 2013). Mutations in α -synuclein, parkin, PINK1, DJ-1 and possibly LRRK2 have been linked to altered mitochondrial function (Shapira & Jenner, 2011). Mitochondrial dysfunction is further increased when mitochondrial protection against oxidative stress is reduced due to the loss of function of DJ-1, parkin and PINK1 (Dexter & Jenner, 2013).

2.6.3 Altered Proteolysis

The presence of most notably α -synuclein and other proteins in Lewy bodies has led to the possible conclusion that, the break-down of proteins that are unwanted, damaged or mutated could possibly be disrupted in PD causing cellular aggregation and neuronal death (Shashidharan *et al.*, 2000). Direct damage to neurons could be caused by protein

aggregates possibly by deforming the cell or interfering with intracellular trafficking in neurons (Dauer & Przedborski, 2003).

2.6.4 Inflammatory Change

Marked increases in cytokine levels found in the striatum and cerebrospinal fluid (CSF) of PD patients have led to the conclusion that neuro-inflammatory reactions occur that lead to cell degeneration (Yacoubian & Standaert, 2009).

2.6.5 Excitotoxic Mechanisms

Glutamate, a primary excitatory transmitter in the CNS in mammals, plays a major role in the excitotoxic process (Yacoubian & Standaert, 2009). The dopaminergic neurons in the substantia nigra contain numerous glutamate receptors, which receive glutamatergic innervation that comes from the subthalamic nucleus and cortex. Overactivation of the N-methyl-D-aspartate (NMDA) receptor by glutamate can result in an increase in intracellular calcium levels which activates pathways responsible for cell death (Mody & MacDonald, 1995).

2.6.6 Apoptosis

Apoptosis is defined as programmed cell death. Cell death pathway activation is likely to represent end-stage processes involved in neurodegeneration mechanisms of PD (Yacoubian & Standaert, 2009). Figure 2.8 shows the various mechanisms that are involved in neurodegeneration.

2.7 Treatment

Current treatment available for PD is focused to a great extent on rectifying the dopaminergic deficit and thus alleviating the motor symptoms (rigidity, bradykinesia, tremors at rest and postural disturbances) of PD (Smith *et al.*, 2011).

2.7.1 Symptomatic Treatment

Since the key molecular events that induce neurodegeneration are not well understood, it provides a major obstacle for the development of neuroprotective therapies for PD (Dauer & Przedborski, 2003). Current treatments are therefore in effect symptomatic, improving the quality of life and functional capabilities (Lees *et al.*, 2009).

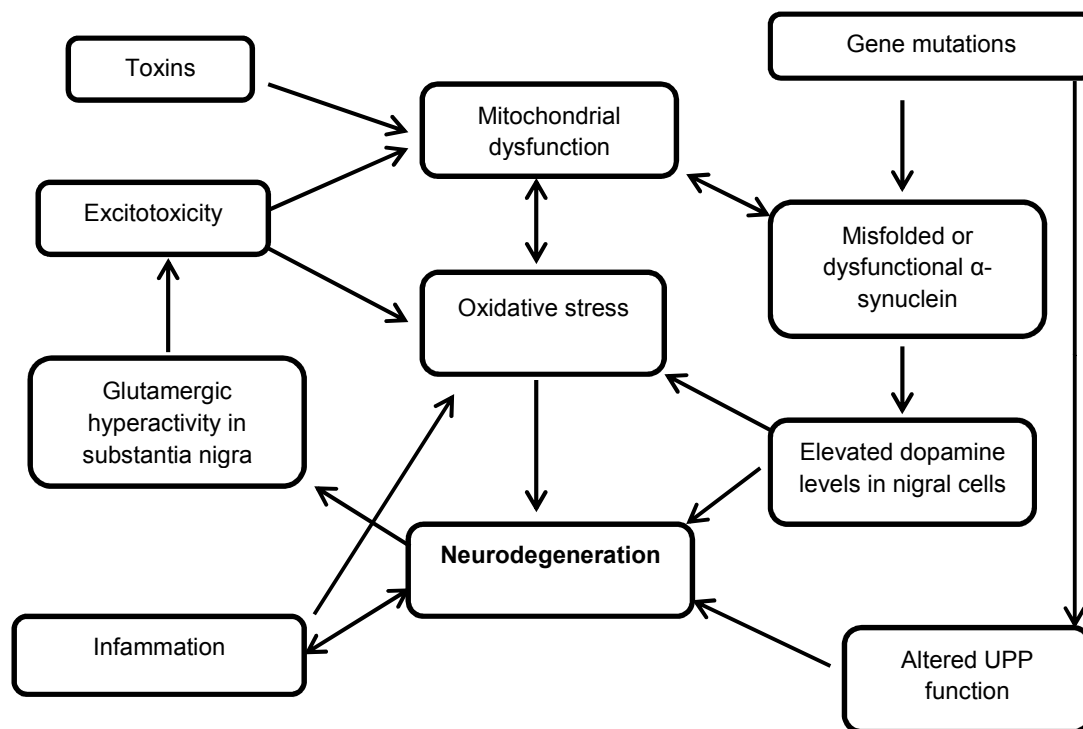
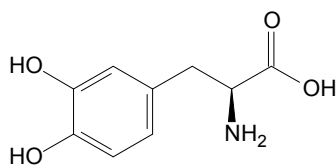


Figure 2.8 Mechanisms of neurodegeneration (Dauer & Przedborski, 2003).

Symptomatic treatment is mainly aimed at restoration of striatal dopamine activity. This is done by either increasing dopamine supply (using the dopamine prodrug levodopa (**15**), direct stimulation of dopamine receptors (dopamine agonists) or by inhibiting the metabolism of dopamine (Lees, 2005).

Levodopa



15 levodopa

Dopamine does not cross the blood-brain barrier, and can thus be metabolized in the periphery resulting in it being ineffective as an antiparkinsonian agent. Levodopa (**15**), a precursor of dopamine, is able to cross the blood brain barrier by making use of active transport. It is then converted inside the brain to dopamine by the pyroxidine-dependant enzyme, aromatic L-amino acid decarboxylase [dopa decarboxylase (DDC)] (Ciccone, 2007). To prevent the peripheral decarboxylation of levodopa, it is usually prescribed with a

dopamine decarboxylase inhibitor such as carbidopa which prevents dopamine decarboxylation in the periphery so as to enhance dopamine levels in the CNS (Olanow, 2004).

The long-term use of levodopa causes dyskinesias (involuntary movements), which can impair quality of life (Dauer & Przedborski, 2003; Smith *et al.*, 2011). It also results in motor response fluctuations (the 'on-off' effect, end of dose akinesia, freezing, and early morning dystonia), and neuropsychiatric complications. Despite these shortcomings, L-dopa is still regarded as the gold standard in therapy for the motor symptoms of PD (Lees, 2005).

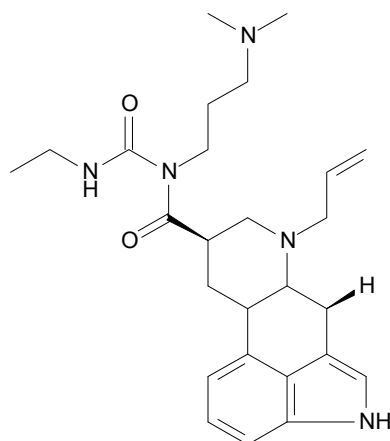
Dopamine Agonists

Dopamine agonists stimulate dopamine receptors directly. Dopamine agonists work mostly on the D₂-like receptors (D₂, D₃ and D₄). Antiparkinsonian activity is linked to stimulation of D₂ postsynaptic receptors, whereas presynaptic stimulation is thought to be linked to neuroprotection (Deleu *et al.*, 2002).

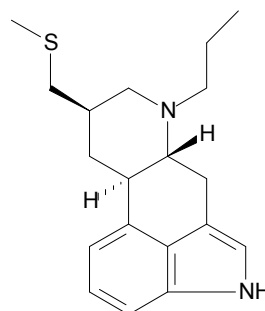
Dopamine agonists can be divided into two groups, namely the ergoline and nonergoline agonists. The ergoline agonists include bromocriptine, carbegoline (**16**), lisuride and pergolide (**17**) while the nonergoline agonists include ropinirole (**18**), apomorphine (**19**), pramipexole, and piribedil (see figure 2.9 for examples).

There is no general agreement on whether dopamine agonists should be given as initial therapy in PD to delay the need for levodopa and therefore lower risk of developing motor complications (this can be done for patients <50 years of age who are more prone to severe motor complications), or for dopamine agonists to be used later in the disease at the end of the levodopa 'honey-moon' phase. In elderly patients, the use of dopamine agonists as initial therapy must be weighed against the risk of side effects caused by these agents such as orthostatic hypotension, oedema and hallucinations, which occur at a higher rate in elderly patients. Dopamine agonists can be given together with levodopa thus allowing the use of lower dosages of levodopa (Lees, 2005).

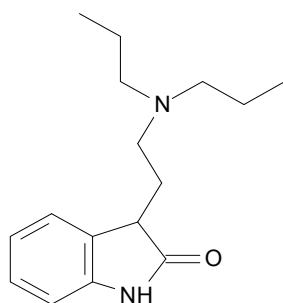
Advantages of dopamine agonists over levodopa include that they do not require carrier mediated transport to enter the brain and their bioavailability are therefore not influenced by the presence of food or amino-acids. They also act directly on dopamine receptors thus requiring no storage or biotransformation by the depleted dopamine neurons found in PD (Lees, 2005; Deleu *et al.*, 2002).



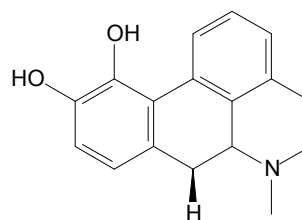
16 Carbegoline



17 Pergolide



18 Ropinirole



19 Apomorphine

Figure 2.9 The chemical structures of selected dopamine agonists.

Adverse effects associated with dopamine agonists include nausea, vomiting, somnolence, orthostatic hypotension, peripheral oedema, and higher doses can cause psychosis. Usually, dopamine agonists are therefore not recommended for use in elderly patients or those who are cognitively impaired (Lees, 2005).

Monoamine Oxidase (MAO) Inhibitors

MAO is a flavin containing enzyme present in the mitochondrial membrane and it exists as two isoforms, namely MAO-A and MAO-B. These two isoforms are different with respect to their substrate preference, distribution in the body, inhibition specificity as well as immunological properties. MAO-A preferentially oxidizes norepinephrine and indolamines, whereas MAO-B preferentially oxidizes phenylethylamines and benzylamines (Deleu *et al.*, 2002).

Early attempts to block dopamine metabolism in the brain by making use of non-selective MAO inhibitors was effective but led to dangerous side effects such as hypertensive crisis, thus making their use in PD unfavorable (Yamada & Yasuhara, 2004). The use of selective MAO-B inhibitors results in increased concentrations of endogenous dopamine as well as exogenous dopamine (such as is obtained from administered levodopa) and generally has an improved side-effect profile. Increased MAO activity has been observed in patients with PD, therefore inhibition of MAO in patients with PD will not only result in an increase in the concentration of monoamines, but will also decrease hydrogen peroxide production, thus decreasing hydroxyl radical formation and the resulting oxidative stress (Youdim and Bakhle, 2006). This coupled to the fact that MAO-B inhibitors inhibit oxidation of MPTP to the toxic metabolite MPP⁺ (Lees, 2005), is indicative of a possible neuroprotective role of MAO inhibitors. MAO-B inhibitors include selegiline (**20**) and rasagiline (**21**) as shown in Figure 2.10. As MAO and its inhibitors are of particular importance to this study, it will be discussed in further detail in section 2.8.



Figure 2.10 Structures of selegiline (**20**) and rasagiline (**21**).

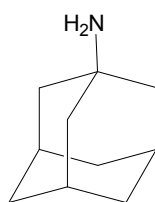
Catechol-O-methyltransferase (COMT) Inhibitors

Decarboxylation to dopamine by DDC is the most predominant metabolic pathway for levodopa. When levodopa is given in combination with a DDC inhibitor such as carbidopa, this major pathway is eliminated thus increasing the effective dose of levodopa (Kaakkola, 2000). When DDC is inhibited O-methylation becomes the dominant pathway for levodopa catabolism. This pathway results in the conversion of levodopa to 3-O-Methyldopa (3-OMD). 3-OMD crosses the blood-brain barrier but it has no affinity for dopamine receptors and no antiparkinsonian activity that has been recorded (Deleu *et al.*, 2002). A peripheral COMT inhibitor such as entacapone, when given in combination with levodopa/carbidopa, enhances the therapeutic activity of levodopa in patients with advanced PD allowing the dosage of levodopa to be decreased. 3-OMD formation is reduced and therefore response to levodopa therapy is improved by this therapeutic combination (Kaakkola, 2000).

Dopamine replacement strategies such as levodopa, dopamine agonists and MAO and COMT inhibitors that are currently used for treating PD are effective against the motor symptoms of PD but have minimal effect on non-motor symptoms (Dexter & Jenner, 2013).

Amantadine

Amantadine (**22**) has numerous mechanisms of action that are of use in the treatment of PD. These include enhancing release of dopamine, blocking the reuptake of dopamine, non-competitive inhibition of NMDA glutamate receptors as well as having some antimuscarinic effects (Lees, 2005; Deleu *et al.*, 2002).



22

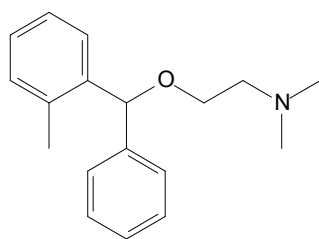
Amantadine may be used as monotherapy or as add-on therapy to dopamine agonists or levodopa/DDC in early or late-stage PD (Deleu *et al.*, 2002).

Anticholinergic Drugs

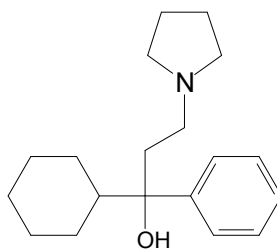
Anticholinergic drugs in PD are believed to act by rectifying the disequilibria present between dopamine and acetylcholine activity in the striatum. Examples of anticholinergic drugs used in PD are shown in figure 2.11. Side effects such as impaired neuropsychiatric activity and cognitive function limit the use anticholinergic drugs (Deleu *et al.*, 2004), while sudden withdrawal of anticholinergic agents could even lead to precipitation of parkinsonism (Comella & Tanner, 1995).

2.7.2 Neuroprotective Drugs

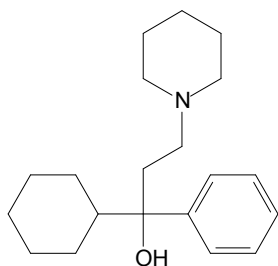
Neuroprotection is defined by LeWitt and Taylor (2008) as slowing the emergence or halting the worsening of disability in everyday functional activities, reducing the decline of ratings focused on distinctive parkinsonian features or avoiding specific clinical events such as use of dopaminergic therapy.



23 Orphenadrine



24 Procyclidine



25 Benzhexol

Figure 2.11 Chemical structures of some anticholinergic drugs used in PD.

As mentioned before, the development of neuroprotective drugs is hindered mainly because the specific molecular events that provoke neurodegeneration in PD are not completely understood (Dauer & Przedborski, 2003). However, several factors have been implicated in the etiology and pathogenesis of PD, thus providing numerous targets for potential neuroprotection as shown in figure 2.12 (Olanow, 2004).

The first clinical study that was done to determine a neuroprotective effect in PD was the DATATOP (Deprenyl and Tocopherol Antioxidative Therapy for Parkinsonism) study (LeWitt & Taylor, 2008). This study consisted of patients with untreated PD that were randomly assigned to receive treatment with the antioxidant vitamin E, the MAO-B inhibitor selegiline or their placebos (Olanow, 2004). The main goal of the study was to determine the time it took patients to reach a stage necessitating introduction of levodopa therapy. Vitamin E proved to be not superior to the placebos even in combination with selegiline. Selegiline, however, were proven to delay emergence of disability. Further studies provided proof that selegiline's ability as neuroprotective agent stems from its propargyl functional group, which has antiapoptotic properties (Tatton *et al.*, 2002). Rasagiline and TCH346, both compounds with propargyl moieties, also show neuroprotective effects. Riluzole, a glutamate release inhibitor has been tested using multiple primary endpoints, but the clinical trial was negative

(Olanow, 2004). There are thus some promising neuroprotective agents, but none have so far been proven to alter disease progression in clinical trials. Currently, there is thus an urgent need for treatment that will effectively slow down disease progression of PD or has the potential to reverse it (Lees, 2005).

Current drugs with potential neuroprotective properties include the dopamine agonists such as bromocriptine, pergolide, ropinirole and pramipexole that can act as free radical scavengers against nitric oxide and hydroxyl radicals (Lange *et al.*, 1995).

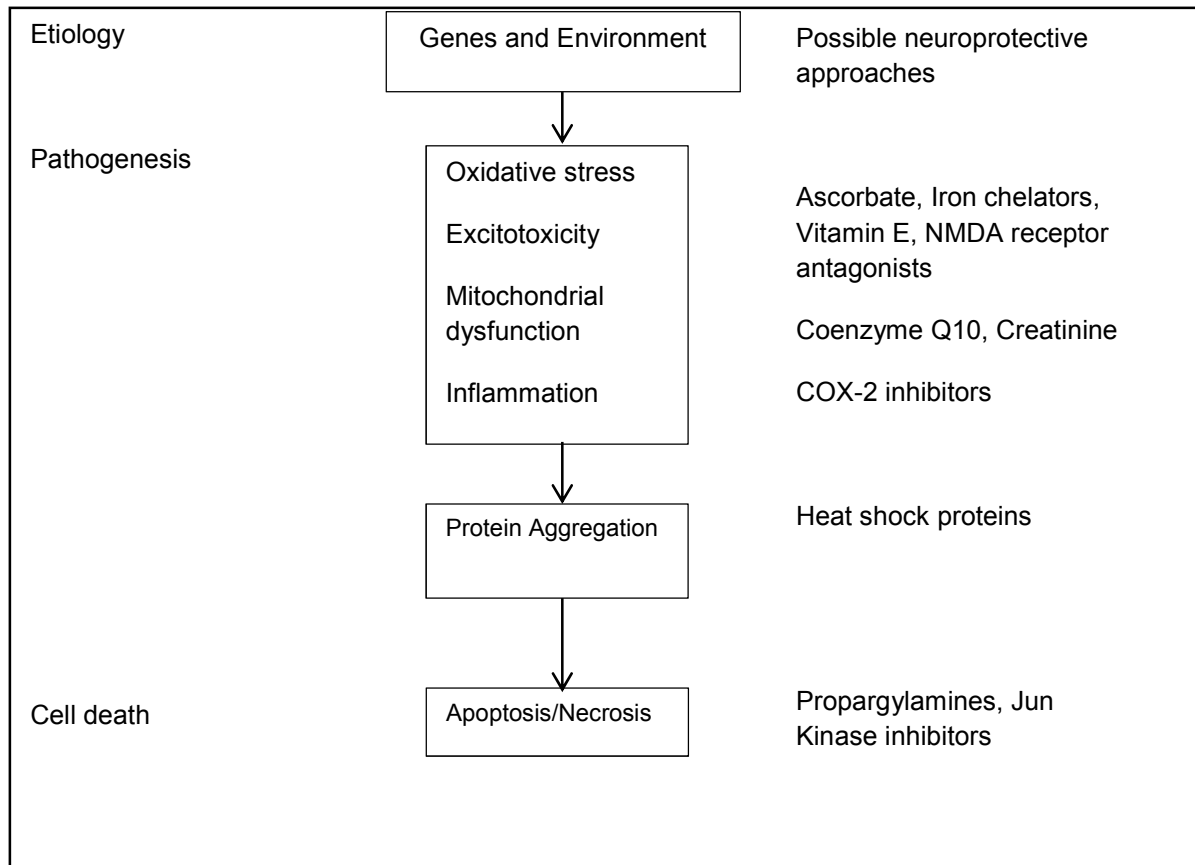


Figure 2.12 Mechanisms of cell death in PD and possible neuroprotective approaches (Olanow, 2004).

The ability of the MAO inhibitors to decrease hydrogen peroxide production and the conversion of toxins such as MPTP to their reactive metabolites is further indicative of the neuroprotective potential of these compounds. However, none of the drugs currently used in the treatment of PD is registered as neuroprotective agents (Lange *et al.*, 1995).

2.8 Monoamine Oxidase (MAO)

2.8.1 General Background

In 1928 an enzyme that catalyzed the oxidative deamination of tyramine was described by Mary Hare-Bernheim as tyramine oxidase. Hugh Blaschko later discovered that tyramine oxidase, noradrenaline oxidase and aliphatic amine oxidase were all the same enzyme that have the ability to metabolize primary, secondary or tertiary amines, but it was Zeller who eventually named the enzyme mitochondrial monoamine oxidase (Youdim *et al.*, 1988).

Over fifty years have passed since MAO inhibitors were first developed as antidepressants. The first potent MAO inhibitor used successfully in the treatment of depressive illness was iproniazid, which is a compound related to the anti-tuberculosis agent isoniazid. The clinical value of iproniazid in depressive illness was however compromised by side effects which included mainly liver toxicity due to its hydrazine structure, leading to the development of other non-hydrazine MAO inhibitors such as tranylcypromine and pargyline. However the use of tranylcypromine was also associated with severe side-effects including the 'cheese reaction' (Youdim *et al.*, 1988).

The cheese reaction is induced by indirect acting sympathomimetic amines, such as tyramine, which are present in food such as cheese, beer and wine. These dietary amines are normally metabolized by MAO in the gut wall and in the liver, thus preventing their entry into systemic circulation. In the presence of a MAO inhibitor, tyramine and other monoamines present in ingested food are not metabolized and can therefore enter the systemic circulation from where they access the brain and induce significant noradrenaline release from the peripheral adrenergic neurons resulting in a severe hypertensive response. This hypertensive response is in some cases, fatal (Youdim & Bakhle, 2006).

An extensive search for novel MAO inhibitors without these severe side-effects thus began (Youdim *et al.*, 2006; Finberg *et al.*, 1981). Selective irreversible MAO-B inhibitors do not cause such side effects because of the small quantity of MAO-B in the small intestines, and tyramine in the small intestines is metabolized to a large extent by MAO-A. Discovery of reversible MAO-A inhibitors such as moclobemide has also been helpful, as their use is not associated with the cheese reaction. Reversible MAO-A inhibitors can inhibit MAO-A adequately in the CNS in order to produce an antidepressant effect, while in the peripheral system, dietary tyramine can displace the inhibitor from MAO-A and allow for its metabolism (Youdim *et al.*, 2006).

2.8.2 Biological Function of MAO

MAO is a flavoprotein present in the mitochondrial outer membranes of numerous cells such as neuronal and glial cells (Wouters, 1998). MAO contains FAD as a cofactor which is essential for MAO to metabolize dopamine to 3,4-dihydroxyphenylacetic acid (DOPAC). This metabolism is shown in figure 2.13 (Kaakkola, 2000; Youdim & Buccafusco, 2005).

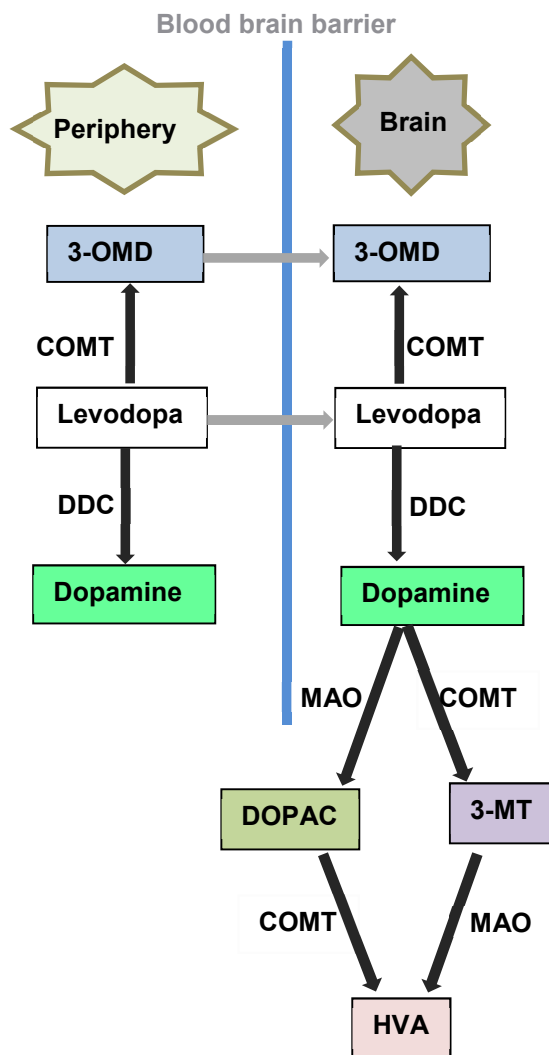


Figure 2.13 Metabolic pathways of levodopa and dopamine in the brain and periphery (Kaakkola, 2000).

MAO catalyzes the oxidative deamination of various biogenic and dietary monoamines as well as catecholamines (Wouters, 1998; Youdim *et al.*, 2006). This catalysis involves the oxidative deamination of primary, secondary and tertiary amines to the corresponding aldehydes, hydrogen peroxide and ammonia as shown in figure 2.14. Aldehyde

dehydrogenase then rapidly metabolizes the aldehyde produced to acidic metabolites such as 5-hydroxyindole acetic acid (produced from serotonin (5-HT) and dihydroxyphenylacetic acid (produced from dopamine). These metabolites can be used to measure MAO activity *in vitro* or *in vivo* (Youdim & Bakhle, 2006).

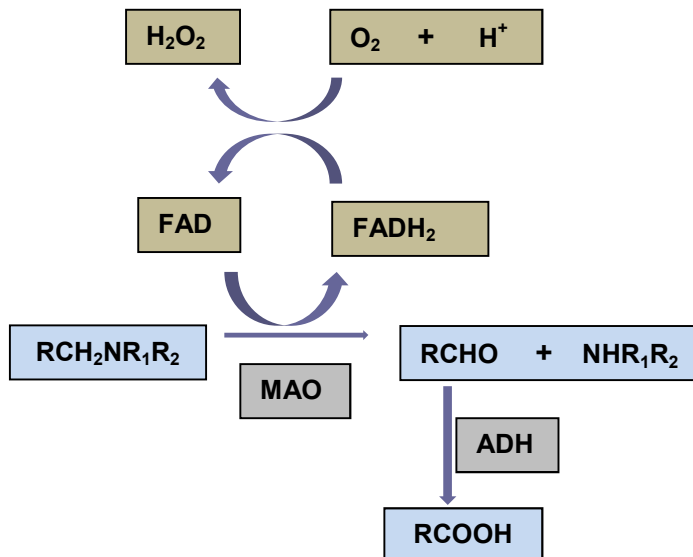


Figure 2.14 Reaction pathway for oxidative deamination of amines by MAO. The main product formed is the aldehyde which is further oxidized to a carboxylic acid (Youdim & Bakhle, 2006).

As previously mentioned, MAO has two isoenzymes (MAO-A and MAO-B), which were initially distinguished by their substrate specificities and by their sensitivities to the inhibitors clorgyline and selegiline (Youdim *et al.*, 2006). MAO-A is inhibited irreversibly by clorgyline and metabolizes adrenaline, NA and 5-HT, while MAO-B is resistant to clorgyline, and prefers phenylethylamine (PEA) as substrate and is inhibited irreversibly by selegiline. Dopamine and tyramine are substrates for both isoforms and are equally metabolized by both MAO-A and MAO-B (Youdim & Buccafusco, 2005).

While the roles of MAO-A and MAO-B in the catalysis of neurotransmitters and dietary amines have been studied quite extensively, very little is known about the functions of the products of MAO activity. One such product is hydrogen peroxide, which may be involved in signaling functions and metabolism in the brain. Aldehydes obtained through deamination of serotonin (5-HT) and noradrenaline play a role in sleep regulation (Jouvet, 1969; Klann & Thiels, 1999). Hydrogen peroxide and ammonia are toxic at high concentrations. While the aldehyde derived from dopamine is cytotoxic, it does not appear to accumulate in healthy brains (Lamensdorf *et al.*, 2000). In Parkinson's disease the levels of aldehyde dehydrogenase in the substantia nigra are depleted therefore the aldehydes from dopamine

metabolism may produce toxic compounds such as tetrahydropapaveroline by forming adducts with amine groups. Tetrahydropapaveroline has been associated with parkinsonism and alcohol-related abnormalities (Shin *et al.*, 2004; Youdim *et al.*, 2006).

2.8.3 Tissue distribution

Both MAO-A and MAO-B are found to be firmly affiliated with the outer mitochondrial membrane, though minute amounts of each enzyme are linked to the microsomal fraction. Both forms of MAO are present in most mammalian tissue but in varying concentrations depending on the type of tissue concerned. The distribution of MAO-A and MAO-B is also uneven in the human brain. The major sites of MAO-A expression in the CNS for example, are the adrenergic and noradrenergic neurons of the locus coeruleus, while MAO-B is found mainly in serotonergic neurons of the raphe and histaminergic neurons of the posterior hypothalamus and also in the astrocytes (Saura *et al.*, 1996). MAO-B is also the main iso-enzyme found in the basal ganglia (Youdim *et al.*, 2006).

Dopamine metabolism in the human brain involves both MAO-A and MAO-B which is contrary to what was found in the mouse striatum where dopamine metabolism is carried out by MAO-A only under basal conditions, but by both iso-enzymes at high concentrations (Fornai *et al.*, 1999).

2.8.4 General structure of MAO

The two MAO isoforms are encoded by separate genes and share a high level of amino acid identity (73%). Both MAO-A and MAO-B in humans contain nine cysteine residues and seven of them are found in highly conserved positions (Hubalek *et al.*, 2003). Close to its N terminus, MAO-A contains an extra stretch of nine amino acids that is not present in MAO-B. The three dimensional structure of both MAO-A and MAO-B in humans and MAO-A in rats have been resolved. MAO isoforms contain a membrane-binding motif α -transmembrane helix, because they are anchored in the outer mitochondrial membrane. This helix is located at the C-terminal of the proteins. In human MAO-B, this region folds into an R-helix that protrudes perpendicularly from the main protein body (Binda *et al.*, 2001; Wang *et al.*, 2013).

Structural differences between the human MAO isoforms include that MAO-A is a monomer while MAO-B is a homodimer (Binda *et al.*, 2001). Substrate binding and oxidation occur in a compact cavity in MAO-A and a bipartite cavity in MAO-B as revealed by the crystal structures in both rats and humans. The cavities extend from the flavin binding site, at the enzyme core to the protein surface, and the volume of the reaction cavity in human MAO-B

is 700 Å³ whilst that of MAO-A is 400 Å³. Despite the considerable structural and mechanistic similarities between MAO-A and MAO-B, they have different substrate and inhibitor specificities. The shape of the inhibitor binding cavity is one of the main factors responsible for the narrower MAO-B cavity with distinct constrictions created by Ile199 and Tyr326. This means that large, rigid inhibitors do not bind but flexible inhibitors can negotiate both sides of the constriction (Veselovsky *et al.*, 2004).

MAO isoforms present in rats are constantly used as tools to screen for potential human MAO enzyme inhibitors. However, reports indicating that rat MAO-A presents different binding affinities for numerous compounds relative to human MAO enzymes have surfaced. There are subtle species differences as suggested by the 3D structural data obtained for human and rat MAO isoforms. Therefore translation of data collected with rodent enzymes to the human MAOs should be done with caution (De Colibus *et al.*, 2005).

Structure of MAO-B

MAO-B (figure 2.15) contains 520 amino acids and the crystal structure shows that the enzyme is dimeric. The crystal structure of MAO-B reveals that the C-terminal residues form an elongated polypeptide chain (amino acids 461-488) found across the monomer surface. This is followed by an α -helix starting at Val 489, which forms the transmembrane helical portion. The helical portion of each monomer projects from the basal face of the dimer, with each helical axis parallel to the molecular two-fold axis. Thus the dimer may bind to the membrane with its two-fold axis perpendicular to the membrane plane, and the C-terminal helices placed within the lipid bilayer. In addition to the C-terminal portion, the structure shows that there may be other protein regions that play a role in membrane binding (Binda *et al.*, 2001).

The MAO-B cavity is made up of two subcavities, that is the substrate-binding cavity (420 Å³) and the entrance cavity (290 Å³), as shown in figure 2.16 (Edmondson *et al.*, 2009; Wang *et al.*, 2013). The substrate binding cavity is outlined by a number of aromatic and aliphatic amino acids that provide the hydrophobic domain as predicted by quantitative structure-activity relationship (QSAR) and substrate binding specificity studies (Walker & Edmondson, 1994). The shape or size of the MAO-B active site is determined to a large extent by conformation of residue Ile199. This is because the side chain of Ile199 presents two different conformations depending on the characteristics of the bound ligand, resulting in either a large single space or a bipartite cavity.

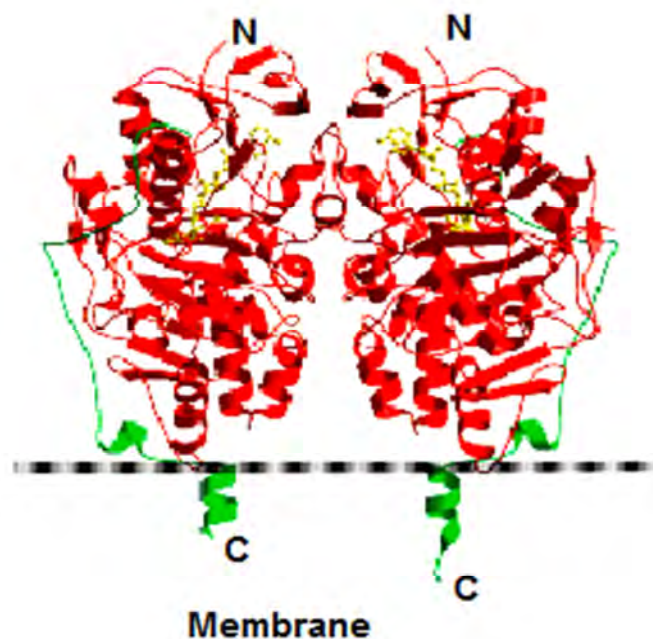


Figure 2.15 Ribbon structure of the MAO-B dimer, with the two-fold axis vertical in the plane of the paper. Monomers A and B are shown on the right and left, respectively. The letter 'N' indicates the observed N-terminal (Lys 4 in both monomers and the letter 'C', the C-terminal (Thr 500 in monomer A and Ile 496 in monomer B). Residues 4–460 are in red, and the C-terminal tail (residues 461–500) is in green. The dimer is anchored to the outer mitochondrial membrane through the C-terminal tails and the neighbouring residues of each monomer. The FAD (in yellow) is shown in ball-and-stick representation (Binda *et al.*, 2001).

The corresponding residue in MAO-A, Phe208 seems not to function as a gating residue as is found in MAO-B. Exchange of Ile199 for Phe in MAO-B in humans, results in decreased binding activity, leading to the conclusion that the bulky Phe side chain inhibits conformational flexibility thus hindering the binding of MAO-B to specific inhibitors (Hubalek *et al.*, 2005). The binding of the substrate or inhibitor to MAO-B involves initial negotiation of the protein loop near the membrane surface, and two hydrophobic cavities known as the entrance cavity and the active site cavity. These two cavities may be separate or fused depending on the Ile199 side chain conformation (Edmondson *et al.*, 2004).

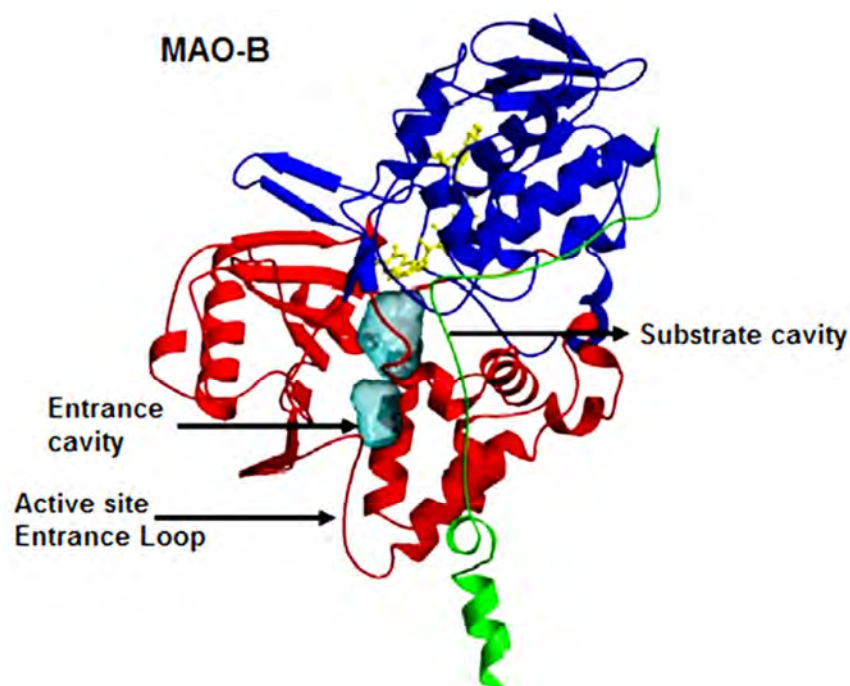


Figure 2.16 Ribbon structure of monomeric unit of human MAO-B. The membrane binding domain is shown in green. The covalent flavin is shown as a ball and stick structure in yellow, the flavin binding domain is shown in blue and the substrate domain is shown in red (Edmondson *et al.*, 2007).

The binding of benzylamine (substrate) in the active site of MAO-B was modeled as shown in figure 2.17a, to determine the mechanistic aspects of the MAO-B catalysis. Benzylamine (**26**) was used because there is much data available on the interaction of benzylamine and its analogues to MAO-B (Walker & Edmondson, 1994). In this model, the benzylamine carbon atom that undergoes flavin-dependant oxidation binds in front of the flavin N5-C4a locus in a highly conserved position, this is a position 3.6 Å away from the flavin N5 (Fraaije & Mattevi, 2000). The flat shape of the cavity restricts orientation of the aromatic ring therefore benzylamine binds between the phenolic side chains of Tyr398 and Tyr435. The flavin and these residues thus form a caged aromatic environment that detects the amino group. MAO prefers to bind to the deprotonated substrate and as such no interaction was observed between the substrate nitrogen and any anionic residues (Miller & Edmondson, 1999). The volume of the benzylamine ($\sim 160 \text{ \AA}^3$), is much smaller than the active site volume (420 \AA^3), highlighting that a region of the active site cavity behind the flavin ring, remains unoccupied by the substrate benzylamine. The cavity may thus allow an aromatic ring to bind to numerous positions away from or closer to the flavin. This explains how MAO-B can oxidize different aromatic amines with variable side chains (Binda *et al.*, 2001).

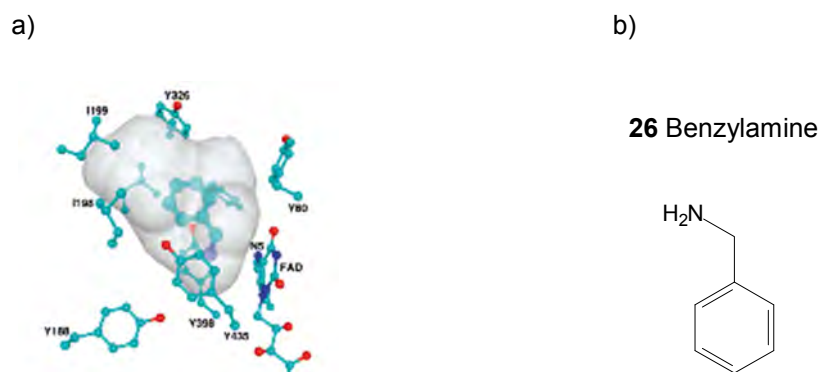


Figure 2.17 (a) Model for the binding of the substrate, benzylamine (**26**), to human MAO-B (Binda *et al.*, 2001), and (b) the structure of benzylamine.

Structure of MAO-A

De Colibus and colleagues (2005), were the first to elucidate the structure of human MAO-A at 3.0 Å. Human MAO-A is different from human MAO-B and rat MAO-A in that it crystallizes as a monomer (figure 2.18) and also exhibits in solution the hydrodynamic behaviour of a monomeric form. The active site of human MAO-A is made up of a single hydrophobic cavity which is ~550 Å. This cavity extends from the flavin ring to the cavity-shaping loop consisting of residues 210-216. The MAO-A cavity is hydrophobic and outlined by 11 aliphatic residues and 5 aromatic residues (De Colibus *et al.*, 2005).

To further understand the MAO-A structure in relation to its function, the low-resolution rat MAO-A structure was extended to the high-resolution wild-type human MAO-A at 2.2 Å. Human MAO-A shows a 90% sequence identity to rat MAO-A with structural differences observed with certain residues, specifically residues 108-118 and 210-216 (Son *et al.*, 2008). Loop 210-216 is important for the structure of the active site in human MAO-A (De Colibus *et al.*, 2005). Both human MAO-A and rat MAO-A exhibit a C-terminal transmembrane helix, a one turn helix parallel to the membrane surface and buried within the membrane (Son *et al.*, 2008).

The 16 residues surrounding the binding cavity are conserved between human and rat MAO-A, but between human MAO-A and human MAO-B, six residues out of the 16 residues are different. In MAO-A, Ile335 plays an important role in inhibitor/substrate binding selectivity which is consistent with rat MAO-A, whilst Tyr326 in MAO-B is crucial for substrate/inhibitor selectivity (Son *et al.*, 2008).

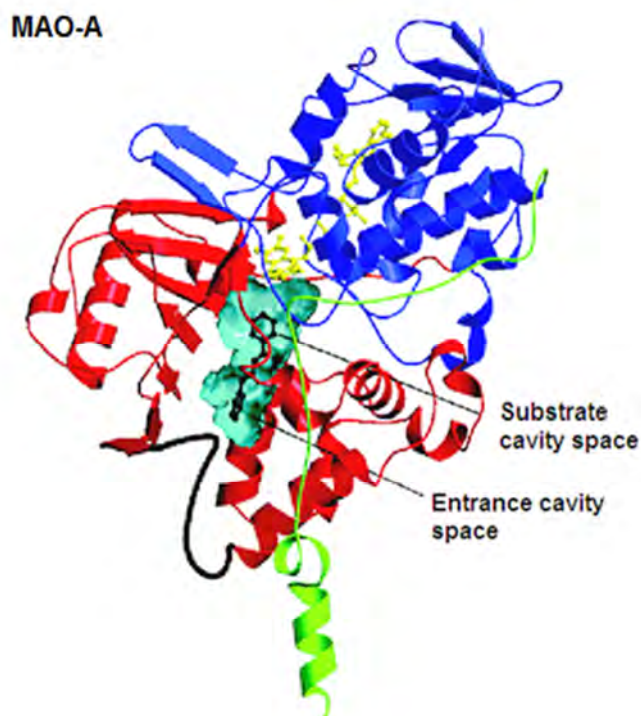


Figure 2.18 Ribbon structure of monomeric human MAO-A. The flavin moiety is shown in ball and stick model in yellow. The substrate domain is shown in red, the flavin binding domain is shown in blue and the membrane binding domain in green (Edmondson *et al.*, 2007).

Flexibility of residues 108-118 is crucial for MAO-A activity. Enzyme anchorage to the mitochondrial membrane is critically important for MAO-A function, and flexibility of residues 108-118 is facilitated by this specific anchorage (Son *et al.*, 2008). Two cysteine residues, Cys321 and Cys323 are found near the catalytic entry site. Catalytic activity is not influenced by serine mutations in either Cys321 or Cys323 (Wu *et al.*, 1993). Mass spectrometry data was used to show the absence of any disulphide bridges in both human MAO-A or MAO-B (Hubalek *et al.*, 2003).

Similarities in human MAO-A and MAO-B exist in their active sites. The covalent FAD cofactors and the two tyrosines of the aromatic cage are identical. Substrate oxidation occurs in these regions of the active site thus the conclusion that both enzymes follow a similar catalytic mechanism (Edmondson *et al.*, 2004). Differences exist in the region of the active site opposite the flavin, and it is this site that recognizes a substrate. Human MAO-A has a single substrate cavity, which is shorter and wider than the longer and narrower

human MAO-B. In conclusion, human MAO-A and MAO-B show structural differences (De Colibus *et al.*, 2005).

2.8.5 Mechanism of Action of MAO

As previously discussed, the MAOs are flavoproteins that catalyze the oxidative deamination of amines to aldehydes, producing hydrogen peroxide and ammonia. In both MAO isoforms, covalently bound FAD is the redox cofactor that is required for catalysis. FAD binds to the MAO enzyme via a thioether linkage between a cysteine residue and 8 α -methylene of the isoalloxazine ring (Kearney *et al.*, 1971). The cysteine residue involved in MAO-A is Cys406 and in MAO-B it is Cys397 (Bach *et al.*, 1988).

The amine substrate binds to the active site of the MAO isoform and the oxidized FAD cofactor is subsequently reduced with the resultant formation of the MAO-FAD_{reduced}-imine complex. The complex reacts with atmospheric oxygen to re-oxidize the FAD. The MAO-FAD_{oxidized}-imine complex dissociates to liberate the imine that undergoes non-enzymatic hydrolysis to give ammonia and the corresponding aldehyde (Wang *et al.*, 2013). This process is summarized in figure 2.19.

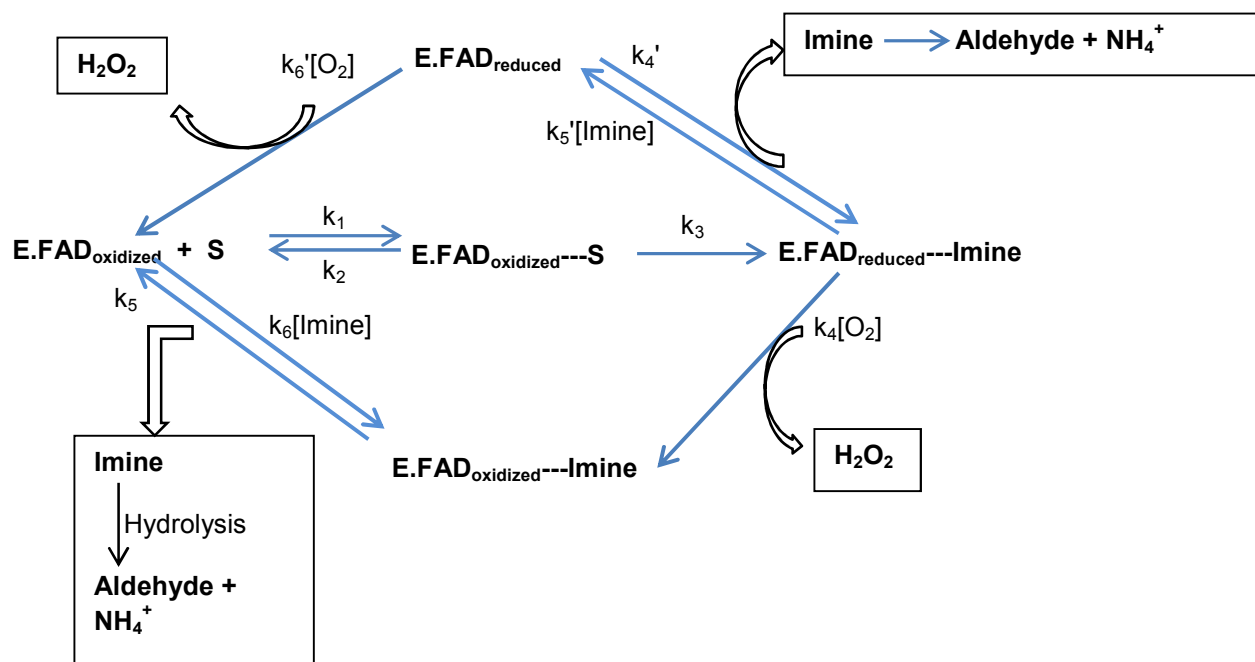


Figure 2.19 Schematic representation of the catalytic reaction pathway followed by MAO-A and MAO-B. Both enzymes follow the lower branch of the pathway with most substrates but MAO-B follows the upper pathway with phenethylamine as substrate (Edmondson *et al.*, 2007).

The single electron transfer (SET) and polar-nucleophilic pathway

Two mechanisms have been proposed to explain the chemical events involved in flavin-dependent amine oxidation (Binda *et al.*, 2001). These mechanisms are the single electron transfer (SET) and the polar nucleophilic pathway (Edmondson *et al.*, 2007). The SET mechanism was proposed by Lu and colleagues (2002) and is well known. This mechanism is shown in figure 2.20.

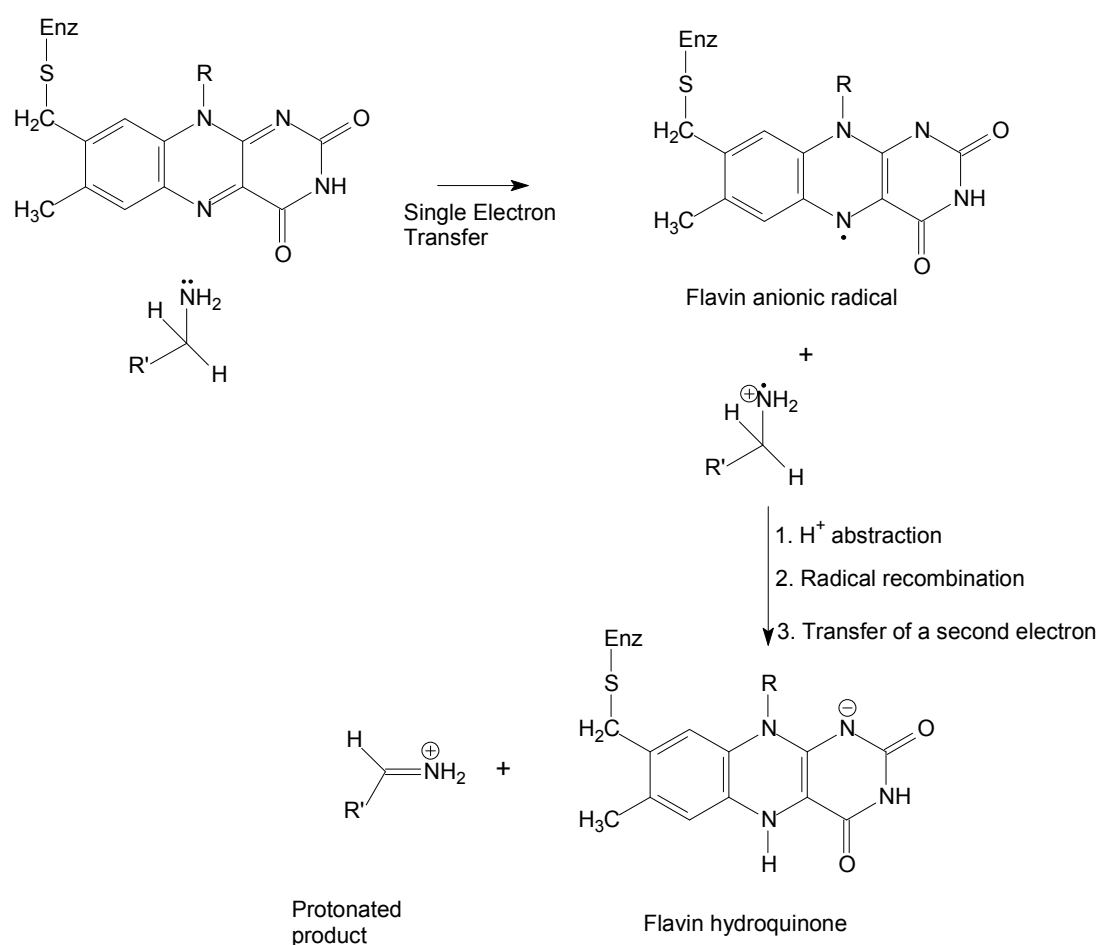


Figure 2.20 The single electron transfer (SET) mechanism (Lu *et al.*, 2002).

The first stage involves the flavin moiety acting as a one-electron oxidant of the lone pair of electrons on the amine nitrogen. This results in formation of an aminium cation radical and a flavin radical. This aminium radical results in the α -proton (α -C-H) becoming sufficiently acidic to enable proton abstraction by a basic amino acid residue in the active site. After a

second electron transfer, the imine and the reduced flavin are formed as products (Binda *et al.*, 2001).

The SET mechanism accounts for the ring-opened products that have been observed for cyclopropylamine substrate analogs (Lu *et al.*, 2002). Thermodynamic considerations, however, suggest that the SET mechanism is highly unlikely because the probability of one electron amine oxidation by a ground state flavin moiety is improbable. There is also no evidence for the formation of flavin radical intermediates during substrate oxidation (Binda *et al.*, 2001; Edmondson *et al.*, 2007).

The polar nucleophilic mechanism is illustrated in figure 2.21, and has more recently been regarded as plausible. This is due to evidence from QSAR data obtained on MAO-A, providing definitive evidence of α -C-H bond cleavage by proton abstraction as shown in figure 2.21. In the polar nucleophilic mechanism, the amine functionality nucleophilically attacks the flavin at the C-4a position, resulting in activation of the flavin N-5 position. This flavin N-5 becomes a strong active site base that can abstract the α -proton from the substrate (Edmondson *et al.*, 2007). This mechanism is believed to be more feasible according to available structural and mechanistic data (Binda *et al.*, 2001).

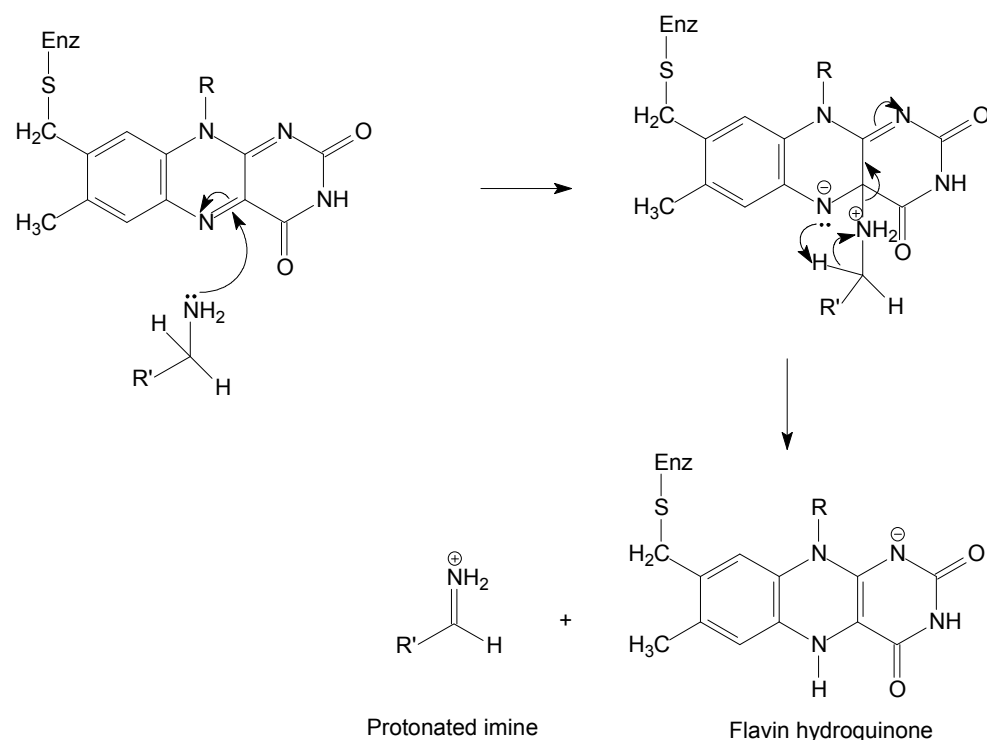


Figure 2.21 Polar nucleophilic mechanism (Edmondson *et al.*, 2007).

2.8.6 MAO-A in depression and PD

MAO inhibitors have antidepressant properties that result from MAO-A inhibition in the CNS. This results in an increase in brain levels of dopamine, NA and 5-HT (Youdim *et al.*, 2006). Reversible MAO-A inhibitors are effective in treating depression in elderly patients (Gareri *et al.*, 2000), while non-selective MAO inhibitors and MAO-A inhibitors are also highly effective in the treatment of phobic anxiety and atypical depressions. MAO-B inhibitors generally do not have antidepressant activity, but neither do they cause the cheese reaction, unless very high concentrations are given that can inhibit MAO-A (Youdim *et al.*, 2006).

Serotonin is broken down by MAO-A, therefore MAO-A inhibitors may further promote what is known as the serotonin syndrome when administered together with serotonin enhancing agents such as selective serotonin reuptake inhibitors (SSRIs). Serotonin syndrome is a life-threatening, centrally mediated condition characterized by restlessness, hallucinations, rapid heart-beat, sudden blood pressure changes, nausea, vomiting, loss of coordination, hyperactive reflexes and diarrhea (Fernandez & Chen, 2007). Although MAO-A is present in the striatum, the concentration is much lower than that of MAO-B (20%) and very little attention has been given to MAO-A inhibition as a way to elevate dopamine levels in the brain (Green *et al.*, 1977). Therefore, a mixture of MAO-A and MAO-B inhibition may effectively enhance DA levels and be more effective in this regard than inhibitors that are selective for a specific MAO isoform. MAO-A inhibition may offer the further advantage of treating depression which is often present in later stages of PD. The use of irreversible MAO-A selective or non-selective MAO inhibitors are however contraindicated in PD patients undergoing levodopa therapy due to the increased risk of hypertensive crisis caused by the cheese reaction (Youdim & Bakhle, 2006).

2.8.7 MAO-B in Parkinson's disease

MAO-B inhibitors may be used as dopamine-sparing agents or as adjunct therapy to levodopa in the treatment of PD. Selective MAO-B inhibitors are used in PD to improve PD motor symptoms by enhancing striatal dopaminergic activity through inhibition of dopamine metabolism (Riederer *et al.*, 1978; Fernandez & Chen, 2007). MAO-B also deaminates β -phenylethylamine, an endogenous amine that inhibits neuronal dopamine uptake and stimulates dopamine release. Although dopamine is equally well metabolized by both MAO-A and MAO-B, the human basal ganglion has higher MAO-B than MAO-A activity. Whereas selective MAO-B inhibitors can significantly elevate synaptic dopamine concentrations, they

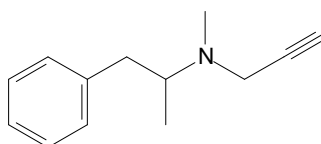
generally do not affect MAO-A activity substantially (Chen & Swope, 2005; Fernandez & Chen, 2007).

Furthermore, in addition to the normal age-related increase in MAO activity, in the PD-affected brain, an increase in MAO-B due to gliosis has been observed, thus, MAO-B and its inhibitors are of particular importance here. As discussed in section 2.6.1, MAO is responsible for the generation of hydrogen peroxide which is converted to the hydroxyl radical in the presence of iron. Inhibition of MAO-B in PD patients will therefore not only increase monoamine levels (such as dopamine levels) that can activate receptors, but also decrease the potential for hydroxyl radical formation and resulting oxidative stress (Youdim & Bakhle, 2006). MAO-B selective inhibitors may furthermore be neuroprotective or modify the disease progress as indicated by the fact that MAO-B inhibition dissipates MPP⁺-induced toxicity and the results obtained in the DATATOP trial (see discussion in section 2.8.8).

2.8.8 Irreversible Inhibitors of MAO-B

Selegiline and rasagiline are examples of irreversible, selective MAO-B inhibitors that inhibit MAO-B by forming covalent bonds between the propargylamine moiety and the enzyme active site (Youdim *et al.*, 2001). Prolonged MAO-B inhibition provides symptomatic improvement in the motor symptoms characteristic of early stage PD. MAO-B inhibitors are thus used as monotherapy and as adjunct therapy to levodopa, as well as to dopamine agonist therapy in PD (Jenner, 2012).

(R)-Deprenyl (*Selegiline*)



20 Selegiline

Selegiline (**20**), also known as *l*-deprenyl, is a propargyl amphetamine derivative that is metabolized in the liver to give desmethylselegiline, L-methamphetamine and L-amphetamine. Selegiline has a low bioavailability (~10%), and the amphetamine metabolites are potentially neurotoxic and may cause various cardiac and psychiatric side effects (Mahmood, 1997; Montastruc *et al.*, 2000). Selegiline may lose MAO-B selectivity at high concentrations which may subsequently result in the 'cheese reaction'. Selegiline administered transdermally (12 mg/day) for example; to healthy subjects in order to

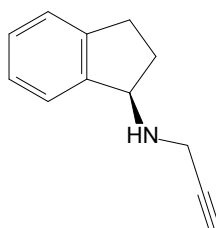
circumvent the first-pass hepatic metabolism resulted in the cheese reaction (Azzaro *et al.*, 2006).

Selegiline efficacy was examined in the DATATOP trial, in which selegiline, tocopherol, their combination, and placebo was given to 800 patients with early untreated PD to examine effects on disease progression. The results obtained showed a modest symptomatic benefit with selegiline, as there was a 9 month delay in the emergence of disability that necessitated levodopa therapy (Parkinson Study Group, 1993; Fernandez & Chen, 2007). A follow up done on the patients in the trial revealed that patients treated with selegiline were less likely to experience the on-off phenomenon or impaired postural balance but highly susceptible to dyskinesias (Parkinson Study Group, 1993). The DATATOP study could however not distinguish between potential neuroprotective effects of selegiline and symptomatic benefits of selegiline use (Fernandez & Chen, 2007).

Selegiline has furthermore shown neuroprotective properties in various preclinical studies. In rodent and non-human primates, pretreatment with selegiline in MPTP-induced parkinsonism animal models, prevented MPTP neurodegeneration (Heikkila *et al.*, 1984). *In vitro*, selegiline decreased oxidative stress linked to MAO-B mediated metabolism of dopamine (Cohen & Spina, 1989). Apoptosis may be prevented by selegiline's capacity to alter gene expression for pro- and anti-apoptotic proteins, thus preserving mitochondria during oxidative stress (Tatton *et al.*, 1996).

At present, selegiline, due to its side effect profile is only used as adjunct therapy to levodopa in PD patients experiencing motor complications, even though it is effective as monotherapy. In essence the benefits of selegiline usage must be weighed against the potential risks of its usage (Fernandez & Chen, 2007). Generally, the combination of selegiline and levodopa is further not recommended in the elderly or advanced PD state because of its low efficacy, frequency of CNS adverse effects and doubts about safety (Olanow *et al.*, 2001).

Rasagiline



21 Rasagiline

Rasagiline (**21**) is a potent, highly selective irreversible inhibitor of MAO-B and irreversibly inhibits MAO-B by attaching covalently via its propargyl moiety to the FAD cofactor of the MAO-B enzyme (Lees, 2005). In addition to preventing dopamine breakdown, rasagiline enhances dopamine release, and antagonizes three cellular processes that subsequently cause apoptosis (LeWitt & Taylor, 2008). In animal studies it has been shown that rasagiline causes functional recovery even when administered after MPTP exposure (Youdim & Buccafusco, 2005).

Metabolism of rasagiline gives rise to aminoindan as the major metabolite as shown in figure 2.22, and this compound possesses weak MAO inhibitory activity and also has neuroprotective effects (Jenner, 2012).

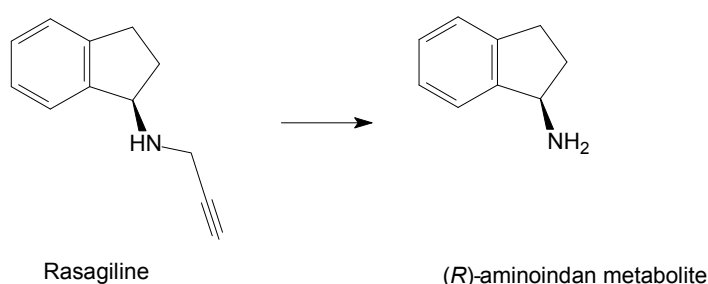


Figure 2.22 Metabolism of rasagiline.

Rasagiline has a greater potency and selectivity than selegiline as reflected in the lower doses required (both *in vitro* and *in vivo*) to obtain neuroprotection after exposure to toxins. When administered prior to MPTP exposure (in MPTP animal models) or lactacystin-treated mice, it has been demonstrated that both selegiline and rasagiline can counteract the effects of the toxins on neuronal dopaminergic loss in the substantia nigra. When administered post-toxin exposure, only rasagiline has the ability to prevent dopaminergic neuronal loss (Zhu *et al.*, 2008).

The (R)-enantiomer is used clinically because the (S)-enantiomer does not possess substantial MAO-B inhibitory activity (Jenner, 2012).

One possible mechanism through which rasagiline provides neuroprotection involves its inhibition of apoptosis by stabilizing the mitochondrial membrane potential that prevents release of cytochrome c and subsequent cell death initiation (figure 2.23) (Maruyama *et al.*, 2001). Through the propargylamine moiety, rasagiline prevents translocation of glyceraldehyde-3-phosphate dehydrogenase (GAPDH) to the nucleus and thus up-regulation of anti-apoptotic proteins. Examples of such anti-apoptotic proteins include Bcl-2 and Bcl-xL,

while pro-apoptotic proteins such as Bad and Bax are down-regulated. These events lead to apoptosis inhibition and cellular function is preserved (Jenner, 2012; Weinreb *et al.*, 2005).

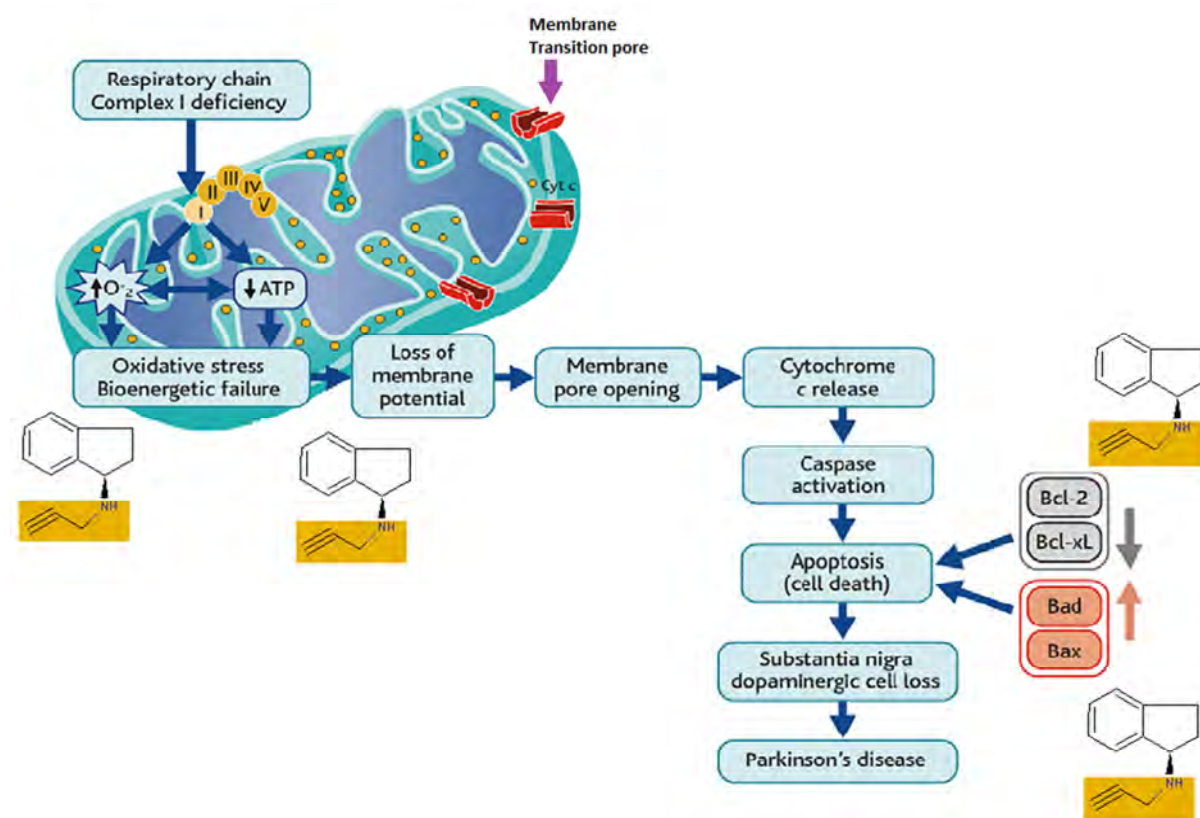


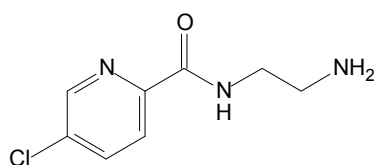
Figure 2.23 The anti-apoptotic mechanism of rasagiline (Jenner & Langston, 2011).

Although the neuroprotective mechanisms of rasagiline are as yet not fully understood, its neuroprotective effects appears to be a result of the actions of the intact molecule itself, the propargylamine domain and the aminoindan metabolite. Numerous *in vitro* studies done to demonstrate neuroprotective effects of rasagiline showed that the concentrations producing neuroprotective effects were much lower than those known to inhibit MAO-B activity (Jenner, 2012).

Comparing rasagiline to selegiline, it is evident that rasagiline may have better efficacy in PD than selegiline. The aminoindan metabolite has neuroprotective activity whilst L-methamphetamine, a metabolite of selegiline has neurotoxic properties *in vitro* and it blocks the neuroprotective effects selegiline and rasagiline (Bar-Am *et al.*, 2004).

2.8.9 Reversible Inhibitors of MAO-B

Lazabemide



27 Lazabemide

Lazabemide (**27**) is a reversible, short acting and highly selective MAO-B inhibitor. It is not a propargylamine derivative like selegiline and thus does not produce amphetamine like metabolites (Parkinson's Study Group, 1993). Lazabemide has the ability to inhibit oxidative damage to a higher degree than selegiline (Mason *et al.*, 2000).

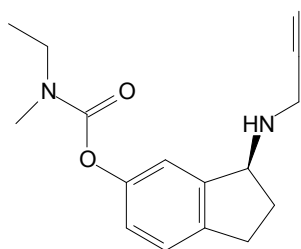
2.8.10 Reversible Inhibitors of MAO-A

Moclobemide

Studies done on selegiline and rasagiline encouraged further development of MAO-A inhibitors that are reversible and selective and not associated with the cheese reaction. Moclobemide is such an example because its reversible binding enables competition to occur such that tyramine or other dietary amines can displace the inhibitor (in this case moclobemide) from the enzyme and be metabolized in the liver or gut (Youdim & Bakhle, 2006). An increase in dopamine release was observed after moclobemide administration in rodent studies. Thus although MAO-A selective inhibition does not affect steady state dopamine levels in the brain, this type of reversible competitive inhibition affects dopamine release (Haefely *et al.*, 1992; Youdim & Bakhle, 2006). Moclobemide has antidepressant activity and is useful in PD patients with significant signs of depression. Clinical studies of moclobemide have shown weak to mild symptomatic relief in PD patients already on L-dopa and dopaminergic agonists. This may be due to the moclobemides' reversibility, as moclobemide may be displaced by dopamine on the MAO-A binding site, allowing dopamine metabolism (Youdim & Bakhle, 2006).

2.8.11 Bifunctional Cholinesterase and MAO-inhibitors

Ladostigil



28 Ladostigil

Ladostigil (**28**) is a butyryl- and acetylcholinesterase (AChE) inhibitor, but it is less potent than rivastigmine or galantamine, which are both well-known acetylcholinesterase inhibitors. Ladostigil is however less toxic than these two AChE inhibitors. It has structural similarities to rasagiline, but it neither inhibits MAO-A nor MAO-B *in vitro* or acutely *in vivo*. Both MAO isoforms are however inhibited in the brain after 1 - 8 weeks of chronic ladostigil treatment, with minimal MAO inhibition in the liver or gut. This tissue selective inhibition of MAO affords irreversible MAO inhibition in the brain without the 'cheese reaction' (Sagi *et al.*, 2005; Youdim & Bakhle, 2006). This non-selective MAO inhibitor increased dopamine, NA and 5-HT levels in rat and mice brain (hippocampus and striatum) with antidepressant activity in animal models. In the mouse model of PD, ladostigil demonstrated MAO selective inhibitor effects by preventing striatal neurodegeneration and dopamine depletion caused by MPTP. Ladostigil is at present in Phase II clinical trials for treatment of Alzheimer's disease and ultimately PD (Youdim & Bakhle, 2006).

2.9 Animal models of Parkinson's disease

Animal models of PD have over the years shown their effectiveness in the continuous search for clues to determine the cause of illness and in the discovery of novel PD treatments (Duty & Jenner, 2011). There are several animal models which include the reserpine, haloperidol, 6-hydroxydopamine, rotenone and paraquat models. Since the MPTP model is the gold standard used, only this model will be discussed in further detail.

2.9.1 MPTP mouse models

MPTP is a toxin, frequently used to create rodent and primate models of PD because it induces persistent parkinsonism in man (Langston *et al.*, 1983). Rats and various other

species are insensitive to the toxic effects of MPTP, which is possibly because MPP⁺, the toxic metabolite of MPTP is rapidly cleared (Johannessen *et al.*, 1985). There is, however, specific strains of mice, namely the black C57 and Swiss Webster which are sensitive to MPTP and have thus enabled the MPTP mouse model of PD to be developed (Sonsalla & Heikkila, 1988).

As MPTP is lipophilic, it readily crosses the blood-brain barrier, is then converted by MAO-B to MPP⁺ which can trigger reactive oxygen species production. It also causes the inhibition of ATP production in the mitochondria (Duty & Jenner, 2011).

The MPTP mouse model has various advantages over the 6-OHDA model, as in MPTP administration, no skilled stereotaxic surgery is required. The systemic injection of MPTP results in a bilateral degeneration of the nigrostriatal tract which closely resembles what happens in PD. The MPTP model thus mimics numerous biochemical features of PD such as decreased glutathione levels and elevated inflammatory markers in the striatum (Duty & Jenner, 2011). With regards to Lewy body presence, it remains controversial whether MPTP-treated mice exhibit Lewy bodies (Duty & Jenner, 2011).

2.9.2 MPTP primate models

MPTP is more effective in the destruction of dopamine neurons in the substantia nigra of primates than in other species. This is thought to be because the toxic metabolite, MPP⁺ persists for a longer time in these species than in other species of animals that are not susceptible to MPTP poisoning (Herkenham *et al.*, 1991). Species of primates that appear to be sensitive to MPTP are macaques, vervet monkeys, squirrel monkeys, baboons and marmosets (Duty & Jenner, 2011).

On systemic administration of MPTP, a parkinsonian-like syndrome develops which consists of akinesia, bradykinesia, rigidity of limbs and trunk and postural abnormalities. This model, due to its ability to represent the symptoms of PD as they occur in man, shows the strongest face validation of all animal models. Postural tremors are observed instead of the usual rest tremors observed in PD (Duty & Jenner, 2011).

On the other hand the pathology and biochemistry of the MPTP-treated primate reveals that this model represents selective nigro-striatal degeneration which does not closely resemble that seen in PD. The dopamine neuron loss in MPTP-treated primate is not progressive and there is no evidence published to suggest the presence of Lewy bodies (Halliday *et al.*, 2009). Though there are variations between the MPTP primate model and PD, this model is

validated in other ways in that, in PD, loss of dopaminergic neurons leads to reactive microgliosis that lasts long after administration, this has been suggested to reflect a continuous loss of dopaminergic neurons that took place in MPTP exposed drug addicts (Langston *et al.*, 1999; Duty & Jenner, 2011).

The MPTP primate model has shown great usefulness, mostly pharmacologically, because levodopa can reverse MPTP-induced motor deficits almost immediately (Burns *et al.*, 1983). Dopamine agonists such as pergolide, bromocriptine and carbegoline, and muscarinic antagonists (such as benhexol) have been shown to be effective as well. The MPTP primate model has been used recently to examine non-dopaminergic therapies for PD, such as the adenosine A_{2A} antagonist istradefylline. Istradefylline has modest symptomatic effect in the primate and its administration did not result in dyskinesia, but when tested in man, its effects on motor function were limited with an increase in dyskinesias being observed (Hauser *et al.*, 2008). This is an example that shows how translation from the MPTP-treated primate has not gone very well with a resultant questionable efficacy in the novel agent istradefylline (Duty & Jenner, 2011).

CHAPTER 3

SYNTHESIS AND CHEMISTRY

3.1 Introduction

The MAO-inhibitory activity of chromone 3-carboxylic acid (**9**) and some of its amide derivatives has been discussed in Chapter 1. Based on the promising MAO inhibitory activity illustrated for these compounds, the aim of the current study was to synthesize ester (**29**) and amide (**30**) derivatives of chromone 3-carboxylic acid by elongating and varying the flexibility of the side chain in position 3. In this chapter the chemistry of the synthesized compounds will be discussed in detail.

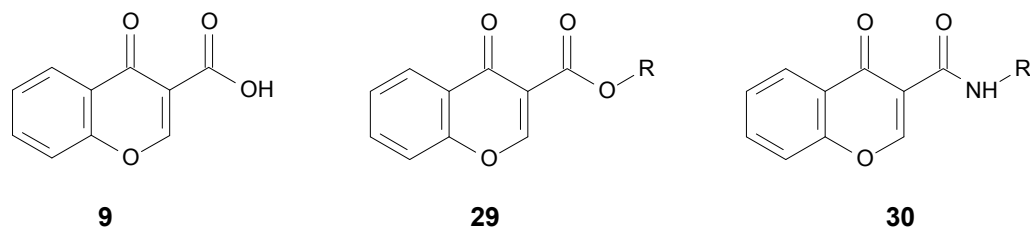


Figure 3.1 Structures of chromone 3-carboxylic acid, proposed ester (**29**) and amide (**30**) derivatives.

3.2 Chemistry

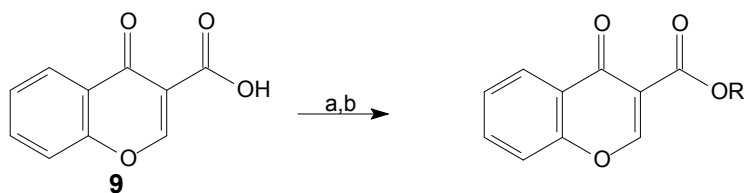
Compounds were synthesized using standard literature procedures and the synthetic strategy employed in the synthesis of both series involved a coupling reaction in the presence of carbonyldiimidazole (CDI) as coupling reagent (Staab, 1962).

3.2.1 Results and Discussion

In total, 15 compounds were successfully synthesized in poor to moderate yields (13 - 70%). All synthesized compounds were characterized by NMR and infrared spectroscopy and mass spectrometry. For all compounds, mass data correlated well with the calculated mass values. For the ester series, three characteristic peaks were present in the IR spectra. These are the absorption bands for the ester carbonyl, ketone carbonyl and the ether group at 1745 cm^{-1} , 1649 cm^{-1} and 1080 cm^{-1} , respectively. On the other hand, absorption bands at 3100 cm^{-1} , 1710 cm^{-1} and 1615 were characteristic of the NH groups, C=O (ketone) and C=O (ester) of series 2, (the presence of an ester group will be explained later). Purity of the compounds was determined by HPLC and was between 75 - 100%. Decomposition of the

ester derivatives (series 1) was observed over time. Melting points generally correlated with reported literature values, however differences in the melting points of series 2 when compared to literature values are most likely due to differences in the ratios of the *E/Z*-isomers (Traven *et al.*, 2010).

Commercially available chromone-3-carboxylic acid (**9**) was used as starting material to synthesize compounds in both series 1 and 2. The synthetic route used in the synthesis of series 1 is depicted in Scheme 3.1



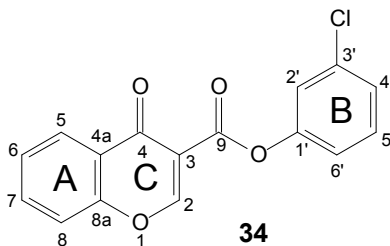
Scheme 3.1: Synthesis of ester chromone derivatives (series 1). Reagents and conditions (a): CDI, DMF, 60 °C, 2 h. (b) R-OH, DMF, rt, overnight.

An equimolar quantity of commercially available chromone-3-carboxylic acid (**9**) and a primary aromatic or aliphatic alcohol were reacted in the presence of carbonyldiimidazole (CDI), a coupling reagent that is both readily available and affordable. Table 3.1 shows the five ester derivatives of series 1 that were successfully synthesized.

Table 3.1: Structures of ester derivatives of series 1 that were successfully synthesized:

Compound	R
31	-C ₆ H ₅
32	-CH ₂ -C ₆ H ₅
33	-(4-Cl-C ₆ H ₄)
34	-(3-Cl-C ₆ H ₄)
35	-CH ₂ -(4-Cl-C ₆ H ₄)

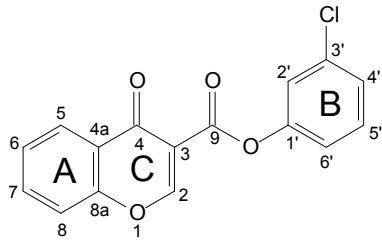
NMR assignments were based on interpretation of both 1D NMR (^{13}C , ^1H , DEPT) and 2D NMR (COSY, HSQC, HMBC) spectra, while NMR data of known compounds were also considered. As an example of a series 1 compound the characterization of compound **34** will be discussed in more detail.



In the ^1H NMR spectrum of the chromone derived ester compound **34**, 9 signals were present accounting for the 9 protons present in the compound. ^1H NMR assignments were made after consideration of the chemical shifts, integration, multiplicities and coupling constants observed for signals in the ^1H NMR spectrum. For example, the most downfield signal, the singlet at δ_{H} 9.27 was thus assigned as H-2. Based on their multiplicities, the two doublet of doublets at δ_{H} 8.13 and δ_{H} 7.76 were assigned as H-5 and H-8 respectively, with H-5 being more downfield due to the deshielding effect of the C-4 carbonyl group. Similarly, the doublet of doublet of doublets at δ_{H} 7.88 and δ_{H} 7.58 were assigned as H-7 and H-6, H-7 being the more downfield signal. The initial assignments of the triplets at δ_{H} 7.50 as H-5' and δ_{H} 7.44 as H-2' were based on the observed coupling constants (8.2 and 2.1 Hz, respectively) and also confirmed by HMBC correlations. A similar approach led to the assignment of the signal at 7.39 as H-4' and the signal at 7.26 ppm as H-6'.

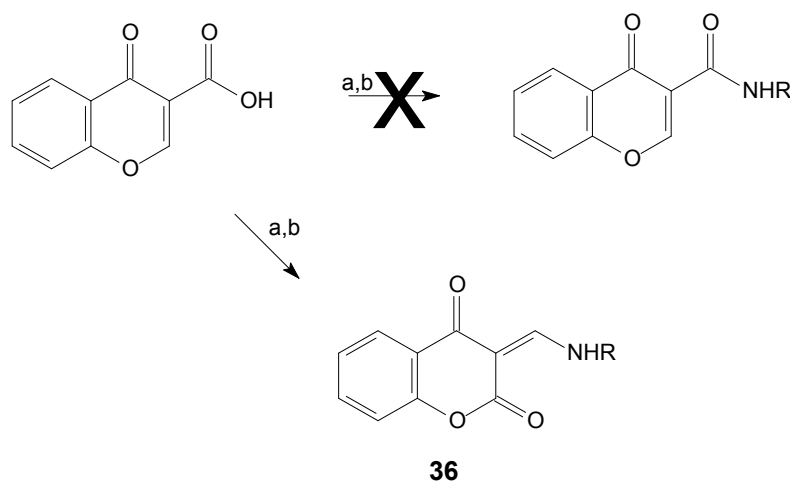
The ^{13}C NMR spectrum in conjunction with the DEPT 135 spectrum showed the presence of 16 carbons of which seven were identified as quaternary carbons and the remaining nine were CH carbons. Assignments of the carbons were performed using the 2D correlations (HMBC and HSQC) and chemical shifts as shown in Table 3.2. For example, the most downfield signal (at 172.5 ppm) was assigned as the C-4 ketone carbonyl group, while the ester carbonyl is present at 160.7 ppm. The nine CH carbons were assigned as follows δ_{C} : 164.4 (C-2), 135.1 (C-7), 131.1 (C-5'), 126.8 (C-6), 126.3 (C-4'), 125.6 (C-5), 122.4 (C-2'), 121.0 (C-6') and 118.8 (C-8). The assignments of signals for the other ester derivatives were done in a similar manner and reported in the experimental data.

Table 3.2: NMR data and HMBC correlations of 3-chlorophenyl 4-oxo-4*H*-chromene-3-carboxylate (**34**):

			
Atom no.	δ_H (multiplicity, <i>J</i> in Hz)	δ_C (Type)	HMBC (δ_H to δ_C)
1			
2	9.27 (s)	164.4 (CH)	3, 4, 8a, 9
3		114.4 (C)	
4		172.5 (C)	
4a		124.3 (C)	
5	8.13 (dd, <i>J</i> = 7.9, 1.7)	125.6 (CH)	4, 7, 8a
6	7.58 (ddd, <i>J</i> = 8.1, 7.2, 1.1)	126.8 (CH)	4a, 5, 7, 8a
7	7.88 (ddd, <i>J</i> = 8.7, 7.2, 1.7)	135.1 (CH)	5, 8, 8a
8	7.76 (dd, <i>J</i> = 8.5, 1.0)	118.8 (CH)	4, 4a, 5, 6, 7, 8a
8a		155.2 (C)	
9		160.7 (C)	
1'		150.9 (C)	
2'	7.44 (t, <i>J</i> = 2.1)	122.4 (CH)	1', 3', 4', 6'
3'		133.4 (C)	
4'	7.39 (ddd, <i>J</i> = 8.1, 2.1, 0.9)	126.3 (CH)	2', 3, 6''

5'	7.50 (t, $J = 8.1$)	131.1 (CH)	1', 3', 4', 6'
6'	7.26 (ddd, $J = 8.2, 2.3, 1.0$)	121.0 (CH)	1', 2', 4'

A similar synthetic approach were followed in the synthesis of the series 2 compounds, where an aromatic or aliphatic amine was coupled to chromone-3-carboxylic acid (**9**) in the presence of CDI as illustrated in scheme 3. 2.



Scheme 3. 2: Synthesis of 3-aminomethylene-2,4-chromandiones. Reagents and conditions (a) CDI, DMF, 60 °C, 2 h. (b) R-NH₂, DMF, rt, overnight.

The results obtained from the synthesis of series 2 were rather surprising, as analogous amide derivatives were obtained using related methodology (Gaspar *et al.*, 2011b; Okumura *et al.*, 1974). Careful consideration of the NMR data revealed that the desired amide derivatives were in fact not synthesized, but that the products that were obtained were the structurally related 3-aminomethylene-2,4-chromandiones illustrated in scheme 3.2 and table 3.3. In the ¹H NMR spectra for example, the presence of a methine proton (H-9) that occurs as a doublet coupling to the adjacent iminoproton provided evidence that the keto-enamines were obtained and not the desired amides (where both H-2 and the NH signals are expected to appear as singlets). A crystal structure was obtained for compound **46** (figure 3.2), and provided further confirmation that this was indeed the case. Tables containing supplementary data on the crystal structure can be found in the addendum on page 155.

Table 3.3 shows the 10 proposed chromone derivatives and the compounds that were actually synthesized in series 2.

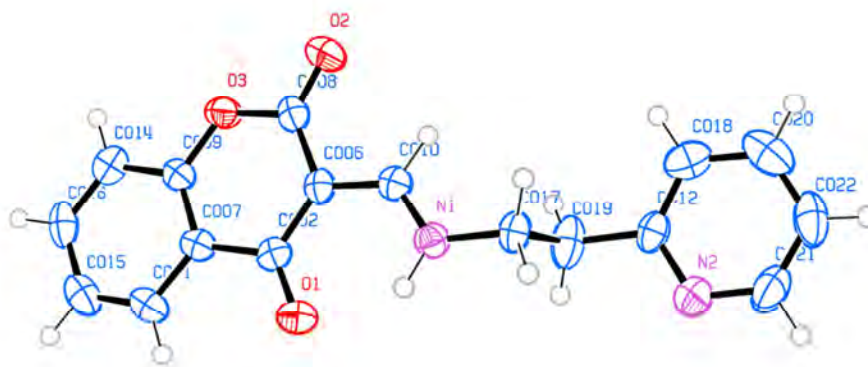
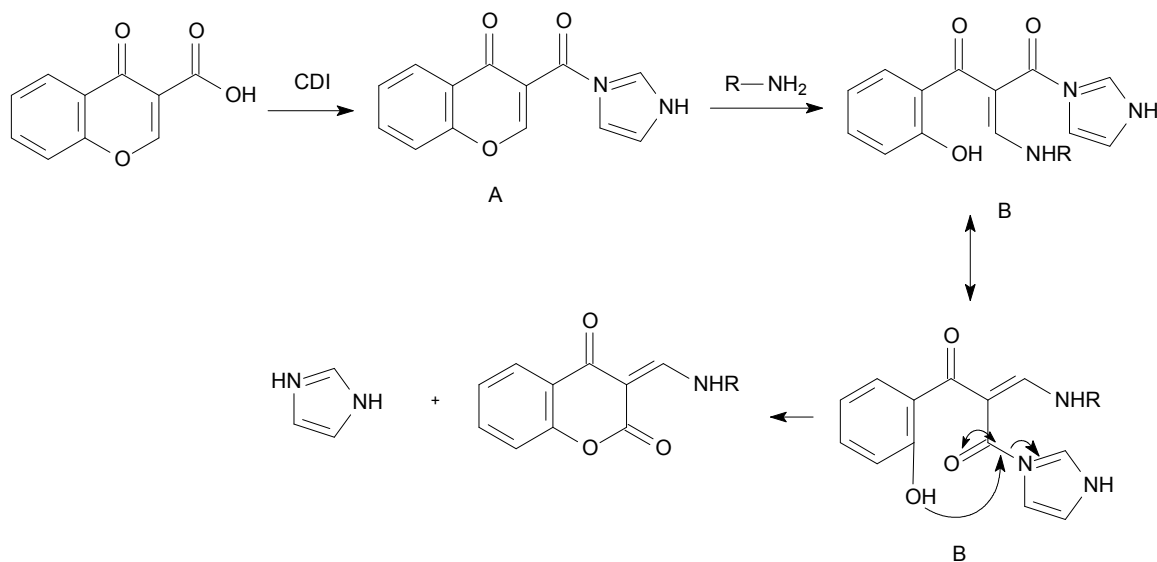


Figure 3.2: ORTEP® drawing representing the crystal structure of the *E*-isomer of compound **46**.

Table 3.3: Structures of proposed and synthesized chromone derivatives of series 2:

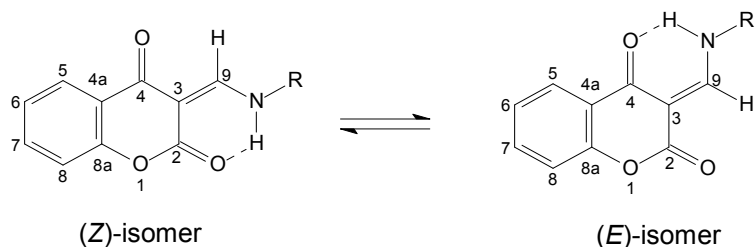
	Proposed	Actual
Compound	R	R
37	-C ₆ H ₅	-C ₆ H ₅
38	-CH ₂ -C ₆ H ₅	-CH ₂ -C ₆ H ₅
39	-(CH ₂) ₂ -C ₆ H ₅	-(CH ₂) ₂ -C ₆ H ₅
40	-(CH ₂) ₃ -C ₆ H ₅	-(CH ₂) ₃ -C ₆ H ₅
41	-(CH ₂) ₄ -C ₆ H ₅	-(CH ₂) ₄ -C ₆ H ₅
42	-(4-Cl-C ₆ H ₄)	-(4-Cl-C ₆ H ₄)
43	-CH ₂ -(4-Cl-C ₆ H ₄)	-CH ₂ -(4-Cl-C ₆ H ₄)
44	-(CH ₂) ₂ -(3-Cl-C ₆ H ₄)	-(CH ₂) ₂ -(3-Cl-C ₆ H ₄)
45	-C ₆ H ₄ N	-C ₆ H ₄ N
46	-(CH ₂) ₂ -C ₆ H ₄ N	-(CH ₂) ₂ -C ₆ H ₄ N

A reaction mechanism for 3-aminomethylene-2,4-chromandione formation, based on one proposed by Ibrahim (2009) for a related system, is illustrated in scheme 3.3. It is postulated that the carboxylic acid is activated by CDI as expected (A). Reaction of the amine however does not result in the displacement of imidazole, but leads to ring opening of the pyrone ring (B), followed by ring closing through lactonization of intermediate B with loss of imidazole.



Scheme 3.3: Proposed mechanism for aminomethylene-2,4-chromandione formation (adapted from Ibrahim, 2009).

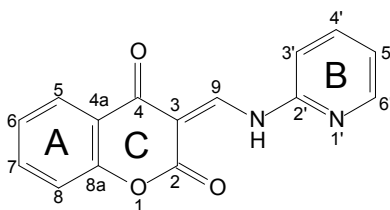
NMR data further revealed that these compounds existed as mixtures of isomers. In the proton spectra there are two distinct NH signals as well as two signals for H-9 and generally also for H-5. Doubling up of almost all carbon signals also occur, but is especially clear for C-4, C-2 and C-9. A literature survey revealed that these compounds exist as mixtures of *E*- and *Z*- isomers, with one isomer predominating (Traven *et al.*, 2010; Milevskii *et al.*, 2013; Ishar *et al.*, 1998; Alberola *et al.*, 2001; Strakova *et al.*, 2006).



Scheme 3.4: The *E*- and *Z*-isomers of the 3-aminomethylene-2,4-chromandiones obtained in this study.

In the ^1H NMR spectrum of compound **45** for example, the two NH signals are present at 13.57 ppm and 11.91 ppm for the major and minor products, respectively. It is postulated that the more downfield signal corresponds to the *E*-isomer, where the NH forms a short, strong intramolecular hydrogen bond with the C(4)=O group. The NH signal for the *Z*-isomer (thus at 11.91 ppm) also forms a hydrogen bond with the ester carbonyl (C2), but it has been reported that this bond is significantly weaker (Traven *et al.*, 2010; Milevskii *et al.*, 2013). On the other hand, the H-9 proton of the minor isomer (presumably the *Z*-isomer) is found more downfield (9.71 ppm) than that of the major *E*-isomer (at 9.61 ppm).

In the ^{13}C NMR spectrum, the signal for the C-4 carbonyl at 182.4 ppm for the major (*E*-isomer) is shifted downfield compared to the signal of the minor *Z*-isomer at 178.8 ppm. The opposite is observed for the C-2 carbonyl, where the signal for the minor *Z*-isomer is the more downfield one (165.3 ppm) compared to the signal for the major *E*-isomer which is present at 163.3 ppm. This is due to the fact that C-4 is hydrogen bonded to the NH proton in the *E*-isomer, whereas C-2 is hydrogen bonded to the NH for the minor *Z*-isomer. The carbonyl that undergoes the hydrogen bonding therefore occurs further downfield than its non-hydrogen bonded counterpart (Traven *et al.*, 2010; Milevskii *et al.*, 2013). Since similar observations were made for all the 3-aminomethylene-2,4-chromandiones synthesized in this study, it is proposed that the *E*-isomer is the major isomer. According to Traven and co-workers, (2010) further evidence for the *E*-isomer as major product is provided by molecular calculations where the energy of formation of the *E*-keto-enamine is lower than that of the *Z*-keto-enamine form.

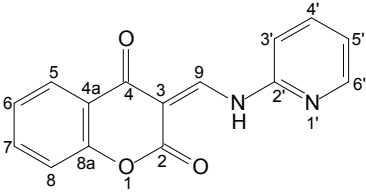


45

As previously discussed for the ester derivative **34**, NMR assignments were based on chemical shifts, integration, multiplicities, coupling constants, correlations in HMBC, HSQC and COSY spectra as well as DEPT data. The assignments and observed HMBC correlations of the major isomer of compound (**45**) are shown in Table 3.4 as an example. The most characteristic difference between the ^1H NMR spectra of these 3-aminomethylene-2,4-chromandiones (**37** - **46**) and those of the ester derivatives (**31** - **35**) were the presence

of H-9 which appears as a doublet coupling to the adjacent imino proton. The NH signals further also occur quite far downfield due to the intramolecular hydrogen bonding with C(4)=O (major isomer) or C(2)=O (minor isomer). The shifts of the aromatic protons of ring A of these derivatives were similar to those of the ester derivatives and were assigned as follows for compound **45**, for example, δ_{H} : 8.05 (H-5), 7.63 - 7.23 (H-7), 7.32 - 7.23 (H-6 and H-8). The ^{13}C NMR spectrum for compound **45** showed the presence of 30 signals, thus providing further evidence of the presence of two isomers. Analysis of the ^{13}C spectrum together with the DEPT 135 spectra indicated the presence of six quaternary carbons and nine CH carbons (for each isomer). Chemical shifts and observed 2D correlations were used to further assign carbon signals (Table 3.4). Similar correlations were observed in all cases for the minor Z-isomer.

Table 3.4: NMR data and HMBC correlations of the major isomer of (3E)-3-[[pyridin-2-yl]amino]methylidene)-3,4-dihydro-2H-1-benzopyran-2,4-dione (**45**):

			
Atom no.	δ_{H} (multiplicity, J in Hz)	δ_{C} (Type)	HMBC (δ_{H} to δ_{C})
1			
2		163.3 (C)	
3		99.7 (C)	
4		182.4 (C)	
4a		120.3 (C)	
5	8.05 (dd, $J = 7.8, 1.7$)	126.0 (CH)	4, 8a, 7
6	7.32 – 7.23 (m)	124.2 (CH)	8a, 8
7	7.63 – 7.56 (m)	135.1 (CH)	8a, 6
8	7.32 – 7.23 (m)	117.5 (CH)	8a, 6
8a		154.4 (C)	

9	9.61 (d, $J = 12.8$)	155.1 (CH)	4, 2, 2', 4a, 3
1'			
2'		149.1 (C)	
3'	7.10 (br d, $J = 8.1$)	113.4 (CH)	5'
4'	7.77 (ddd, $J = 8.1, 7.4, 1.9$)	139.01 (CH)	2'
5'	7.20 (ddd, $J = 7.4, 4.8, 0.9$)	122.1 (CH)	6'
6'	8.49 – 8.43 (m)	149.4 (CH)	2', 4', 5'
NH	13.57 (d, $J = 12.5$)		

Ratios of the *E:Z*-mixtures were calculated using the integral intensities of the H-9 signals. Interestingly, Traven and co-workers (2010) noted that the rate of equilibration between these isomers strongly depends on solvent polarity, where for 3-(*p*-tolyliminomethyl)chromane-2,4-dione, equilibrium is almost immediately established after dissolution in methanol, 4 hours after dissolution in DMSO and 24 hours after dissolution in chloroform (Traven *et al.*, 2010). Thus, if a different solvent was used to dissolve these compounds and if they were observed over time, the observed ratios of these isomers could change. In order to investigate the effect of temperature on the ratios of isomers, variable temperature NMR experiments were performed. The results from compound **38** are shown in figure 3.3.

Based on these results it appears that changes in temperature from -10 to 45 °C do not alter the observed ratios of the *E*- and *Z*-isomers.

The experimental data of compound **42** and compound **12**, synthesized by Gaspar *et al.*, (2011b) was further compared, as the original idea was to synthesize compound **12** as reference compound. In table 3.5, the melting points and ¹H NMR data of these two compounds are given. In both cases, the solvent used was deuterated dimethylsulfoxide (DMSO-*d*₆).

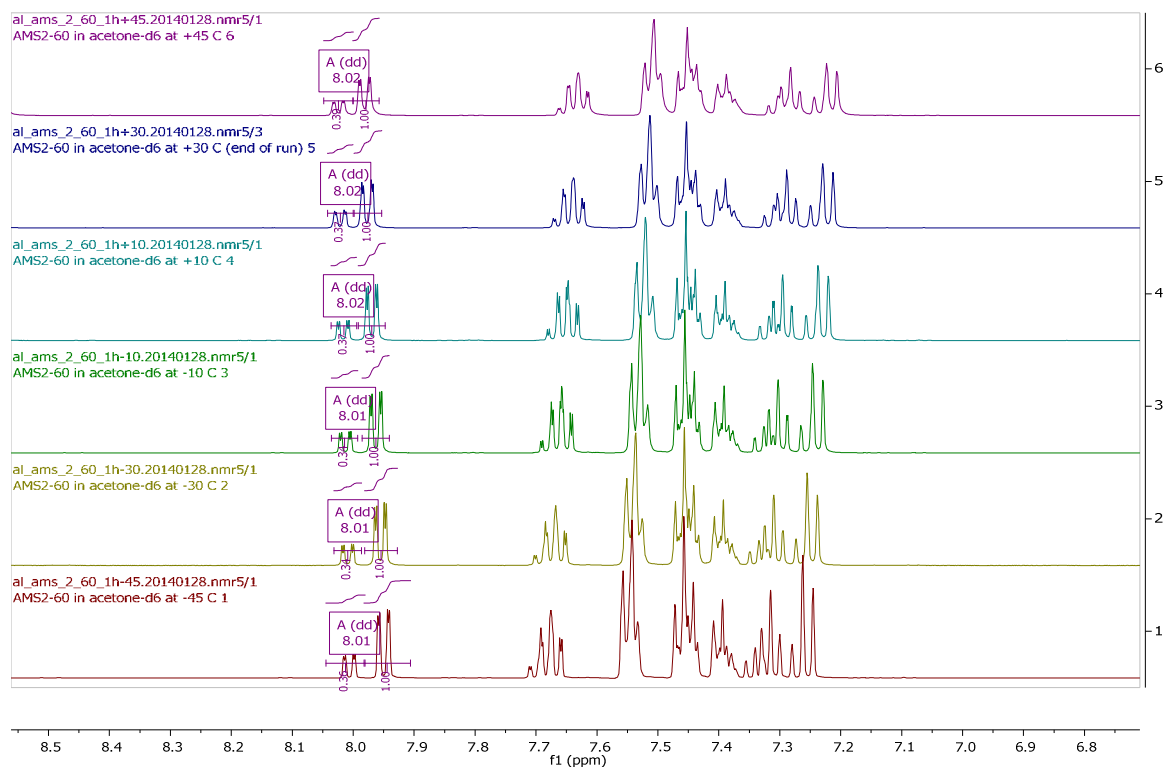
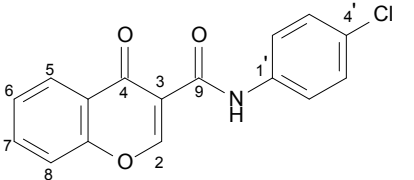
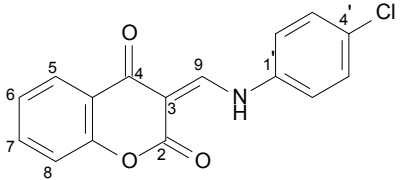


Figure 3.3: Compound **38** dissolved in acetone. NMR experiments performed at 45, 30, 10, -10, -30 and -45 °C.

Both the melting points and ^1H NMR data for these two compounds are very similar. Furthermore, no explanation is provided by these workers for the occurrence of H-2 and the amide proton as doublets with similar coupling constants in the ^1H NMR spectrum. Thus, based on the close similarity of these data, and a comparison between the ^1H NMR data of these workers (Gaspar *et al.*, 2011a) and those of other groups (Traven *et al.*, 2010; Bandyopadhyay *et al.*, 2000; Ishar *et al.*, 1998), it is most likely that the compounds synthesized by Gaspar and co-workers (2011a) were erroneously identified and were in fact also 3-aminomethylene-2,4-chromandiones instead of the amide derivatives as reported. In order to synthesize the desired amides, the in situ generation of an acyl chloride with phosphorus (V) oxychloride (POCl_3) could possibly be used in stead of the coupling with CDI (Cagide *et al.*, 2015).

Table 3.5: Comparison of melting points and ^1H NMR data of compounds **12** (Gaspar *et al.*, 2011a) and **42**.

	Compound 12 (Gaspar <i>et al.</i> , 2011a)		Compound 42
Atom		Atom	
	mp: 255 – 259 °C		mp: 251.7 – 252.7 °C
	^1H NMR data (DMSO-d_6)		^1H NMR data (DMSO-d_6)
2 (1)	8.85 (0.7H, d, $J = 13.8$ Hz)	9-(<i>E</i>)	8.84 (1H, d, $J = 13.8$ Hz)
2 (2)	8.88 (0.3H, d, $J = 14.8$ Hz)	9-(<i>Z</i>)	8.86 (0.4H, d, $J = 14.8$ Hz)
5	7.99 (dd, $J = 7.8, 1.5$ Hz)	5	8.00 – 7.95 (m)
6	7.38 (1H, dd, $J = 7.6$ Hz)	6	7.39 – 7.30 (m)
7	7.70 – 7.73 (m)	7	7.74 – 7.67 (m)
8	7.34 (d, $J = 7.8$ Hz)	8	7.39 - 7.30 (m)
2'/6'	7.70 – 7.73 (m)	2'/6'	7.74 – 7.76 (m)
3'/5'	7.54 (d, $J = 8.8$ Hz)	3'/5'	7.56 – 7.49 (m)
NH (1)	11.84 (0.3H, d, $J = 14.8$ Hz)	NH (<i>Z</i>)	11.83 (0.4H, d, $J = 14.5$ Hz)
NH (2)	13.39 (0.7H, d, $J = 13.8$ Hz)	NH (<i>E</i>)	13.37 (1H, d, $J = 13.8$ Hz)

3.3 Experimental

3.3.1 Materials and Instrumentation

All reagents and chemicals were purchased from Sigma-Aldrich® and used without further purification. All solvents used were obtained from ACE, whilst deuterated solvents used for NMR spectroscopy were purchased from Merck®.

Thin Layer Chromatography

Routine reaction monitoring was performed by making use of thin layer chromatography. Silica gel 60 F254 plates (Merck) with UV₂₅₄ fluorescent indicator was used for TLC detection. Mobile phase systems that were used included ethyl acetate: methanol 8:2 and ethyl acetate: petroleum ether 8:2.

Nuclear Magnetic Resonance (NMR) spectroscopy

Carbon (¹³C) and proton (¹H) NMR spectra were recorded on a Bruker® Avance III 600 spectrometer at frequencies of 150 MHz and 600 MHz, respectively. All NMR samples were dissolved in either deuterated chloroform (CDCl₃) or deuterated dimethyl-sulfoxide (DMSO-*d*₆). The chemical shifts (δ) were reported in parts per million (ppm). ¹H NMR data is reported showing the chemical shifts, the integration (for example 1H), the multiplicity and coupling constant (*J*) in Hz. The spin multiplicities are given in abbreviated format namely: s (singlet), br s (broad singlet), d (doublet), br d (broad doublet), dd (doublet of doublets), ddd (doublet of doublet of doublets), t (triplet), br t (broad triplet), q (quartet), p (pentet/quintet), s (septet) or m (multiplet). Chemical shifts are referenced to the residual solvent signal, at 7.26 ppm for ¹H and 77.0 ppm for ¹³C in CDCl₃, and at 2.50 ppm for ¹H and 39.5 ppm for ¹³C in DMSO-*d*₆.

Mass Spectrometry

High resolution mass spectra (HRMS) were recorded on a Bruker micrOTOF-Q II mass spectrometer in atmospheric-pressure chemical ionization (APCI) in positive ionisation mode.

HPLC

Purity of the synthesized compounds was determined by high performance liquid chromatography (HPLC) using an Agilent® 1100 HPLC system equipped with a quaternary pump and an Agilent® 1100 series diode array detector. HPLC grade acetonitrile obtained from Merck® and Milli-Q water obtained from Millipore® was used for the chromatography. A Venusil XBP C18 column (4.60 x 150 mm, 5 μm) was used with acetonitrile (30%) and Milli-Q water (70%) as the initial mobile phase at a flow rate of 1 ml/min. A solvent gradient program was initiated at the start of each HPLC run. The concentration of acetonitrile in the mobile phase was linearly increased up to 85% over a period of 5 minutes. Each HPLC run was 15 min long with a 5 min allowance for equilibration between runs. The test compound was injected (20 μl, 1 mM) into the HPLC system and the eluent was monitored at

wavelengths of 210, 254 and 300 nm. Most organic compounds absorb UV light at these wavelengths; therefore any impurities present will elute and be detected under these conditions. The HPLC chromatograms are supplied in the addendum on page 148.

Melting Point

Melting points were determined on a Büchi® melting point apparatus, model B-545 and are uncorrected.

Infra-red (IR) spectroscopy

An Alpha FT-IR spectrometer (Bruker®), platinum ATR was used to further characterize the synthesized compounds. The OPUS/Mentor software interface was used to process the spectrometer readings.

Single-crystal X-ray diffraction analysis

X-ray crystallographic studies were done using a Bruker® SMART X2S benchtop crystallographic system. For this purpose a single colourless crystal of compound **46** was mounted on a Mitegen Micromount. Intensity measurements were performed using monochromated (doubly curved silicon crystal) Mo-K α -radiation (0.71073 Å) from a sealed microfocus tube. Generator settings were 50 kV, 1 mA. APEX2 software was used for preliminary determination of the unit cell and determination of integrated intensities and unit cell refinement were performed using Bruker® SAINT. The data collection temperature was -73 °C. Data were corrected for absorption effects with SADABS using the multiscan technique. The structure was solved with XS and subsequent structure refinements were performed with XL.

3.3.2 Synthetic Procedures

General Procedure for synthesis of ester derivatives (31 - 35)

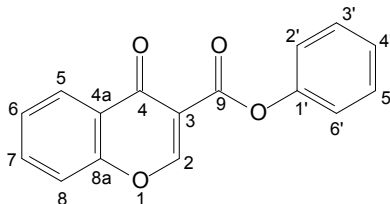
1,1'-Carbonyldiimidazole (CDI) (5.26 mmol, 1 equivalent) was added to a stirred suspension of chromone-3-carboxylic acid (5.26 mmol, 1 equivalent) in *N,N*-dimethyl-formamide (DMF) (20 ml). This mixture was stirred for 2 - 3 hours at 60 °C under nitrogen, after which the reaction was cooled to 0 °C and the alcohol (5.26 mmol, 0.8 equivalents) was added. The mixture was then brought to room temperature and stirred overnight. On completion, 20 ml of ethyl acetate (organic layer) and 40 ml of distilled water (aqueous layer) were added. The two layers were separated and the aqueous layer was further extracted using ethyl acetate (2 x 20 ml) then the ethyl acetate fractions were combined. This organic fraction was washed with distilled water (5 x 40 ml), and washed further with brine, dried over magnesium sulphate and concentrated (*in vacuo*). The resulting crude product was purified by re-crystallization from methanol.

General Procedure for synthesis of 3-aminomethylene-2,4-chromandiones (37 - 46)

1,1'-Carbonyldiimidazole (CDI) (5.26 mmol, 1 equivalent) was added to a stirred suspension of chromone-3-carboxylic acid (5.26 mmol, 1 equivalent) in 20 ml *N,N*-dimethyl-formamide (DMF). This mixture was stirred for 2 - 3 hours at 60 °C under nitrogen, after which the reaction was cooled to 0 °C and the amine (5.26 mmol, 1 equivalent) was added. The mixture was then brought to room temperature and stirred overnight. On reaction completion, 20 ml of ethyl acetate (organic layer) and 40 ml of distilled water (aqueous layer) were added. The two layers were separated and the aqueous layer was further extracted using ethyl acetate (2 x 20 ml), where after the ethyl acetate fractions were combined. This organic fraction was washed with distilled water (5 x 40 ml), and washed further with brine, dried over magnesium sulphate and concentrated (*in vacuo*). The resulting crude product was purified by re-crystallization from methanol.

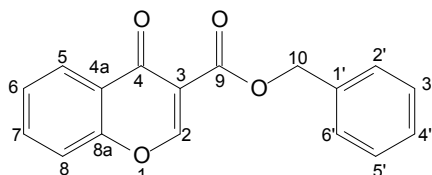
3.3.3 Physical and spectroscopic data of synthesized compounds

Phenyl 4-oxo-4*H*-chromene-3-carboxylate (**31**)



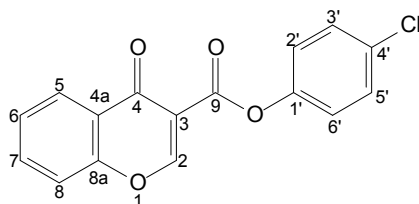
The title compound was prepared from chromone-3-carboxylic acid and phenol in a yield of 22%: mp. 154.7-155.5 °C (methanol), pale yellow crystals. $^1\text{H NMR}$ (600 MHz, DMSO- d_6) δ 9.26 (s, 1H, H-2), 8.13 (dd, $J = 7.9, 1.7$ Hz, 1H, H-5), 7.88 (ddd, $J = 8.7, 7.2, 1.7$ Hz, 1H, H-7), 7.76 (dd, $J = 8.5, 1.0$ Hz, 1H, H-8), 7.58 (ddd, $J = 8.1, 7.2, 1.1$ Hz, 1H, H-6), 7.50 – 7.43 (m, 2H, H-3'/5'), 7.34 – 7.27 (m, 1H, H-4'), 7.28 – 7.22 (m, 2H, H-2'/6'). $^{13}\text{C NMR}$ (151 MHz, DMSO- d_6) δ 172.5 (C-4), 164.0 (C-2), 161.1 (C-9), 155.2 (C-8a), 150.2 (C-1'), 135.0 (C-7), 129.6 (C-3'/5'), 126.7 (C-6), 126.1 (C-4'), 125.5 (C-5), 124.3 (C-4a), 121.9 (C-2'/6'), 118.7 (C-8), 114.8 (C-3). **IR** ν_{max} (cm^{-1}) 3057, 1746, 1645, 1614, 1486, 1094, 750. **APCI-HRMS** m/z calcd. for $\text{C}_{16}\text{H}_{11}\text{O}_4$, 267.0652, $[M+H]^+$ found 267.0658. **Purity** (HPLC): 81 %.

Benzyl 4-oxo-4*H*-chromene-3-carboxylate (**32**)



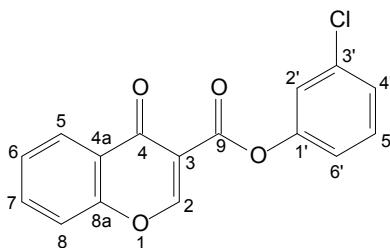
The title compound was prepared from chromone-3-carboxylic acid and benzyl alcohol in a yield of 16%: mp. 107.3 – 108.3 °C (methanol), pale brown crystals. $^1\text{H NMR}$ (600 MHz, CDCl_3) δ 8.65 (s, 1H, H-2), 8.27 (dd, $J = 8.0, 1.7$ Hz, 1H, H-5), 7.67 (ddd, $J = 8.7, 7.1, 1.7$ Hz, 1H, H-7), 7.48 – 7.40 (m, 4H, H-6, H-8, H-2'/6' or H-3'/5')*, 7.39 – 7.33 (m, 2H, H-2'/6' or H-3'/5')*, 7.34 – 7.28 (m, 1H, H-4'), 5.35 (s, 2H, H-10). $^{13}\text{C NMR}$ (151 MHz, CDCl_3) δ 173.3 (C-4), 163.1 (C-9), 161.9 (C-2), 155.5 (C-8a), 135.5 (C-1'), 134.2 (C-7), 128.6 (C-2'/6' or C-3'/5'), 128.24 (C-4'), 128.16 (C-2'/6' or C-3'/5'), 126.5 (C-5 or C-6), 126.2 (C-5 or C-6), 125.1 (C-4a), 118.1 (C-8), 116.0 (C-3), 66.9 (C-10). **IR** ν_{max} (cm^{-1}) 3087, 1727, 1650, 1613, 1462, 1079, 754. **APCI-HRMS** m/z calcd. for $\text{C}_{17}\text{H}_{13}\text{O}_4$, 281.0808, $[M+H]^+$ found 281.0809. **Purity** (HPLC): 97 %. * In no particular order.

4-chlorophenyl-4-oxo-4*H*-chromene-3-carboxylate (**33**)



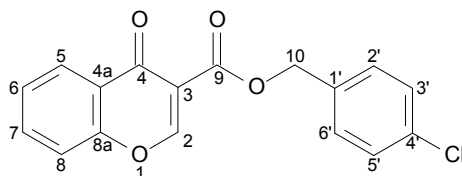
The title compound was prepared from chromone-3-carboxylic acid and 4-chlorophenol in a yield of 21%: mp. 181.9-182.3 °C (methanol), pale yellow crystals. **¹H NMR** (600 MHz, CDCl₃) δ 8.83 (s, 1H, H-2), 8.29 (dd, *J* = 8.0, 1.7 Hz, 1H, H-5), 7.72 (ddd, *J* = 8.7, 7.2, 1.7 Hz, 1H, H-7), 7.54 – 7.45 (m, 2H, H-6, H-8)*, 7.35 (d, *J* = 8.8 Hz, 2H, H-3'/5'), 7.16 (d, *J* = 8.8 Hz, 2H, H-2'/6'). **¹³C NMR** (151 MHz, CDCl₃) δ 173.0 (C-4), 162.8 (C-2), 161.6 (C-9), 155.5 (C-8a), 148.7 (C-1'), 134.5 (C-7), 131.5 (C-4'), 129.5 (C-3'/5'), 126.61, 126.57 (C-5, C-6)*, 125.0 (C-4a), 123.1 (C-2'/6'), 118.2 (C-8), 115.3 (C-3). **IR** ν_{\max} (cm⁻¹) 3056, 1752, 1643, 1615, 1461, 1070, 758. **APCI-HRMS** *m/z* calcd. for C₁₆H₁₀ClO₄, 301.0262, [*M*+*H*]⁺ found 301.0268. **Purity** (HPLC): 83 %. * In no particular order.

3-chlorophenyl 4-oxo-4*H*-chromene-3-carboxylate (**34**)



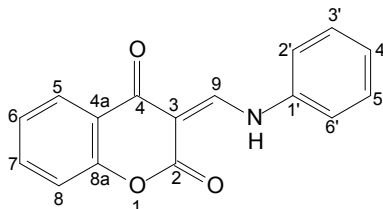
The title compound was prepared from chromone-3-carboxylic acid and 3-chlorophenol in a yield of 19%: mp. 151.2 - 155 °C (methanol), yellow crystals. **¹H NMR** (600 MHz, DMSO-*d*₆) δ 9.27 (s, 1H, H-2), 8.13 (dd, *J* = 7.9, 1.7 Hz, 1H, H-5), 7.88 (ddd, *J* = 8.7, 7.2, 1.7 Hz, 1H, H-7), 7.76 (dd, *J* = 8.5, 1.0 Hz, 1H, H-8), 7.58 (ddd, *J* = 8.1, 7.2, 1.1 Hz, 1H, H-6), 7.50 (t, *J* = 8.1 Hz, 1H, H-5'), 7.44 (t, *J* = 2.1 Hz, 1H, H-2'), 7.39 (ddd, *J* = 8.1, 2.1, 0.9 Hz, 1H, H-4'), 7.26 (ddd, *J* = 8.2, 2.3, 1.0 Hz, 1H, H-6'). **¹³C NMR** (151 MHz, DMSO-*d*₆) δ 172.5 (C-4), 164.4 (C-2), 160.7 (C-9), 155.2 (C-8a), 150.9 (C-1'), 135.1 (C-7), 133.4 (C-3'), 131.1 (C-5'), 126.8 (C-6), 126.3 (C-4'), 125.6 (C-5), 124.3 (C-4a), 122.4 (C-2'), 121.0 (C-6'), 118.8 (C-8), 114.4 (C-3). **IR** ν_{\max} (cm⁻¹) 3072, 1738, 1642, 1615, 1462, 1088, 755. **APCI-HRMS** *m/z* calcd. for C₁₆H₁₀ClO₄, 301.0262, [*M*+*H*]⁺ found 301.0272. **Purity**: Sample decomposed upon standing. Unable to obtain purity data using HPLC. Purity acceptable based on NMR spectra.

(4-chlorophenyl)methyl-4-oxo-4*H*-chromene-3-carboxylate (**35**)



The title compound was prepared from chromone-3-carboxylic acid and 4-chlorobenzyl-alcohol in a yield of 59%: mp. 116.6-117.7 °C (methanol), yellow crystals. **¹H NMR** (600 MHz, DMSO-*d*₆) δ 9.00 (s, 1H, H-2), 8.09 (dd, *J* = 8.0, 1.7 Hz, 1H, H-5), 7.83 (ddd, *J* = 8.6, 7.1, 1.7 Hz, 1H, H-7), 7.70 (br d, *J* = 8.4, 1H, H-8), 7.57 – 7.49 (m, 3H, H-6, H-2'/6' or H-3'/5'), 7.45 (d, *J* = 8.4 Hz, 2H, H-2'/6' or H-3'/5'), 5.29 (s, 2H, H-10). **¹³C NMR** (151 MHz, DMSO-*d*₆) δ 172.5 (C-4), 162.9 (C-2), 162.6 (C-9), 155.2 (C-8a), 135.0 (C-1'), 134.8 (C-7), 132.6 (C-4'), 129.6 (C-2'/6' or C-3'/5'), 128.4 (C-2'/6' or C-3'/5'), 126.5 (C-6), 125.5 (C-5), 124.4 (C-4a), 118.6 (C-8), 115.5 (C-3), 65.2 (C-10). **IR** ν_{\max} (cm⁻¹): 3080, 1732, 1647, 1614, 1461, 1083, 766. **APCI-HRMS** *m/z* calcd. for C₁₇H₁₂ClO₄, 315.0419 [*M*+*H*]⁺ found 315.0388. **Purity** (HPLC): 97 %.

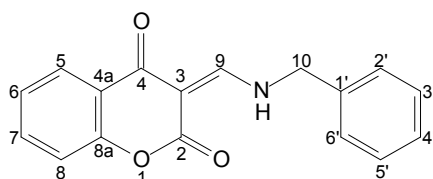
(3*E/Z*)-3-[(phenylamino)methylidene]-3,4-dihydro-2*H*-1-benzopyran-2,4-dione (**37**)



The title compound was prepared from chromone-3-carboxylic acid and aniline in a yield of 62%: mp. 206.7 - 209.5 °C (methanol), (lit. 208 – 210 °C, Traven *et al.*, 2010; 204 – 208 °C; Bandyopadhyay *et al.*, 2000, 201– 202 °C (DMSO), Okumura *et al.*, 1974; 194 – 236 °C (CHCl₃ – petroleum ether), Ishar *et al.*, 1998), yellow fluffy crystals. Ratio of major isomer: minor isomer 1:0.9. **¹H NMR** (600 MHz, CDCl₃) δ **Major isomer**: 13.68 (d, *J* = 13.5 Hz, 1H, NH), 8.88 (d, *J* = 13.6 Hz, 1H, H-9), 8.05 (dd, *J* = 7.8, 1.7 Hz, 1H, H-5), 7.62 – 7.55 (m, 1H, H-7), 7.49 – 7.42 (m, 2H, H-2'/6' or H-3'/5'), 7.39 – 7.22 (m, 5H, H-2'/6' or H-3'/5', H-4', H-6, H-8). **Minor isomer**: 11.92 (d, *J* = 14.4 Hz, 1H, NH), 9.02 (d, *J* = 14.5 Hz, 1H, H-9), 8.12 (dd, *J* = 7.8, 1.7 Hz, 1H, H-5), 7.62 – 7.55 (m, 1H, H-7), 7.49 – 7.42 (m, 2H, H-2'/6' or H-3'/5'), 7.39 – 7.22 (m, 5H, H-2'/6' or H-3'/5', H-4', H-6, H-8). **¹³C NMR** (151 MHz, CDCl₃) δ **Major isomer**: 181.8 (C-4), 163.6 (C-2), 154.95 (C-8a), 154.92 (C-9), 137.7 (C-1'), 134.8 (C-7),

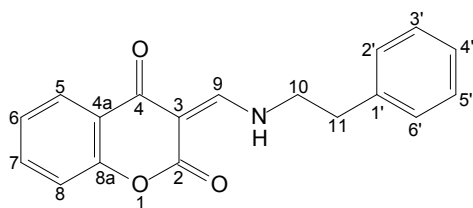
130.18 (C-3'/5'), 127.5 (C-4'), 126.6 (C-5), 124.2 (C-6), 120.3 (C-4a), 118.45 (C-2'/6'), 117.43 (C-8), 98.7 (C-3). **Minor isomer:** 178.6 (C-4), 165.2 (C-2), 154.7 (C-8a), 153.4 (C-9), 137.7 (C-1'), 134.7 (C-7), 130.16 (C-3'/5'), 127.4 (C-4'), 125.8 (C-5), 124.4 (C-6), 120.6 (C-4a), 118.51 (C-2'/6'), 117.37 (C-8), 98.8 (C-3). **IR** ν_{\max} (cm⁻¹) 3180, 1684, 1594, 1567, 755. **APCI-HRMS** m/z calcd. for C₁₆H₁₂NO₃, 266.0812, $[M+H]^+$ found 266.0807. **Purity** (HPLC): 90 %.

(3*E/Z*)-3-[(benzylamino)methylidene]-3,4-dihydro-2*H*-1-benzopyran-2,4-dione (**38**)



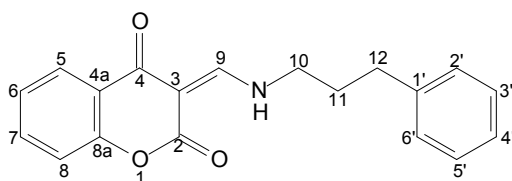
The title compound was prepared from chromone-3-carboxylic acid and benzylamine in a yield of 58%: mp. 163.8-164.6 °C (methanol), (lit. 165 – 167 °C, Traven *et al.*, 2010), pink crystals. Ratio of major isomer: minor isomer 1:0.3. **¹H NMR** (600 MHz, DMSO-*d*₆) δ **Major isomer:** 11.96 – 11.88 (m, 1H, NH), 8.62 (d, J = 14.6 Hz, 1H, H-9), 7.89 (dd, J = 7.8, 1.4 Hz, 1H, H-5), 7.67 – 7.58 (m, 1H, H-7), 7.44 – 7.23 (m, 7H, H-6, H-8, H-2' - 6')*, 4.82 (d, J = 6.2 Hz, 2H, H-10). **Minor isomer:** 10.71 – 10.65 (m, 1H, NH), 8.72 (d, J = 15.4 Hz, 1H, H-9), 7.93 (br d, J = 7.7 Hz, 1H, H-5), 7.67 – 7.58 (m, 1H, H-7), 7.44 – 7.23 (m, 7H, H-6, H-8, H-2' - 6')*, 4.82 (d, J = 6.2 Hz, 2H, H-10). **¹³C NMR** (151 MHz, DMSO-*d*₆) δ **Major isomer:** 179.4 (C-4), 162.7 (C-2), 162.2 (C-9), 154.2 (C-8a), 136.7 (C-1'), 134.3 (C-7), 128.8 (C-2'/C-6' or C-3'/C-5'), 128.0 (C-2'/C-6' or C-3'/C-5'), 127.98 (C-4'), 125.3 (C-5), 123.9 (C-6), 120.2 (C-4a), 116.9 (C-8), 96.0 (C-3), 53.2 (C-10). **Minor isomer:** 177.1 (C-4), 163.2 (C-2), 160.6 (C-9), 154.1 (C-8a), 137.0 (C-1'), 134.4 (C-7), 128.8 (C-2'/C-6' or C-3'/C-5'), 128.0 (C-2'/C-6' or C-3'/C-5'), 127.9 (C-4'), 125.8 (C-5), 124.0 (C-6), 120.4 (C-4a), 117.0 (C-8), 95.9 (C-3), 53.1 (C-10). **IR** ν_{\max} (cm⁻¹) 3033, 1708, 1592, 1463, 746. **APCI-HRMS** m/z calcd. for C₁₇H₁₄NO₃, 280.0968, $[M+H]^+$ found 280.0972. **Purity** (HPLC): 100 %. * In no particular order.

(3*E/Z*)-3-[[2-phenylethyl]amino]methylidene}-3,4-dihydro-2*H*-1-benzopyran-2,4-dione (**39**)



The title compound was prepared from chromone-3-carboxylic acid and phenethylamine in a yield of 59%: mp. 178.2-178.7 °C (methanol), white crystals. Ratio of major isomer: minor isomer 1:0.5. **¹H NMR** (600 MHz, DMSO-*d*₆) δ **Major isomer:** 11.68 – 11.62 (m, 1H, NH), 8.34 (d, *J* = 14.3 Hz, 1H, H-9), 7.90 (dd, *J* = 7.7, 1.7 Hz, 1H, H-5), 7.66 – 7.59 (m, 1H, H-7), 7.33 – 7.17 (m, 7H, H-2' - 6', H-8, H-6)*, 3.83 (q, *J* = 6.7 Hz, 2H, H-10), 2.96 (t, *J* = 7.2 Hz, 2H, H-11). **Minor isomer:** 10.40 (br s, 1H, NH), 8.45 (d, *J* = 14.8 Hz, 1H, H-9), 7.90 (dd, *J* = 7.7, 1.7 Hz, 1H, H-5), 7.66 – 7.59 (m, 1H, H-7), 7.33 – 7.17 (m, 7H, H-2' - 6', H-8, H-6)*, 3.83 (q, *J* = 6.7 Hz, 2H, H-10), 2.96 (t, *J* = 7.2 Hz, 2H, H-11). **¹³C NMR** (151 MHz, DMSO-*d*₆) δ **Major isomer:** 179.3 (C-4), 162.7 (C-2), 162.2 (C-9), 154.2 (C-8a), 137.9 (C-1'), 134.3 (C-7), 128.9, 128.5 (C-2'/6', C-3'/5')*, 126.6 (C-4'), 125.3 (C-5), 123.95 (C-6), 120.3 (C-4a), 116.9 (C-8), 95.6 (C-3), 51.6 (C-10), 35.8 (C-11). **Minor isomer:** 177.0 (C-4), 163.2 (C-2), 160.6 (C-9), 154.1 (C-8a), 137.9 (C-1'), 134.4 (C-7), 128.9, 128.5 (C-2'/6', C-3'/5')*, 126.6 (C-4'), 125.8 (C-5), 124.04 (C-6), 120.4 (C-4a), 117.0 (C-8), 95.3 (C-3), 51.7 (C-10), 35.9 (C-11). **IR** ν_{max} (cm⁻¹) 3063, 1708, 1590, 1463, 741. **APCI-HRMS** *m/z* calcd. for C₁₈H₁₆NO₃, 294.1125, [*M*+*H*]⁺ found 294.1129. **Purity** (HPLC): 100 %.*In no particular order.

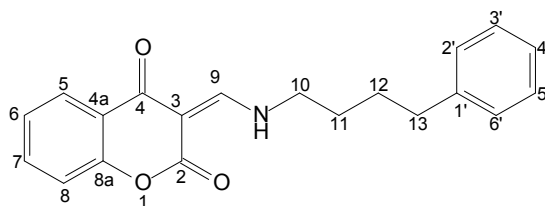
(3*E/Z*)-3-[[3-phenylpropyl]amino]methylidene}-3,4-dihydro-2*H*-1-benzopyran-2,4-dione (**40**)



The title compound was prepared from chromone-3-carboxylic acid and 3-phenyl-1-propylamine in a yield of 58%: mp. 171.3-171.6 °C (methanol), white crystals. Ratio of major isomer: minor isomer 1:0.7. **¹H NMR** (600 MHz, DMSO-*d*₆) δ **Major isomer:** 11.76 – 11.57 (m, 1H, NH), 8.44 (d, *J* = 14.7 Hz, 1H, H-9), 7.96 – 7.89 (m, 1H, H-5), 7.68 – 7.61 (m, 1H, H-

7), 7.40 – 7.08 (m, 7H, H-6, H-8, H-2' - 6')*, 3.60 (q, $J = 6.8$ Hz, 2H, H-10), 2.64 – 2.57 (m, 2H, H-12), 1.95 (p, $J = 7.3$ Hz, 2H, H-11). **Minor isomer:** 10.52 – 10.21 (m, 1H, NH), 8.55 (d, $J = 15.5$ Hz, 1H, H-9), 7.96 – 7.89 (m, 1H, H-5), 7.68 – 7.61 (m, 1H, H-7), 7.40 – 7.08 (m, 7H, H-6, H-8, H-2' - 6'), 3.60 (q, $J = 6.8$ Hz, 2H, H-10), 2.64 – 2.57 (m, 2H, H-12), 1.95 (p, $J = 7.3$ Hz, 2H, H-11). **^{13}C NMR** (151 MHz, DMSO- d_6) δ **Major isomer:** 179.3 (C-4), 162.7 (C-2), 162.2 (C-9), 154.2 (C-8a), 140.9 (C-1'), 134.28 (C-7), 128.4, 128.3 (C-2'/6', C-3'/5')*, 125.9 (C-4'), 125.3 (C-5), 123.9 (C-6), 120.3 (C-4a), 116.9 (C-8), 95.7 (C-3), 50.0 (C-10), 31.9 (C-12), 31.15 (C-11). **Minor isomer:** 177.1 (C-4)**, 163.5 (C-2), 160.6 (C-9), 154.2 (C-8a), 140.9 (C-1'), 134.33 (C-7), 128.4, 128.3 (C-2'/6', C-3'/5')*, 125.7 (C-4'), 125.3 (C-5), 124.0 (C-6), 120.5 (C-4a), 117.0 (C-8), 95.7 (C-3), 50.2 (C-10), 31.9 (C-12), 31.2 (C-11). **IR** ν_{max} (cm^{-1}) 3023, 1711, 1603, 1462, 752. **APCI-HRMS** m/z calcd. for $\text{C}_{19}\text{H}_{18}\text{NO}_3$, 308.1281, $[M+H]^+$ found 308.1280. **Purity** (HPLC): 100 %.* In no particular order. **Shift based on HMBC correlation, signal not visible on ^{13}C NMR spectrum.

3(*E/Z*)-3-[[4-phenylbutyl]amino]methylidene}-3,4-dihydro-2*H*-1-benzopyran-2,4-dione (**41**)

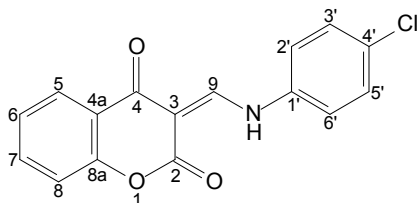


The title compound was prepared from chromone-3-carboxylic acid and 4-phenylbutylamine in a yield of 13%: mp. 142.4 – 143.3 °C (methanol), white crystals. Ratio of major isomer: minor isomer 1:0.4. **^1H NMR** (600 MHz, CDCl_3) δ **Major isomer:** 11.86 (br s, 1H, NH), 8.34 (d, $J = 14.1$ Hz, 1H, H-9), 7.99 (dd, $J = 7.8, 1.7$ Hz, 1H, H-5), 7.54 (ddd, $J = 8.4, 7.4, 1.7$ Hz, 1H, H-7), 7.30 – 7.12 (m, 7H, H-6, H-8, H-2' - H-6')*, 3.50 (q, $J = 6.4$ Hz, 2H, H-10), 2.65 (t, $J = 6.8$ Hz, 2H, H-13), 1.79 – 1.66 (m, 4H, H-11, H-12)*. **Minor isomer:** 10.21 (br s, 1H, NH), 8.50 (d, $J = 14.9$ Hz, 1H, H-9), 8.07 (dd, $J = 7.8, 1.6$ Hz, 1H, H-5), 7.57 – 7.53 (m, 1H, H-7), 7.30 – 7.12 (m, 7H, H-6, H-8, H-2' - H-6')*, 3.52 (q, $J = 6.4$ Hz, 2H, H-10), 2.65 (t, $J = 6.8$ Hz, 2H, H-13), 1.79 – 1.66 (m, 4H, H-11, H-12)*. **^{13}C NMR** (151 MHz, CDCl_3) δ **Major isomer:** 181.3 (C-4), 163.9 (C-2), 162.2 (C-9), 154.8 (C-8a), 141.08 (C-1'), 134.2 (C-7), 128.5, 128.3 (C-2'/6', C-3'/5')* 126.1 (C-5), 125.6 (C-4'), 123.9 (C-6), 120.5 (C-4a), 117.3 (C-8), 96.83 (C-3), 50.9 (C-10), 35.2 (C-13), 29.57, 28.0 (C-11, C-12)*. **Minor isomer:** 178.4 (C-4), 165.2 (C-2), 160.6 (C-9), 154.6 (C-8a), 141.10 (C-1'), 134.3 (C-7), 128.5, 128.3 (C-2'/6', C-3'/5')*, 126.3 (C-5), 125.6 (C-4'), 124.1 (C-6), 120.7 (C-4a), 117.2 (C-8), 96.76 (C-3), 50.8 (C-10), 35.2 (C-13), 29.64, 28.0 (C-11, C-12)*. **IR** ν_{max} (cm^{-1}) 3195, 1687, 1606, 1463, 754. **APCI-**

HRMS m/z calcd. for $C_{20}H_{20}NO_3$, 322.1438, $[M+H]^+$ found 322.1445. **Purity** (HPLC): 100 %.

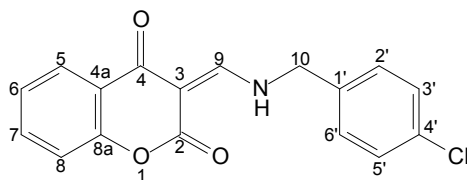
*In no particular order.

(3*E/Z*)-3-[[4-chlorophenyl]amino]methylidene}-3,4-dihydro-2*H*-1-benzopyran-2,4-dione (**42**)



The title compound was prepared from chromone-3-carboxylic acid and 4-chloroaniline in a yield of 57%: mp. 251.7-252.7 °C (methanol), (lit. 250 °C, Fitton 1979), yellow solid. Ratio of major isomer: minor isomer 1:0.4. **¹H NMR** (600 MHz, DMSO- d_6) δ **Major isomer**: 13.37 (d, $J = 13.8$ Hz, 1H, NH), 8.84 (d, $J = 13.8$ Hz, 1H, H-9), 8.00 – 7.95 (m, 1H, H-5), 7.74 – 7.67 (m, 3H, H-7, H-2'/6'), 7.56 – 7.49 (m, 2H, H-3'/5'), 7.39 – 7.30 (m, 2H, H-6, H-8)*. **Minor isomer**: 11.83 (d, $J = 14.5$ Hz, 1H, NH), 8.86 (d, $J = 14.8$ Hz, 1H, H-9), 8.00 – 7.95 (m, 1H, H-5), 7.74 – 7.67 (m, 3H, H-7, H-2'/6'), 7.56 – 7.49 (m, 2H, H-3'/5'), 7.39 – 7.30 (m, 2H, H-6, H-8)*. **¹³C NMR** (151 MHz, DMSO- d_6) δ **Major isomer**: 180.3 (C-4), 162.3 (C-2), 155.8 (C-9), 154.4 (C-8a), 137.1 (C-1'), 135.1 (C-7), 131.2 (C-4'), 129.6 (C-3'/5'), 125.5 (C-5), 124.4 (C-6), 121.3 (C-2'/6'), 119.9 (C-4a), 117.2 (C-8), 98.3 (C-3). **Minor isomer**: 177.5 (C-4), 163.1 (C-2), 154.5 (C-9), 154.2 (C-8a), 137.6 (C-1'), 135.0 (C-7), 131.1 (C-4'), 129.5 (C-3'/5'), 125.9 (C-5), 124.5 (C-6), 121.7 (C-2'/6'), 120.2 (C-4a), 117.3 (C-8), 98.2 (C-3). **IR** ν_{max} (cm⁻¹) 3076, 1711, 1614, 1463, 750. **APCI-HRMS** m/z calcd. for $C_{16}H_{11}ClNO_3$, 300.0422, $[M+H]^+$ found 300.0439. **Purity** (HPLC): 79 %. *In no particular order.

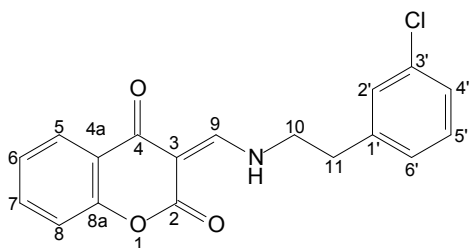
(3*E/Z*)-3-({[4-chlorophenyl]methyl}amino)methylidene)-3,4-dihydro-2*H*-1-benzopyran-2,4-dione (**43**)



The title compound was prepared from chromone-3-carboxylic acid and 4-chlorobenzylamine in a yield of 37%: mp. 182.7-183.1 °C (methanol), white crystals. Ratio of major isomer: minor isomer 1:0.5. **¹H NMR** (600 MHz, DMSO- d_6) δ **Major isomer**: 11.87 (br

s, 1H, NH), 8.61 (br s, 1H, H-9), 7.95 – 7.86 (m, 1H, H-5), 7.67 – 7.60 (m, 1H, H-7), 7.48 – 7.38 (m, 4H, H-2'/6', H-3'/5')*, 7.32 – 7.23 (m, 2H, H-6, H-8), 4.80 (s, 2H, H-10). **Minor isomer:** 10.66 (br s, 1H, NH), 8.71 (br s, 1H, H-9), 7.95 – 7.86 (m, 1H, H-5), 7.67 – 7.60 (m, 1H, H-7), 7.48 – 7.38 (m, 4H, H-2'/6', H-3'/5')*, 7.32 – 7.23 (m, 2H, H-6, H-8), 4.80 (s, 2H, H-10). **¹³C NMR** (151 MHz, DMSO-*d*₆) δ **Major isomer:** 179.5 (C-4), 162.8 (C-2), 162.3 (C-9), 154.3 (C-8a), 135.9 (C-1'), 134.5 (C-7), 132.7 (C-4'), 130.0, 128.8 (C-2'/6', C-3'/5')*, 125.3 (C-5), 124.0 (C-6), 120.3 (C-4a), 117.0 (C-8), 96.2 (C-3), 52.5 (C-10). **Minor isomer:** 177.3 (C-4), 163.2 (C-2), 160.8 (C-9), 154.3 (C-8a), 136.1 (C-1'), 134.5 (C-7), 132.7 (C-4'), 130.0, 128.8 (C-2'/6', C-3'/5')*, 125.8 (C-5), 124.1 (C-6), 120.4 (C-4a), 117.1 (C-8), 96.0 (C-3), 52.5 (C-10). **IR** ν_{\max} (cm⁻¹) 3183, 1698, 1617, 1464, 753. **APCI-HRMS** *m/z* calcd. for C₁₇H₁₃ClNO₃, 314.0578, [*M+H*]⁺ found 314.0557. **Purity** (HPLC): 100 %. *In no particular order.

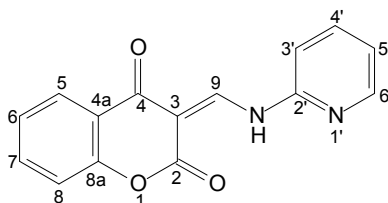
(3*E/Z*)-3-({[2-(3-chlorophenyl)ethyl]amino}methylidene)-3,4-dihydro-2*H*-1-benzopyran-2,4-dione (**44**)



The title compound was prepared from chromone-3-carboxylic acid and 2-(3-chlorophenyl)ethan-1-amine in a yield of 70%: mp. 216.3-217.6 °C (methanol), white fluffy crystals. The ratio of major isomer: minor isomer 1:0.5. **¹H NMR** (600 MHz, DMSO-*d*₆) δ **Major isomer:** 10.45 – 10.35 (m, 1H, NH), 8.37 (d, *J* = 14.6 Hz, 1H, H-9), 7.94 – 7.88 (m, 1H, H-5), 7.68 – 7.60 (m, 1H, H-7), 7.39 – 7.18 (m, 6H, H-2',H-4', H-5', H-6', H-6, H-8), 3.83 (q, *J* = 7.0 Hz, 2H, H-10), 3.01 – 2.94 (m, 2H, H-11). **Minor isomer:** 11.66 – 11.61 (m, 1H, NH), 8.48 (d, *J* = 15.5 Hz, 1H, H-9), 7.94 – 7.88 (m, 1H, H-5), 7.68 – 7.60 (m, 1H, H-7), 7.39 – 7.18 (m, 6H, H-2',H-4', H-5', H-6', H-6, H-8), 3.83 (q, *J* = 7.0 Hz, 2H, H-10), 3.01 – 2.94 (m, 2H, H-11). **¹³C NMR** (151 MHz, DMSO-*d*₆) δ **Major isomer:** 179.3 (C-4), 162.7 (C-2), 162.3 (C-9), 154.2 (C-8a), 140.5 (C-1'), 134.3 (C-7), 133.1 (C-3'), 130.3, 128.9, 127.7, 126.6 (C-2', C-4', C-5', C-6')*, 125.3 (C-5), 124.0 (C-6) 120.3 (C-4a), 116.9 (C-8), 95.6 (C-3), 51.2 (C-10), 35.3 (C-11). **Minor isomer:** 177.0 (C-4), 163.2 (C-2), 160.7 (C-9), 154.1 (C-8a), 140.5 (C-1'), 134.4 (C-7), 133.1 (C-3'), 130.3, 128.9, 127.7, 126.5 (C-2', C-4', C-5', C-6')*, 125.8 (C-5), 124.1 (C-6), 120.3 (C-4a), 117.0 (C-8), 95.4 (C-3), 51.3 (C-10), 35.3 (C-11). **IR**

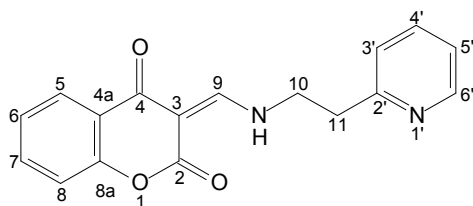
ν_{\max} (cm^{-1}) 3140, 1705, 1623, 1464, 752. **APCI-HRMS** m/z calcd. for $\text{C}_{18}\text{H}_{15}\text{ClNO}_3$, 328.0735, $[M+H]^+$ found 328.0734. **Purity** (HPLC): 98 %. *In no particular order.

(3*E/Z*)-3-[[pyridin-2-yl]amino]methylidene}-3,4-dihydro-2*H*-1-benzopyran-2,4-dione (**45**)



The title compound was prepared from chromone-3-carboxylic acid and 2-aminopyridine in a yield of 65%: mp. 212.2-214.9 °C (methanol), (lit. 237 – 240 °C (DMF), Strakova *et al.*, 2006), yellow solid. Ratio of major isomer: minor isomer 1:0.4. **¹H NMR** (600 MHz, CDCl_3) δ **Major isomer:** 13.57 (d, $J = 12.5$ Hz, 1H, NH), 9.61 (d, $J = 12.8$ Hz, 1H, H-9), 8.49 – 8.43 (m, 1H, H-6'), 8.05 (dd, $J = 7.8, 1.7$ Hz, 1H, H-5), 7.77 (ddd, $J = 8.1, 7.4, 1.9$ Hz, 1H, H-4'), 7.63 – 7.56 (m, 1H, H-7), 7.32 – 7.23 (m, 2H, H-6, H-8), 7.20 (ddd, $J = 7.4, 4.8, 0.9$ Hz, 1H, H-5'), 7.10 (br d, $J = 8.1$ Hz, 1H, H-3'). **Minor isomer:** 11.91 (d, $J = 13.7$ Hz, 1H, NH), 9.71 (d, $J = 13.7$ Hz, 1H, H-9), 8.49 – 8.43 (m, 1H, H-6'), 8.13 (dd, $J = 7.8, 1.7$ Hz, 1H, H-5), 7.77 (ddd, $J = 8.1, 7.4, 1.9$ Hz, 1H, H-4'), 7.63 – 7.56 (m, 1H, H-7), 7.32 – 7.23 (m, 2H, H-6, H-8), 7.20 (ddd, $J = 7.4, 4.8, 0.9$ Hz, 1H, H-5'), 7.12 (br d, $J = 8.1$ Hz, 1H, H-3'). **¹³C NMR** (151 MHz, CDCl_3) δ **Major isomer:** 182.4 (C-4), 163.3 (C-2), 155.1 (C-9), 154.4 (C-8a), 149.4 (C-6'), 149.1 (C-2'), 139.0 (C-4'), 135.1 (C-7), 126.0 (C-5), 124.2 (C-6), 122.1 (C-5'), 120.3 (C-4a), 117.5 (C-8), 113.4 (C-3'), 99.7 (C-3). **Minor isomer:** 178.8 (C-4), 165.3 (C-2), 154.7 (C-9), 154.5 (C-8a), 149.3 (C-6'), 149.25 (C-2'), 139.0 (C-4'), 134.9 (C-7), 126.7 (C-5), 124.5 (C-6), 122.0 (C-5'), 120.7 (C-4a), 117.4 (C-8), 113.2 (C-3'), 100.0 (C-3). **IR** ν_{\max} (cm^{-1}) 3218, 1685, 1640, 1459, 760. **APCI-HRMS** m/z calcd. for $\text{C}_{15}\text{H}_{11}\text{N}_2\text{O}_3$, 267.0764, $[M+H]^+$ found 267.0748. **Purity** (HPLC): 99 %.

(3*E/Z*)-3({[2-(pyridin-2-yl)ethyl]amino}methylidene)-3,4-dihydro-2*H*-1-benzopyran-2,4-dione
(46)



The title compound was prepared from chromone-3-carboxylic acid and 2-(2-pyridyl)ethylamine in a yield of 53%: mp. 144.7-145.8 °C (methanol), colorless crystals. Ratio of major isomer: minor isomer 1:0.4. **¹H NMR** (600 MHz, DMSO-*d*₆) δ **Major isomer:** 11.81 (s, 1H, NH), 8.56 – 8.49 (m, 1H, H-6'), 8.40 (br s, 1H, H-9), 7.93 – 7.86 (m, 1H, H-5), 7.76 – 7.69 (m, 1H, H-4'), 7.66 – 7.58 (m, 1H, H-7), 7.33 – 7.21 (m, 4H, H-3', H-5', H-6, H-8), 4.01 (t, *J* = 6.7 Hz, 2H, H-10), 3.16 (t, *J* = 6.6 Hz, 2H, H-11). **Minor isomer:** 10.61 (s, 1H, NH), 8.56 – 8.49 (m, 2H, H-9, H-6'), 7.93 – 7.86 (m, 1H, H-5), 7.76 – 7.69 (m, 1H, H-4'), 7.66 – 7.58 (m, 1H, H-7), 7.33 – 7.21 (m, 4H, H-3', H-5', H-6, H-8), 4.01 (t, *J* = 6.7 Hz, 2H, H-10), 3.16 (t, *J* = 6.6 Hz, 2H, H-11). **¹³C NMR** (151 MHz, DMSO-*d*₆) δ **Major isomer:** 179.2 (C-4), 162.7 (C-2), 162.2 (C-9), 157.8 (C-2'), 154.1 (C-8a), 149.1 (C-6'), 136.7 (C-4'), 134.2 (C-7), 125.3 (C-5), 123.9 (C-6), 123.6, 121.9 (C-3', C-5')*, 120.3 (C-4a), 116.9 (C-8), 95.6 (C-3), 49.3 (C-10), 36.97 (C-11). **Minor isomer:** 176.9 (C-4), 163.2 (C-2), 160.6 (C-9), 157.9 (C-2'), 154.2 (C-8a), 149.0 (C-6'), 136.7 (C-4'), 134.3 (C-7), 125.7 (C-5), 124.0 (C-6), 123.6, 121.9, (C-3', C-5')*, 120.4 (C-4a), 117.0 (C-8), 95.4 (C-3), 49.5 (C-10), 37.1 (C-11). **IR** ν_{\max} (cm⁻¹): 3197, 1708, 1605, 1463, 762. **APCI-HRMS** *m/z* calcd. for C₁₇H₁₅N₂O₃, 295.1077, [*M+H*]⁺ found 295.1071. **Purity** (HPLC): 100 %. * In no particular order.

3.4 Summary

A total of fifteen chromone derivatives were synthesized. Five of these were ester derivatives, while 10 3-aminomethylene-2,4-chromandiones were obtained instead of the expected amide derivatives. All compounds were characterized using NMR and IR spectroscopy, as well as mass spectrometry. A crystal structure was obtained for compound **46** to further confirm its structure. HPLC data were further obtained to confirm purity of the compounds.

CHAPTER 4

BIOLOGICAL EVALUATION

4.1 Introduction

In this chapter, the biological evaluation of all the compounds synthesized as detailed in chapter 3 will be discussed. The objectives of this chapter are:

1. To determine the IC₅₀ values of the synthesized compounds for inhibition of the MAO-A and MAO-B enzymes. Sigmoidal concentration-inhibition curves will be drawn for this purpose.
2. To determine if the test inhibitors of MAO-A and/or MAO-B are competitive inhibitors. For this outcome Lineweaver-Burk plots will be constructed.
3. To determine the reversibility of binding of the inhibitors to MAO-A and MAO-B by use of dialysis of the enzyme-inhibitor complexes.

4.2 Enzyme Kinetics

Enzyme kinetics is the quantitative analysis of the rates of enzyme-catalyzed reactions and the factors affecting these rates. Kinetic analysis aids in elucidating the catalytic mechanisms involved in enzyme-catalyzed processes (Kennelly & Rodwell, 2009). Enzymes work by converting the substrate (S) into the product. The formation of a complex between the enzyme (E) and the substrate (ES complex) is characteristic of enzyme-catalyzed reactions.

For a typical enzyme, the initial velocity (v_i) increases with an increase in substrate concentration [S], until a maximum velocity (V_{max}) is reached (figure 4.1). Any further increase in substrate concentration does not result in an increase of v_i , the enzyme is thus 'saturated' with substrate (Kennelly & Rodwell, 2009).

The Michaelis-Menten equation shows the relationship between v_i and [S], as obtained graphically from figure 4.1.

$$v_i = \frac{V_{max} [S]}{K_m + [S]} \quad \mathbf{1}$$

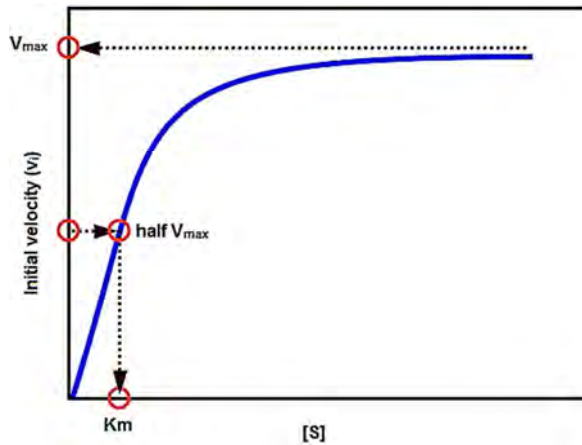


Figure 4.1 Michaelis-Menten plot showing effect of substrate concentration on V_i .

K_m is a constant which represents the substrate concentration at which v_i is half the maximal velocity at a specific concentration of the enzyme. Manipulation of this equation will result in equation 2, which represents an equation of a straight line in the form $y = ax + b$.

$$\frac{1}{v_i} = \left(\frac{K_m}{V_{max}} \right) \frac{1}{[S]} + \frac{1}{V_{max}} \quad 2$$

This equation (2), when plotted is called a double reciprocal or Lineweaver-Burk plot as shown in figure 4.2.

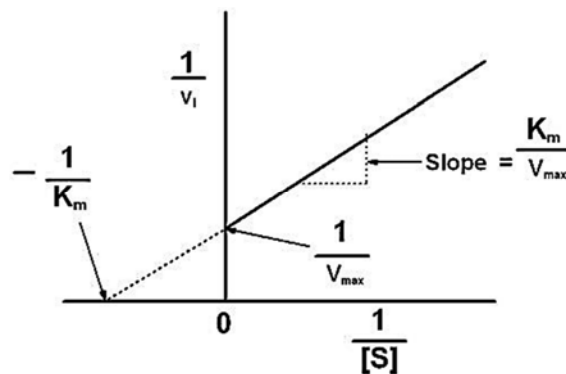


Figure 4.2 Lineweaver-Burk plot of $1/v_i$ as the y-axis and $1/[S]$ as the x-axis. The x-axis intercept represents $-1/K_m$, and $1/V_{max}$ represents the y-intercept.

The Lineweaver-Burk plot is useful for comparison of inhibitory mechanisms, thereby distinguishing competitive and non-competitive inhibitors. In competitive inhibition, the presence of an inhibitor decreases the ability of the enzyme to bind with its substrate, whilst a non-competitive inhibitor binds to a distinct site on the enzyme which is not the substrate binding site and acts by reducing the turnover rate of the reaction (Rogers & Gibon, 2009).

4.2.1 Competitive inhibition

Several substrate concentrations are used to ascertain the value of v_i both in the presence and absence of the inhibitor. In a graph representing competitive inhibition, the lines connecting the experimental data points intersect at the y-axis as shown in figure 4.3.

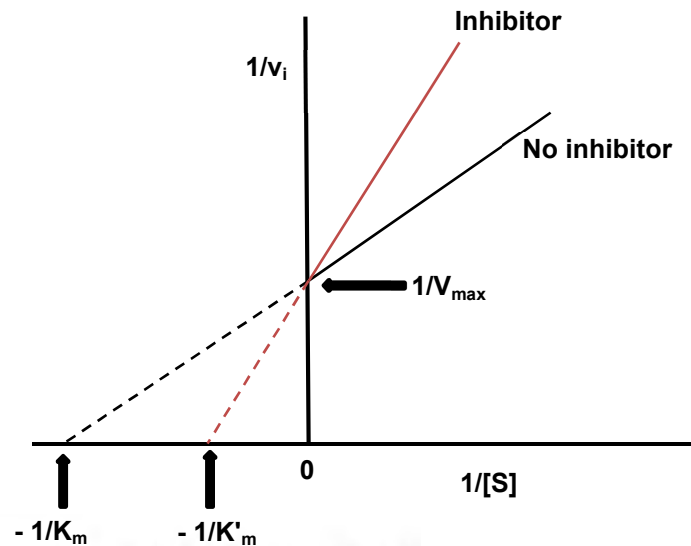


Figure 4.3 Lineweaver-Burk plot of competitive inhibition. The x-intercept is $-1/K_m$ when no inhibitor is present and $-1/K'_m$ in the presence of an inhibitor. The y-intercept is $1/V_{max}$.

From the graph (figure 4.3) it can be deduced that as $1/[S]$ approaches 0, the value of v_i is unaffected by the presence of the inhibitor. However, the x-intercept is dependent on the inhibitor concentration (Kennelly & Rodwell, 2009). An increase in the concentration of the competitive inhibitor will result in an increase in K_m of the enzyme. However, no effect is observed on V_{max} because an infinite substrate concentration will exclude the effect of the competitive inhibitor (Rogers & Gibon, 2009).

The K_i may be calculated from x-intercept, which is the dissociation constant for the inhibitor by using equation 3:

$$x = \frac{-1}{K_m} \left(1 + \frac{[I]}{K_i} \right) \quad 3$$

4.2.2 Non-competitive inhibition

In non-competitive inhibition, the presence of the inhibitor does not affect substrate binding. The enzyme-inhibitor complex and the enzyme-inhibitor-substrate complex can both be formed. In simple non-competitive inhibition affinity for the substrate is unaffected by the presence of the inhibitor, but there are inhibitors that may affect substrate binding affinity (Kennelly & Rodwell, 2009). Figure 4.4 shows a graphical representation of a non-competitive inhibitor.

V_{\max} cannot be recovered by increasing the substrate concentration because the inhibitor does not bind at the active site (Rogers & Gibon, 2009).

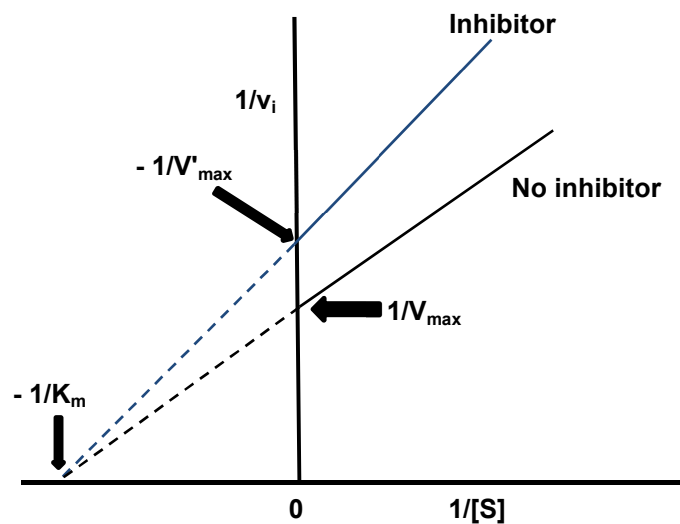


Figure 4.4 Lineweaver-Burk plot showing non-competitive inhibition. The x-intercept is $1/K_m$ and it remains constant, whilst the y-intercept is $1/V_{\max}$ in the presence of the inhibitor, and $1/V'_{\max}$ when no inhibitor is present.

4.2.3 K_i Determination

The Michaelis equation can be used to determine the value of K_i as illustrated above in equation 3. However a simple method of calculating K_i was discovered by Dixon (1953). The K_i value may be used to compare the potency of various inhibitors acting on the same target (Burlingham & Widlanski, 2003). Plotting $1/v_i$ against the inhibitor concentration $[I]$ for a competitive inhibitor, and keeping the substrate constant, a straight line would be obtained. If two substrate concentrations are used the lines would intersect on the left of the y-axis as shown in figure 4.5 (Dixon, 1953).

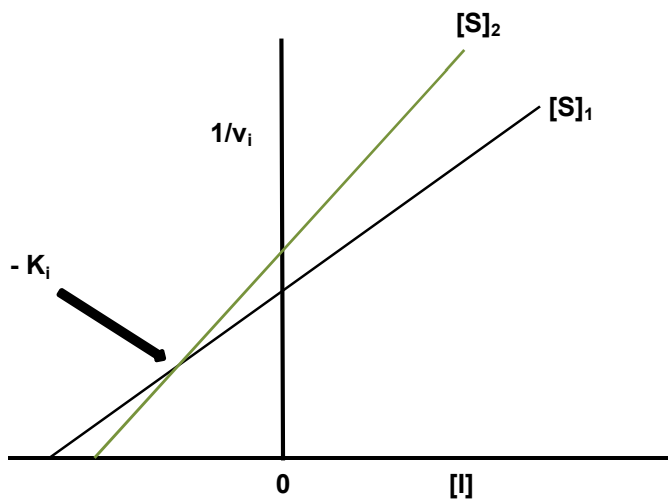


Figure 4.5 K_i determination for competitive inhibition.

In a non-competitive inhibitor the lines do not cross but they intersect at a point on the x-axis and this point is equal to $-K_i$, as shown in figure 4.6 (Dixon, 1953).

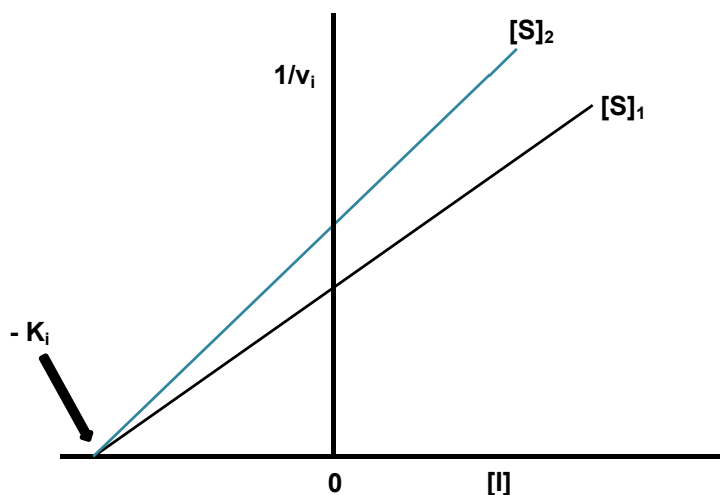


Figure 4.6 K_i determination for non-competitive inhibition.

4.2.4 IC_{50} determination and its relationship to K_i

Inhibitor potency can also be expressed in terms of the IC_{50} value. The IC_{50} denotes the concentration of inhibitor required to half the reaction rate of an enzyme-catalyzed reaction *in vitro* or under stipulated assay conditions (Burlingham & Widlanski, 2003). K_i and IC_{50} values are used to compare relative inhibitor potency, though IC_{50} values are the most commonly used for assessing enzyme-inhibitor interaction (Burlingham & Widlanski, 2003).

The lower the K_i , the tighter the binding and similarly for IC_{50} values, the lower values indicate better inhibition. For competitive inhibitors, the relationship between the IC_{50} and K_i is given by equation 4 as described by Cheng and Prusoff (1973).

$$IC_{50} = K_i \left(1 + \frac{[S]}{K_m} \right) \quad 4$$

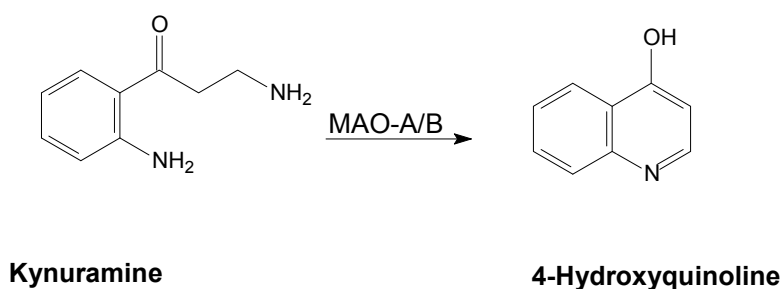
For a non-competitive inhibitor, the relationship between K_i and IC_{50} is described using equation 5 (Cheng & Prusoff, 1973).

$$IC_{50} = K_i \left(1 + \frac{K_m}{[S]} \right) \quad 5$$

In this study, the inhibitor potencies for the MAO enzyme of the synthesized compounds (**31** - **35** and **37** - **46**) will be expressed as IC_{50} values, and these values will be determined from sigmoidal concentration curves.

4.3 IC_{50} Value Determination of the Test Inhibitors

The compounds synthesized in this study were evaluated as inhibitors of MAO-A and MAO-B. Recombinant human MAO-A and MAO-B enzymes were used for this purpose. MAO activity was measured by making use of a fluorometric assay with kynuramine as the enzyme substrate. Kynuramine is a non-selective substrate for both MAO-A and MAO-B and is oxidized to 4-hydroxyquinoline (scheme 4.1), a metabolite that fluoresces in alkaline media at an excitation wavelength of 310 nm and an emission wavelength of 400 nm (Strydom *et al.*, 2010).



Scheme 4.1 Oxidation of kynuramine by MAO-A or MAO-B to give 4-hydroxyquinoline.

In the presence of a MAO inhibitor, the concentration of 4-hydroxyquinoline is reduced as the oxidation of kynuramine is inhibited. This decrease in concentration of 4-hydroxyquinoline can be measured fluorometrically since 4-hydroxyquinoline is fluorescent. This fluorescence is measured at an excitation wavelength of 310 nm and an emission

wavelength of 400 nm (Novaroli *et al.*, 2005). Fluorescence will decrease with increasing concentration of the MAO inhibitor. The test inhibitors and kynuramine do not fluoresce at the specified assay conditions, thus fluorescence of the generated 4-hydroxyquinoline can be measured efficiently.

Selectivity index (SI) refers to the degree of selectivity of the test inhibitor for the MAO-B isoform. This ratio is calculated as follows:

$$SI = \frac{IC_{50}(MAO-A)}{IC_{50}(MAO-B)}$$

4.3.1 Chemicals and Instrumentation

Fluorescence spectrophotometry was conducted on a Varian® Cary Eclipse® fluorescence spectrophotometer. The MAO enzymes were obtained from microsomes from insect cells containing recombinant human MAO-A and MAO-B (5 mg/ml). These enzymes and kynuramine.2HBr were all obtained from Sigma-Aldrich®. Sodium hydroxide (NaOH) and potassium phosphate (buffer) (KH₂PO₄) were obtained from Merck®. 96-well plates were obtained from Corning.

4.3.2 Method: IC₅₀ value determination

The incubations were prepared as follows. The recombinant human MAO-A and MAO-B were stored at -70 °C and only prepared just before use. The enzymatic reactions were carried out in white 96-well microtiter plates (Eppendorf®) to a final volume of 200 µl and were carried out in triplicate. Potassium phosphate was used as buffer at pH 7.4 [100 mM, made isotonic with potassium chloride (KCl)]. 92 µl of buffer was added first, followed by 50 µl of kynuramine, then the inhibitor (8 µl). Concentrations for the test inhibitors were varied for the assay (0, 0.003, 0.01, 0.1, 1, 10 and 100 µM). The reactions were incubated in a convection oven at 37 °C for at least 20 min. DMSO (co-solvent), at a concentration of 4% was added to each reaction. The enzyme reaction was initiated by adding MAO-A or MAO-B (0.0075 mg protein/ml), then incubated at 37 °C for 20 min. Termination of the reactions was done using 80 µl of NaOH (2 N). The concentrations of the MAO generated 4-hydroxyquinoline were measured using the fluorescence spectrophotometer ($\lambda_{ex} = 310$ nm; $\lambda_{em} = 400$ nm) (Strydom *et al.*, 2010; Legoabe *et al.*, 2014). Figure 4.7 shows the general workflow for IC₅₀ determination done for this study.

For quantitative estimations of 4-hydroxyquinoline, a linear calibration curve was constructed, containing known concentrations of 4-hydroxyquinoline (0.0469, 0.09375, 0.1875, 0.375, 0.75 and 1.5 μM), each dissolved in potassium phosphate buffer to a final volume of 200 μl . 80 μl of NaOH (2 N) was added to each standard. Sigmoidal-dose response curves were obtained by plotting the initial rate of kynuramine oxidation against the logarithm of the test inhibitor concentration. Prism® 5 software package (GraphPad® Software) was used to fit the kinetic data obtained. The IC_{50} values are expressed as mean \pm standard deviation (SD) and as stated earlier, the IC_{50} values were experimentally determined in triplicate (Strydom *et al.*, 2010).

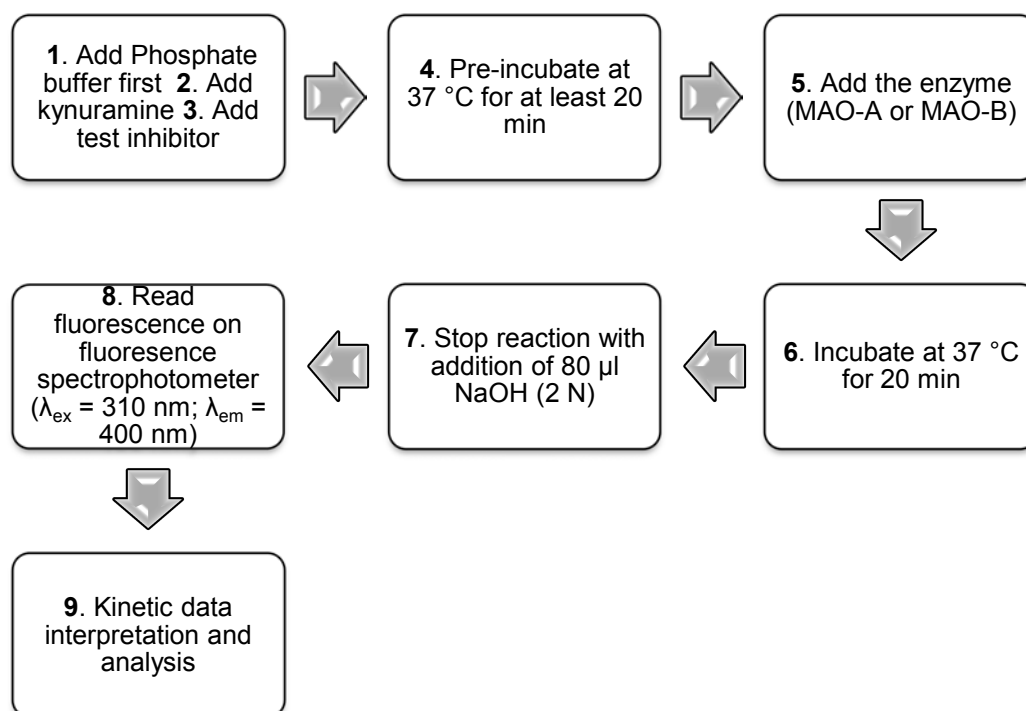


Figure 4.7 Workflow for IC_{50} determination.

4.3.3 Results and Discussion (IC_{50} determination)

The sigmoidal-dose response curves of the test inhibitors were constructed by plotting the logarithms of the different concentrations of the test inhibitors against the rate of MAO catalyzed oxidation of kynuramine. The concentration of the inhibitor required to decrease the rate of catalysis to half the maximal value is the IC_{50} . Figure 4.8 shows an example of a sigmoidal concentration inhibition curve that is used to determine the IC_{50} value.

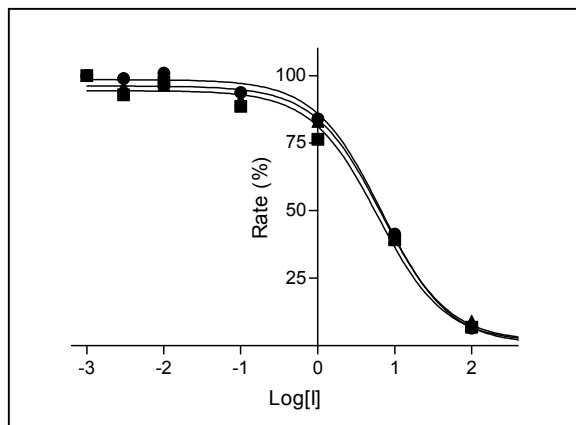
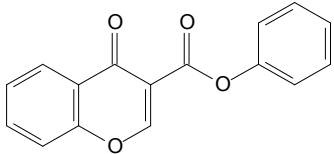
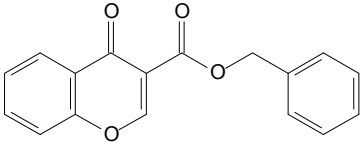
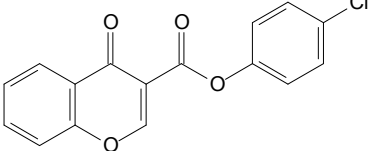
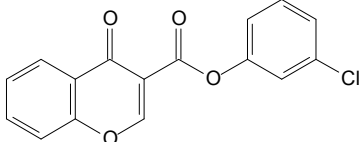
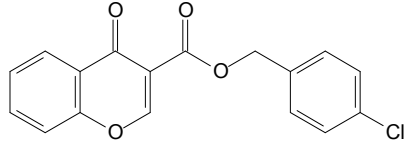


Figure 4.8 A sigmoidal dose response curve that may be used to calculate the IC_{50} .

In table 4.1 and 4.2 the results obtained for MAO inhibitory activity for series 1 (ester derivatives) and 2 (3-aminomethylene-2,4-chromandiones), are summarized respectively. Selectivity index (SI) values are also given to show the selectivity of the compounds for MAO-B inhibition over MAO-A.

Table 4.1: IC_{50} and SI values of synthesized ester derivatives for hMAO-A and hMAO-B inhibitory activity.

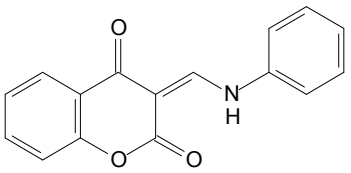
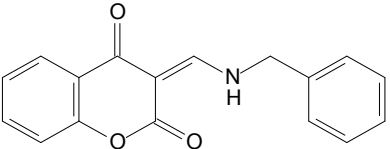
Name	Structure	MAO-A $IC_{50} \pm SD$ (μM)	MAO-B $IC_{50} \pm SD$ (μM)	SI
31		66.7 ± 2.06	27.3 ± 0.946	2.4
32		26.8 ± 0.560	14.7 ± 0.416	1.8
33		21.6 ± 8.72	14.8 ± 1.09	1.5
34		18.5 ± 8.85	12.0 ± 0.400	1.5

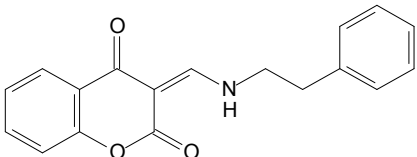
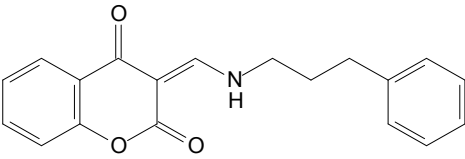
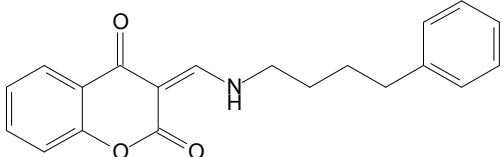
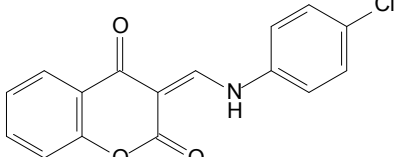
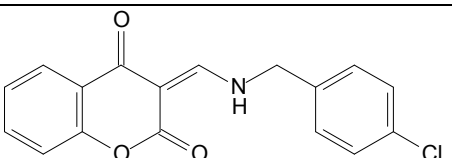
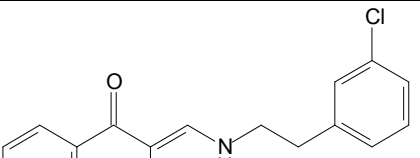
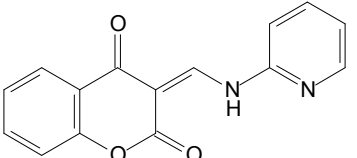
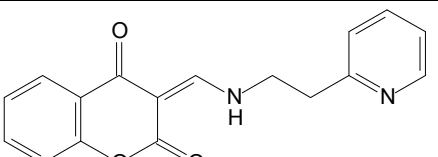
35		18.6 ± 3.27	9.74 ± 0.123	1.9
-----------	---	-----------------	------------------	-----

From Table 4.1 (ester derivatives), the following observations and conclusions can be made:

- The ester derivatives are generally weak MAO-A and MAO-B inhibitors.
- Comparing the MAO-A and MAO-B potencies of compound **31** (a phenyl substituted ester derivative) and **32** (a benzyl substituted ester derivative), it is evident that the benzyl derivative is more potent than the phenyl derivative. Thus chain elongation from phenyl to benzyl improved MAO inhibition activity. A similar trend is observed when the activity of compound **33** is compared to that of **35**.
- 4-Chlorophenyl substitution (**33**) has improved MAO inhibition activity compared to unsubstituted phenyl side chain (**31**). This can also be seen when comparing compound **35**, a 4-chlorobenzyl substituted derivative, to compound **32**, a unsubstituted benzyl ester derivative which is less potent than compound **35**.
- Comparing the 4-chlorophenyl side chain (**33**) with 3-chlorophenyl side chain (**34**), it is clear that changing the position of the chlorine group does not have significant effect on the MAO inhibition activity.
- Therefore it can be concluded that elongation of the side chain from phenyl to benzyl and substituting with a chlorine group in the 3'- or 4'-position results in improved MAO activity.

Table 4.2: IC₅₀ and SI values of synthesized for 3-aminomethylene-2,4-chromanones for hMAO-A and hMAO-B inhibitory activity.

Name	Structure	MAO-A IC ₅₀ ± SD (μM)	MAO-B IC ₅₀ ± SD (μM)	SI
37		79.6 ± 30.2	0.947 ± 0.125	84
38		77.9 ± 25.5	0.638 ± 0.287	122

39		101 ± 3.49	0.897 ± 0.166	113
40		312 ± 89.1	1.43 ± 0.103	219
41		155 ± 19.1	142 ± 47.2	1.1
42		72.1 ± 6.53	3.08 ± 0.279	23
43		288 ± 61.8	No Inhibition ^a	-
44		No Inhibition ^a	No Inhibition ^a	-
45		73.1 ± 20.4	38.7 ± 1.73	1.9
46		41.6 ± 2.29	16.6 ± 1.04	2.5

^a No inhibition at a maximum tested concentration of 100 μM.

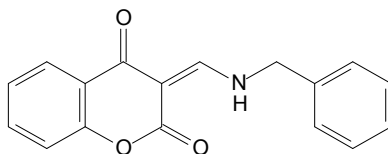
From table 4.2, the following conclusions can be made:

- The 3-aminomethylene-2,4-chromandiones are selective inhibitors of MAO-B with IC₅₀ values in the micromolar range.

- Generally, the 3-aminomethylene-2,4-chromandiones have more potent MAO-B inhibitory activity compared to the ester derivatives (they are however weaker inhibitors of MAO-A).
- Compound **38** is the most potent inhibitor for the MAO-B isoform with an IC₅₀ value of 0.638 μM.
- Compound **40** is the most selective MAO-B inhibitor with a SI value of 219.
- The most potent MAO-A inhibitor is compound **46** with an IC₅₀ value for MAO-A inhibition of 41.6 μM and an SI value of 2.5. This compound is thus not selective and has poor MAO activity.
- MAO-B inhibitory activity increases with side chain elongation from compound **37** to **38** (phenyl to benzyl), and is similar for compounds **37** and **39**, but from compound **40** to **41**, as further chain elongation occurs MAO-B inhibitory activity decreases. This may be due to the compound becoming too large to fit into the MAO-B active site.
- Comparing the MAO-A and MAO-B inhibitory activity of compounds **42**, **43** and **44**, it is evident that chain elongation results in loss of activity. Interestingly, compounds **43** and **44** do not have any MAO-B inhibitory activity. This may be due to lengthening of the side chain in combination with the addition of extra bulk.
- Comparing the MAO activity of compounds **37** – **39** with that of compounds **42** – **44**, one can see that the presence of a chlorine moiety in the side chain results in weakening the MAO-B inhibition activity.
- The compounds with pyridine-containing side chains, (compounds **45** and **46**) both show poor MAO inhibitory activity, but in this case chain elongation from pyridyl (**45**) to ethylpyridyl (**46**), resulted in a two-fold increase in MAO inhibition activity.
- Comparing **31** to **37**, compound **37** is approximately 30-fold more potent than compound **31**. Both have a phenyl group in their side chains, but the presence of the aminomethylene-2,4-chromandione shows precedence over the ester chromone. In fact, the 3-aminomethylene-2,4-chromandiones **37**, **38** and **42**, are all more potent MAO-B inhibitors than their corresponding ester derivatives **31**, **32** and **33**.
- Interestingly, comparing compound **35** to compound **43**, it is noted that inhibitory activity for MAO-B is lost from the ester derivative to the aminomethylene chromandione derivative. Both contain a chlorine moiety in the 4'-position, therefore this characteristic loss of MAO-B inhibition could be attributed to the keto-enamine derivative.

- These compounds were obtained as inseparable mixtures of *E* and *Z* isomers, and the contribution of each isomer to the activity could not be determined.

4.4 Mode of MAO Inhibition



38

Sets of Lineweaver-Burk plots were constructed to determine the mode of inhibition. Compound **38** was used as the representative inhibitor because it was the most potent MAO-B inhibitor of the series. To determine whether compound **38** exhibits a competitive or non-competitive mode of inhibition, Lineweaver-Burk plots were constructed for this compound for the inhibition of MAO-B. Only the mode of inhibition for MAO-B was determined because the IC₅₀ values showed general selectivity of these compounds for MAO-B with poor MAO-A inhibitory activity.

4.4.1 Construction of Lineweaver-Burk plots

Four Lineweaver-Burk plots were constructed to examine the mode of MAO-B inhibition by compound **38**. The first plot was constructed in the absence of compound **38** and the remaining three plots in the presence of different concentrations of compound **38** (0.1595 - 0.7975 μM). Kynuramine at eight different concentrations (15 - 250 μM) was used as substrate. Pre-incubation of substrate and inhibitor was done for 15 min at 37 °C before the enzyme was added.

Recombinant human MAO-B (5 mg/ml) was stored at -70 °C until required and prepared just before use. The concentration of MAO-B enzyme that was subsequently used was 0.015 mg protein/ml. The incubations were prepared in 500 μl potassium phosphate buffer (100 mM, pH 7.4, made isotonic with KCl) and all contained compound **38**, kynuramine and 4% DMSO as cosolvent. These were incubated for 20 min at 37 °C. The reactions were stopped with 400 μl NaOH (2N) and 1000 μl distilled water as added. These reactions were then centrifuged at 16 000 g for 10 min.

The rate of MAO-catalyzed formation of 4-hydroxyquinoline (main metabolite of kynuramine oxidation), was measured using a fluorescence spectrophotometer ($\lambda_{\text{ex}} = 310 \text{ nm}$; $\lambda_{\text{em}} = 400 \text{ nm}$). 4-Hydroxyquinoline fluoresces whilst kynuramine and compound **38** do not fluoresce under these assay conditions. Linear regression analysis was performed using Prism® 5 (Manley-King *et al.*, 2011). The K_i value was estimated from the x-axis intercept ($-K_i$) from the replot of the four slopes of the Lineweaver-Burk plots versus concentration of the inhibitor (compound **38**). A calibration curve was constructed with known concentrations of 4-hydroxyquinoline dissolved in 500 μl of potassium phosphate buffer. 400 μl of NaOH (2 N) as well as 1000 μl of distilled water were added to each calibration standard.

4.4.2 Results and Discussion (Mode of Inhibition)

Figure 4.9 shows the set of constructed Lineweaver-Burk plots. The results show linear lines that intersect at a single point just to the left of the y-axis.

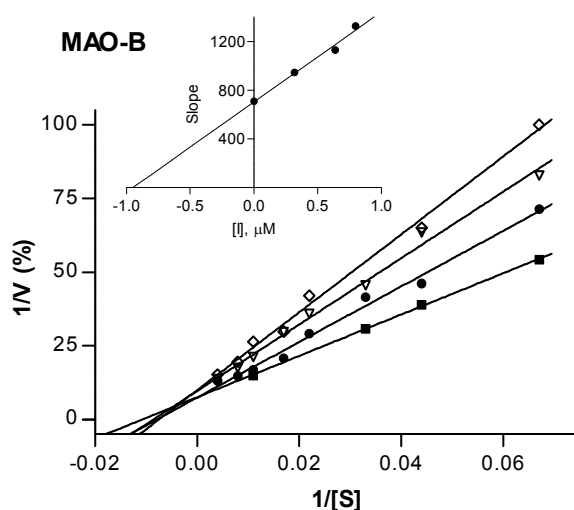
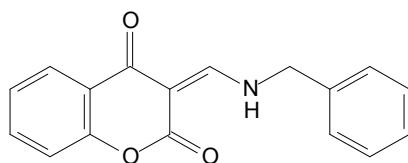


Figure 4.9 Lineweaver-Burk plots of the inhibition of recombinant human MAO-B by various concentrations of compound **38**. The filled black squares represent the plot constructed in the absence of compound **38** and the other three plots were obtained in the presence of compound **38**. The inset is a plot of the slopes of the Lineweaver-Burk plots versus the concentration of compound **38** (inhibitor [I]).

This therefore suggests that compound **38** interacts competitively with the MAO-B enzyme. From the re-plot of the slopes of the Lineweaver-Burk plots versus the concentration of compound **38** (figure 4.9 inset), the K_i value is estimated to be 0.949 μM for MAO-B inhibition.

4.5 Reversibility studies for MAO inhibition using Dialysis

4.5.1 Dialysis



38

The reversibility of the MAO inhibition by compound **38** was examined using dialysis (Harfenist *et al.*, 1996). Compound **38** was selected because it is the most potent MAO-B inhibitor in this study with an IC_{50} value of 0.638 μ M. None of the synthesized inhibitors were potent MAO-A inhibitors therefore reversibility of MAO-A inhibition was not examined. For these studies Slide-A-Lyzer® dialysis cassettes (Thermo Scientific) with a sample volume of 0.5 – 3 ml and a molecular cut off weight of 10 000 was used. The MAO-B enzyme (0.03 mg/ml) was combined with compound **38** at concentrations equal to fourfold the IC_{50} value for the inhibition of MAO-B. The final volume was 0.8 ml. These mixtures were prepared in sucrose buffer which consists of sodium phosphate buffer (100 mM, pH 7.4, 5% sucrose), and DMSO (4%) was used as co-solvent. These enzyme/inhibitor mixtures were then pre-incubated at 37 °C for 15 min. As controls, the MAO-B enzyme was preincubated in the presence and absence of an irreversible MAO-B inhibitor (*R*)-deprenyl. (*R*)-Deprenyl has an IC_{50} value of 79 nM (Petzer *et al.*, 2012) for MAO-B inhibition. The concentrations employed for (*R*)-deprenyl were also fourfold that of its IC_{50} value for the inhibition of MAO-B. After preincubation the enzyme/inhibitor mixtures were injected into the dialysis cassettes and dialyzed at 4 °C in 80 ml of outer dialysis buffer (100 mM potassium phosphate, pH 7.4, 5% sucrose) for 24 h. The outer dialysis buffer was replaced with fresh buffer at 3 h and also 7 h after the start of dialysis. The reactions were diluted twofold with kynuramine at 24 h after the start of dialysis. This kynuramine was prepared using potassium phosphate buffer (100 mM, pH 7.4, made isotonic with KCl). The final concentration of kynuramine in these reactions was 50 μ M with the final inhibitor concentrations in the reactions being equal to twofold their IC_{50} values. Undialyzed mixtures of the MAO-B enzyme and the test inhibitor were also kept at 4 °C over the same time period (24 h) for comparison. All the reactions were terminated by the addition of 400 μ l NaOH (2N) and 1000 μ l milli-Q water. Fluorescence spectrophotometry was subsequently used to measure residual MAO activities in each reaction mixture. All reactions were done in triplicate, with the residual MAO catalytic

rates expressed as mean \pm SD. Figure 4.10 shows the summary of steps of the dialysis method.

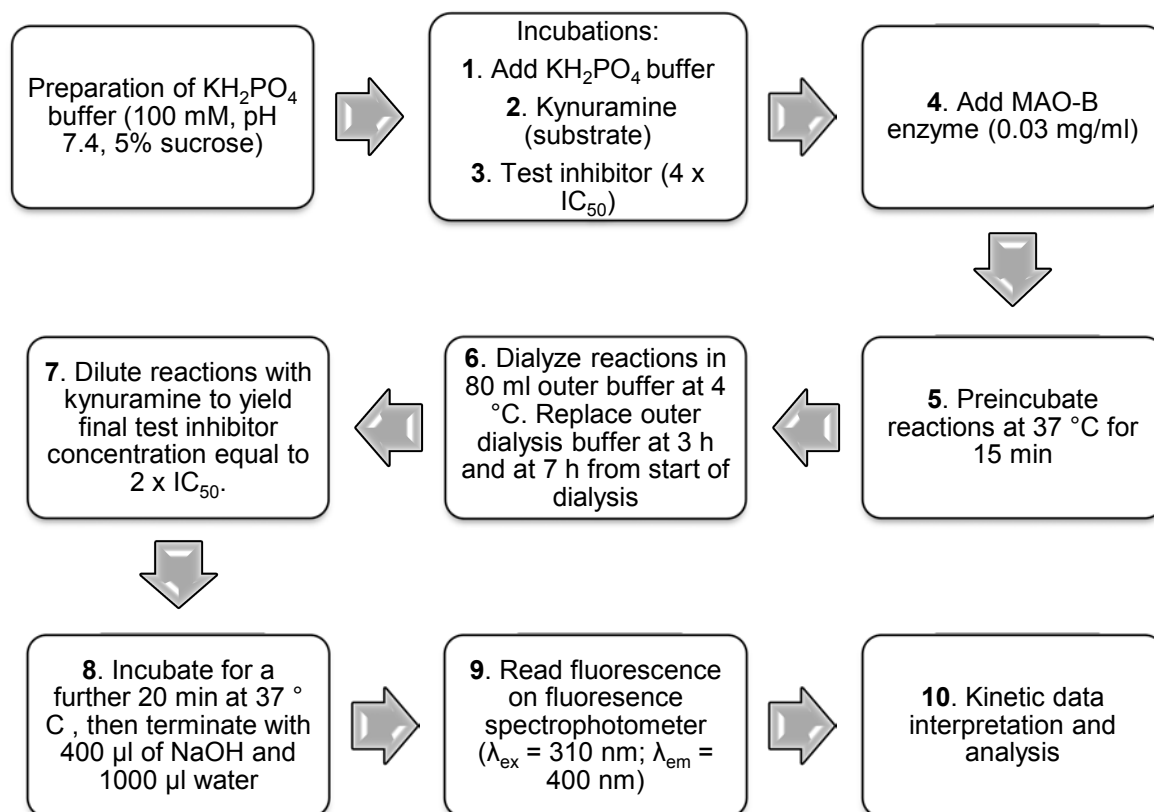


Figure 4.10 Summary of method used to determine reversibility of MAO-B inhibition using dialysis.

4.5.2 Results and Discussion (Reversibility Studies)

Figure 4.11, shows the results obtained in the reversibility assay. Inhibition of MAO-B by compound **38** was completely reversed after 24 h of dialysis. After dialysis of mixtures containing compound **38** and MAO-B, the MAO-B catalytic activity was recovered to 115% of the control value. This suggests that compound **38**, is a reversible inhibitor of MAO-B. After dialysis of mixtures containing the irreversible MAO-B inhibitor, (*R*)-deprenyl, and MAO-B, the catalytic activity of MAO-B was not recovered, with only 3% activity remaining.

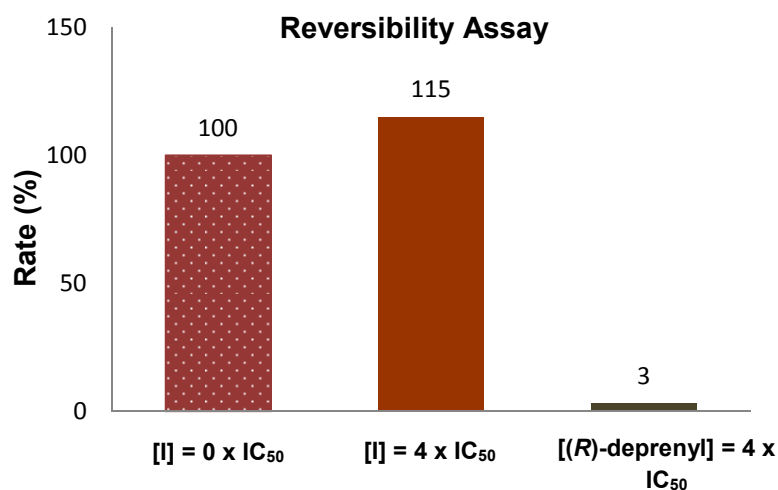
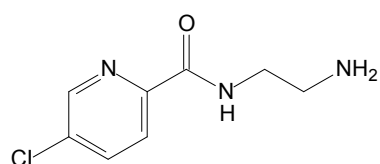


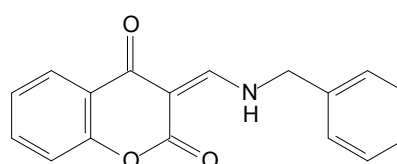
Figure 4.11 The reversibility of inhibition of MAO-B by compound **38**. Recombinant human MAO-B (0.03 mg/ml) was dialyzed in the absence of inhibitor, presence of inhibitor **38** (at 4 x IC₅₀) and presence of (*R*)-deprenyl (at 4 x IC₅₀). The enzyme was added to the substrate (50 μM) to yield final [Enzyme] 0.015 mg/mL and residual MAO-B activities were recorded.

4.6 Summary

In this chapter, *in vitro* biological evaluation of synthesized chromone derivatives was accomplished and the results discussed. In general, the compounds show poor MAO-A inhibitory activity but the aminomethylene chromandione derivatives in particular show promising MAO-B inhibition. When compared to lazabemide (**27**) (IC₅₀ = 0.091 μM) (Petzer *et al.*, 2013), a reversible inhibitor of MAO-B, compound **38** was 7-fold less potent for MAO-B inhibition under similar conditions.



27 Lazabemide



38

CHAPTER 5

CONCLUSION

Parkinson's disease is a progressive neurodegenerative disorder affecting the central nervous system. This disease is the result of the death of dopaminergic neurons in the substantia nigra. The motor symptoms associated with Parkinson's disease include bradykinesia, muscle rigidity, resting tremor and an impairment of postural balance. The key molecular events that result in the neurodegenerative characteristics of Parkinson's disease are not well understood thus hindering development of neurotherapeutic agents (Dauer & Przedborski, 2003).

All current available treatments used in Parkinson's disease are symptomatic, and none have been substantially proven to halt or retard neurodegeneration. Levodopa is a highly effective anti-Parkinsonian agent, however, long term levodopa therapy has numerous side effects that affect the quality of life of the individual. There is thus an urgent need for novel drugs for the treatment of Parkinson's disease with better side effect profiles.

The MAO-A and MAO-B enzymes are flavoenzymes which play an important role in the oxidative degradation of amine neurotransmitters such as dopamine, serotonin and epinephrine. Inhibition of the MAOs can potentially modulate neurotransmitter levels (for example dopamine) in the brain that are actively involved in the pathogenesis of some neurodegenerative, age-related diseases such as Parkinson's disease. Inhibition of specifically MAO-B in the brain will result in increased dopamine levels, thus alleviating Parkinson's disease symptoms, with possible neuroprotective effects (Youdim *et al.*, 2006).

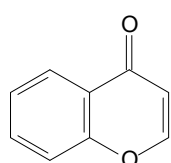
The MAO inhibitory potential of chromone derivatives has been illustrated previously (Legoabe *et al.*, 2012a). The present study aimed to synthesize and evaluate chromone derivatives as potential MAO inhibitors and thus to contribute to the structure-activity relationships of the MAO inhibitory activity of this class of compounds.

Aim

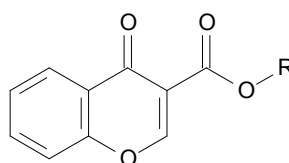
The aim of this project was to design, synthesize and evaluate chromone derivatives as inhibitors of monoamine oxidase. The ideal inhibitor in this case is postulated to be a selective, reversible MAO-B inhibitor for the treatment of Parkinson's disease.

Chemistry

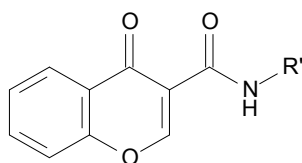
This study aimed to synthesize ester (**29**) and amide derivatives (**30**) of chromone 3-carboxylic acid. This was to be achieved by elongating and varying the flexibility of the side chain in position 3 of the chromone ring scaffold (**1**). Chromone ester derivatives were successfully synthesized but the desired amide chromone derivatives (**30**), were not obtained and 3-aminomethylene-2,4-chromandiones (**36**) were synthesized instead. Careful qualitative analysis using 2D NMR, X-ray crystallography and variable temperature NMR aided in structure elucidation of the 3-aminomethylene-2,4-chromandiones. The present study therefore investigated the MAO inhibitory properties of series of chromone derivatives **29** and **36**.



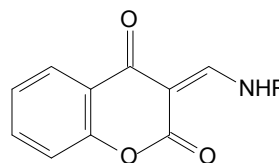
1



29

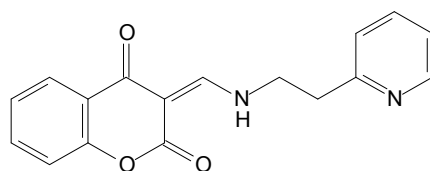


30



36

Fifteen chromone derivatives were successfully synthesized using standard literature synthetic procedures. All compounds were synthesized through a one-step coupling reaction, using CDI as a coupling agent. Characterization of all compounds was done by NMR spectroscopy, mass spectrometry and IR spectroscopy. HPLC was used to assess purity of all compounds with the purity ranging from 75 - 100%. The crystal structure of compound **46** was obtained (figure 5.1) to further prove the synthesis of 3-aminomethylene-2,4-chromandiones instead of the expected amide derivatives.



46

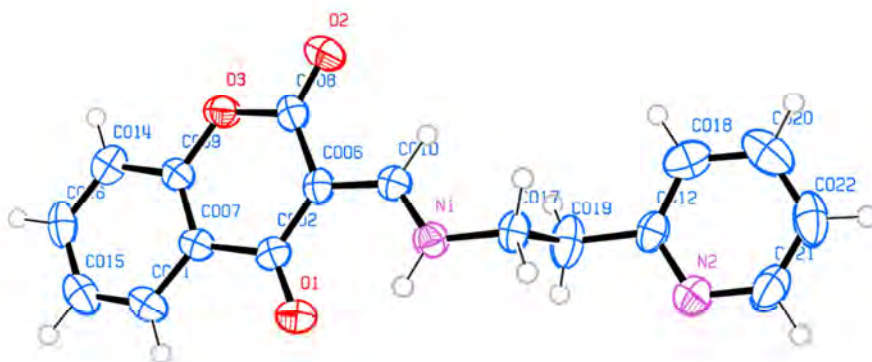


Figure 5.1 Ortep® drawing representing the crystal structure of the *E*-isomer of compound **46**.

In vitro assays

Biological assays were conducted to determine MAO inhibitory activity of the chromone derivatives. The MAO inhibitory activities of the synthesized chromone derivatives were assessed by employing a fluorometric assay using recombinant human MAO-A and MAO-B, and kynuramine as substrate for both MAO-A and MAO-B. Kynuramine is oxidized to yield 4-hydroxyquinoline, a fluorescent product. To measure the MAO catalytic activity, a fluorescence spectrophotometer was used at an excitation wavelength of 310 nm, and an emission wavelength of 400 nm. The biological assay revealed that the ester derivatives were weak MAO-A and MAO-B inhibitors, while several of the 3-aminomethylene-2,4-chromandiones exhibited promising MAO-B inhibitory activities with SI values ranging generally from 1.1 – 219, but poor MAO-A inhibition. The most potent MAO-B inhibitor was compound **38** with an IC_{50} value of 0.638 μ M. Compared to the reversible MAO-B selective inhibitor, lazabemide (IC_{50} = 0.091 μ M), compound **38** is 7-fold less potent.

To determine whether the binding of these aminomethylene derivatives to the MAO-B enzyme is reversible or irreversible, a dialysis assay was conducted. Compound **38** was used as the test inhibitor, and (*R*)-deprenyl was used as a positive control. This study revealed a reversible mode of inhibition.

Kinetic studies were conducted to determine the mode of inhibition. Lineweaver-Burk plots were constructed for the inhibition of human MAO-B by **38**. The lines of the Lineweaver-Burk plots intersected just to the left of the y-axis. This therefore suggests a competitive mode of binding of compound **38** to MAO-B.

Chromone derivatives were synthesized and evaluated as inhibitors of MAO. The effect of chain elongation and the introduction of a more flexible substituent in position 3 was explored. The MAO inhibitory activities of the ester derivatives were generally poor, whilst the 3-aminomethylene-2,4-chromandiones showed promising, reversible MAO-B inhibitory activity. An analysis of the structure–activity relationships (SARs) for MAO-B inhibition revealed some interesting trends. For the ester series, the results showed that weak MAO-A and MAO-B inhibitors are obtained when focusing on this specific position, and not highly potent, selective MAO-B inhibitors as postulated. A 2 carbon side chain appears to be optimal for the 3-aminomethylene-2,4-chromandione series as the addition of extra carbons or further substitution with a chlorine group results in a decrease in activity.

The inadvertent synthesis of the 3-aminomethylene-2,4-chromandione series resulted in this first report of the MAO inhibitory activities of 3-aminomethylene-2,4-chromandiones as inhibitors of MAO. Substitution in position 3 generally appears to result in less potent inhibitors than C6 and C7 substitution as previously investigated by Legoabe and colleagues (2012a,b). Further structural modifications are therefore required to optimize these compounds for further development as potent, reversible inhibitors of MAO-B. One suggestion to enhance the MAO-B inhibitory activity of these compounds would be to add less bulky substituents such as methyl or fluorine to the 3'- and/or 4'-position instead of the chlorine substituent.

BIBLIOGRAPHY

Adler, C.H. 2005. Nonmotor complications in Parkinson's disease. *Movement disorders*, 20:S23-S29.

Alberola, A., Calvo, L., Gonzalez-Ortega, A., Encabo, A.P., Sanudo, M.C. 2001. Synthesis of [1]benzopyrano[4,3-b]pyrrol-4(1H)-ones from 4-chloro-3-formylcoumarin. *Synthesis*, 13:1941-1948.

Alcaro, S., Gaspar, A., Ortuso, F., Milhazes, N., Orallo, F., Uriarte, E., Yáñez, M., Borges, F. 2010. Chromone-2- and -3-carboxylic acids inhibit differently monoamine oxidases A and B. *Bioorganic & medicinal chemistry letters*, 20:2709-2712.

Ascherio, A., Weisskopf, M.G., O'Reilly, E.J., McCullough, M.L., Calle, E.E., Rodriguez, C., Thun, M.J. 2004. Coffee consumption, gender, and Parkinson's disease mortality in the cancer prevention study II cohort: The modifying effects of estrogen. *American journal of epidemiology*, 160:977-984.

Ascherio, A., Zhang, S.M., Hernán, M.A., Kawachi, I., Colditz, G.A., Speizer, F.E., Willett, W.C. 2001. Prospective study of caffeine consumption and risk of Parkinson's disease in men and women. *Annals of neurology*, 50:56-63.

Ashok, P.P., Radhakrishnan, K., Sridharan, R., Mousa, M.E. 1986. Epidemiology of Parkinson's disease in Benghazi, North-East Libya. *Clinical neurology and neurosurgery*, 88:109-113.

Azzaro, A.J., Vandenberg, C.M., Blob, L.F., Kemper, E.M., Sharoky, M., Oren, D.A., Campbell, B.J. 2006. Tyramine pressor sensitivity during treatment with the selegiline transdermal system 6 mg/24 h in healthy subjects. *Journal of clinical pharmacology*, 46:933-944.

Bach, A.W., Lan, N.C., Johnson, D.L., Abell, C.W., Bembenek, M.E., Kwan, S.W., Seeburg, P.H., Shih, J.C. 1988. cDNA cloning of human liver monoamine oxidase A and B: Molecular basis of differences in enzymatic properties. *Proceedings of the national academy of sciences of the United States of America*, 85:4934-4938.

Bandyopadhyay, C., Ranabir Sur, K., Patra, R., Sen, A. 2000. Synthesis of coumarin derivatives from 4-oxo-4H-1-benzopyran-3-carboxaldehyde via 3(arylaminoethylene)chroman-2,4-dione. *Tetrahedron*, 56:3583-3587.

Bar-Am, O., Amit T., Youdim, M.B.H. 2004. Contrasting neuroprotective and neurotoxic actions of respective metabolites of anti-Parkinson drugs rasagiline and selegiline. *Neuroscience letters*, 355:169-172.

Barichella, M., Pezzoli, G., Mauri, A., Savardi, C. 2010. Neural lipids in Parkinson's disease. (In Lajtha, A., Tettamanti, G. & Goracci, G., eds. Handbook of neurochemistry and molecular neurobiology. 3rd ed. United States: Springer. p. 583-592).

Binbuga, N., Ruhs, C., Hasty, J.K., Henry, W.P., Schultz, T.P. 2008. Developing environmentally benign and effective organic wood preservatives by understanding the biocidal and non-biocidal properties of extractives in naturally durable heartwood. *Holzforschung*, 62:264-269.

Binda, C., Newton-Vinson, P., Hubálek, F., Edmondson, D.E., Mattevi, A. 2001. Structure of human monoamine oxidase B, a drug target for the treatment of neurological disorders. *Nature structural & molecular biology*, 9:22-26.

Brichta, L., Greengard, P., Flajolet, M. 2013. Advances in the pharmacological treatment of Parkinson's disease: Targeting neurotransmitter systems. *Trends in neurosciences*, 36:543-554.

Burlingham, B.T., Widlanski, T.S. 2003. An intuitive look at the relationship of K_i and IC_{50} : A more general use for the Dixon plot. *Journal of chemical education*, 80:214.

Burns, R.S., Chiueh, C.C., Markey, S.P., Ebert, M.H., Jacobowitz, D.M., Kopin, I.J. 1983. A primate model of parkinsonism: Selective destruction of dopaminergic neurons in the pars compacta of the substantia nigra by N-methyl-4-phenyl-1,2,3,6-tetrahydropyridine. *Proceedings of the national academy of sciences of the United States of America*, 80:4546-4550.

- Cagide, F., Silva, T., Reis, J., Gaspar, A., Borges, F., Gomes, L.R., Low, J.N.** 2015. Discovery of two new classes of potent monoamine oxidase-B inhibitors by tricky chemistry *Chemical communications*, 51:2832-2835.
- Chaudhuri, K., Healy, D.G., Schapira, A.H.** 2006. Non-motor symptoms of Parkinson's disease: Diagnosis and management. *The lancet neurology*, 5:235-245.
- Chen, J.J., Swope, D.M.** 2005. Clinical pharmacology of rasagiline: A novel, second-generation propargylamine for the treatment of Parkinson disease. *The journal of clinical pharmacology*, 45:878-894.
- Cheng, Y., C., Prusoff, W.H.** 1973. Relationship between the inhibition constant (K_i) and the concentration of inhibitor which causes 50 per cent inhibition (IC_{50}) of an enzymatic reaction. *Biochemical pharmacology*, 22:3099-3108.
- Chung, K.K., Dawson, V.L., Dawson, T.M.** 2003. New insights into Parkinson's disease. *Journal of neurology*, 250:iii15-iii24.
- Cicccone, C.D.** 2007. Pharmacology in rehabilitation. 4th ed. Philadelphia: FA Davis. p. 704.
- Cohen, G., Spina, M.B.** 1989. Deprenyl suppresses the oxidant stress associated with increased dopamine turnover. *Annals of neurology*, 26:689-690.
- Comella, C., Tanner, C.M.** 1995. Anticholinergic drugs in the treatment of Parkinson's disease. *Neurological disease and therapy*, 34:109.
- Dauer, W., Przedborski, S.** 2003. Parkinson's disease: Mechanisms and models. *Neuron*, 39:889-909.
- Day, B.J., Patel, M., Calavetta, L., Chang, L.Y., Stamler, J.S.** 1999. A mechanism of paraquat toxicity involving nitric oxide synthase. *Proceedings of the national academy of sciences of the United States of America*, 96:12760-12765.
- De Colibus, L., Li, M., Binda, C., Lustig, A., Edmondson, D.E., Mattevi, A.** 2005. Three-dimensional structure of human monoamine oxidase A (MAO A): Relation to the structures

of rat MAO A and human MAO B. *Proceedings of the national academy of sciences of the United States of America*, 102:12684-12689.

Deleu, D., Hanssens, Y., Northway, M.G. 2004. Subcutaneous apomorphine. *Drugs & aging*, 21:687-709.

Deleu, D., Northway, M.G., Hanssens, Y. 2002. Clinical pharmacokinetic and pharmacodynamic properties of drugs used in the treatment of Parkinson's disease. *Clinical pharmacokinetics*, 41:261-309.

Dexter, D.T., Jenner, P. 2013. Parkinson disease: from pathology to molecular disease mechanisms. *Free radical biology and medicine*, 62:132-144.

Dixon, M. 1953. The determination of enzyme inhibitor constants. *The biochemical journal*, 55:170-171.

Djemgou, P.C., Gatsing, D., Tchuendem, M., Ngadjui, B.T., Tane, P., Ahmed, A.A., Gamal-Eldeen, A.M., Adoga, G.I., Hirata, T., Mabry, T.J. 2006. Antitumor and immunostimulatory activity of two chromones and other constituents from *Cassia petersiana*. *Natural product communications*, 1:961-968.

Duty, S., Jenner, P. 2011. Animal models of Parkinson's disease: a source of novel treatments and clues to the cause of the disease. *British journal of pharmacology*, 164:1357-1391.

Edmondson, D.E., Binda, C., Mattevi, A. 2007. Structural insights into the mechanism of amine oxidation by monoamine oxidases A and B. *Archives of biochemistry and biophysics*, 464:269-276.

Edmondson, D.E., Binda, C., Wang, J., Upadhyay, A.K., Mattevi, A. 2009. Molecular and mechanistic properties of the membrane-bound mitochondrial monoamine oxidases. *Biochemistry*, 48:4220-4230.

Edmondson, D.E., Mattevi, A., Binda, C., Li, M., Hubalek, F. 2004. Structure and mechanism of monoamine oxidase. *Current medicinal chemistry*, 11:1983-1993.

- Edwards, A.M., Howell, J.B.** 2000. The chromones: History, chemistry and clinical development. A tribute to the work of Dr R. E. C. Altounyan. *Clinical & experimental allergy*, 30:756-774.
- Ellis, G.P.** 2009. The chemistry of heterocyclic compounds, chromenes, chromanones, and chromones. New York: Wiley. p. 1196.
- Fearnley, J.M., Lees, A.J.** 1991. Ageing and Parkinson's disease: Substantia nigra regional selectivity. *Brain: A journal of neurology*, 114:2283-2301.
- Fernandez, H.H., Chen, J.J.** 2007. Monoamine oxidase-B inhibition in the treatment of Parkinson's disease. *Pharmacotherapy: The journal of human pharmacology and drug therapy*, 27:174S-185S.
- Fiedorowicz, J.G., Swartz, K.L.** 2004. The role of monoamine oxidase inhibitors in current psychiatric practice. *Journal of psychiatric practice*, 10:239-248.
- Finberg, J.P.M., Tenne, M., Youdim, M.B.H.** 1981. Tyramine antagonistic properties of AGN 1135, an irreversible inhibitor of monoamine oxidase type B. *British journal of pharmacology*, 73:65-74.
- Fitton, A.O., Frost, J.R., Houghton, P.G., Suschitzky, H.** 1979. Reactions of formyl chromone derivatives. Part 2. Addition reactions of 3-(aryliminoethyl)chromones. *Journal of the Chemical Society, Perkin Transactions*, 1:1691-1694.
- Foley, P., Riederer, P.** 2000. Influence of neurotoxins and oxidative stress on the onset and progression of Parkinson's disease. *Journal of neurology*, 247:1182-1194.
- Fornai, F., Chen, K., Giorgi, F.S., Gesi, M., Alessandri, M.G., Shih, J.C.** 1999. Striatal dopamine metabolism in monoamine oxidase B-deficient mice: A brain dialysis study. *Journal of neurochemistry*, 73:2434-2440.
- Forno, L.S.** 1996. Neuropathology of Parkinson's disease. *Journal of neuropathology and experimental neurology*, 55:259-272.
- Fox, S.H., Brotchie, J.M., Lang, A.E.** 2008. Non-dopaminergic treatments in development for Parkinson's disease. *The lancet neurology*, 7:927-938.

Fraaije, M.W., Mattevi, A. 2000. Flavoenzymes: Diverse catalysts with recurrent features. *Trends in biochemical sciences*, 25:126-132.

Gabor, M. 1986. Anti-inflammatory and anti-allergic properties of flavonoids. *Progress in clinical and biological research*, 213:471-480.

Gamal-Eldeen, A.M., Djemgou, P.C., Tchuendem, M., Ngadjui, B.T., Tane, P., Toshifumi, H. 2007. Anti-cancer and immunostimulatory activity of chromones and other constituents from *Cassia petersiana*. *Zeitschrift fur naturforschung C - A journal of biosciences*, 62:331-338.

Gareri, P., Falconi, U., De Fazio, P., De Sarro, G. 2000. Conventional and new antidepressant drugs in the elderly. *Progress in neurobiology*, 61:353-396.

Gaspar, A., Reis, J., Fonseca, A., Milhazes, N., Viña, D., Uriarte, E., Borges, F. 2011b. Chromone 3-phenylcarboxamides as potent and selective MAO-B inhibitors. *Bioorganic & medicinal chemistry letters*, 21:707-709.

Gaspar, A., Silva, T., Yáñez, M., Vina, D., Orallo, F., Ortuso, F., Uriarte, E., Alcaro, S., Borges, F. 2011a. Chromone, a privileged scaffold for the development of monoamine oxidase inhibitors. *Journal of medicinal chemistry*, 54:5165-5173.

Gibb, W.R., Lees, A.J. 1988. The relevance of the Lewy body to the pathogenesis of idiopathic Parkinson's disease. *Journal of neurology, neurosurgery & psychiatry*, 51:745-752.

Green, A.R., Mitchell, B.D., Tordoff, A.F.C., Youdim, M.B.H. 1977. Evidence for dopamine deamination by both type A and type B monoamine oxidase in rat brain *in vivo* and for the degree of inhibition of enzyme necessary for increased functional activity of dopamine and 5-hydroxytryptamine. *British journal of pharmacology*, 60:343-349.

Greenamyre, J.T., Sherer, T.B., Betarbet, R., Panov, A.V. 2001. Complex I and Parkinson's disease. *International union of biochemistry and molecular biology life*, 52:135-141.

Grindlay, D., Reynolds, T. 1986. The *Aloe vera* phenomenon: A review of the properties and modern uses of the leaf parenchyma gel. *Journal of ethnopharmacology*, 16:117-151.

Haefely, W., Burkard, W.P., Cesura, A.M., Kettler, R., Lorez, H.P., Martin, J.R., Richards, J.G., Scherschlicht, R., Da Prada, M. 1992. Biochemistry and pharmacology of moclobemide, a prototype RIMA. *Psychopharmacology*, 106:S6-14.

Halliday, G., Herrero, M.T., Murphy, K., McCann, H., Ros-Bernal, F., Barcia, C., Mori, H., Blesa, F.J., Obeso, J.A. 2009. No Lewy pathology in monkeys with over 10 years of severe MPTP parkinsonism. *Movement disorders*, 24:1519-1523.

Harfenist, M., Heuser, D.J., Joyner, C.T., Batchelor, J.F., White, H.L. 1996. Selective inhibitors of monoamine oxidase. Structure-activity relationship of tricyclics bearing imidazoline, oxadiazole, or tetrazole groups. *Journal of medicinal chemistry*, 39:1857-1863.

Huang, R.H., Faulkner, R. 1981. The role of phospholipid in the multiple functional forms of brain monoamine oxidase. *Journal of biological chemistry*, 256:9211-9215.

Hauser, R.A., Shulman, L.M., Trugman, J.M., Roberts, J.W., Mori, A., Ballerini, R., Sussman, N.M. 2008. Study of istradefylline in patients with Parkinson's disease on levodopa with motor fluctuations. *Movement disorders*, 23:2177-2185.

Heikkila, R.E., Manzino, L., Cabbat, F.S., Duvoisin, R.C. 1984. Protection against the dopaminergic neurotoxicity of 1-methyl-4-phenyl-1,2,5,6-tetrahydropyridine by monoamine oxidase inhibitors. *Nature*, 311:467-469.

Helguera, A.M., Pérez-Garrido, A., Gaspar, A., Reis, J., Cagide, F., Vina, D., Cordeiro, M., Borges, F. 2013. Combining QSAR classification models for predictive modelling of human monoamine oxidase inhibitors. *European journal of medicinal chemistry*, 59:75-90.

Heligman, L., Chen, N., Babakol, O. 2000. Shifts in the structure of population and deaths in less developed regions. (In Gribble, J.N. & Preston, S.H., eds. *The epidemiological transition policy and planning implications for developing countries*. Washington, D.C: National Academy Press. p. 9-41).

Henchcliffe, C., Beal, M.F. 2008. Mitochondrial biology and oxidative stress in Parkinson's disease pathogenesis. *Nature clinical practice neurology*, 4:600-609.

Henchcliffe, C., Schumacher, H.C., Burgut, F.T. 2005. Recent advances in Parkinson's disease therapy: Use of monoamine oxidase inhibitors. *Expert review of neurotherapeutics*, 5:811-821.

Herkenham, M., Lynn, A.B., Johnson, M.R., Melvin, L.S., de Costa, B.R., Rice, K.C. 1991. Characterization and localization of cannabinoid receptors in rat brain: A quantitative in vitro autoradiographic study. *The journal of neuroscience: The official journal of the society for neuroscience*, 11:563-583.

Hu, G., Bidel, S., Jousilahti, P., Antikainen, R., Tuomilehto, J. 2007. Coffee and tea consumption and the risk of Parkinson's disease. *Movement disorders*, 22:2242-2248.

Hubálek, F., Binda, C., Khalil, A., Li, M., Mattevi, A., Castagnoli, N., Edmondson, D.E. 2005. Demonstration of isoleucine 199 as a structural determinant for the selective inhibition of human monoamine oxidase B by specific reversible inhibitors. *Journal of biological chemistry*, 280:15761-15766.

Hubálek, F., Pohl, J., Edmondson, D.E. 2003. Structural comparison of human monoamine oxidases A and B: mass spectrometry monitoring of cysteine reactivities. *Journal of biological chemistry*, 278:28612-28618.

Ibrahim, M.A. 2009. Ring transformation of chromone-3-carboxamide. *Tetrahedron*, 65:7687-7690.

Ishar, M.P.S., Kumar, K., Singh, R. 1998. Thermal rearrangements of C-(4-oxo-4H[1]benzopyran-3-yl)-N-phenylnitronone-a route to novel quinolino[2,3-b]chroman-12-ones. *Tetrahedron letters*, 39:6547-6550.

Jenner, P. 2012. Mitochondria, monoamine oxidase B and Parkinson's disease. *Basal ganglia*, 2:S3-S7.

Jenner, P., Langston, J.W. 2011. Explaining ADAGIO: A critical review of the biological basis for the clinical effects of rasagiline. *Movement disorders*, 26:2316-2323.

Johannessen, J.N., Chiueh, C.C., Burns, R.S., Markey, S.P. 1985. IV. Differences in the metabolism of MPTP in the rodent and primate parallel differences in sensitivity to its neurotoxic effects. *Life sciences*, 36:219-224.

- Jouvet, M.** 1969. Biogenic amines and the states of sleep. *Science*, 163:32-41.
- Jovanovic, S.V., Steenken, S., Tosic, M., Marjanovic, B., Simic, M.G.** 1994. Flavonoids as antioxidants. *Journal of the American chemical society*, 116:4846-4851.
- Kaakkola, S.** 2000. Clinical pharmacology, therapeutic use and potential of COMT inhibitors in Parkinson's disease. *Drugs*, 59:1233-1250.
- Kearney, E.B., Salach, J.I., Walker, W.H., Seng, R.L., Kenney, W., Zeszotek, E., Singer, T.P.** 1971. The covalently-bound flavin of hepatic monoamine oxidase. *European journal of biochemistry*, 24:321-327.
- Kennelly, P., Rodwell, V.** 2009. Enzymes: Mechanism of action. (In Murray, K., Bender, D., Botham, K. M., Kennelly, P. J., Rodwell, V., Weil, P. A., eds. Harper's illustrated biochemistry. 28th ed. New York: McGraw-Hill. p. 62-74).
- Klann, E., Thiels, E.** 1999. Modulation of protein kinases and protein phosphatases by reactive oxygen species: Implications for hippocampal synaptic plasticity. *Progress in neuro-psychopharmacology and biological psychiatry*, 23:359-376.
- Kuroda, M., Uchida, S., Watanabe, K., Mimaki, Y.** 2009. Chromones from the tubers of *Eranthis cilicica* and their antioxidant activity. *Phytochemistry*, 70:288-293.
- Lamensdorf, I., Eisenhofer, G., Harvey-White, J., Nechustan, A., Kirk, K., Kopin, I.J.** 2000. 3,4-Dihydroxyphenylacetaldehyde potentiates the toxic effects of metabolic stress in PC12 cells. *Brain research*, 868:191-201.
- Lange, K.W., Paul, G.M., Naumann, M., Gsell, W.** 1995. Dopaminergic effects on cognitive performance in patients with Parkinson's disease. *Journal of neural transmission*, 46:423-432.
- Langston, J., Forno, L., Tetrud, J., Reeves, A., Kaplan, J., Karluk, D.** 1999. Evidence of active nerve cell degeneration in the substantia nigra of humans years after 1-methyl-4-phenyl-1, 2, 3, 6-tetrahydropyridine exposure. *Annals of neurology*, 46:598-605.
- Langston, J.W.** 2006. The Parkinson's complex: parkinsonism is just the tip of the iceberg. *Annual neurology*, 59:591-596.

Langston, J.W., Ballard, P., Tetrud, J.W., Irwin, I. 1983. Chronic parkinsonism in humans due to a product of meperidine-analog synthesis. *Science*, 219:979-980.

Lees, A. 2005. Alternatives to levodopa in the initial treatment of early Parkinson's disease. *Drugs & aging*, 22:731-740.

Lees, A.J., Hardy, J., Revesz, T. 2009. Parkinson's disease. *The lancet*, 373:2055-2066.

Legoabe, L.J., Petzer, A., Petzer, J.P. 2012a. Inhibition of monoamine oxidase by selected C6-substituted chromone derivatives. *European journal of medicinal chemistry*, 49:343-353.

Legoabe, L.J., Petzer, A., Petzer, J.P. 2012b. Selected C7-substituted chromone derivatives as monoamine oxidase inhibitors. *Bioorganic chemistry*, 45:1-11.

Legoabe, L.J., Petzer, A., Petzer, J.P. 2012c. Selected chromone derivatives as inhibitors of monoamine oxidase. *Bioorganic & medicinal chemistry letters*, 22:5480-5484.

Legoabe, L.J., Petzer, A., Petzer, J.P. 2014. α -Tetralone derivatives as inhibitors of monoamine oxidase. *Bioorganic & medicinal chemistry letters*, 24:2758-2763.

LeWitt, P.A., Taylor, D.C. 2008. Protection against Parkinson's disease progression: Clinical experience. *Neurotherapeutics*, 5:210-225.

Lu, X., Rodriguez, M., Silverman, R.B., Vintem, A.P.B., Ramsay, R.R. 2002. Irreversible inactivation of mitochondrial monoamine oxidase. (*In* Chapman, S.K., Perham, R.N. & Scrutton, N.S., eds. *Flavins and flavoproteins: Proceedings of the 14th International Symposium*. Berlin, Germany: Rudolf Weber. p. 817-830).

Machado, N.F.L., Marques, M.P.M. 2010. Bioactive chromone derivatives - structural diversity. *Current bioactive compounds*, 6:76.

Mahmood, I. 1997. Clinical pharmacokinetics and pharmacodynamics of selegiline. an update. *Clinical pharmacokinetics*, 33:91-102.

Manley-King, C.I., Bergh, J.J., Petzer, J.P. 2011. Inhibition of monoamine oxidase by selected C5- and C6-substituted isatin analogues. *Bioorganic and medicinal chemistry*, 19:261-274.

Martens, S., Mithöfer, A. 2005. Flavones and flavone synthases. *Phytochemistry*, 66:2399-2407.

Maruyama, W., Youdim, M.B.H., Naoi, M. 2001. Antiapoptotic properties of rasagiline, N-propargylamine-1(*R*)-aminoindan, and its optical (*S*)-isomer, TV1022. *Annals of the New York academy of sciences*, 939:320-329.

Mason, R.P., Olmstead Jr, E.G., Jacob, R.F. 2000. Antioxidant activity of the monoamine oxidase B inhibitor lazabemide. *Biochemical pharmacology*, 60:709-716.

Milevskii, B., Chibisova, T., Solov'eva, N., Anisimova, O., Lebedev, V., Ivanov, I., Traven, V. 2013. Synthesis and structure of Schiff bases derived from 3-formyl-4-hydroxycoumarin and diamines. *Chemistry of heterocyclic compounds*, 48:1781-1792.

Miller, J.R., Edmondson, D.E. 1999. Structure-activity relationships in the oxidation of para-substituted benzylamine analogues by recombinant human liver monoamine oxidase A. *Biochemistry*, 38:13670-13683.

Mody, I., MacDonald, J.F. 1995. NMDA receptor-dependent excitotoxicity: The role of intracellular Ca^{2+} release. *Trends in pharmacological sciences*, 16:356-359.

Montastruc, J., Chaumerliac, C., Desboeuf, K., Manika, M., Bagheri, H., Rascol, O., Lapeyre-Mestre, M. 2000. Adverse drug reactions to selegiline: A review of the French pharmacovigilance database. *Clinical neuropharmacology*, 23:271-275.

Morelli, M., Di Paolo, T., Wardas, J., Calon, F., Xiao, D., Schwarzschild, M.A. 2007. Role of adenosine A_{2A} receptors in parkinsonian motor impairment and L-DOPA-induced motor complications. *Progress in neurobiology*, 83:293-309.

Muramatsu, Y., Araki, T. 2002. Glial cells as a target for the development of new therapies for treating Parkinson's disease. *Drug news & perspectives*, 15:586-590.

Nicklas, W.J., Vyas, I., Heikkila, R.E. 1985. Inhibition of NADH-linked oxidation in brain mitochondria by 1-methyl-4-phenyl-pyridine, a metabolite of the neurotoxin 1-methyl-4-phenyl-1,2,5,6-tetrahydropyridine. *Life science*, 36:2503-2508.

- Novaroli, L., Reist, M., Favre, E., Carotti, A., Catto, M., Carrupt, P.** 2005. Human recombinant monoamine oxidase B as reliable and efficient enzyme source for inhibitor screening. *Bioorganic and medicinal chemistry*, 13:6212-6217.
- Okubadejo, N.U., Bower, J.H., Rocca, W.A., Maraganore, D.M.** 2006. Parkinson's disease in Africa: A systematic review of epidemiologic and genetic studies. *Movement disorders*, 21:2150-2156.
- Okumura, K., Kondo, K., Oine, T., Inoue, I.** 1974. Synthesis of chromone-3-carboxanilides. *Chemical & pharmaceutical bulletin*, 22:331-336.
- Olanow, C.W.** 2004. The scientific basis for the current treatment of Parkinson's disease. *Annual review of medicine*, 55:41-60.
- Olanow, C.W., Tatton, W.G.** 1999. Etiology and pathogenesis of Parkinson's disease. *Annual review of neuroscience*, 22:123-144.
- Olanow, C.W., Watts, R.L., Koller, W.C.** 2001. An algorithm (decision tree) for the management of Parkinson's disease. *Neurology*, 56:S1-S88.
- Ortwine, D.F.** 2004. Chromone derivatives as matrix metalloproteinase inhibitors. (Patent: WO2004014880 A1).
- Parkinson Study Group.** 1993. Effects of tocopherol and deprenyl on the progression of disability in early Parkinson's disease. *New England journal of medicine*, 328:176-183.
- Parmar, N. S., Tariq, M., Ageel, A. M.** 1987. Effect of thromboxane A₂ and leukotriene C₄ inhibitors on the experimentally induced gastric lesions in the rat. *Research Communications in Chemical Pathology and Pharmacology*, 58: 15-25.
- Petzer, A., Harvey, B.H., Wegener, G., Petzer, J.P.** 2012. Azure B, a metabolite of methylene blue, is a high-potency, reversible inhibitor of monoamine oxidase. *Toxicology and applied pharmacology*, 258:403-409.
- Petzer, A., Pienaar, A., Petzer, J.P.** 2013. The inhibition of monoamine oxidase by esomeprazole. *Drug research*, 63:462-467.

Pisani, L., Barletta, M., Soto-Otero, R., Nicolotti, O., Mendez-Alvarez, E., Catto, M., Introcaso, A., Stefanachi, A., Cellamare, S., Altomare, C., Carotti, A. 2013. Discovery, biological evaluation, and structure–activity and –selectivity relationships of 6'-substituted (E)-2-(benzofuran-3(2H)-ylidene)-N-methylacetamides, a novel class of potent and selective monoamine oxidase inhibitors. *Journal of medicinal chemistry*, 56:2651-2664.

Popat, R.A., Van Den Eeden, S.K., Tanner, C.M., McGuire, V., Bernstein, A.L., Bloch, D.A., Leimpeter, A., Nelson, L.M. 2005. Effect of reproductive factors and postmenopausal hormone use on the risk of Parkinson's disease. *Neurology*, 65:383-390.

Priyadarshi, A., Khuder, S.A., Eric A. Schaub, E.A., Priyadarshi, S.S. 2001. Environmental risk factors and Parkinson's disease: A metaanalysis. *Environmental research*, 86:122-127.

Ragonese, P., D'Amelio, M., Salemi, G., Aridon, P., Gammino, M., Epifanio, A., Morgante, L., Savettieri, G. 2004. Risk of Parkinson's disease in women: effect of reproductive characteristics. *Neurology*, 62:2010-2014.

Riederer, P., Youdim, M., Rausch, W., Birkmayer, W., Jellinger, K., Seemann, D. 1978. On the mode of action of L-deprenyl in the human central nervous system. *Journal of neural transmission*, 43:217-226.

Rogers, A., Gibon, Y. 2009. Enzyme kinetics: Theory and practice. (*In Plant Metabolic Networks*. Schwender, J., ed. New York: Springer. p. 71-103).

Ross, G.W., Abbott, R.D. 2014. Living and dying with Parkinson's disease. *Movement disorders*, 13:1571-1573.

Ross, G.W., Abbott, R.D., Petrovitch, H., Morens, D.M., Grandinetti, A., Tung, K.H., Tanner, C.M., Masaki, K.H., Blanchette, P.L., Curb, J.D., Popper, J.S., White, L. 2000. Association of coffee and caffeine intake with the risk of Parkinson disease. *Journal of the American medical association*, 283:2674-2679.

Sagi, Y., Drigues, N., Youdim, M.B. 2005. The neurochemical and behavioral effects of the novel cholinesterase-monoamine oxidase inhibitor, ladostigil, in response to l-dopa and l-tryptophan, in rats. *British journal of pharmacology*, 146:553-560.

- Saura, J., Bleuel, Z., Ulrich, J., Mendelowitsch, A., Chen, K., Shih, J.C., Malherbe, P., Da Prada, M., Richards, J.G.** 1996. Molecular neuroanatomy of human monoamine oxidases A and B revealed by quantitative enzyme radioautography and in situ hybridization histochemistry. *Neuroscience*, 70:755-774.
- Schapira, A.H.** 2006. Mitochondrial disease. *The lancet*, 368:70-82.
- Schapira, A.H., Jenner, P.** 2011. Etiology and pathogenesis of Parkinson's disease. *Movement disorders*, 26:1049-1055.
- Schapira, A.V.** 2011. Monoamine oxidase B inhibitors for the treatment of Parkinson's disease. *CNS drugs*, 25:1061-1071.
- Schwarzschild, M.A., Agnati, L., Fuxe, K., Chen, J., Morelli, M.** 2006. Targeting adenosine A_{2A} receptors in Parkinson's disease. *Trends in neurosciences*, 29:647-654.
- Shashidharan, P., Good, P.F., Hsu, A., Perl, D.P., Brin, M.F., Olanow, C.W.** 2000. Torsin A accumulation in Lewy bodies in sporadic Parkinson's disease. *Brain research*, 877:379-381.
- Shin, M.H., Jang, J.H., Surh, Y.J.** 2004. Potential roles of NF-kappa B and ERK1/2 in cytoprotection against oxidative cell death induced by tetrahydropapaveroline. *Free radical biology & medicine*, 36:1185-1194.
- Singh, R., Sharma, N.** 2014. Monoamine oxidase inhibitors for neurological disorders: A review. *Chemical biology letters*, 1:33-39.
- Smith, Y., Wichmann, T., Factor, S.A., DeLong, M.R.** 2011. Parkinson's disease therapeutics: New developments and challenges since the introduction of levodopa. *Neuropsychopharmacology*, 37:213-246.
- Son, S., Ma, J., Kondou, Y., Yoshimura, M., Yamashita, E., Tsukihara, T.** 2008. Structure of human monoamine oxidase A at 2.2-Å resolution: The control of opening the entry for substrates/inhibitors. *Proceedings of the national academy of sciences of the United States of America*, 105:5739-5744.

Sonsalla, P.K., Heikkila, R.E. 1988. Neurotoxic effects of 1-methyl-4-phenyl-1,2,3,6-tetrahydropyridine (MPTP) and methamphetamine in several strains of mice. *Progress in neuro-psychopharmacology and biological psychiatry*, 12:345-354.

Speciale, S.G. 2002. MPTP: Insights into parkinsonian neurodegeneration. *Neurotoxicology and teratology*, 24:607-620.

Spillantini, M.G., Crowther, R.A., Jakes, R., Hasegawa, M., Goedert, M. 1998. Alpha-synuclein in filamentous inclusions of Lewy bodies from Parkinson's disease and dementia with Lewy bodies. *Proceedings of the national academy of sciences of the United States of America*, 95:6469-6473.

Staab, H.A. 1962. New methods of preparative organic chemistry IV. Synthesis using heterocyclic amides (azolides). *Angewandte chemie*, international edition, 1:351-367.

Standaert, D.G., Roberson, E.D. 2011. Treatment of central nervous system degenerative disorders. (In Brunton, L.L., Chabner, B.A. & Knollmann, B.C., eds. Goodman & Gilman's The pharmacological basis of therapeutics. 12th ed. New York: McGraw-Hill. p. 611-619).

Stocchi, F. 2014. Therapy for Parkinson's disease: What is in the pipeline? *Neurotherapeutics*, 11:24-33.

Strakova, I., Petrova, M., Belyakov, S., Strakovs, A. 2006. Reactions of 4-chloro-3-formyl-coumarin with primary amines. *Chemistry of heterocyclic compounds*, 42:574-582.

Strydom, B., Malan, S.F., Castagnoli Jr., N., Bergh, J.J., Petzer, J.P. 2010. Inhibition of monoamine oxidase by 8-benzyloxycaffeine analogues. *Bioorganic and medicinal chemistry*, 18:1018-1028.

Sumiyoshi, M., Kimura, Y. 2010. Enhancing effects of a chromone glycoside, eucryphin, isolated from *Astilbe* rhizomes on burn wound repair and its mechanism. *Phytomedicine*, 17:820-829.

Tanner, C.M., Langston, J.W. 1990. Do environmental toxins cause Parkinson's disease? A critical review. *Neurology*, 40: 17-30.

Tatton, W.G., Chalmers-Redman, R.M.E., Ju, W.J.H. 2002. Propargylamines induce antiapoptotic new protein synthesis in serum- and nerve growth factor (NGF)-withdrawn, NGF-differentiated PC-12 cells. *Journal of pharmacology and experimental therapeutics*, 301:753-764.

Tatton, W.G., Wadia, J.S., Ju, W.Y., Chalmers-Redman, R.M., Tatton, N.A. 1996. (-)-Deprenyl reduces neuronal apoptosis and facilitates neuronal outgrowth by altering protein synthesis without inhibiting monoamine oxidase. *Journal of neural transmission*, 48:45-59.

Timar, J. 1988. Recovery of MAO-B enzyme activity after (-)deprenyl (selegiline) pretreatment, measured in vivo. *Acta physiologica hungarica*, 74:259-266.

Traven, V., Ivanov, I., Lebedev, V., Chibisova, T., Milevskii, B., Solov'eva, N., Polshakov, V., Alexandrov, G., Kazheva, O., Dyachenko, O. 2010. E/Z (C=C)-isomerization of enamines of 3-formyl-4-hydroxycoumarin induced by organic solvents. *Russian chemical bulletin*, 59:1605-1611.

Veselovsky, A.V., Ivanov, A.S., Medvedev, A.E. 2004. Computer modelling and visualization of active site of monoamine oxidases. *Neurotoxicology*, 25:37-46.

Walker, M.C., Edmondson, D.E. 1994. Structure-activity relationships in the oxidation of benzylamine analogs by bovine liver mitochondrial monoamine oxidase B. *Biochemistry*, 33:7088-7098.

Wang, C.C., Billett, E., Borchert, A., Kuhn, H., Ufer, C. 2013. Monoamine oxidases in development. *Cellular and molecular life sciences*, 70:599-630.

Weinreb, O., Amit, T., Bar-Am, O., Chillag-Talmor, O., Youdim, M.B.H. 2005. Novel neuroprotective mechanism of action of rasagiline is associated with its propargyl moiety: Interaction of bcl-2 family members with PKC pathway. *Annals of the New York academy of sciences*, 1053:348-355.

Wichmann, T., DeLong, M.R. 1993. Neurocircuitry of Parkinson's disease. (In Davis, K.L., Charney, D., Coyle, J.T., Nemeroff, C., eds. *Neuropsychopharmacology: The fifth generation of progress*. Philadelphia: Lippincott; Williams & Wilkins, 122:1761-1779).

Wouters, J. 1998. Structural aspects of monoamine oxidase and its reversible inhibition. *Current medicinal chemistry*, 5:137-162.

Wu, H.F., Chen, K., Shih, J.C. 1993. Site-directed mutagenesis of monoamine oxidase A and B: Role of cysteines. *Molecular pharmacology*, 43:888-893.

Yacoubian, T.A., Standaert, D.G. 2009. Targets for neuroprotection in Parkinson's disease. *Biochimica et biophysica acta - molecular basis of disease*, 1792:676-687.

Yamada, M., Yasuhara, H. 2004. Clinical pharmacology of MAO inhibitors: Safety and future. *Neurotoxicology*, 25:215-221.

Youdim, M.B., Buccafusco, J.J. 2005. Multi-functional drugs for various CNS targets in the treatment of neurodegenerative disorders. *Trends in pharmacological sciences*, 26:27-35.

Youdim, M.B.H., Bakhle, Y.S. 2006. Monoamine oxidase: Isoforms and inhibitors in Parkinson's disease and depressive illness. *British journal of pharmacology*, 147:S287-S296.

Youdim, M.B.H., Edmondson, D., Tipton, K.F. 2006. The therapeutic potential of monoamine oxidase inhibitors. *Nature reviews neuroscience*, 7:295-309.

Youdim, M.B.H., Finberg, J.P.M., Tipton, K.F. 1988. Monoamine oxidase. (In Trendelenburg, U. & Weiner, U., eds. Catecholamines. 1st ed. Berlin: Springer-Verlag. p. 119-192).

Youdim, M.B.H., Gross, A., Finberg, J.P.M. 2001. Rasagiline [N-propargyl-1R(+)-aminoindan], a selective and potent inhibitor of mitochondrial monoamine oxidase B. *British journal of pharmacology*, 132:500-506.

Zecca, L., Youdim, M.B.H., Riederer, P., Connor, J.R., Crichton, R.R. 2004. Iron, brain ageing and neurodegenerative disorders. *Nature reviews neuroscience*, 5:863-873.

Zhou, T., Shi, Q., Lee, K.H. 2010. Anti-AIDS agents 83. Efficient microwave-assisted one-pot preparation of angular 2,2-dimethyl-2H-chromone containing compounds. *Tetrahedron letters*, 51:4382-4386.

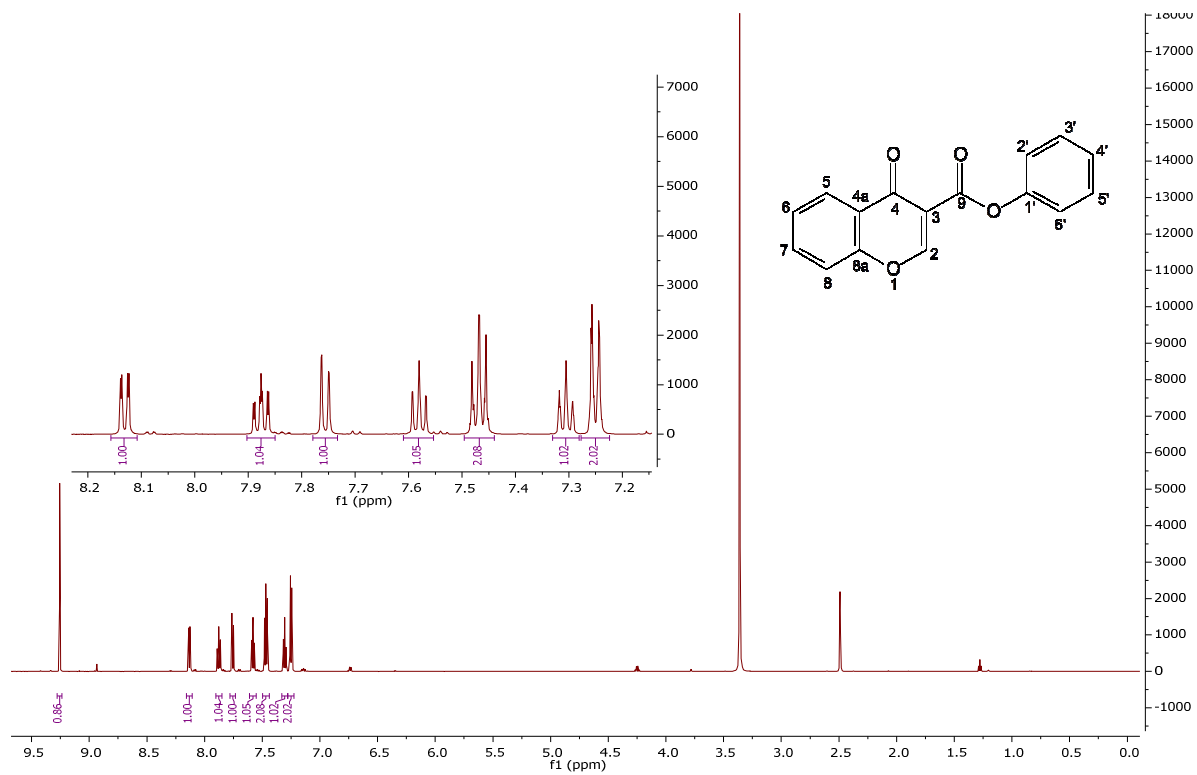
Zhu, W., Xie, W., Pan, T., Jankovic, J., Li, J., Youdim, M.B.H., Le, W. 2008. Comparison of neuroprotective and neurorestorative capabilities of rasagiline and selegiline against lactacystin-induced nigrostriatal dopaminergic degeneration. *Journal of neurochemistry*, 105:1970-1978.

ADDENDUM

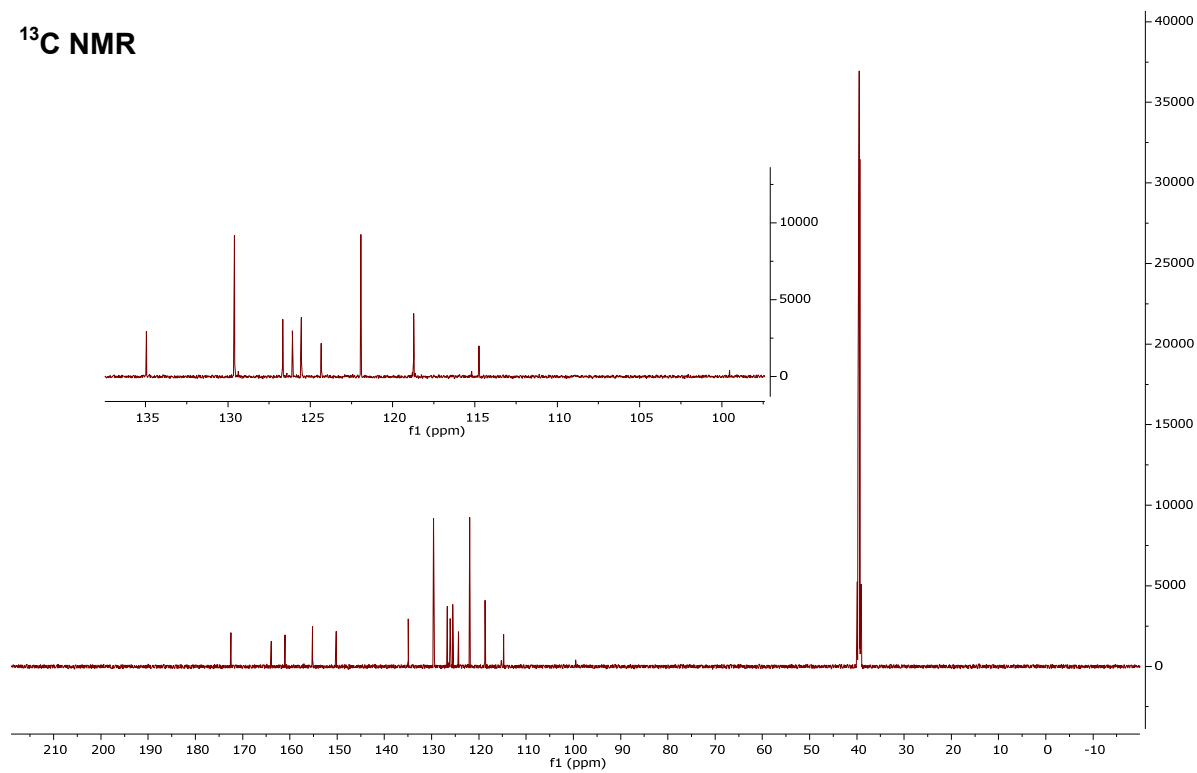
LIST OF ¹ H NMR AND ¹³ C NMR SPECTRA	113
LIST OF MASS SPECTROMETRY DATA	132
LIST OF INFRA-RED SPECTRA.....	140
LIST OF HPLC DATA.....	148
SUPPLEMENTARY DATA ON CRYSTAL STRUCTURE.....	155

Phenyl 4-oxo-4*H*-chromene-3-carboxylate (**31**)

¹H NMR

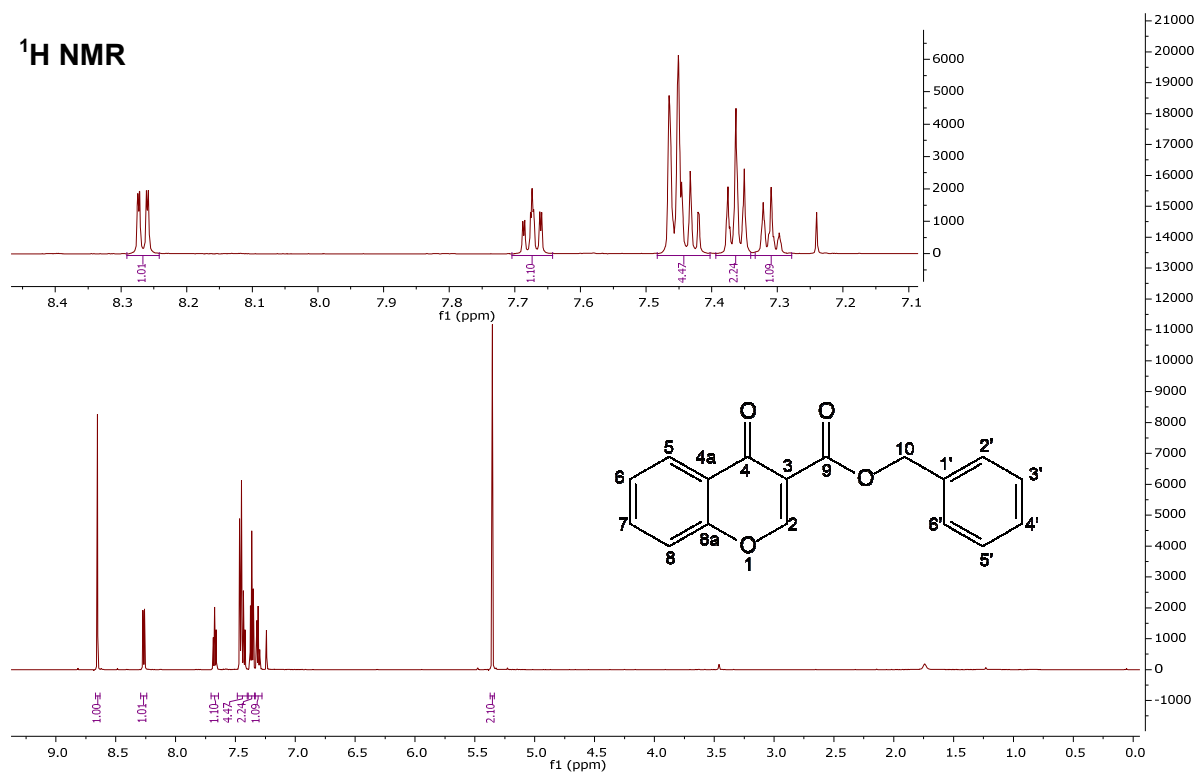


¹³C NMR

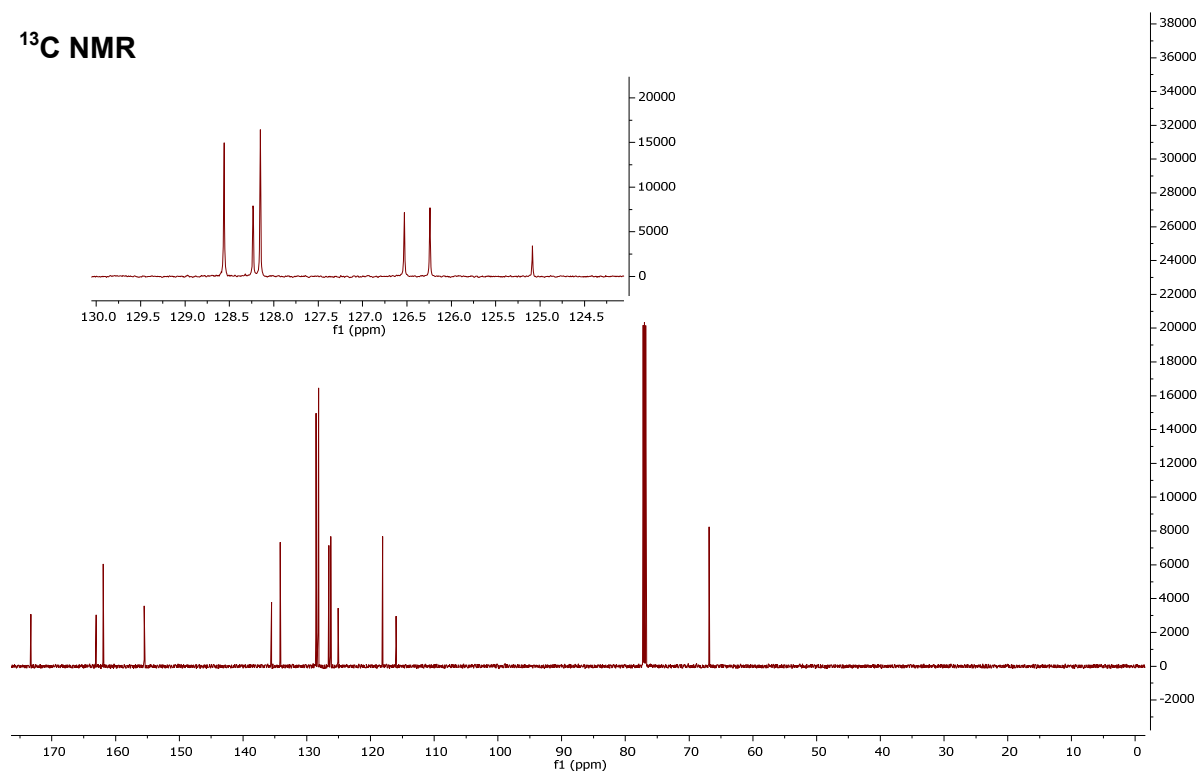


Benzyl 4-oxo-4*H*-chromene-3-carboxylate (**32**)

¹H NMR

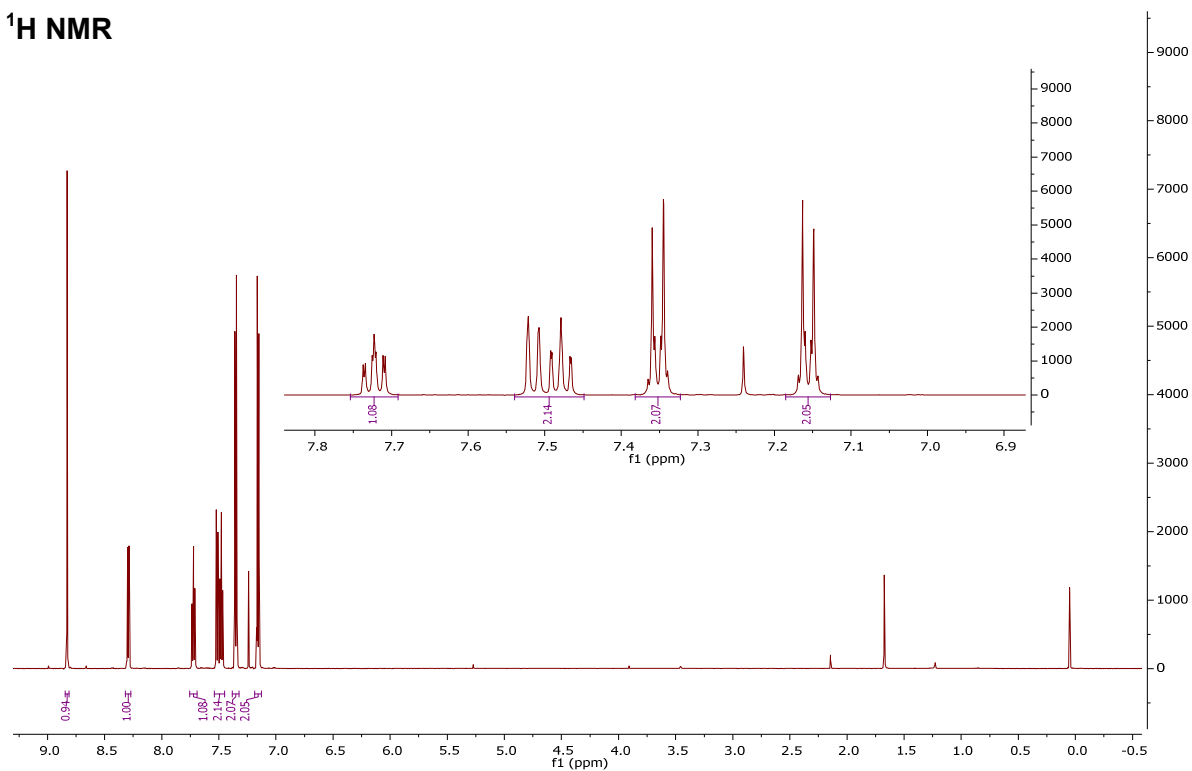


¹³C NMR

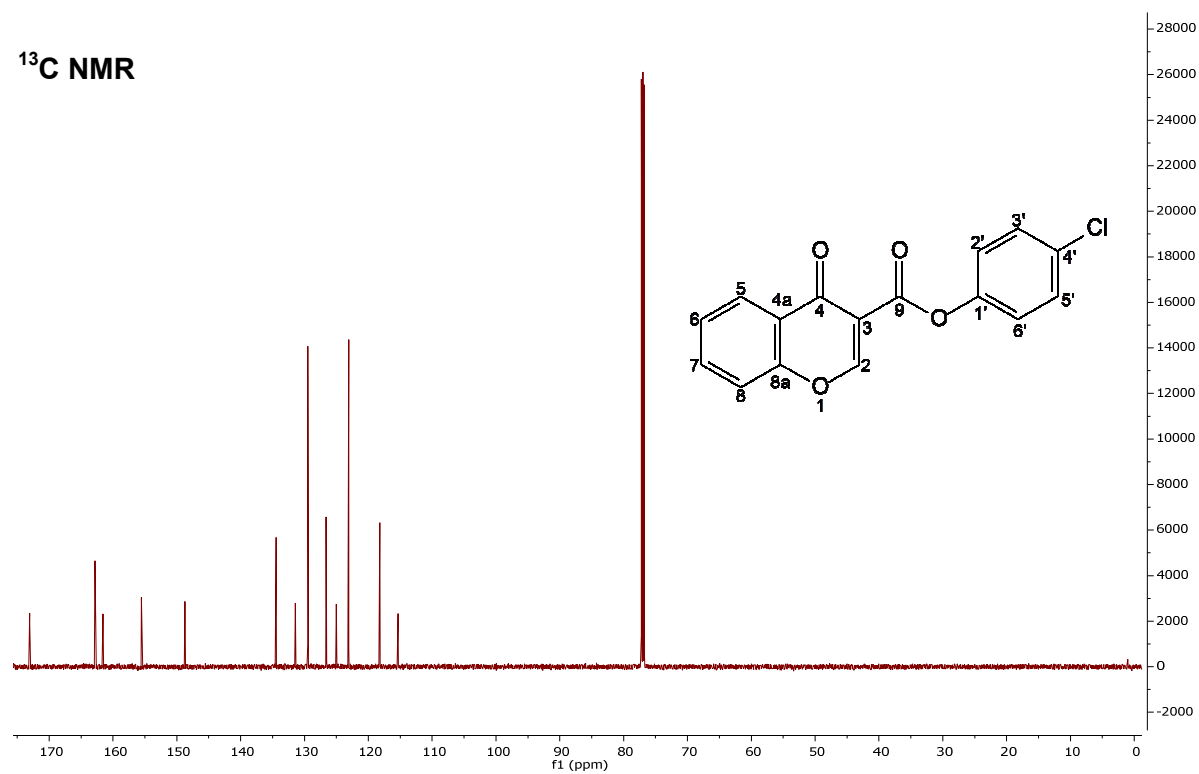


4-chlorophenyl-4-oxo-4H-chromene-3-carboxylate (**33**)

¹H NMR

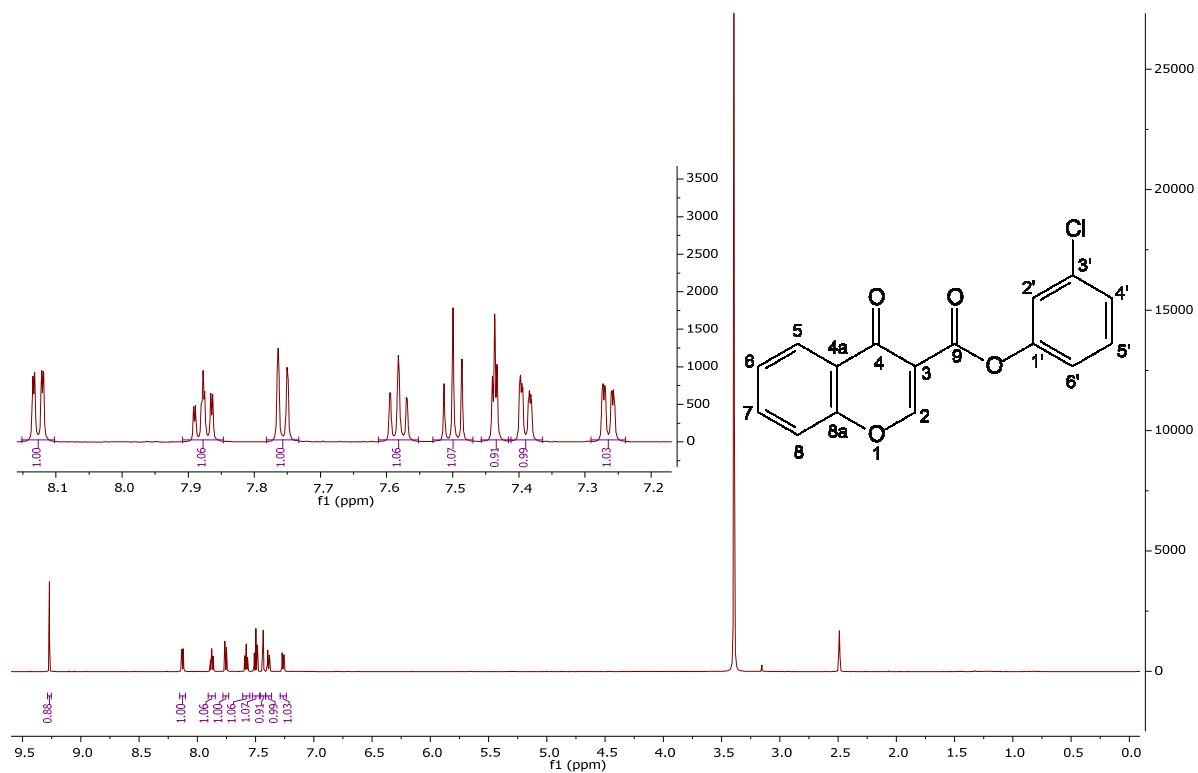


¹³C NMR

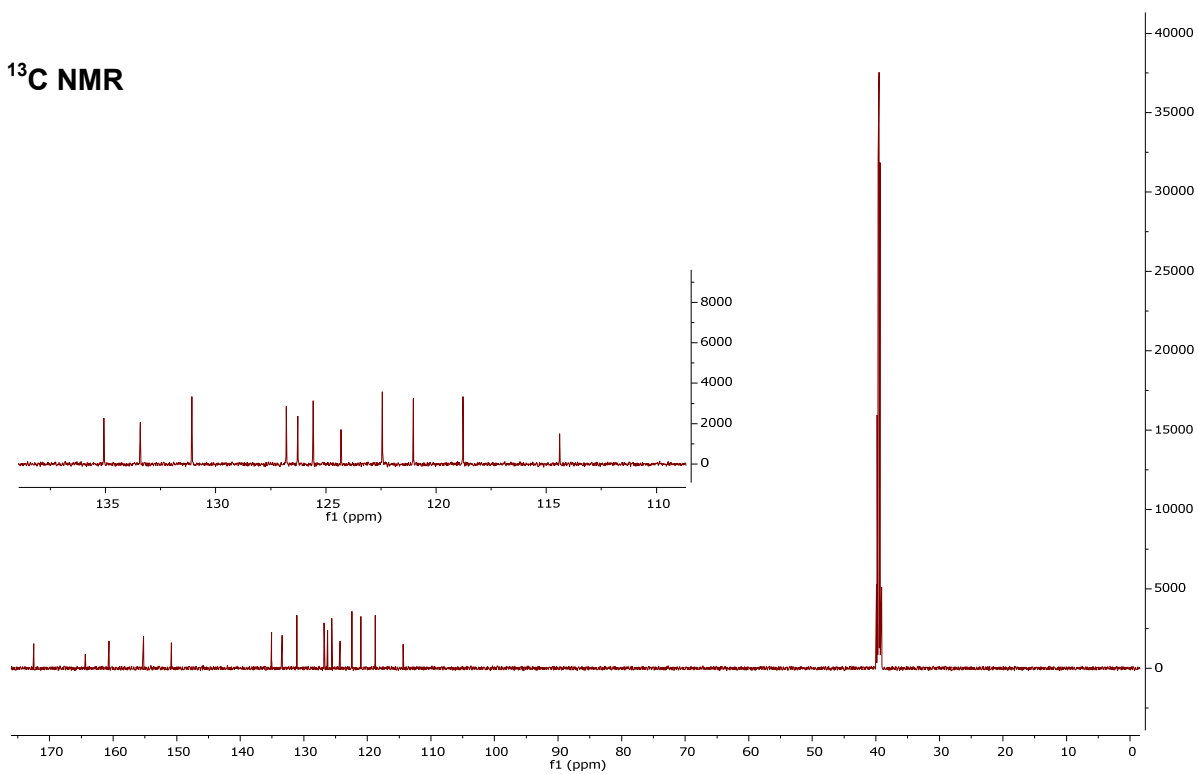


3-chlorophenyl 4-oxo-4*H*-chromene-3-carboxylate (**34**)

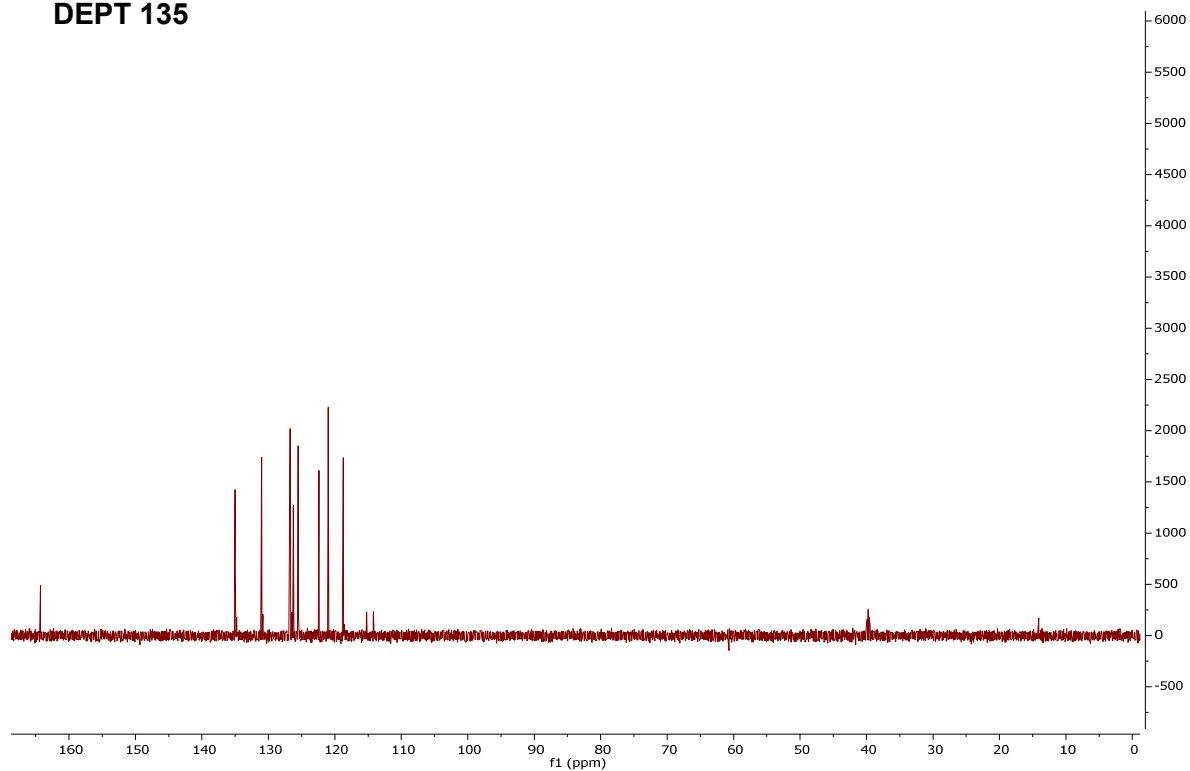
¹H NMR



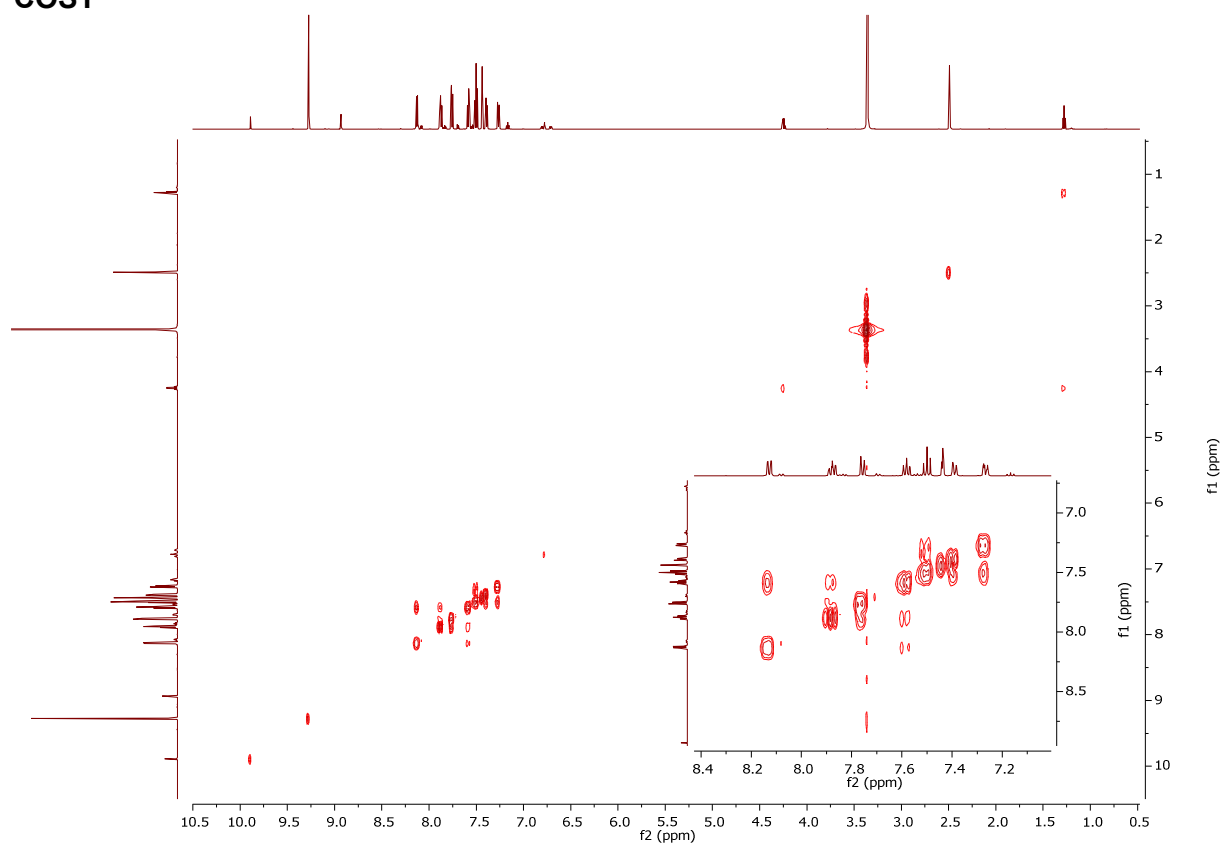
¹³C NMR



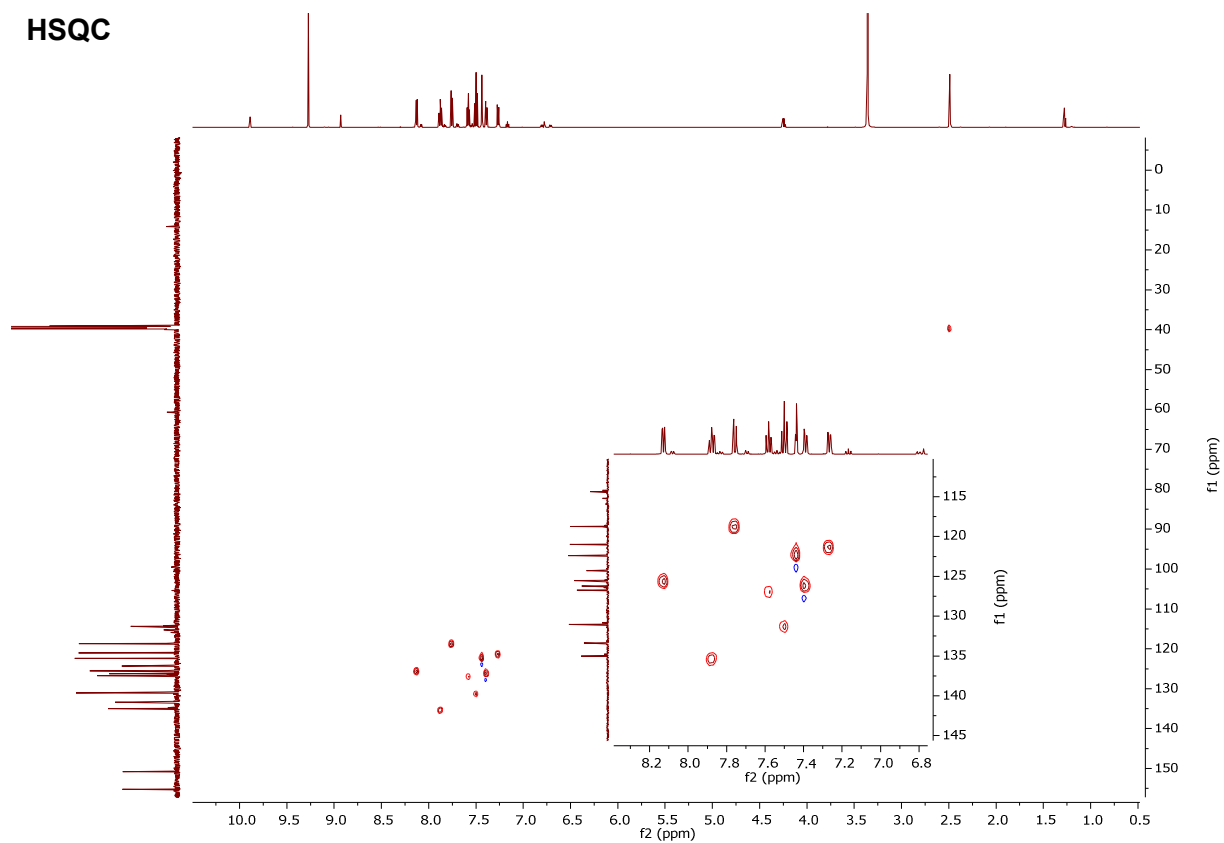
DEPT 135



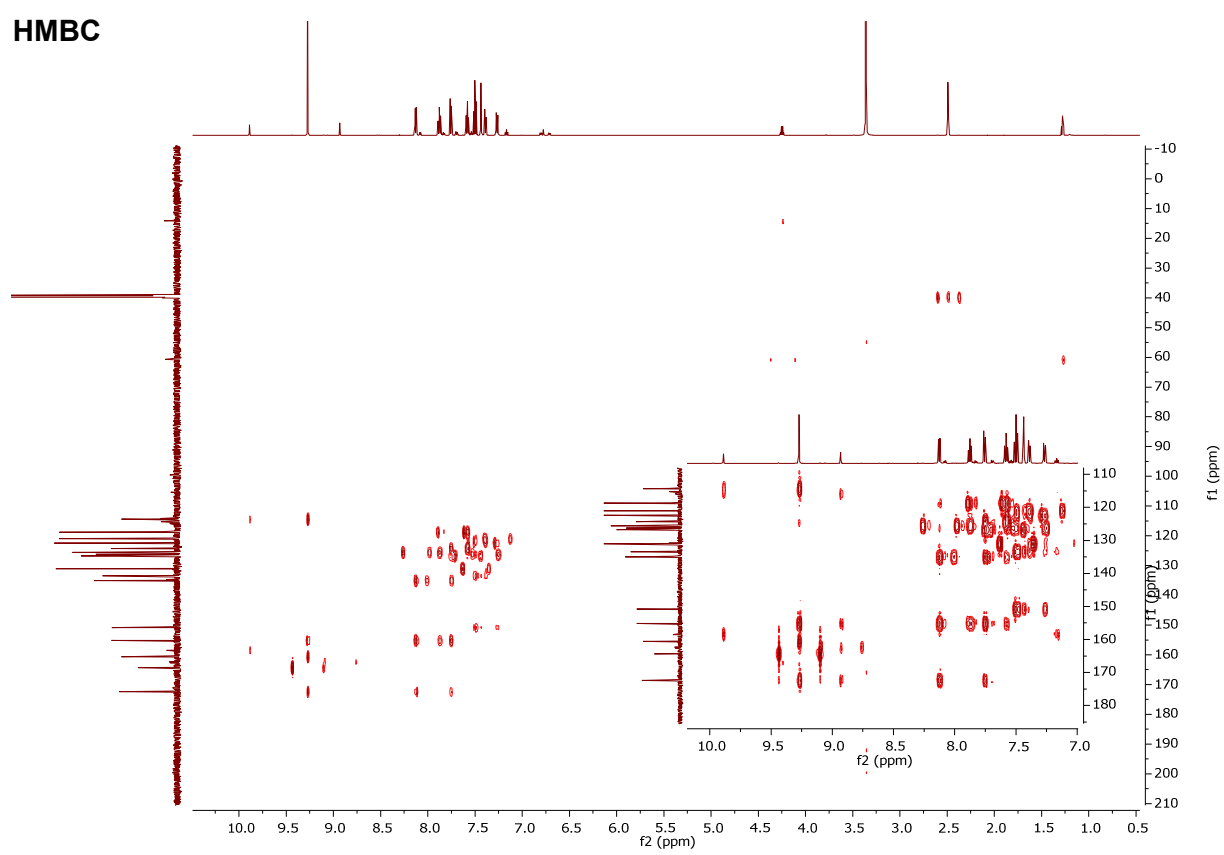
COSY



HSQC

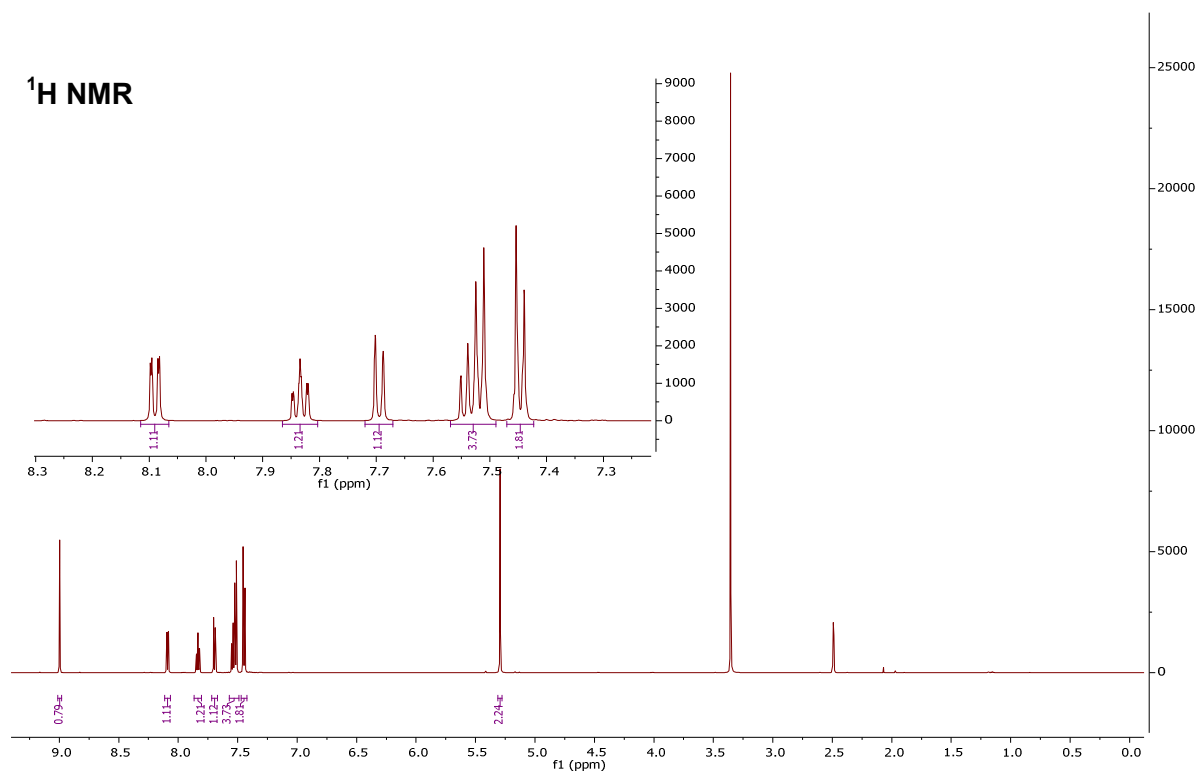


HMBC

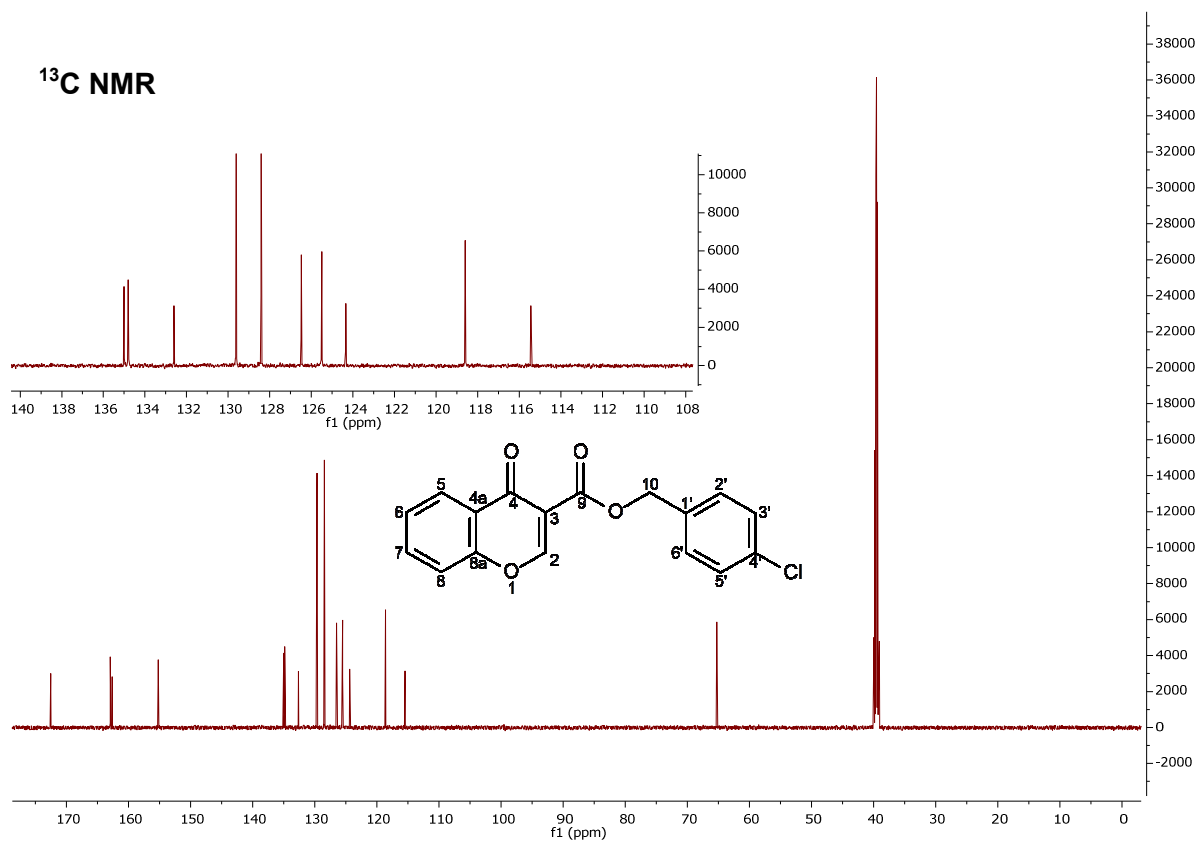


(4-chlorophenyl)methyl-4-oxo-4H-chromene-3-carboxylate (35)

¹H NMR

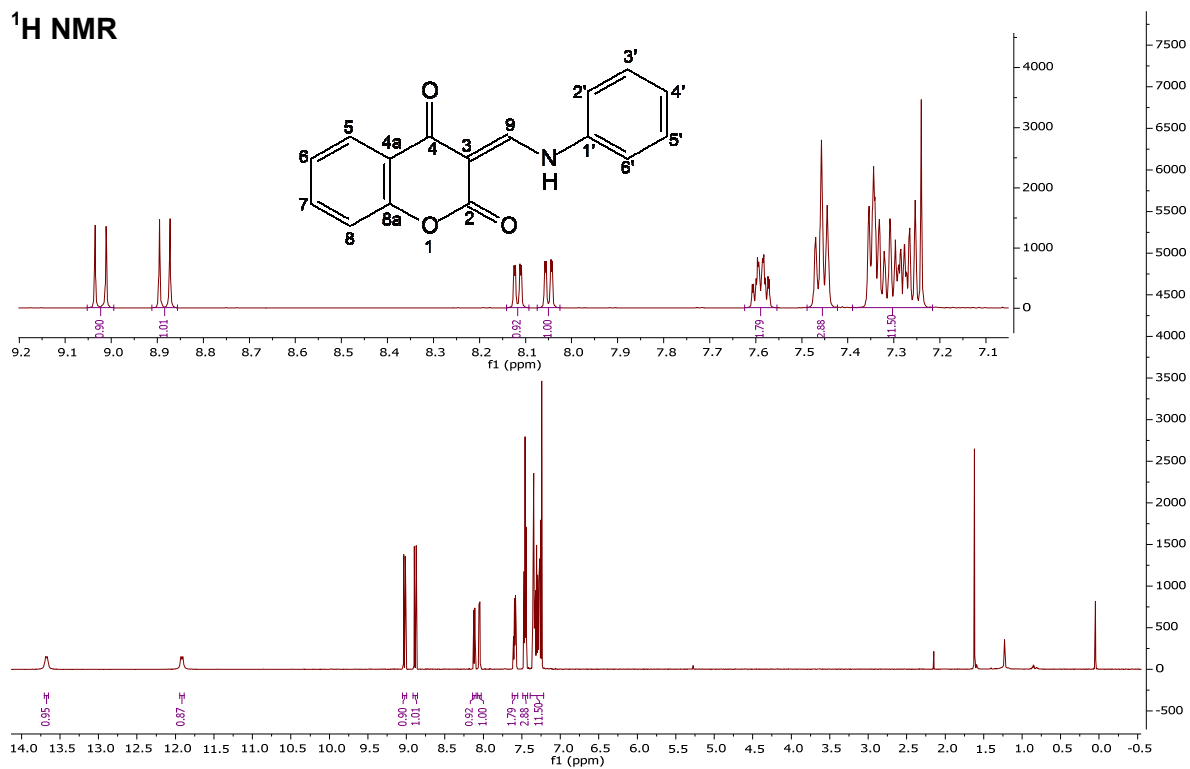


¹³C NMR

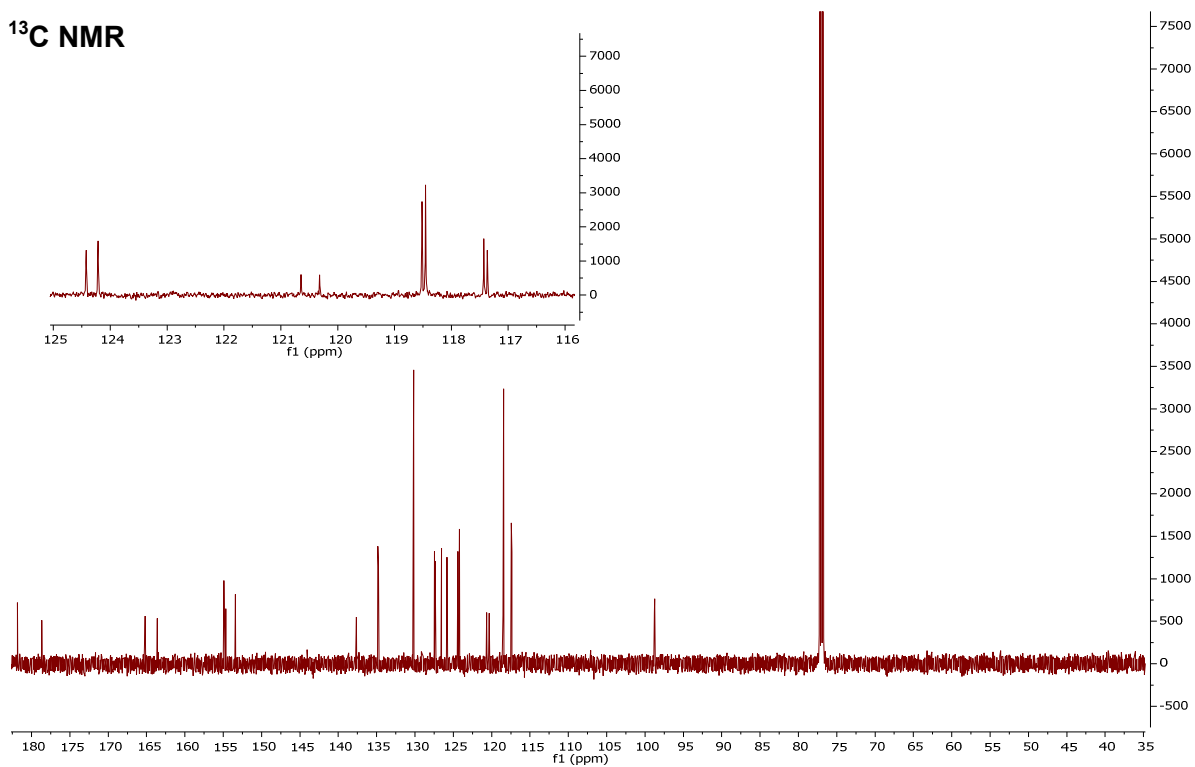


(3E/Z)-3-[(phenylamino)methylidene]-3,4-dihydro-2H-1-benzopyran-2,4-dione (37)

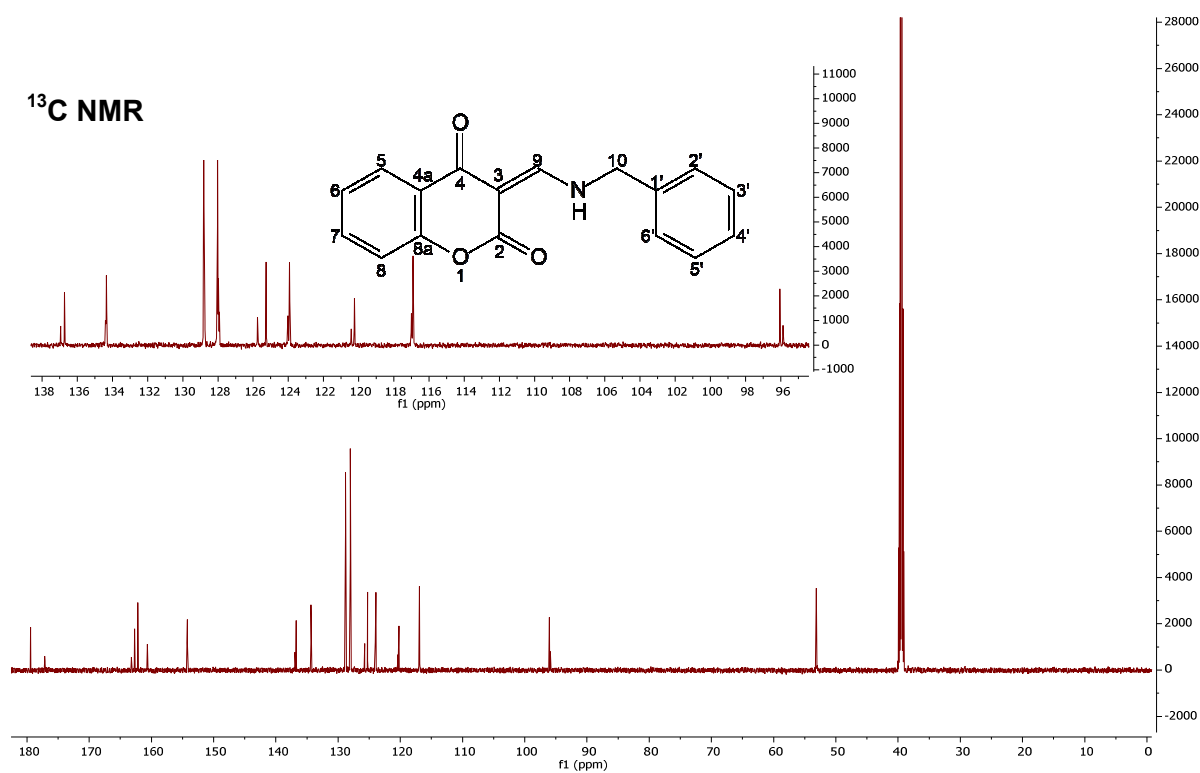
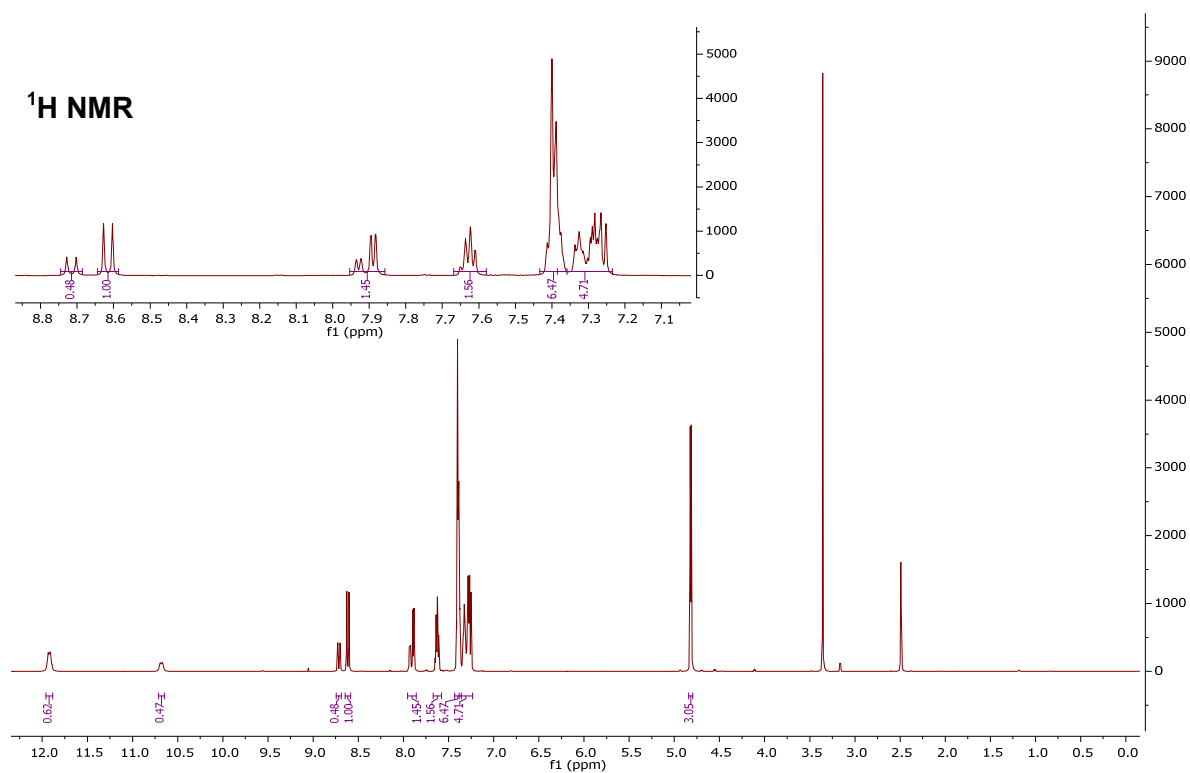
¹H NMR



¹³C NMR

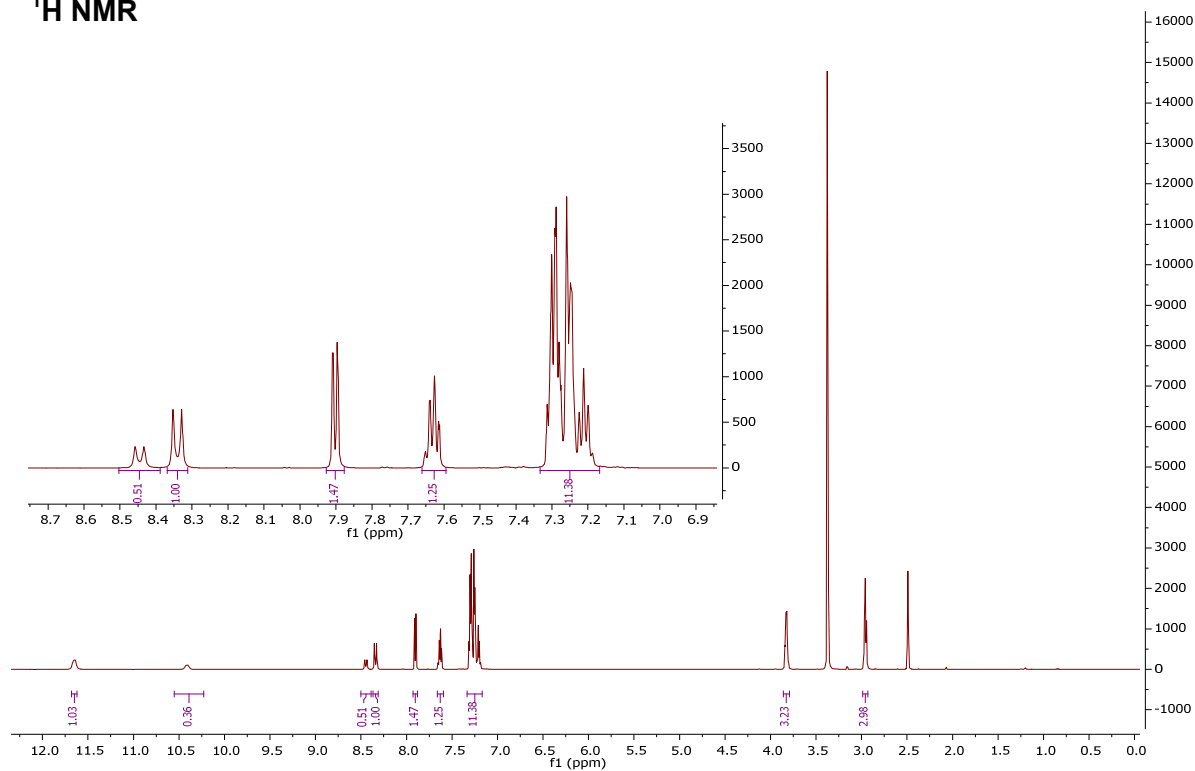


(3E/Z)-3-[(benzylamino)methylidene]-3,4-dihydro-2H-1-benzopyran-2,4-dione (38)

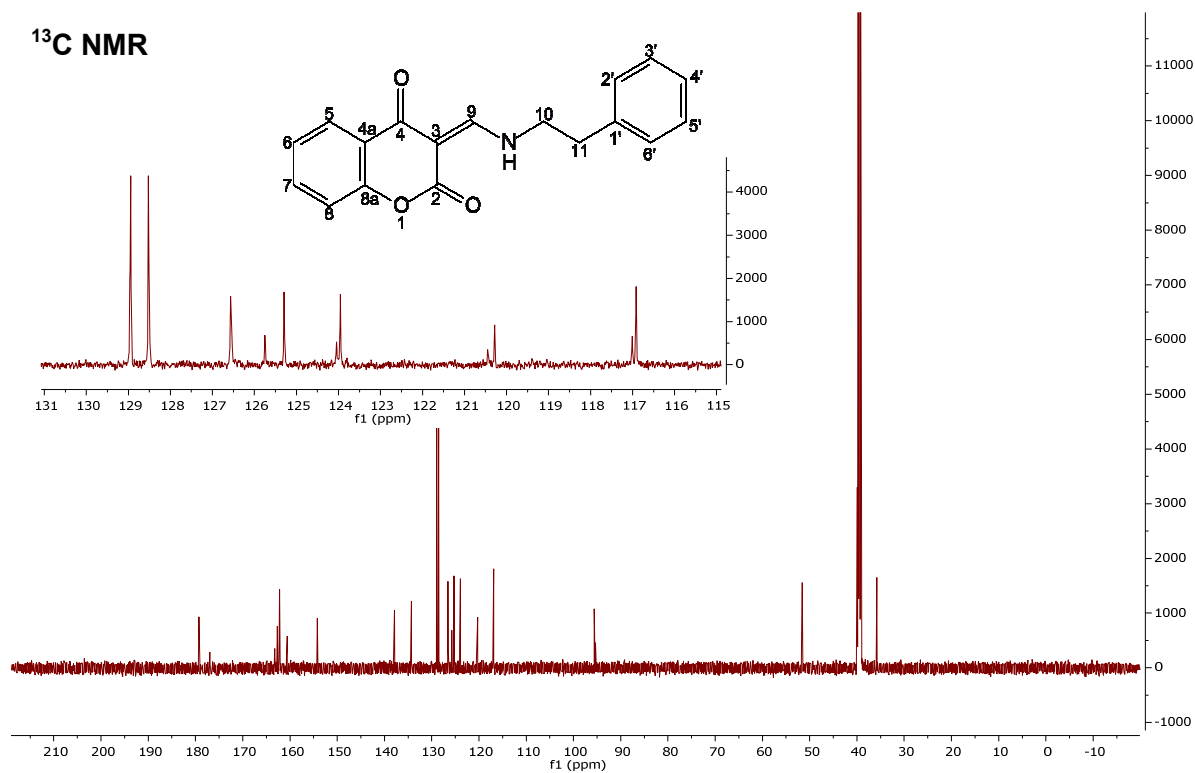


(3E/Z)-3-[(2-phenylethyl)amino]methylidene}-3,4-dihydro-2H-1-benzopyran-2,4-dione (39)

¹H NMR

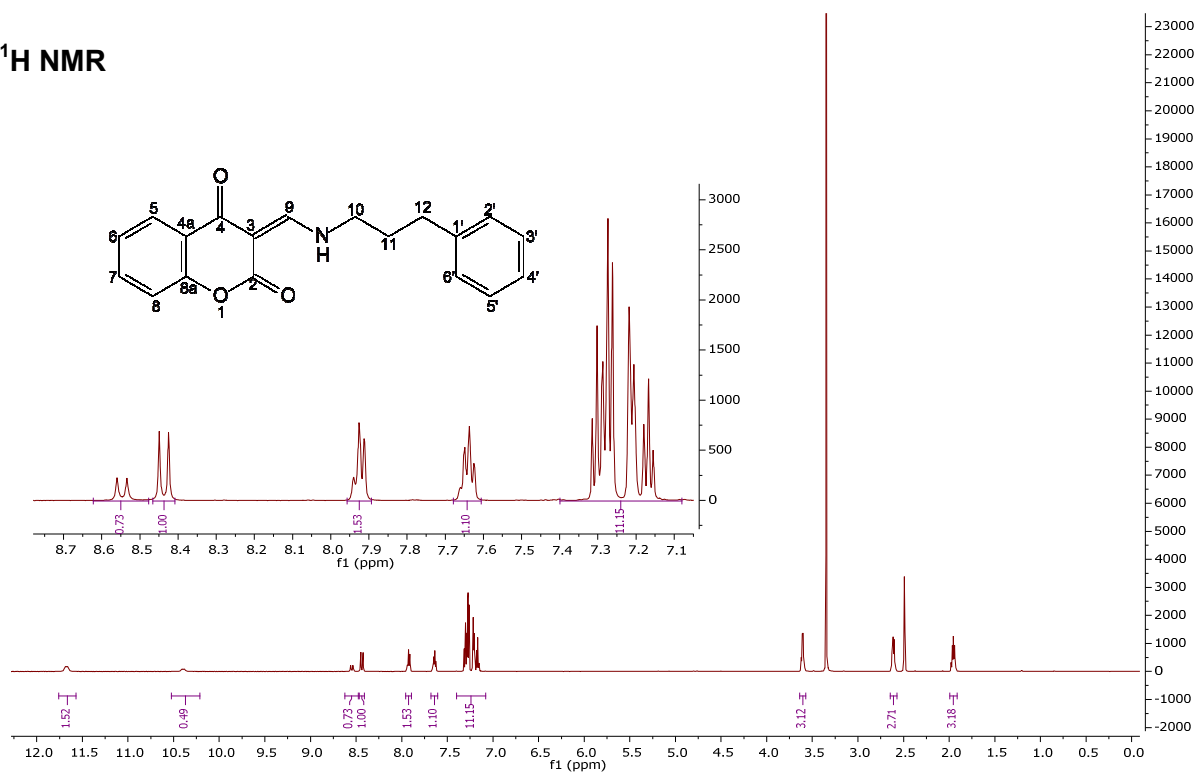


¹³C NMR

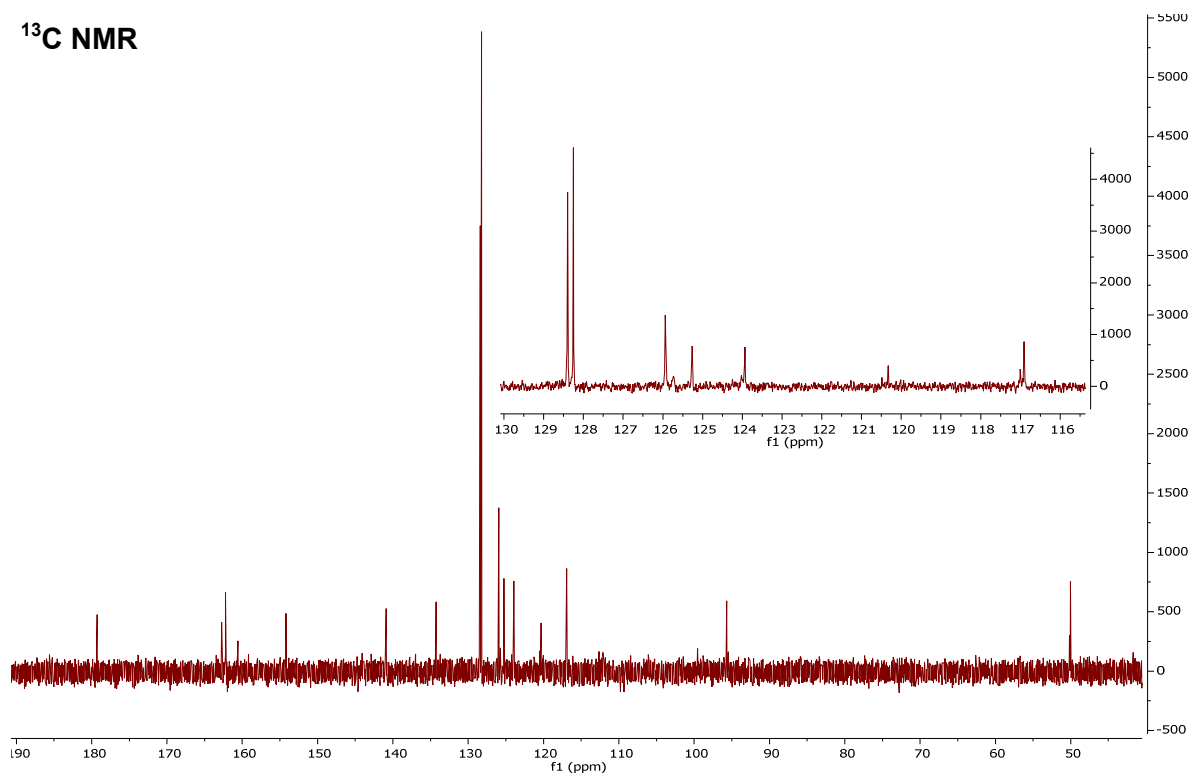


(3E/Z)-3-[(3-phenylpropyl)amino]methylidene}-3,4-dihydro-2H-1-benzopyran-2,4-dione (40)

¹H NMR

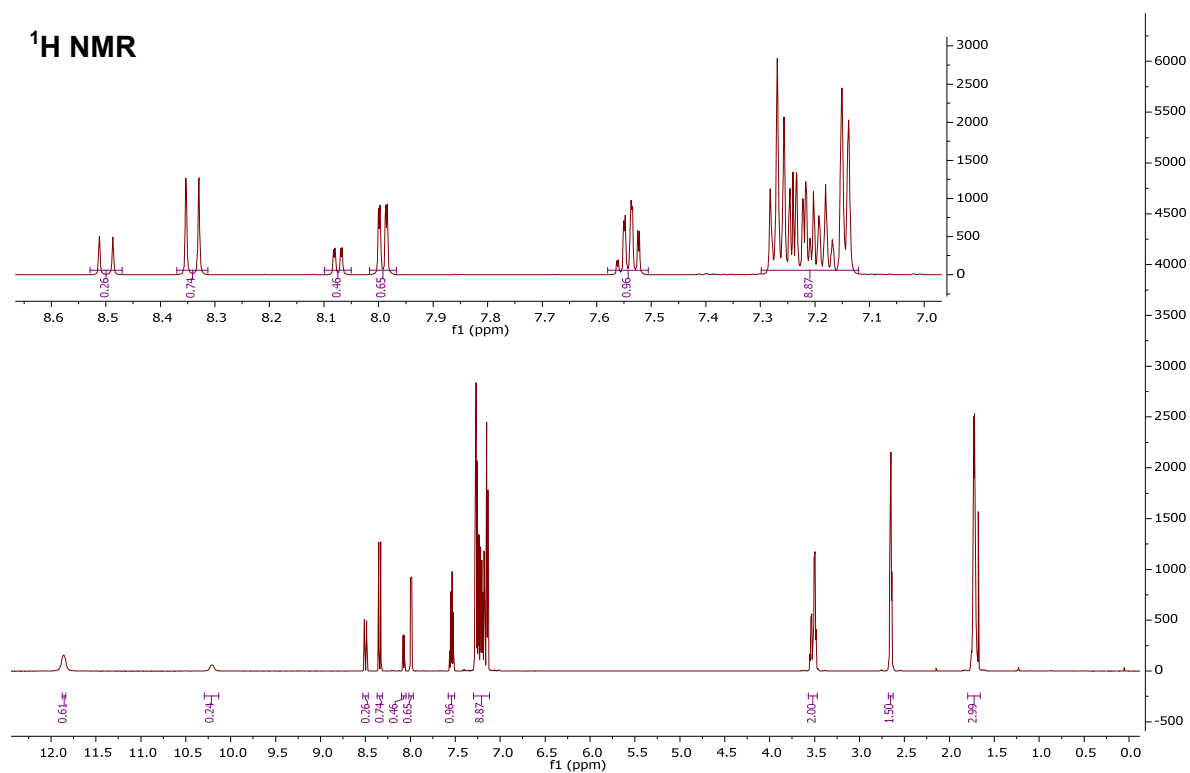


¹³C NMR

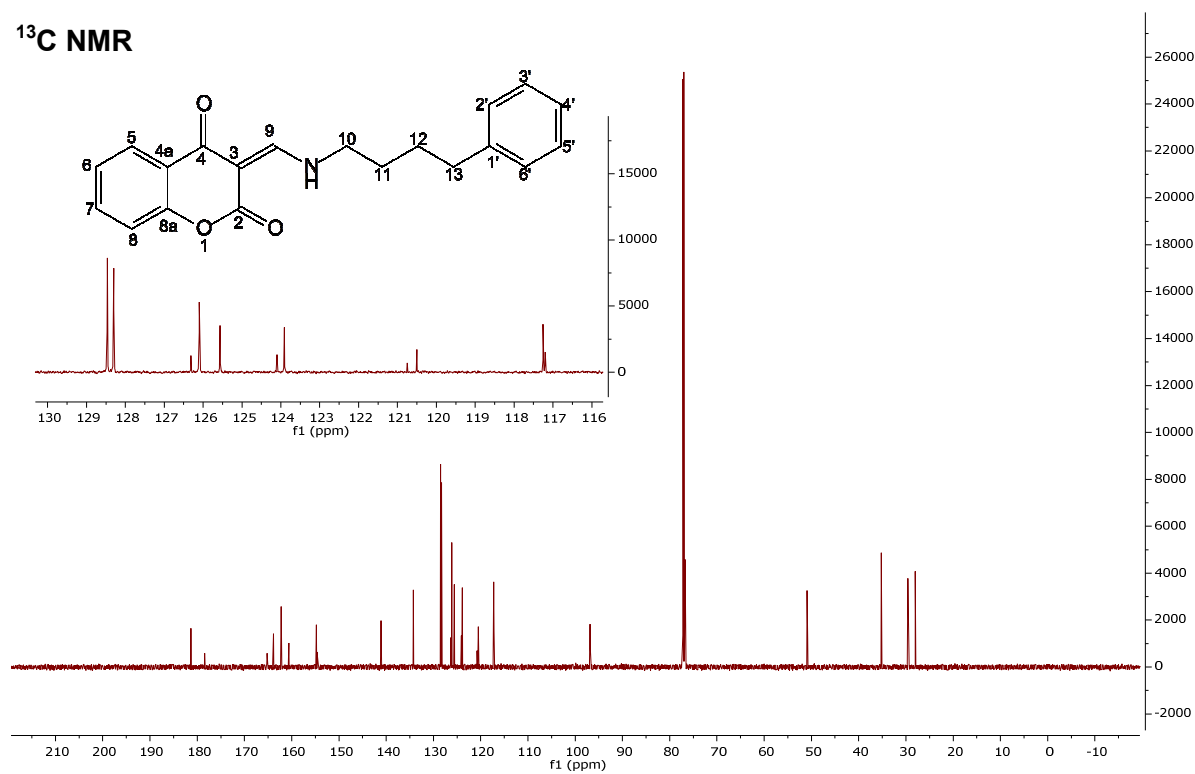


3(*E/Z*)-3-[(4-phenylbutyl)amino]methylidene}-3,4-dihydro-2*H*-1-benzopyran-2,4-dione (**41**)

¹H NMR

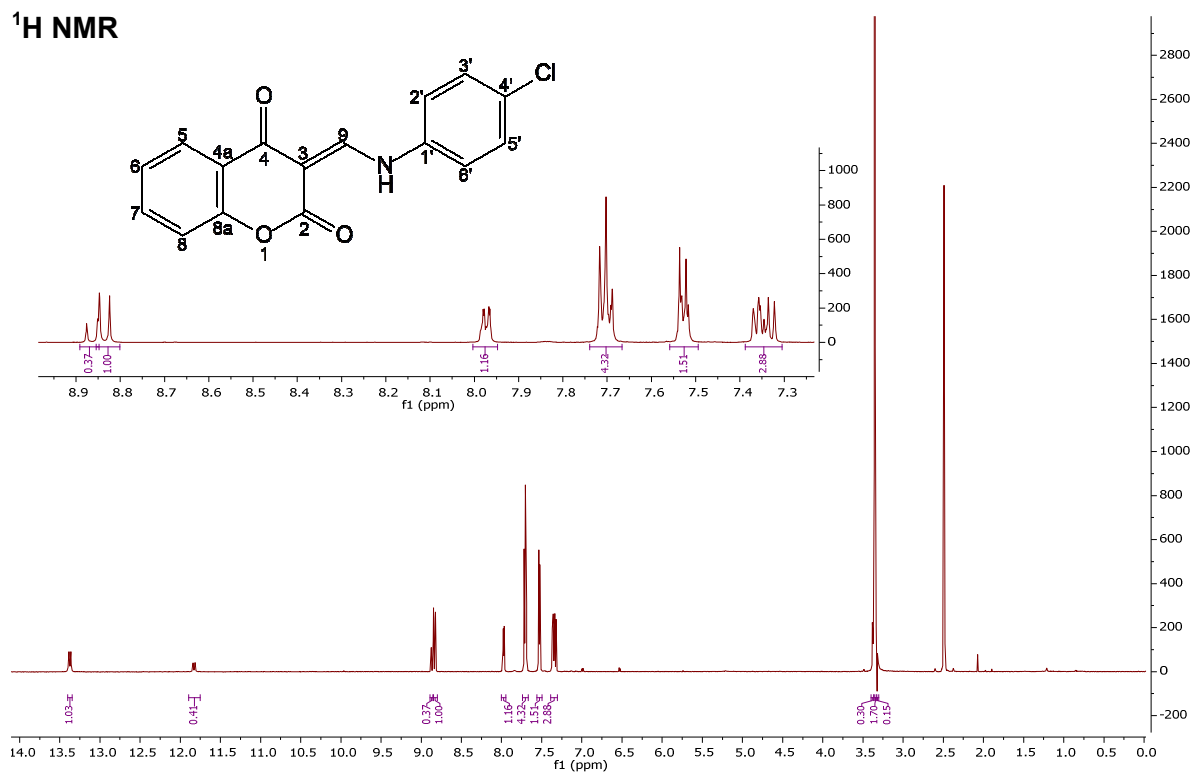


¹³C NMR

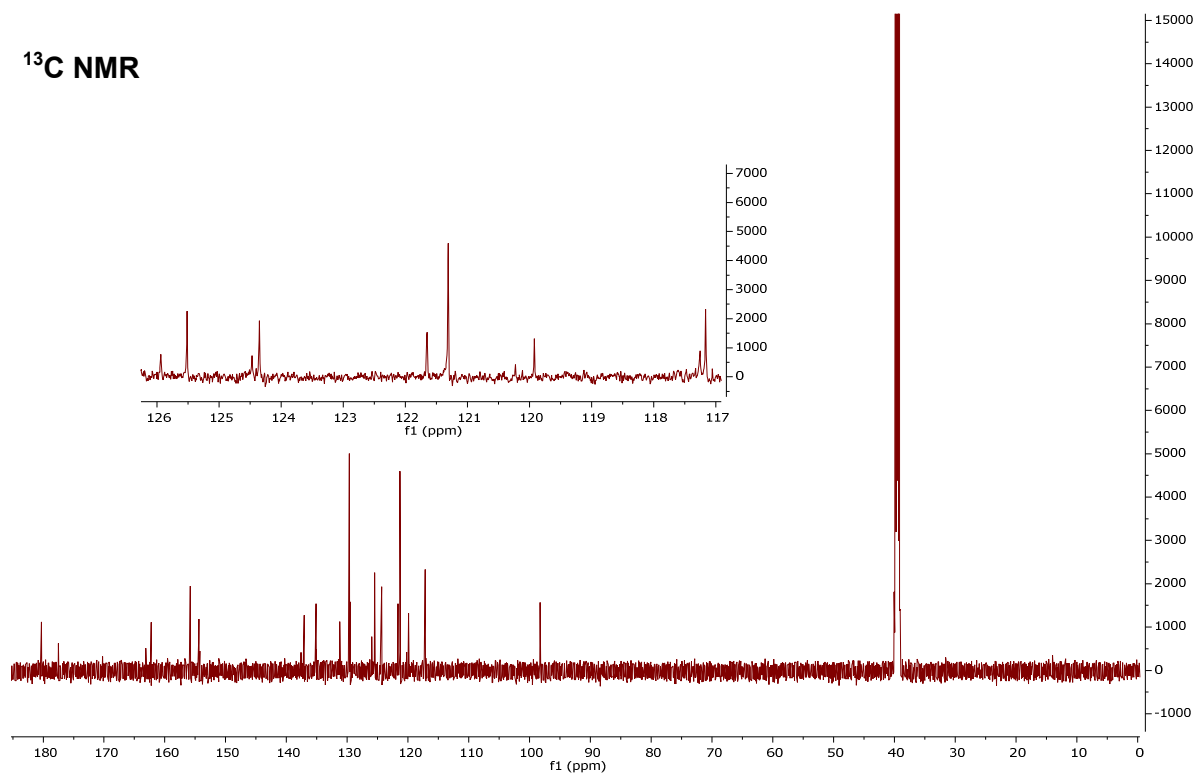


(3E/Z)-3-[(4-chlorophenyl)amino]methylidene}-3,4-dihydro-2H-1-benzopyran-2,4-dione (42)

¹H NMR

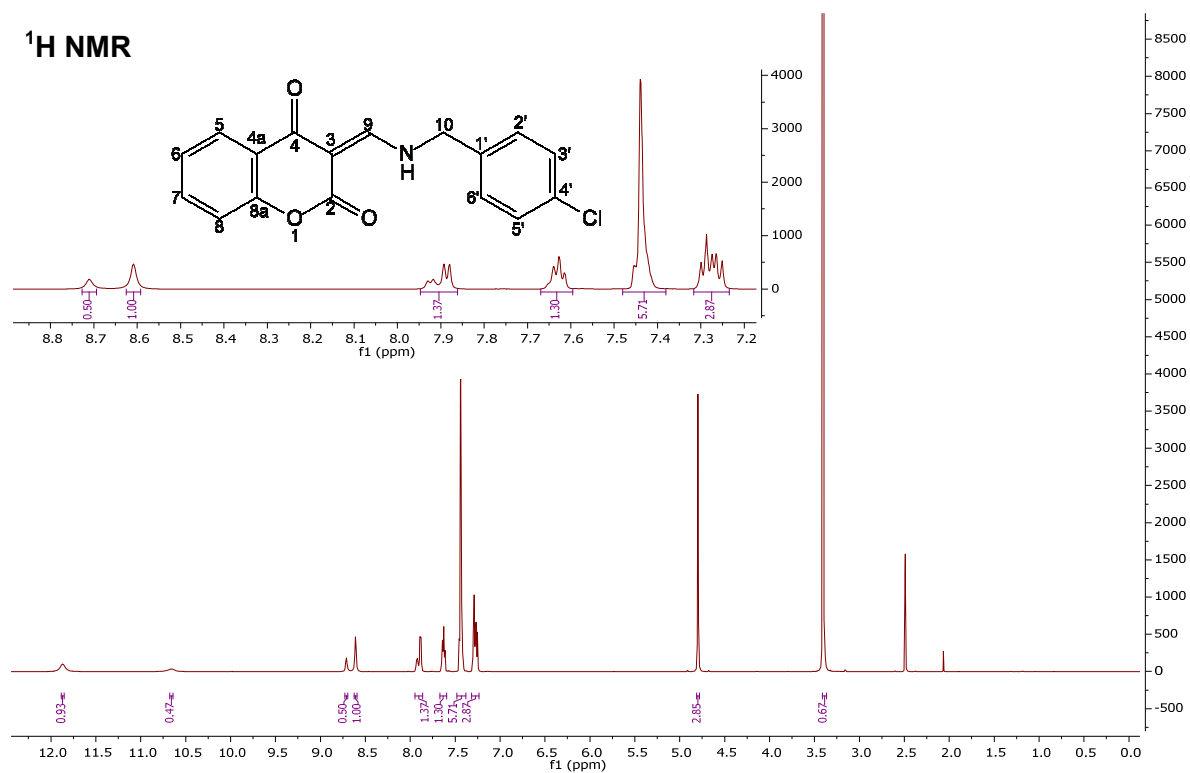


¹³C NMR

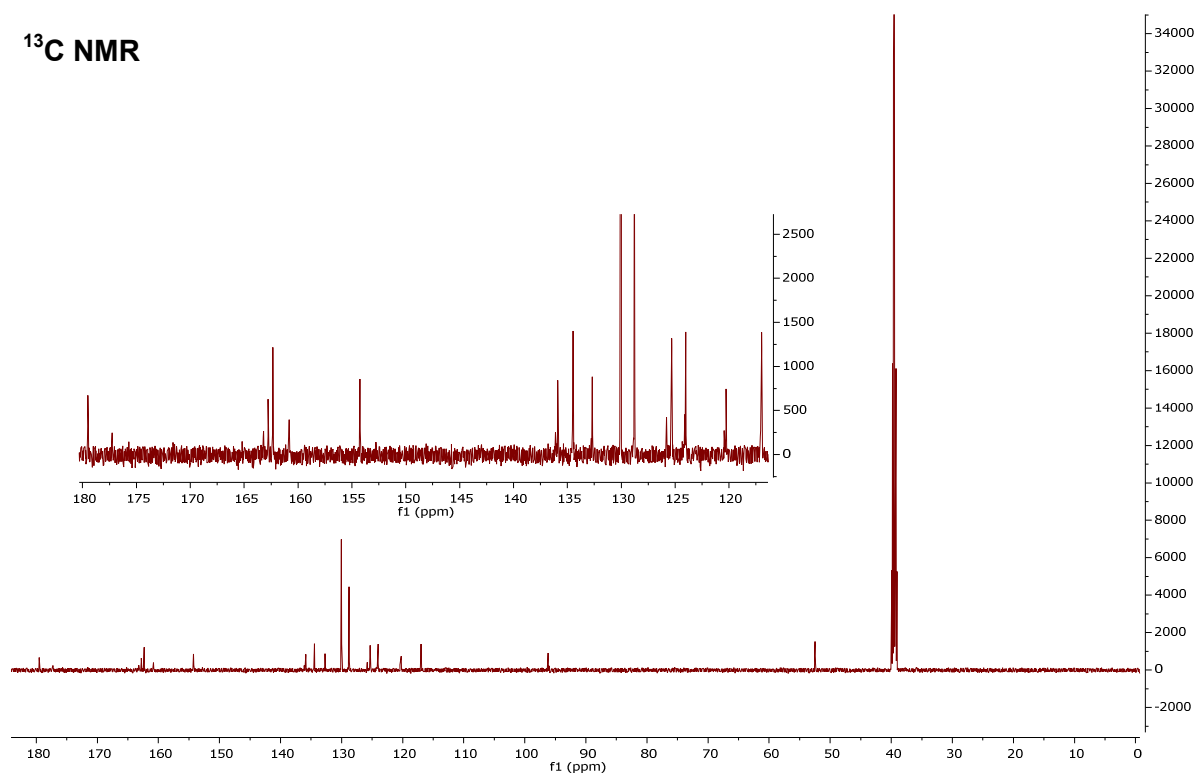


(3E/Z)-3-({(4-chlorophenyl)methyl}amino)methylidene)-3,4-dihydro-2H-1-benzopyran-2,4-dione (43)

¹H NMR

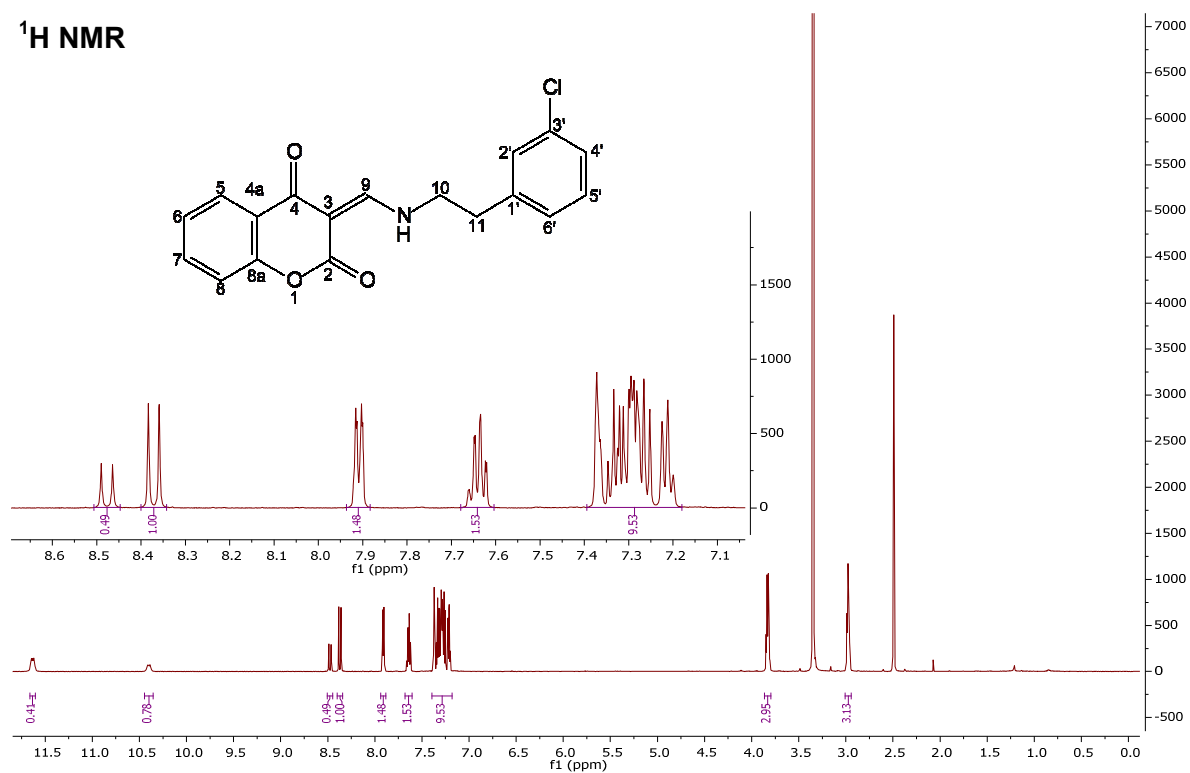


¹³C NMR

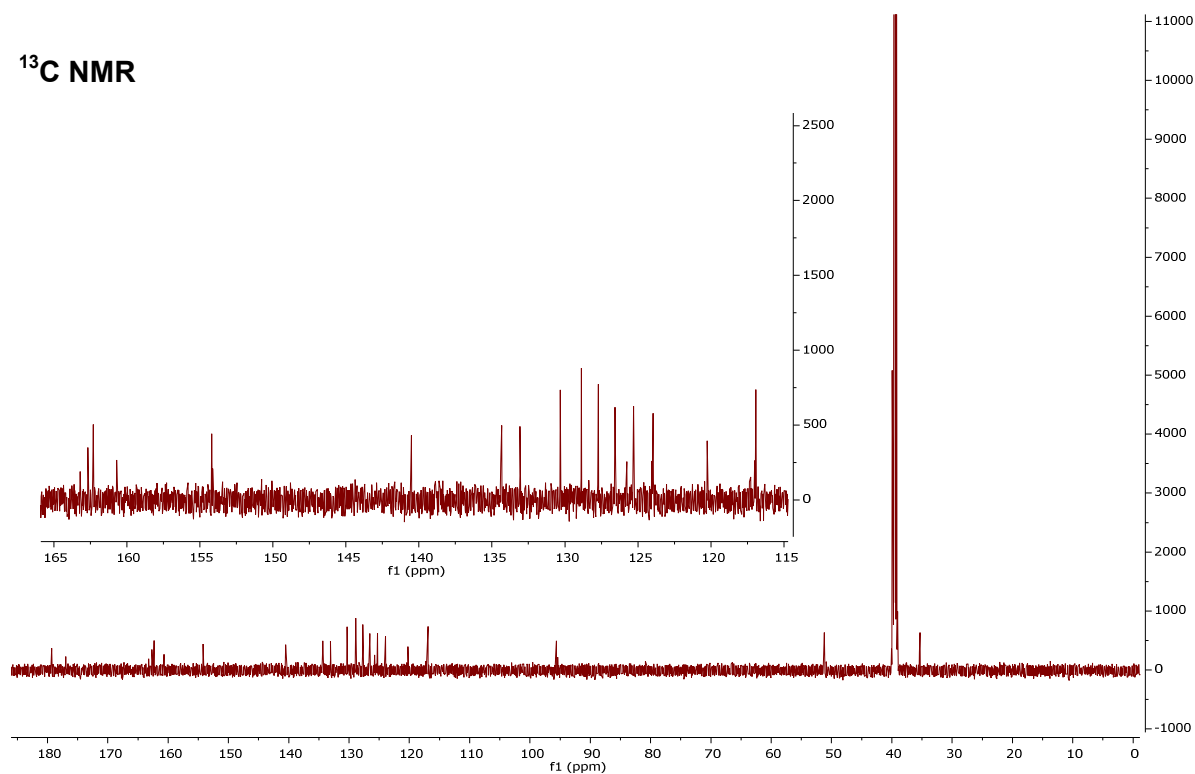


(3E/Z)-3-({[2-(3-chlorophenyl)ethyl]amino}methylidene)-3,4-dihydro-2H-1-benzopyran-2,4-dione (44)

¹H NMR

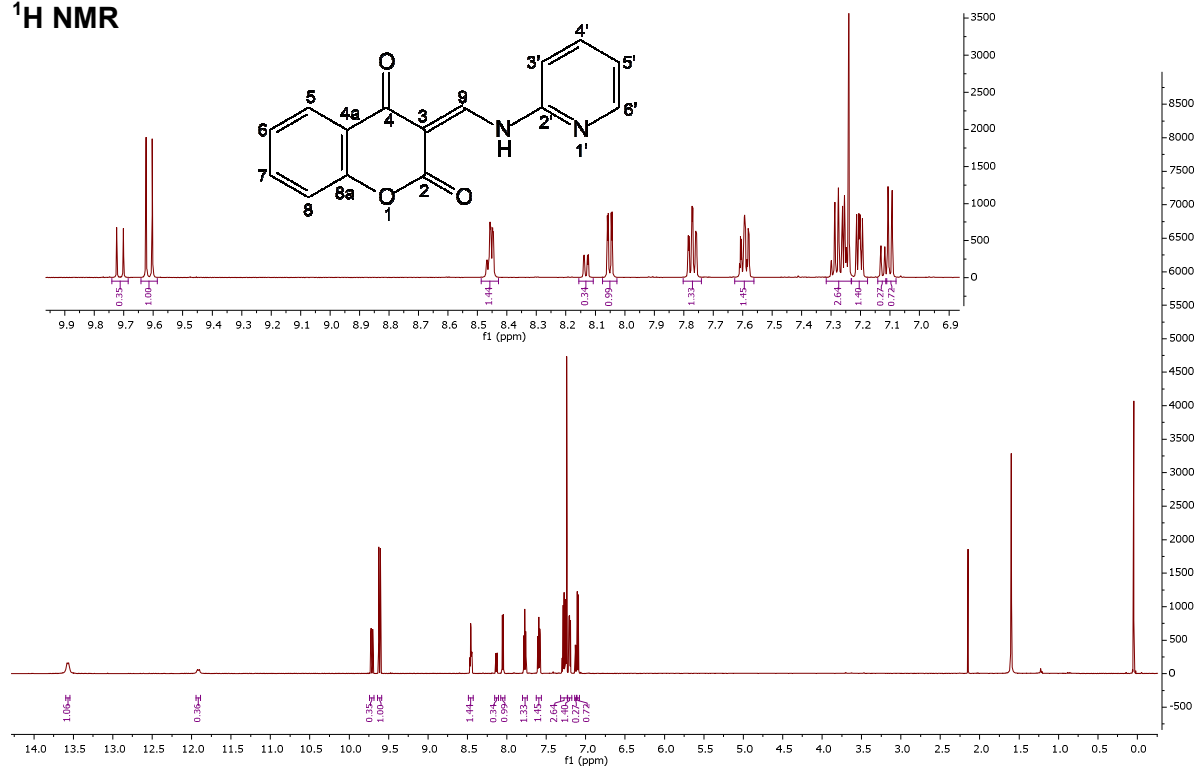


¹³C NMR

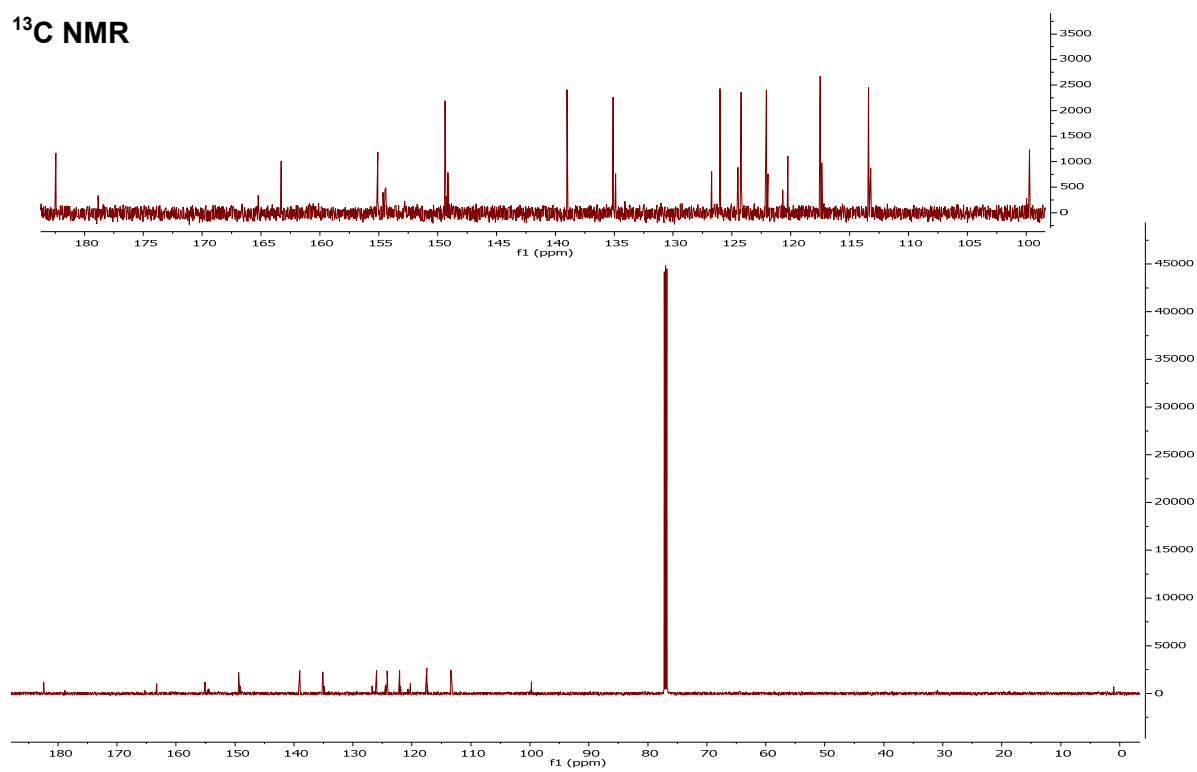


(3E/Z)-3-[(pyridin-2-yl)amino]methylidene}-3,4-dihydro-2H-1-benzopyran-2,4-dione (45)

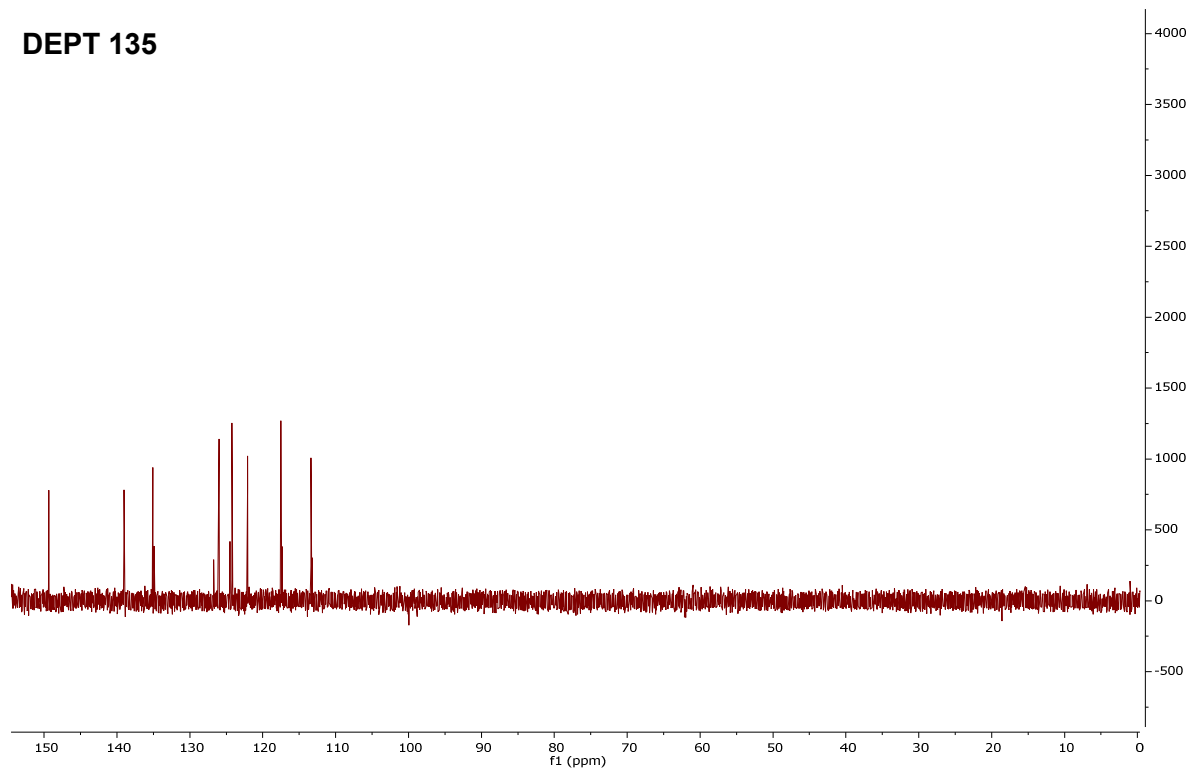
¹H NMR



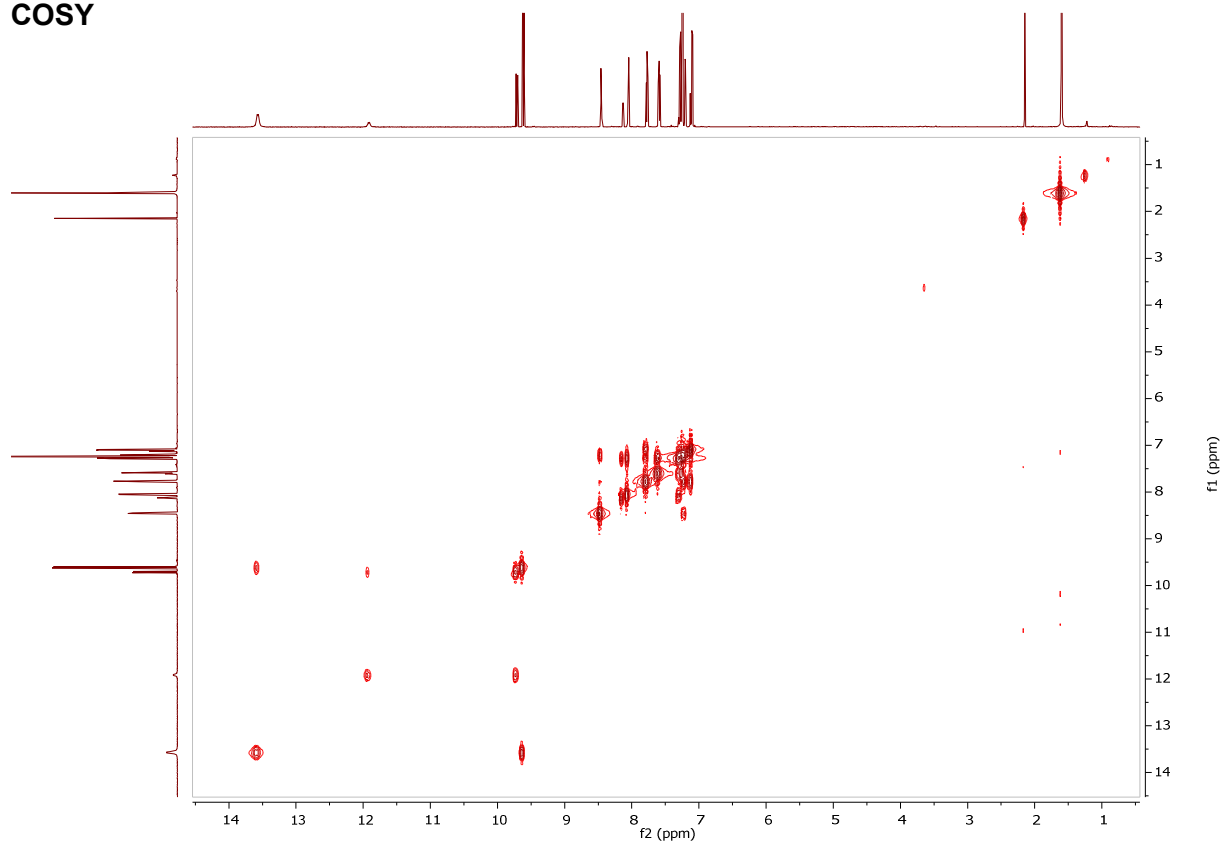
¹³C NMR



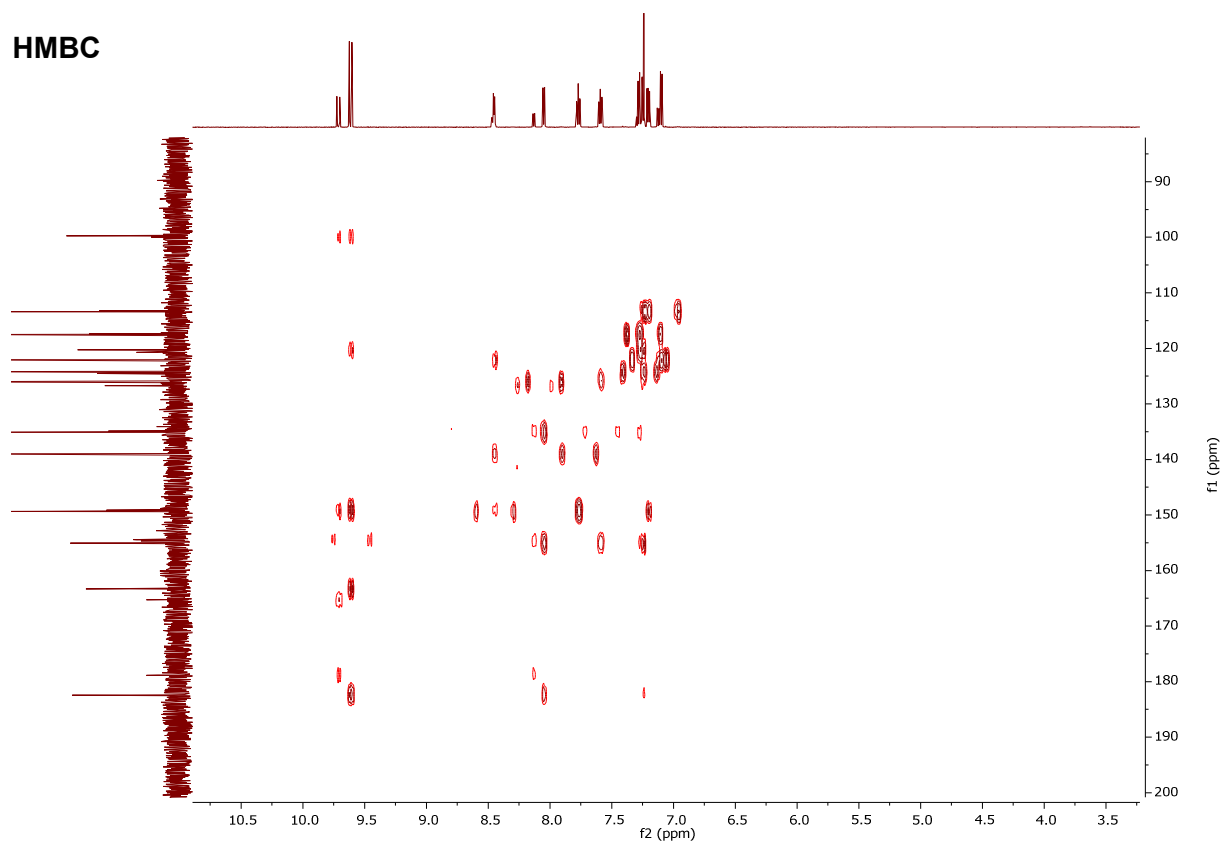
DEPT 135



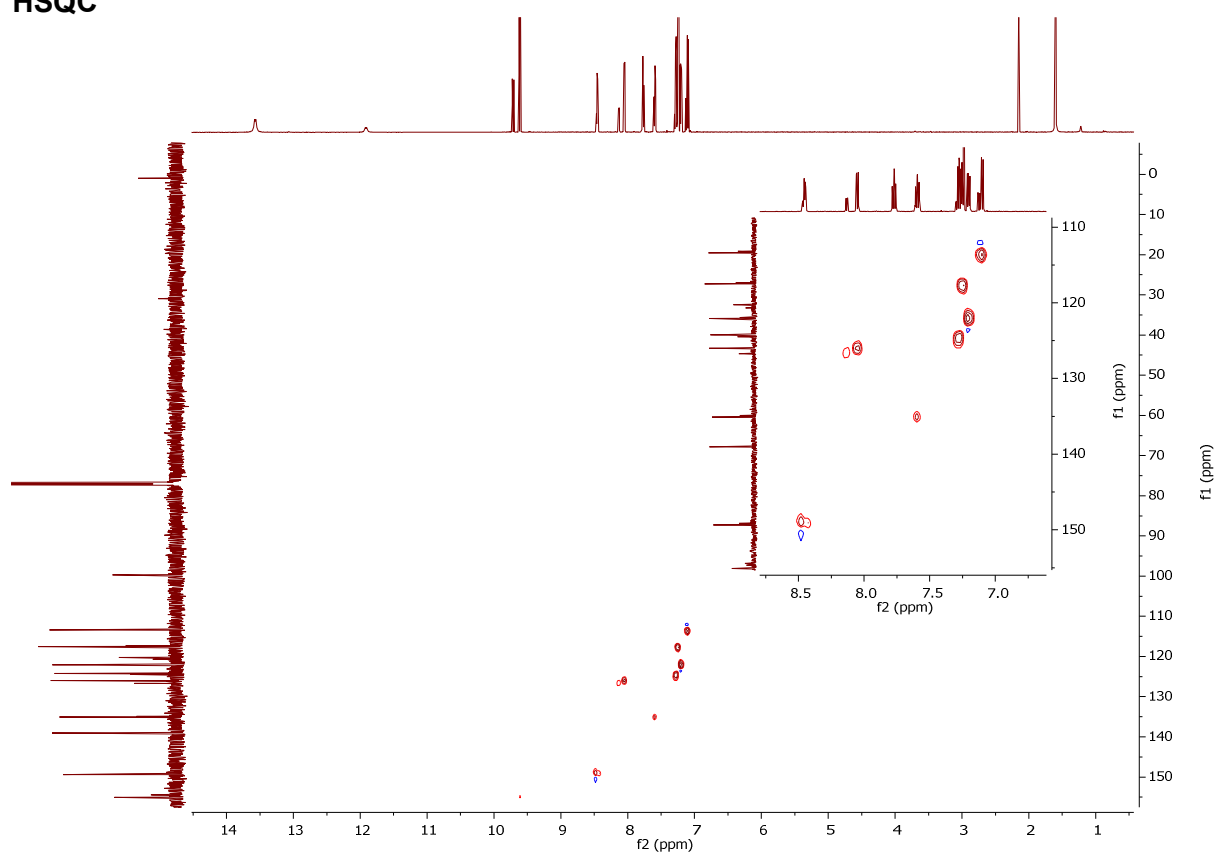
COSY



HMBC



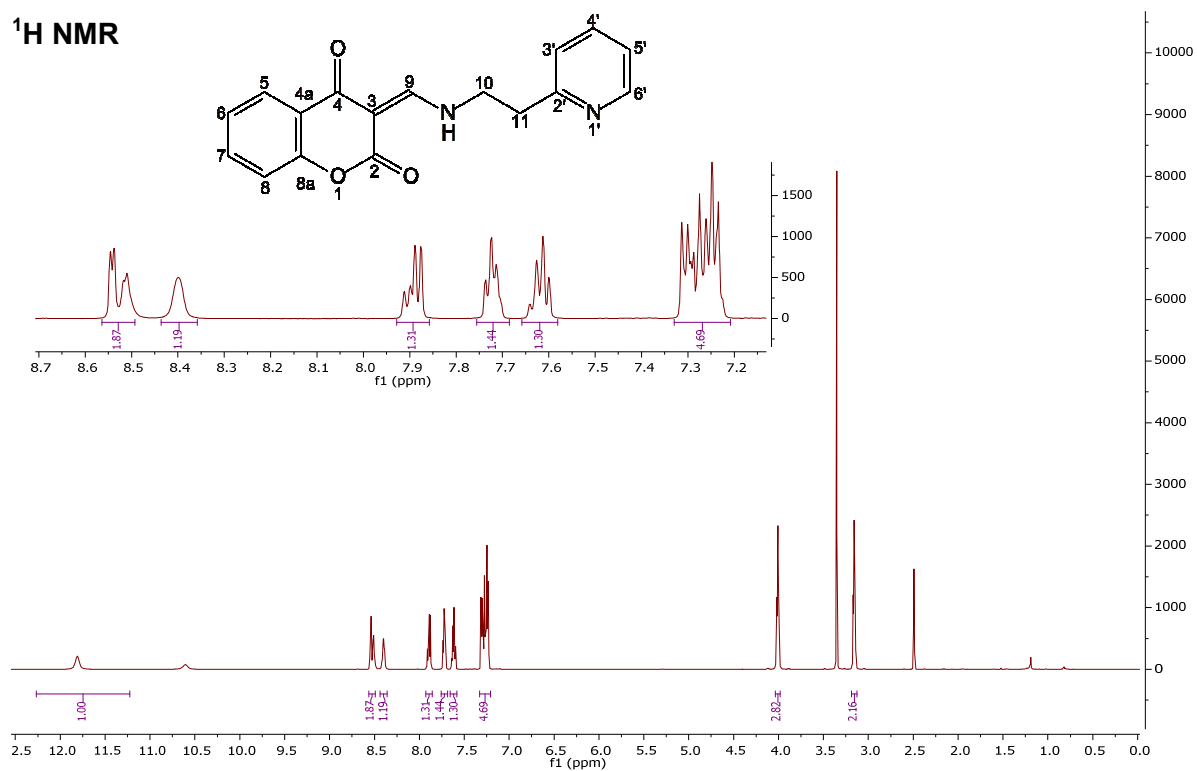
HSQC



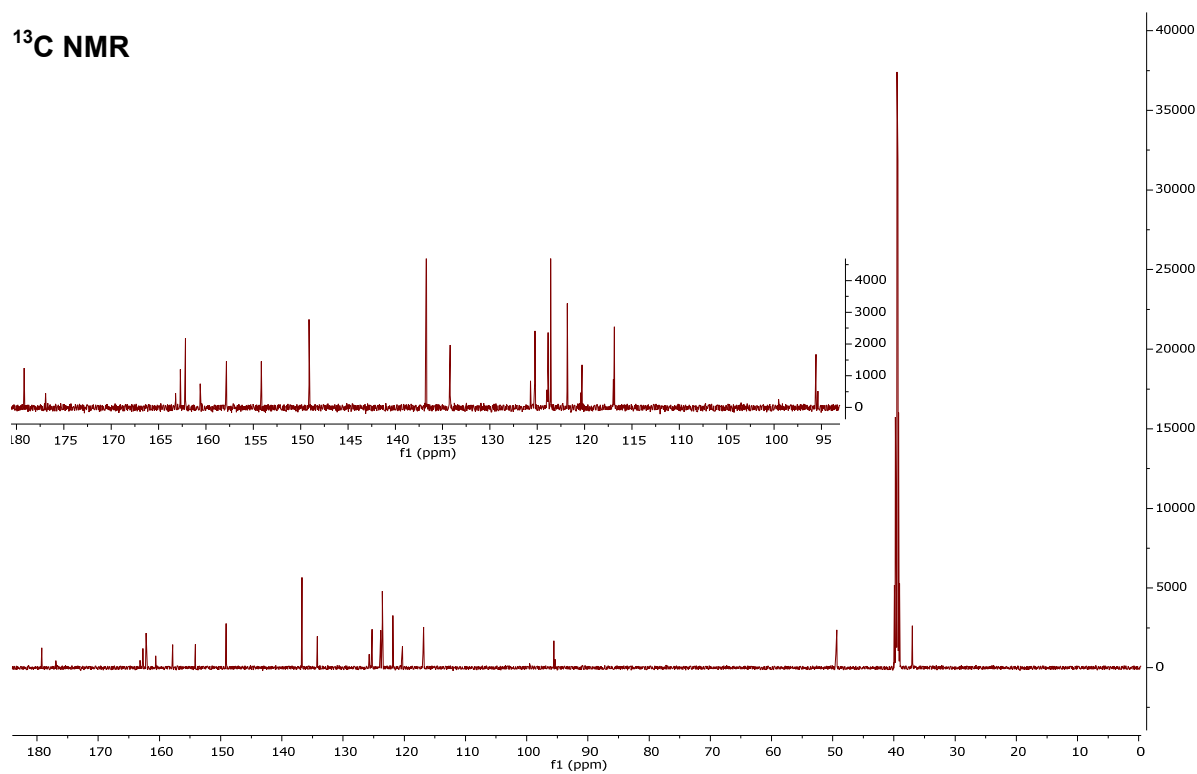
(3E/Z)-3({[2-(pyridin-2-yl)ethyl]amino}methylidene)-3,4-dihydro-2H-1-benzopyran-2,4-dione

(46)

¹H NMR

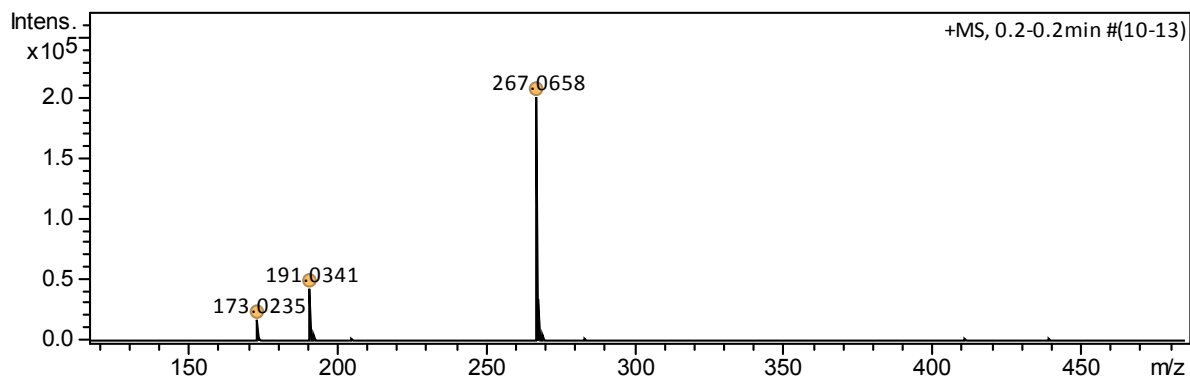


¹³C NMR



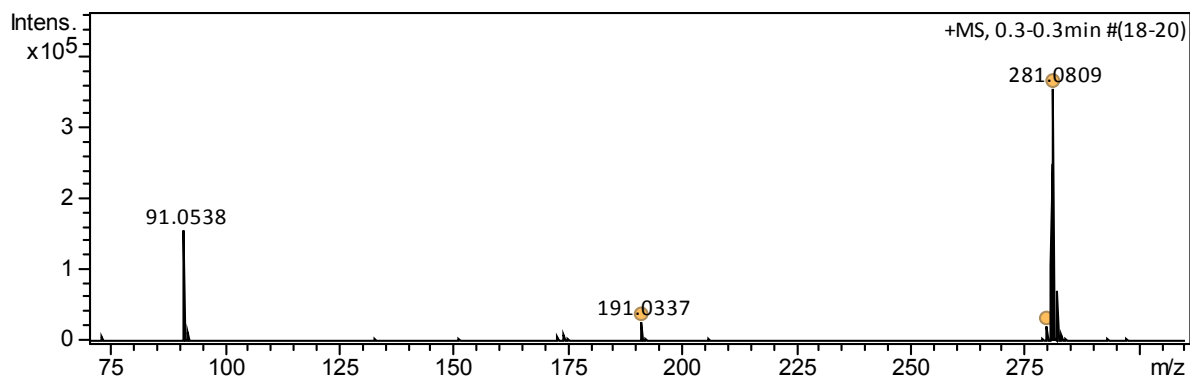
MASS SPECTRA

Phenyl 4-oxo-4*H*-chromene-3-carboxylate (**31**)



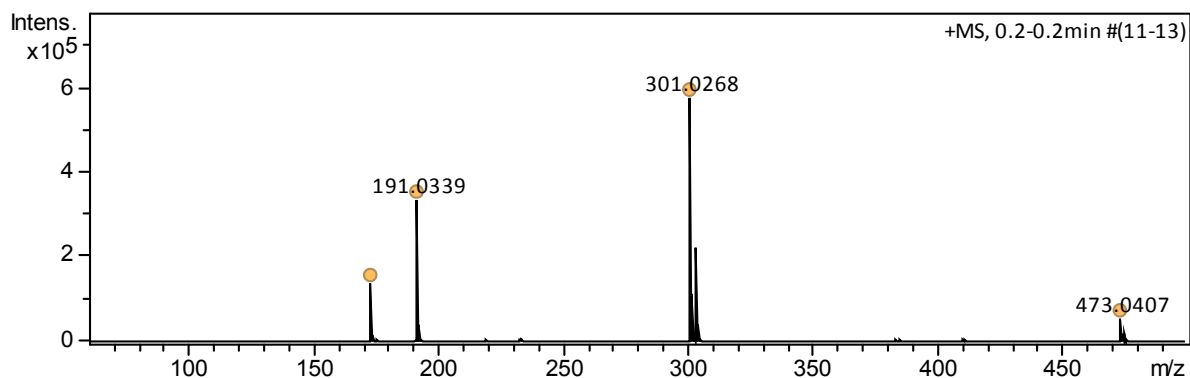
Meas. m/z	Formula	Score	m/z	err [mDa]	err [ppm]	mSigma	rdb	N-rule	e ⁻ Conf
267.0658	C ₁₆ H ₁₁ O ₄	100.00	267.0652	-0.6	-2.3	1.5	11.5	ok	Even

Benzyl 4-oxo-4*H*-chromene-3-carboxylate (**32**)



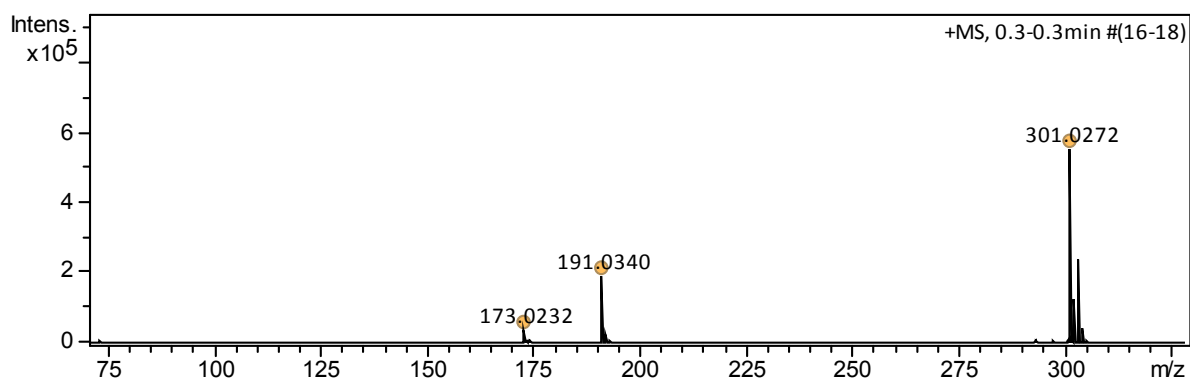
Meas. m/z	Formula	Score	m/z	err [mDa]	err [ppm]	mSigma	rdb	N-rule	e ⁻ Conf
281.0809	C ₁₇ H ₁₃ O ₄	100.00	281.0808	-0.0	-0.1	8.3	11.5	ok	even

4-chlorophenyl-4-oxo-4H-chromene-3-carboxylate (33)



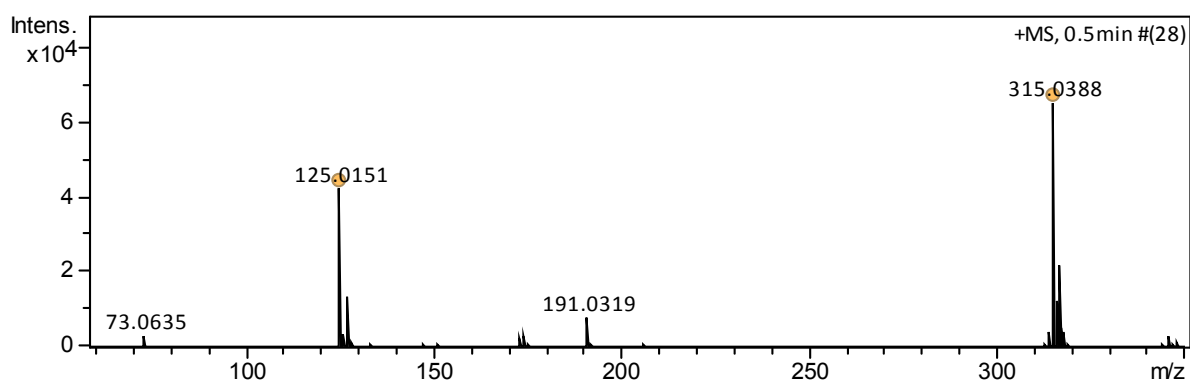
Meas. m/z	Formula	Score	m/z	err [mDa]	err [ppm]	mSigma	rdb	N-rule	e ⁻ Conf
301.0268	C ₁₆ H ₁₀ ClO ₄	100.00	301.0262	-0.6	-2.0	23.8	11.5	ok	even

3-chlorophenyl 4-oxo-4H-chromene-3-carboxylate (34)



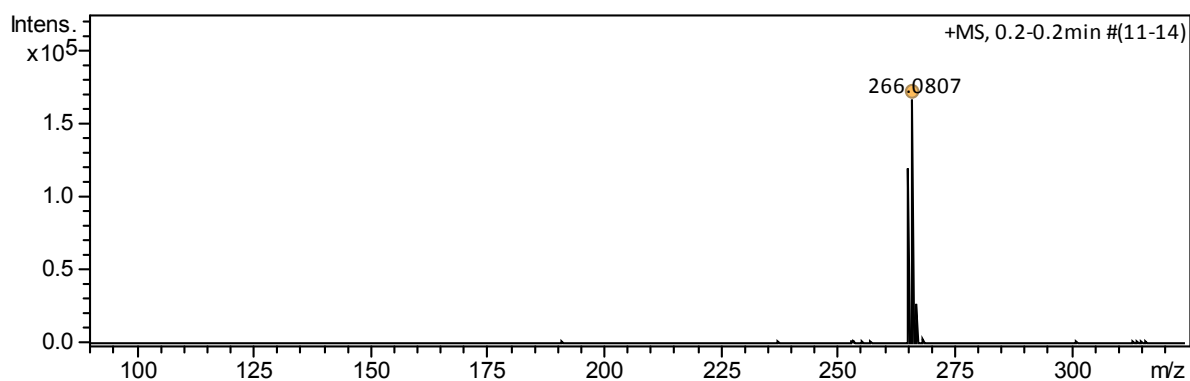
Meas. m/z	Formula	Score	m/z	err [mDa]	err [ppm]	mSigma	rdb	N-rule	e ⁻ Conf
301.0272	C ₁₆ H ₁₀ ClO ₄	100.00	301.0262	-1.0	-3.4	47.6	11.5	ok	even

(4-chlorophenyl)methyl-4-oxo-4H-chromene-3-carboxylate (35)



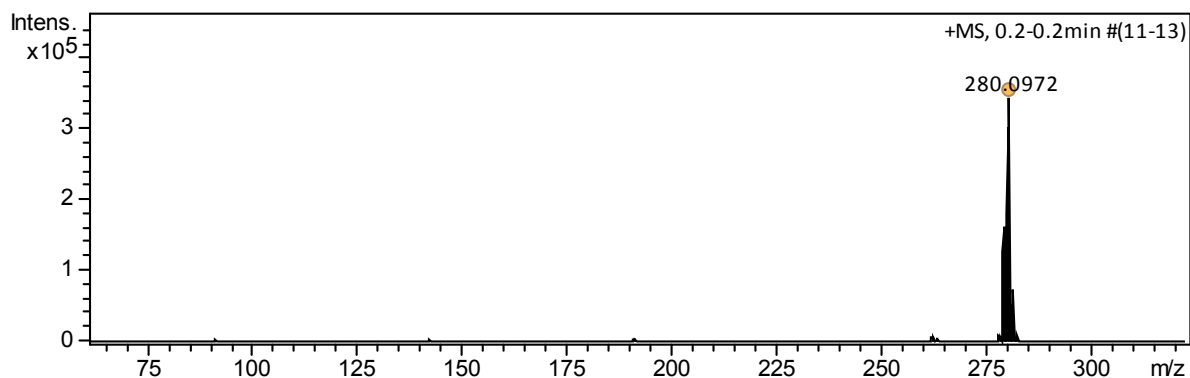
Meas. m/z	Formula	Score	m/z	err [mDa]	err [ppm]	mSigma	rdb	N-rule	e ⁻ Conf
315.0388	C ₁₇ H ₁₂ ClO ₄	100.00	315.0419	3.0	9.6	5.7	11.5	ok	even

(3E/Z)-3-[(phenylamino)methylidene]-3,4-dihydro-2H-1-benzopyran-2,4-dione (37)



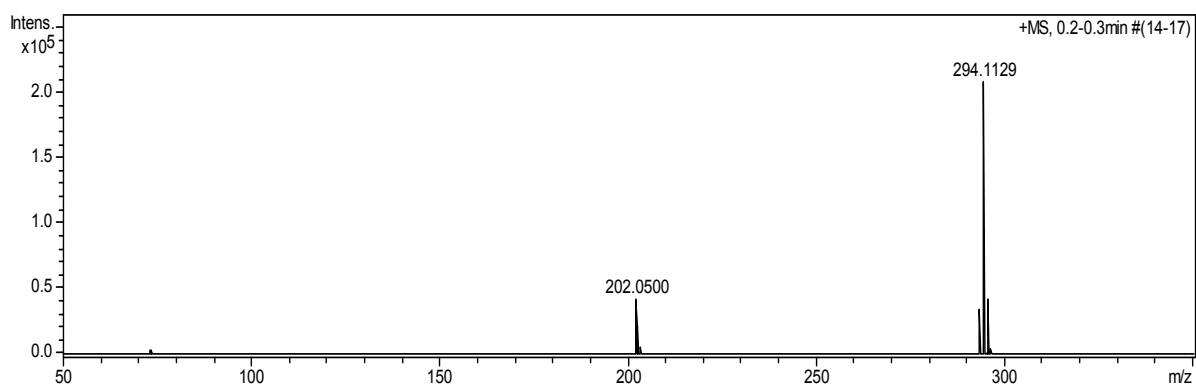
Meas. m/z	Formula	Score	m/z	err [mDa]	err [ppm]	mSigma	rdb	N-rule	e ⁻ Conf
266.0807	C ₁₆ H ₁₂ NO ₃	100.00	266.0812	0.5	1.9	7.4	11.5	ok	even

(3E/Z)-3-[(benzylamino)methylidene]-3,4-dihydro-2H-1-benzopyran-2,4-dione (38)



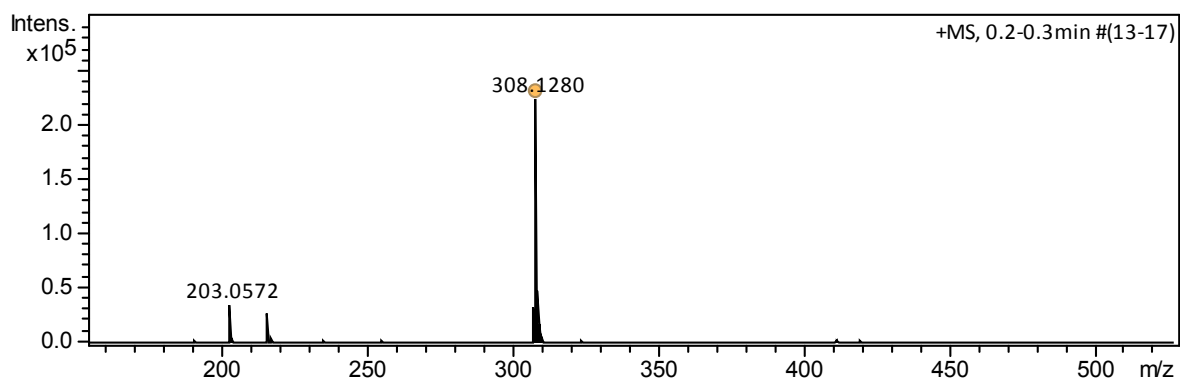
Meas. m/z	Formula	Score	m/z	err [mDa]	err [ppm]	mSigma	rdb	N-rule	e ⁻ Conf
280.0972	C ₁₇ H ₁₄ NO ₃	100.00	280.0968	-0.4	-1.5	16.5	11.5	ok	even

(3E/Z)-3-[(2-phenylethyl)amino]methylidene}-3,4-dihydro-2H-1-benzopyran-2,4-dione (39)



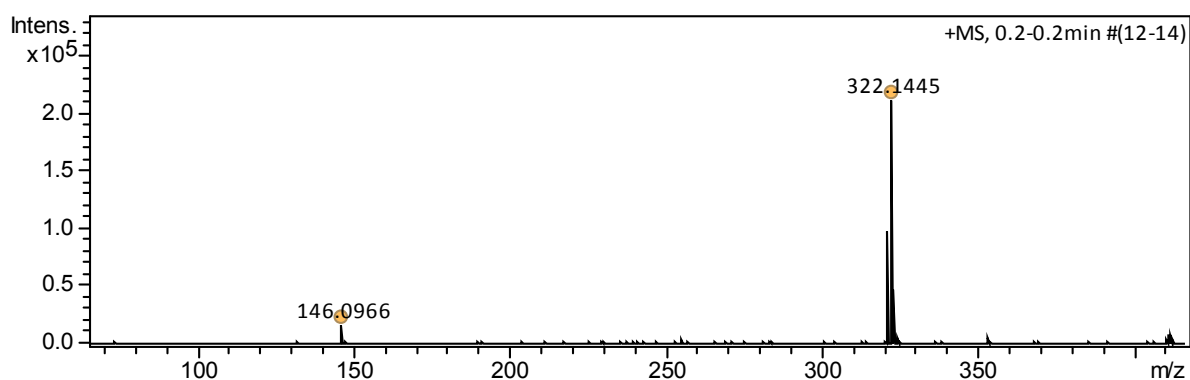
Meas. m/z	Formula	Score	m/z	err [mDa]	err [ppm]	mSigma	rdb	N-rule	e ⁻ Conf
294.1129	C ₁₈ H ₁₆ NO ₃	100.00	294.1125	-0.4	-1.5	1.4	11.5	ok	even

(3E/Z)-3-[(3-phenylpropyl)amino]methylidene}-3,4-dihydro-2H-1-benzopyran-2,4-dione (40)



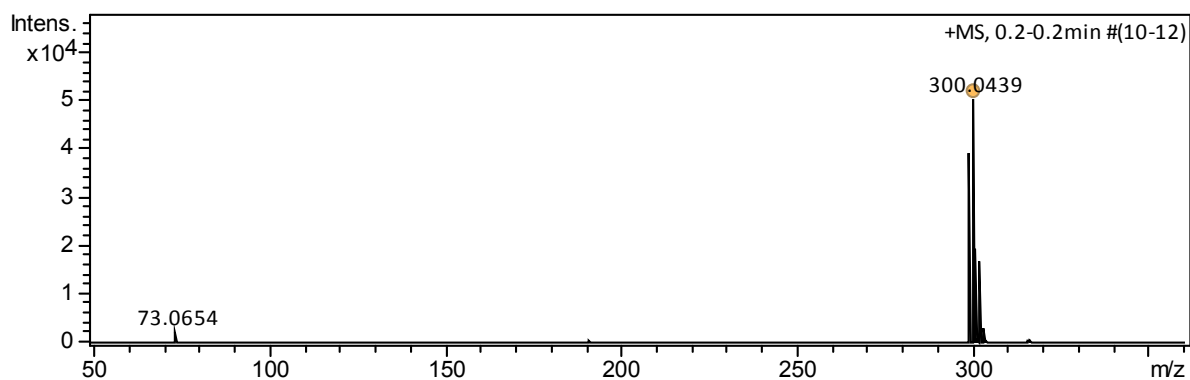
Meas. m/z	Formula	Score	m/z	err [mDa]	err [ppm]	mSigma	rdb	N-rule	e ⁻ Conf
308.1280	C ₁₉ H ₁₈ NO ₃	100.00	308.1281	0.1	0.3	0.3	11.5	ok	even

3(E/Z)-3-[(4-phenylbutyl)amino]methylidene}-3,4-dihydro-2H-1-benzopyran-2,4-dione (41)



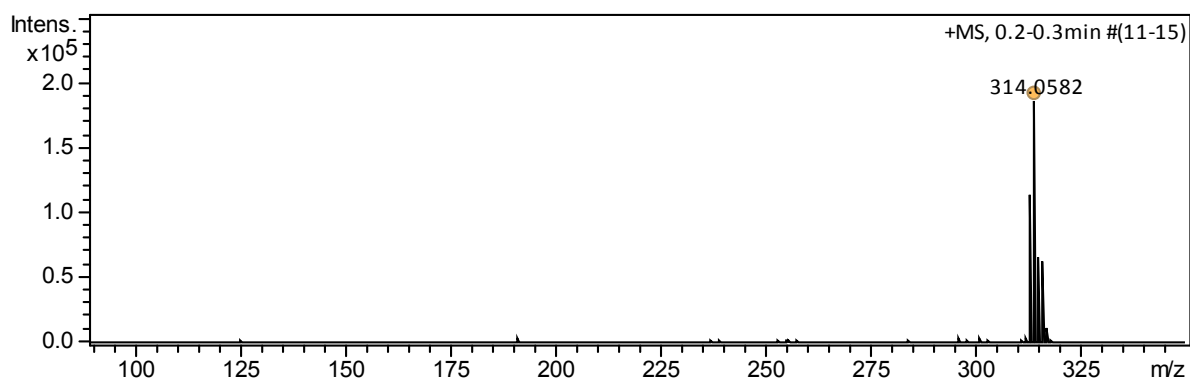
Meas. m/z	Formula	Score	m/z	err [mDa]	err [ppm]	mSigma	rdb	N-rule	e ⁻ Conf
322.1445	C ₂₀ H ₂₀ NO ₃	100.00	322.1438	-0.7	-2.2	2.2	11.5	ok	even

(3E/Z)-3-([(4-chlorophenyl)amino]methylidene)-3,4-dihydro-2H-1-benzopyran-2,4-dione (42)



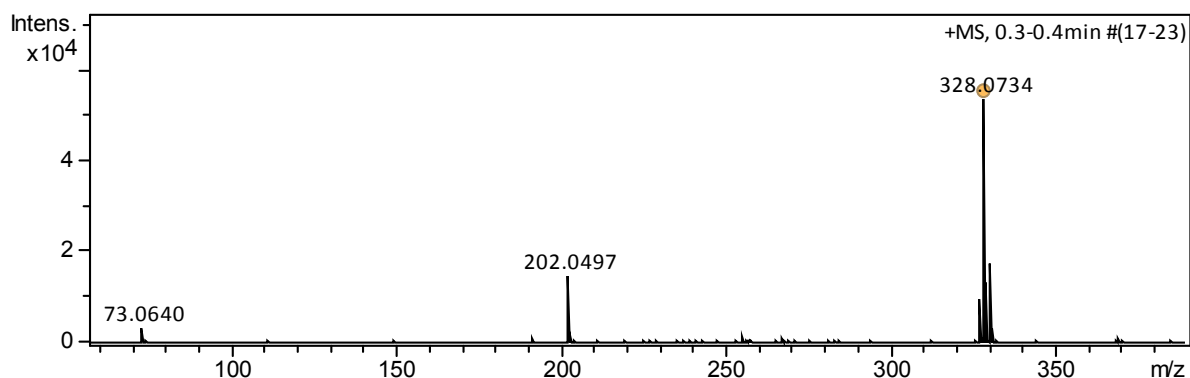
Meas. m/z	Formula	Score	m/z	err [mDa]	err [ppm]	mSig ma	rdb	N-rule	e ⁻ Conf
300.0439	C ₁₆ H ₁₁ ClNO ₃	100.00	300.0422	-1.7	-5.7	94.1	11.5	ok	even

(3E/Z)-3-([(4-chlorophenyl)methyl]amino)methylidene)-3,4-dihydro-2H-1-benzopyran-2,4-dione (43)



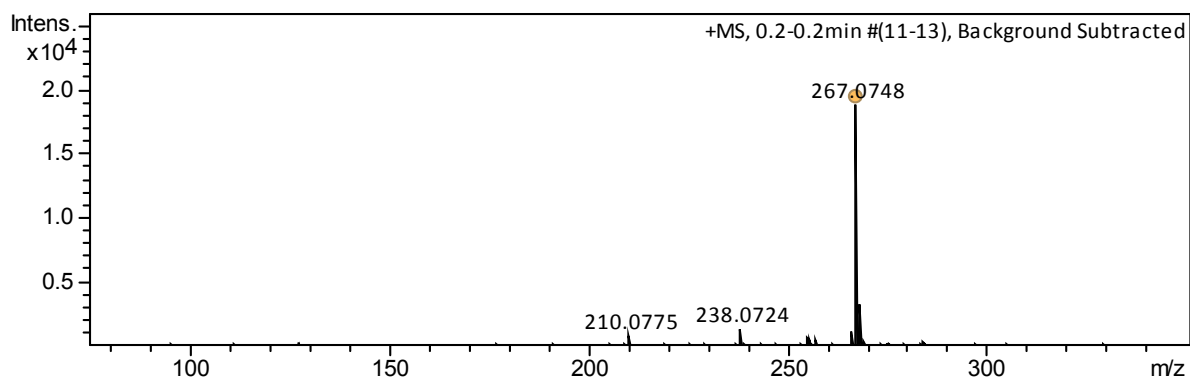
Meas. m/z	Formula	Score	m/z	err [mDa]	err [ppm]	mSigma	rdb	N-rule	e ⁻ Conf
314.0582	C ₁₇ H ₁₃ ClNO ₃	100.00	314.0578	-0.4	-1.1	71.8	11.5	ok	even

(3E/Z)-3-([2-(3-chlorophenyl)ethyl]amino)methylidene)-3,4-dihydro-2H-1-benzopyran-2,4-dione (44)



Meas. m/z	Formula	Score	m/z	err [mDa]	err [ppm]	mSigma	rdb	N-rule	e ⁻ Conf
328.0734	C ₁₈ H ₁₅ ClNO ₃	100.00	328.0735	0.1	0.3	22.6	11.5	ok	even

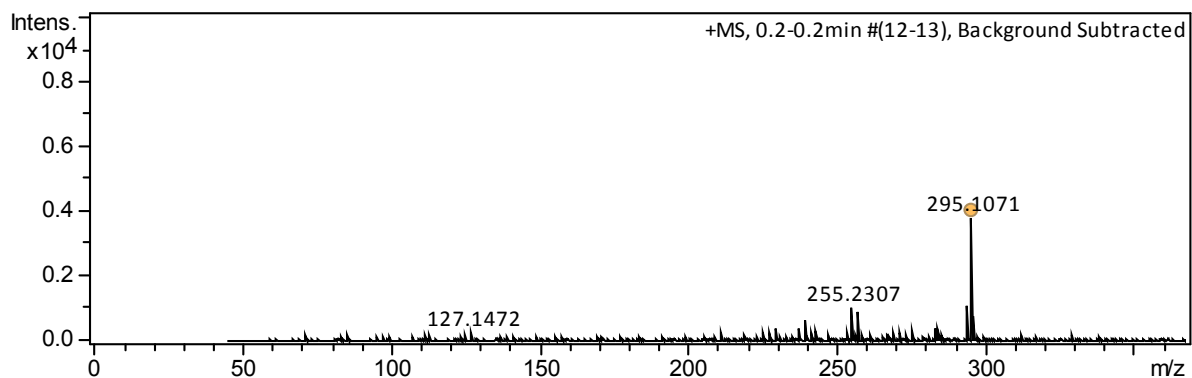
(3E/Z)-3-[(pyridin-2-yl)amino]methylidene}-3,4-dihydro-2H-1-benzopyran-2,4-dione (45)



Meas. m/z	Formula	Score	m/z	err [mDa]	err [ppm]	mSigma	rdb	N-rule	e ⁻ Conf
267.0748	C ₁₅ H ₁₁ N ₂ O ₃	100.00	267.0764	1.6	6.0	11.4	11.5	ok	even

(3E/Z)-3-([2-(pyridin-2-yl)ethyl]amino)methylidene)-3,4-dihydro-2H-1-benzopyran-2,4-dione

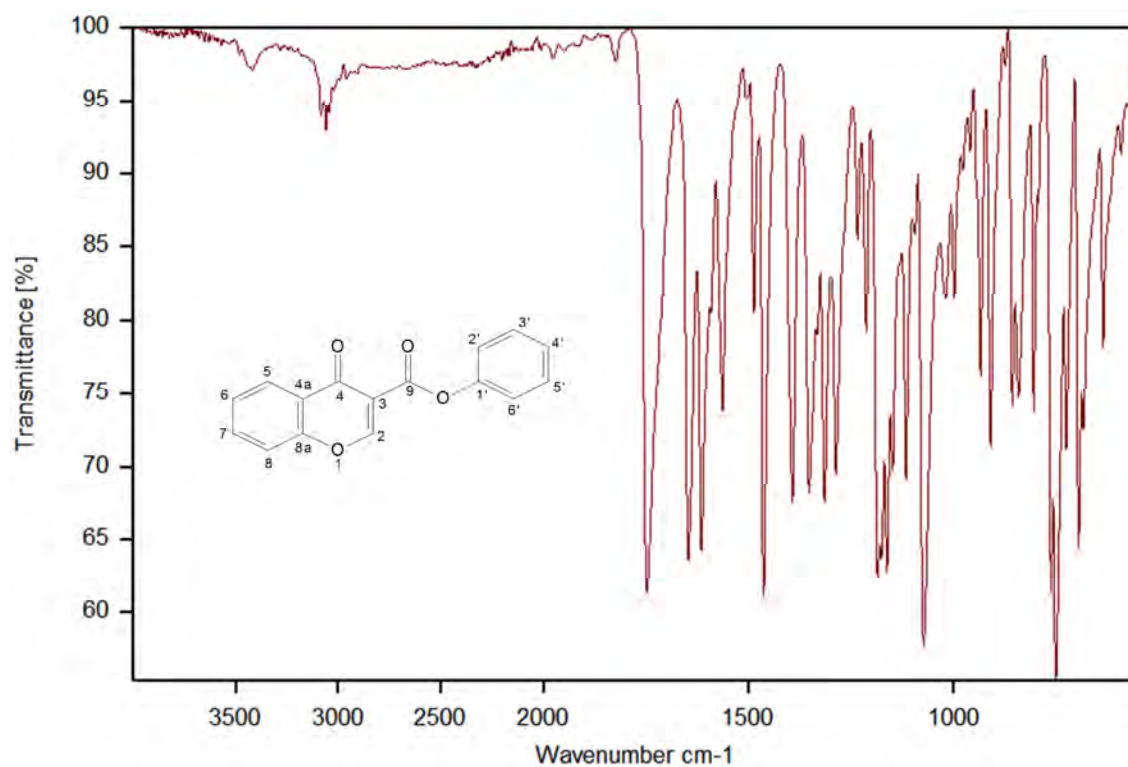
(46)



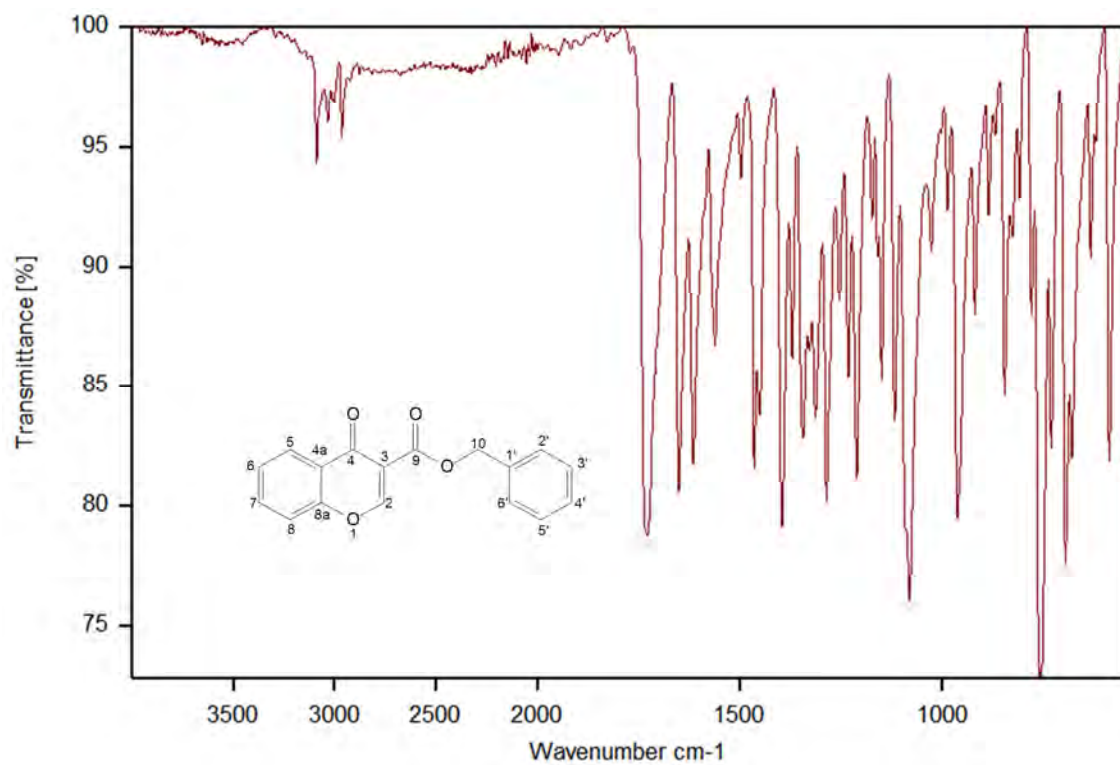
Meas. m/z	Formula	Score	m/z	err [mDa]	err [ppm]	mSigma	rdb	N-rule	e ⁻ Conf
295.1071	C ₁₇ H ₁₅ N ₂ O ₃	100.00	295.1077	0.6	2.1	15.0	11.5	ok	even

INFRA-RED SPECTRA

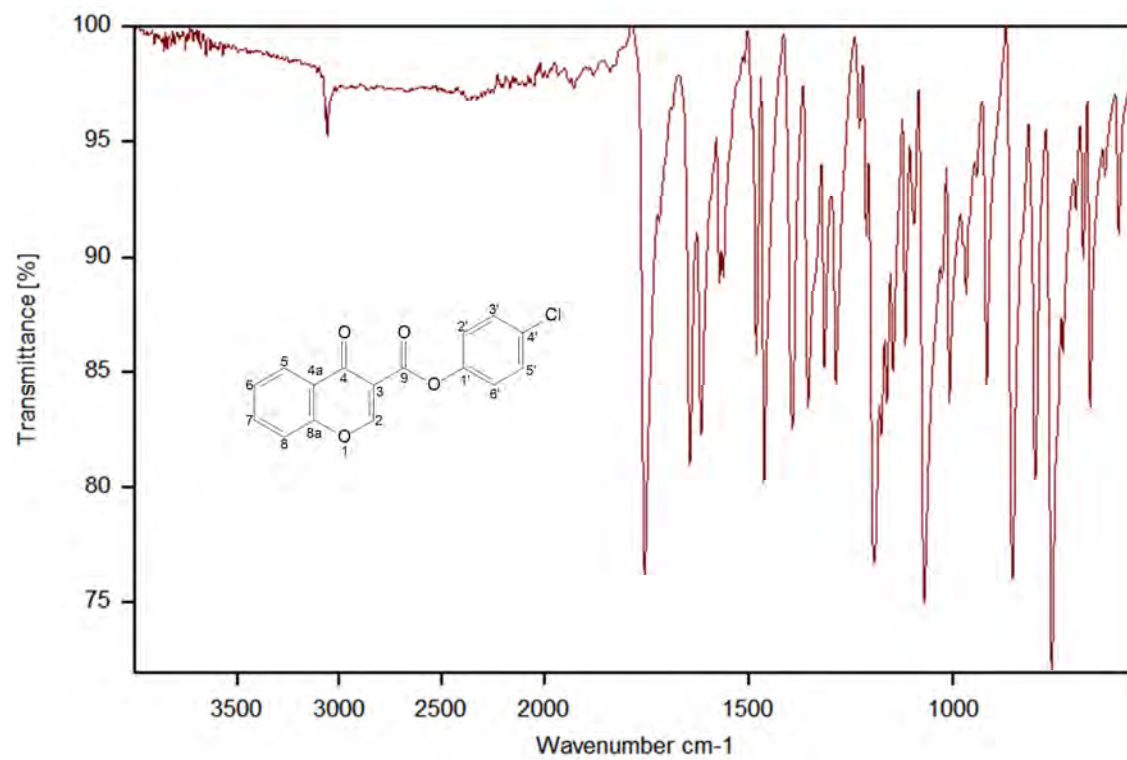
Phenyl 4-oxo-4*H*-chromene-3-carboxylate (31)



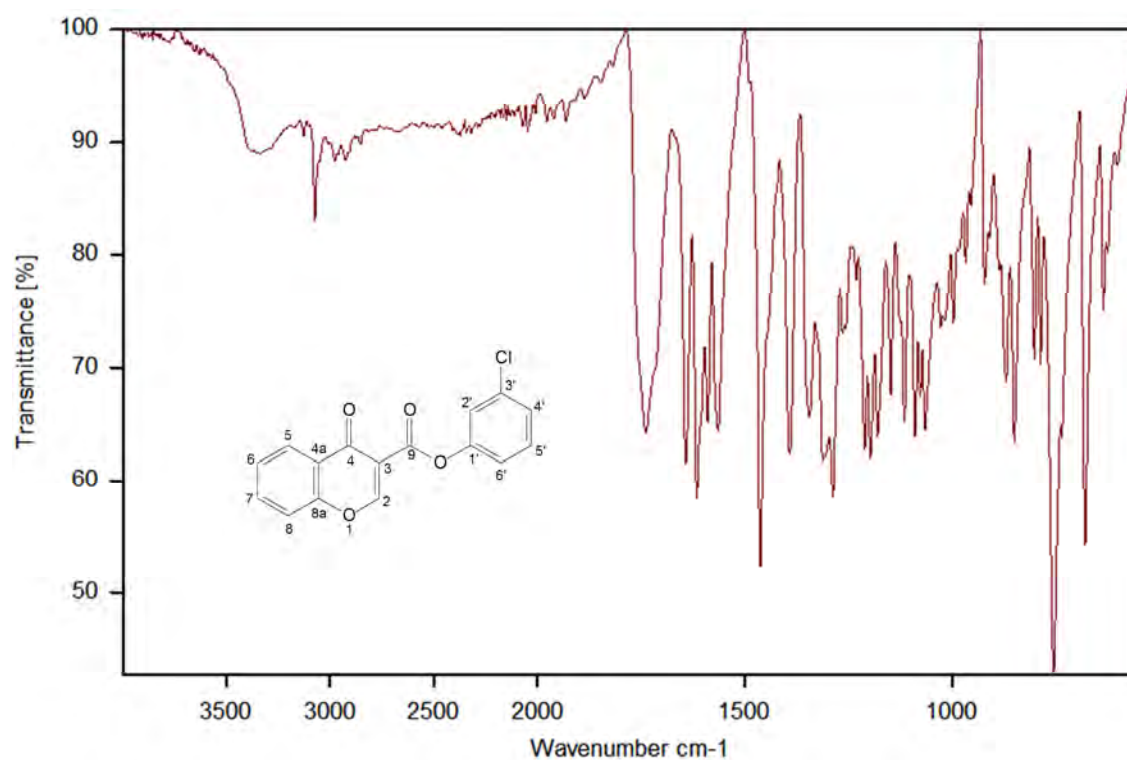
Benzyl 4-oxo-4*H*-chromene-3-carboxylate (32)



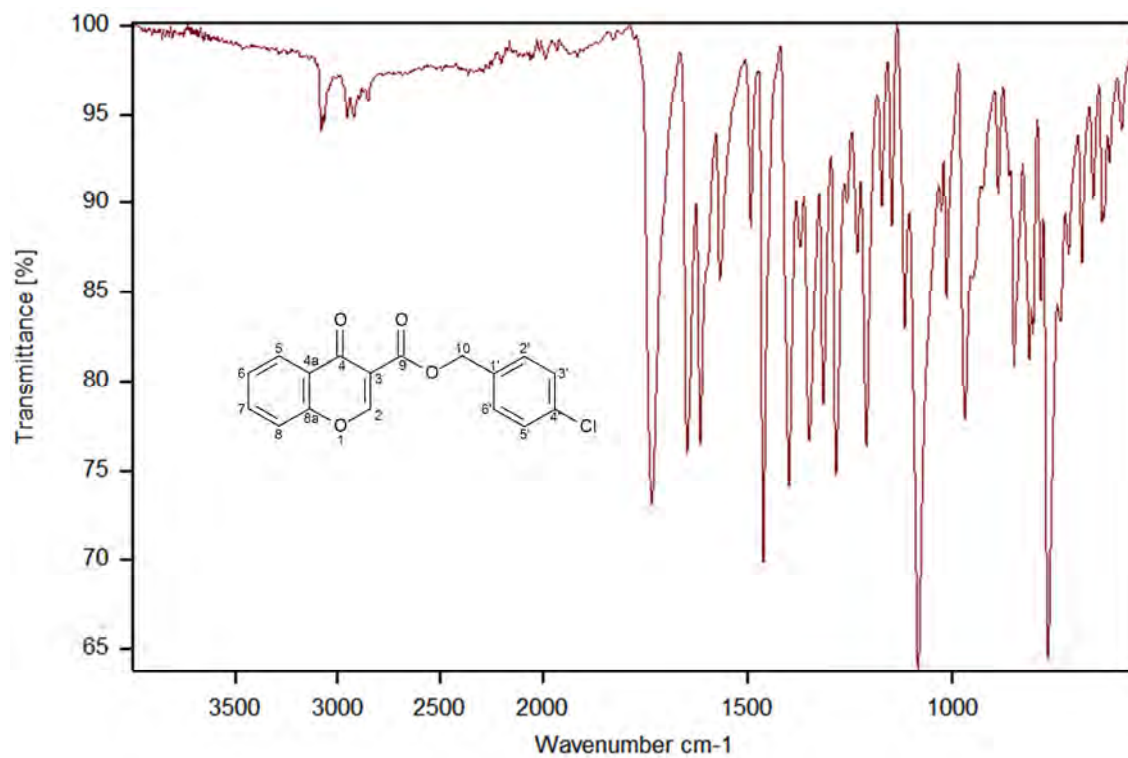
4-chlorophenyl-4-oxo-4H-chromene-3-carboxylate (33)



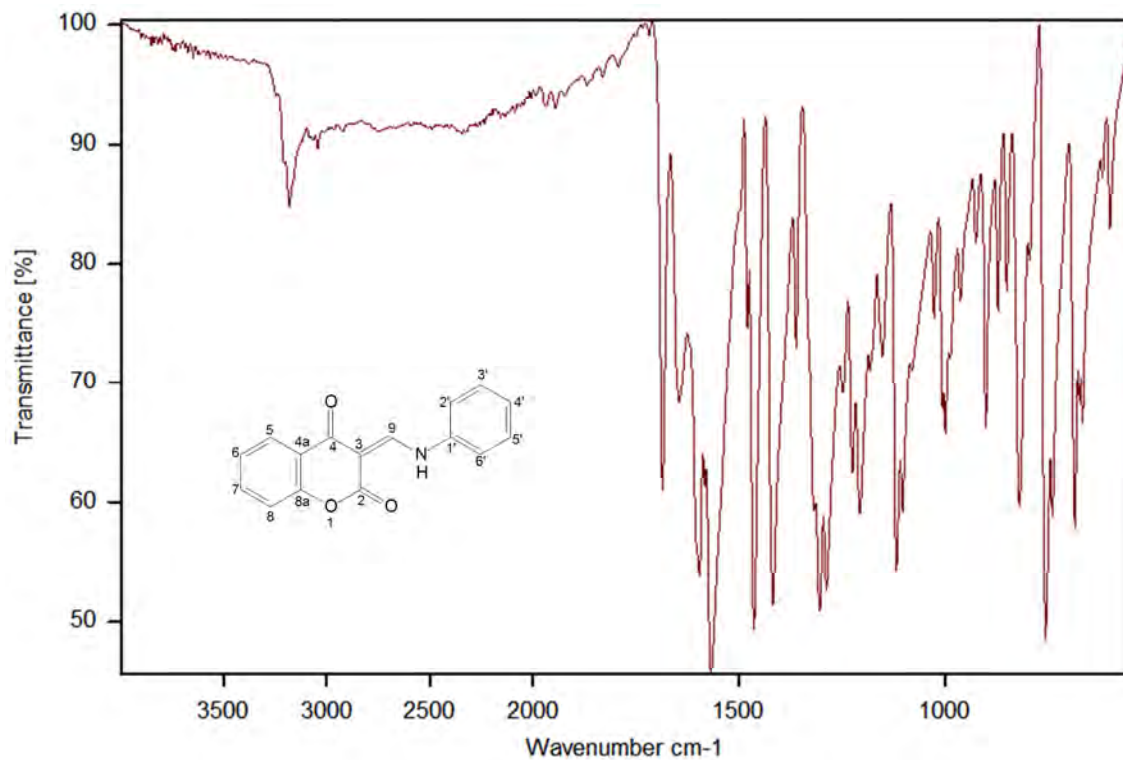
3-chlorophenyl 4-oxo-4H-chromene-3-carboxylate (34)



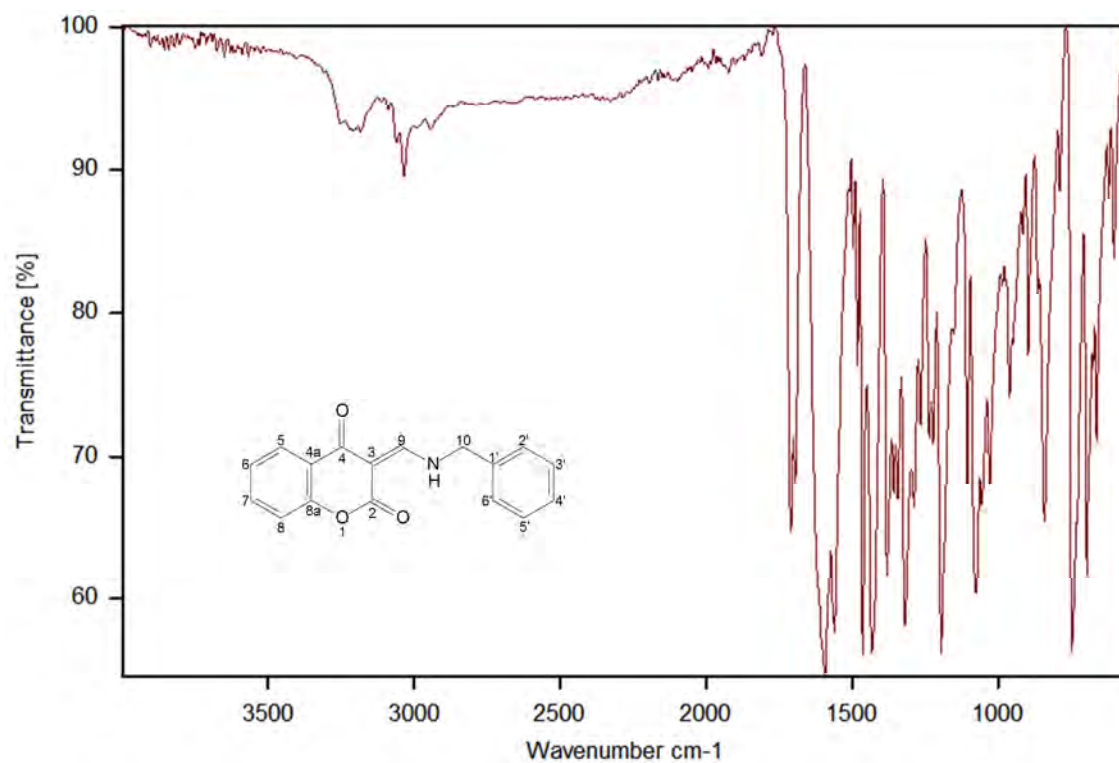
(4-chlorophenyl)methyl-4-oxo-4H-chromene-3-carboxylate (35)



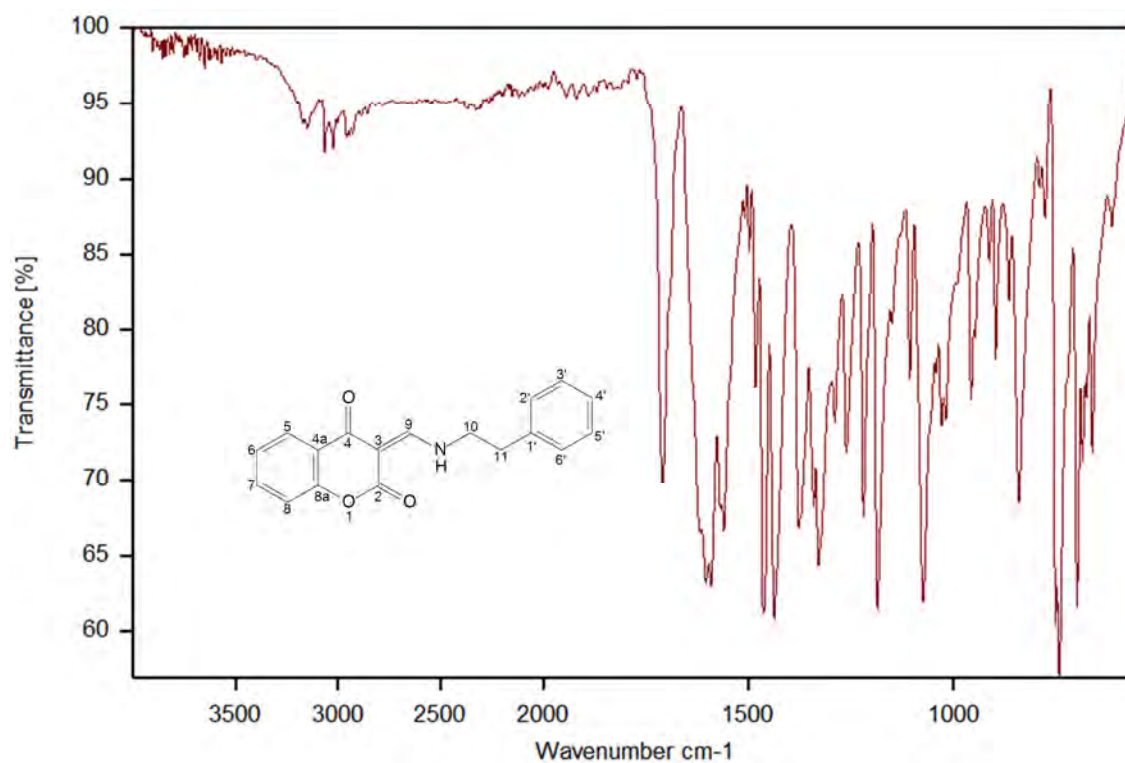
(3E/Z)-3-[(phenylamino)methylidene]-3,4-dihydro-2H-1-benzopyran-2,4-dione (37)



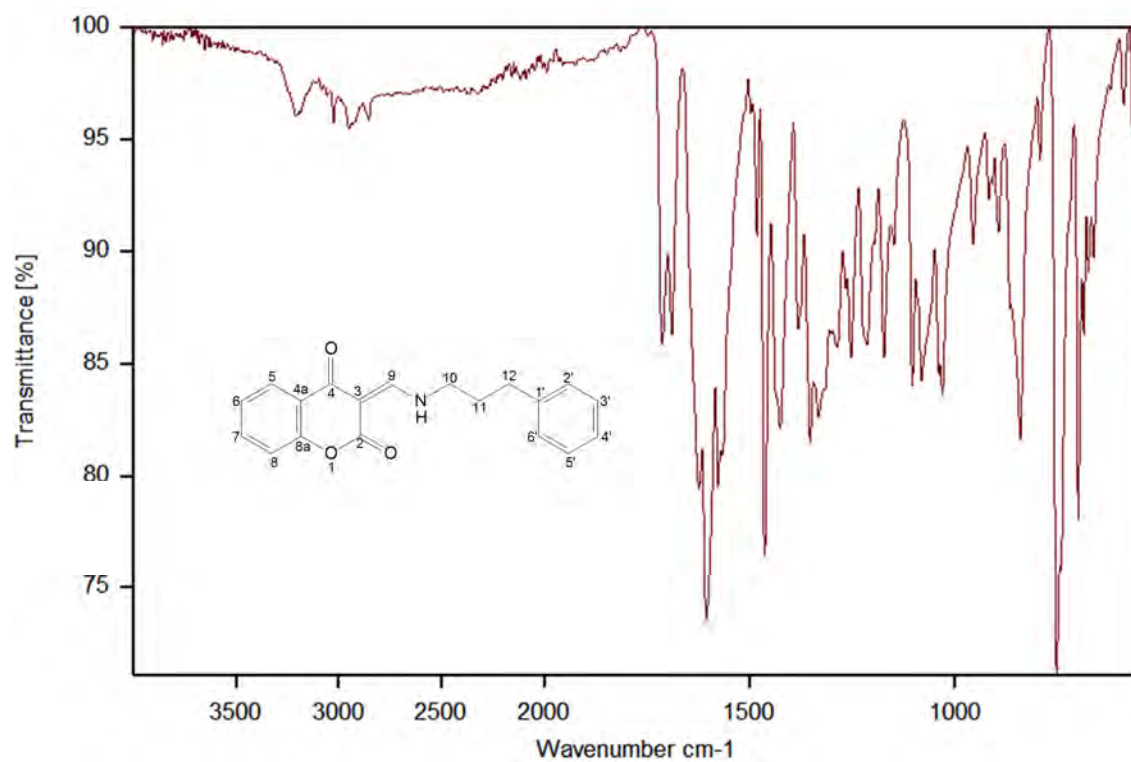
(3E/Z)-3-[(benzylamino)methylidene]-3,4-dihydro-2H-1-benzopyran-2,4-dione (38)



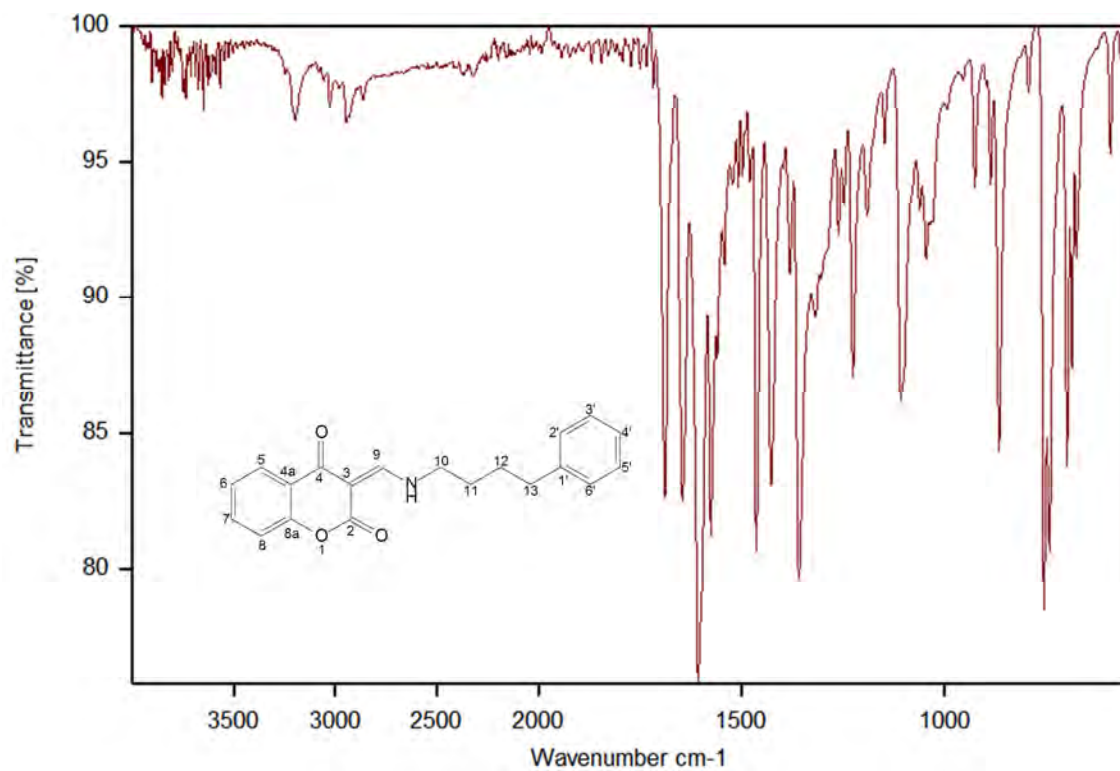
(3E/Z)-3-[(2-phenylethyl)amino]methylidene}-3,4-dihydro-2H-1-benzopyran-2,4-dione (39)



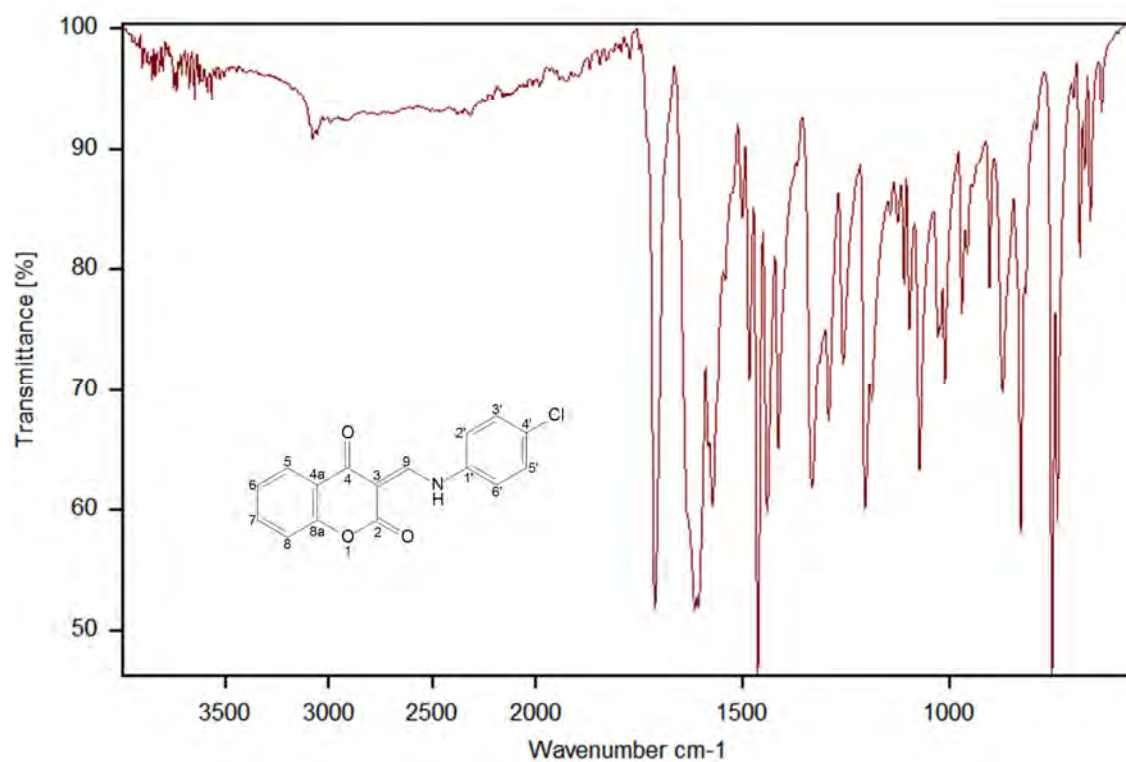
3(E/Z)-3-[(3-phenylpropyl)amino]methylidene}-3,4-dihydro-2H-1-benzopyran-2,4-dione (40)



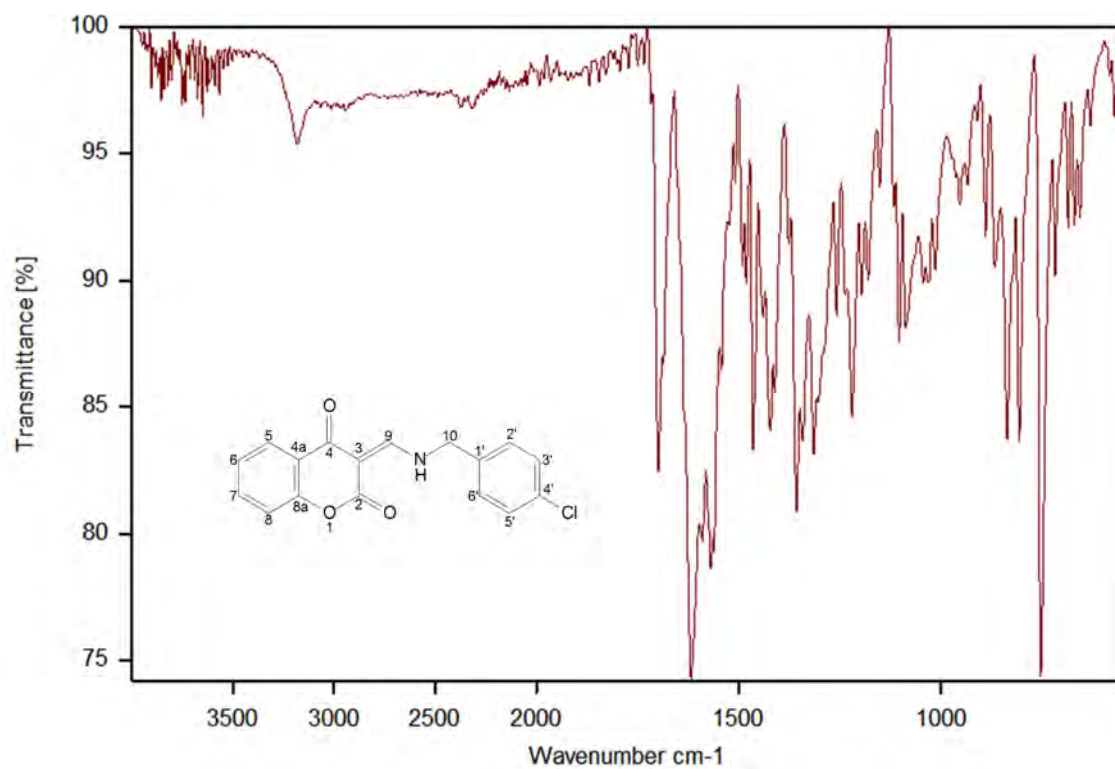
3(E/Z)-3-[(4-phenylbutyl)amino]methylidene}-3,4-dihydro-2H-1-benzopyran-2,4-dione (41)



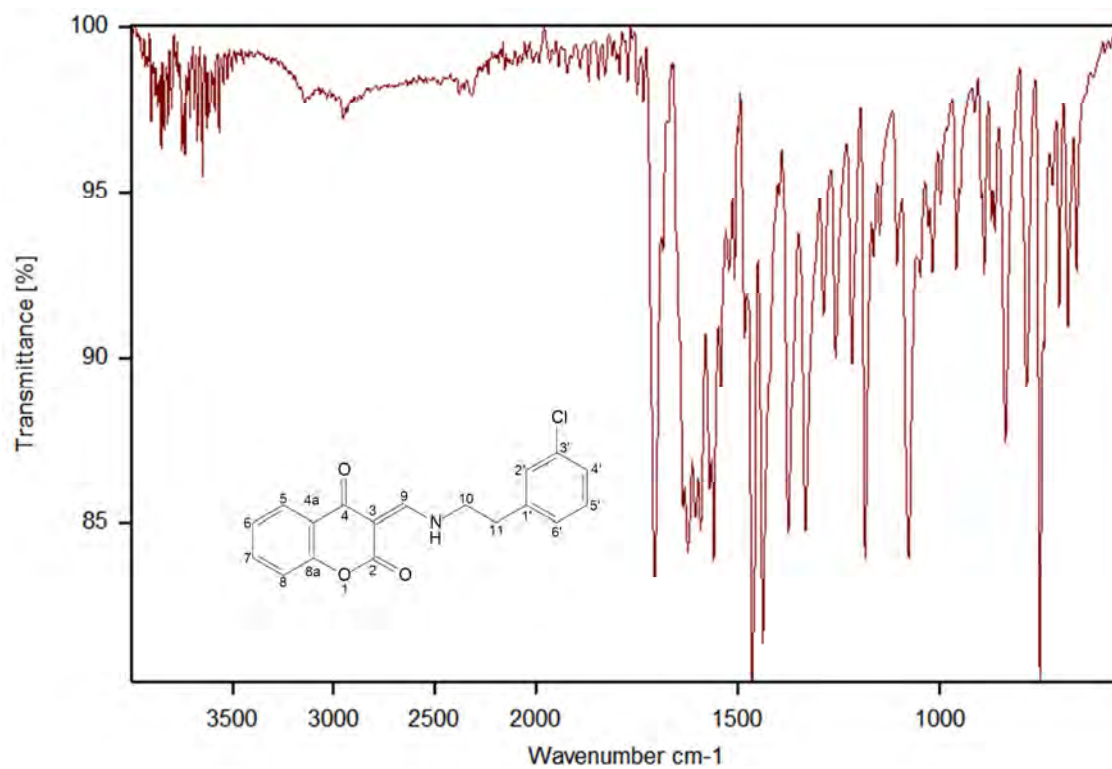
(3E/Z)-3-[(4-chlorophenyl)amino]methylidene)-3,4-dihydro-2H-1-benzopyran-2,4-dione (42)



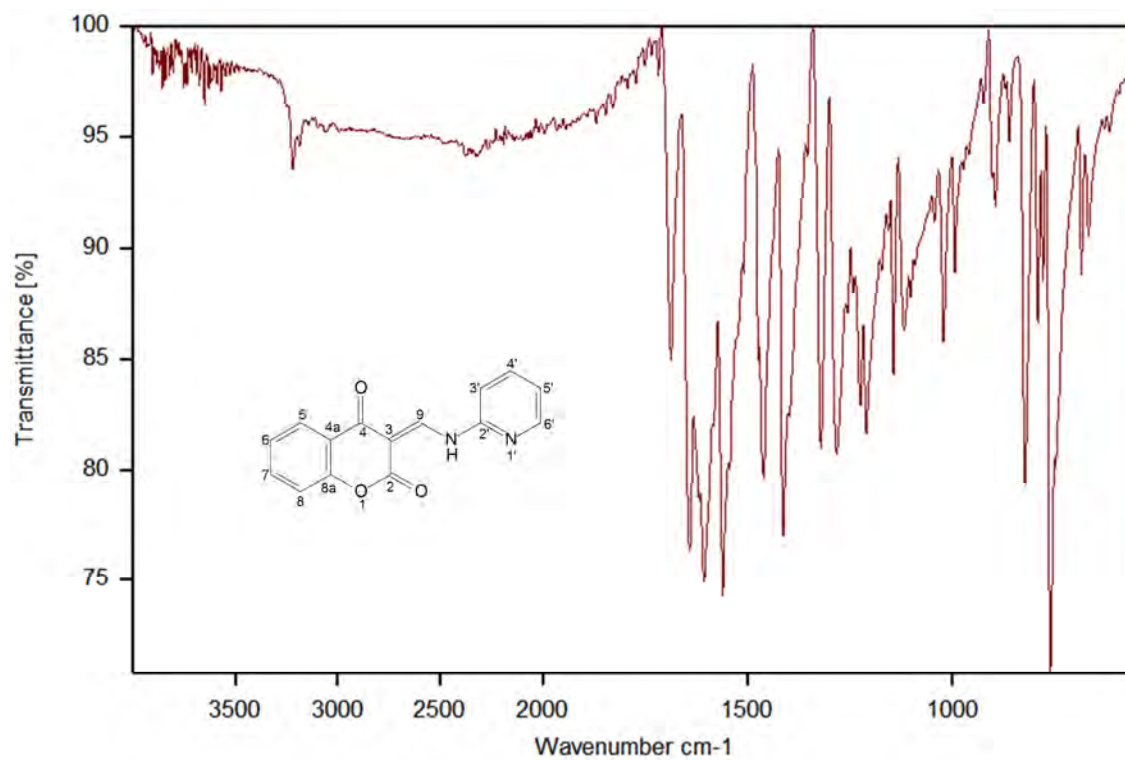
(3E/Z)-3-([(4-chlorophenyl)methyl]amino)methylidene)-3,4-dihydro-2H-1-benzopyran-2,4-dione (43)



(3E/Z)-3-([2-(3-chlorophenyl)ethyl]amino)methylidene)-3,4-dihydro-2H-1-benzopyran-2,4-dione (44)

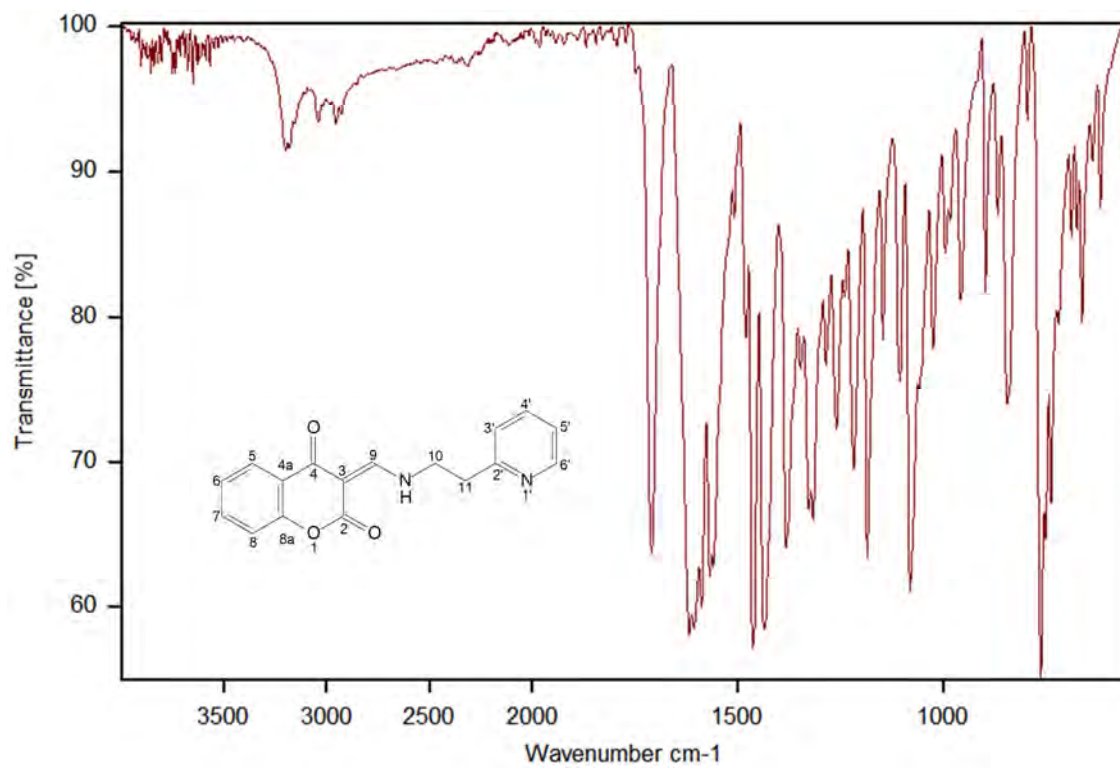


(3E/Z)-3-[(pyridin-2-yl)amino]methylidene}-3,4-dihydro-2H-1-benzopyran-2,4-dione (45)



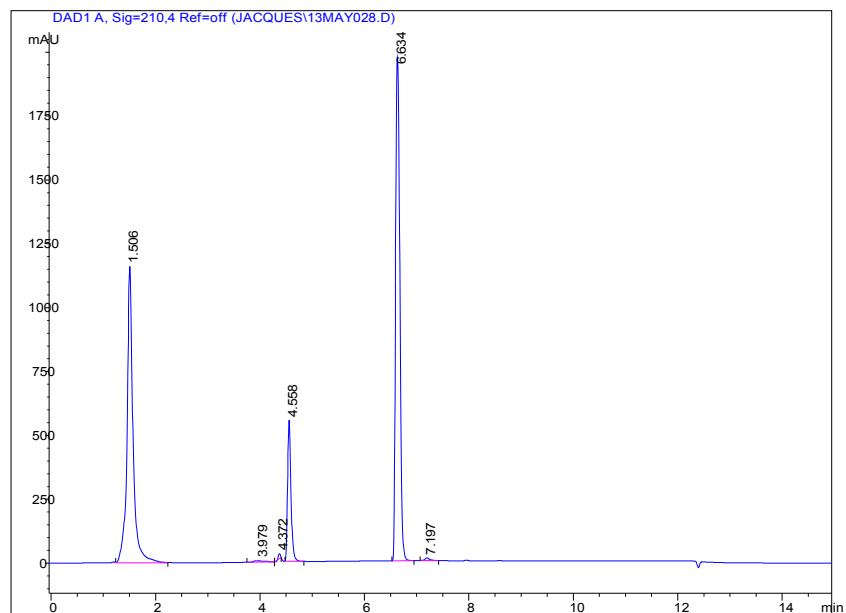
(3E/Z)-3-([2-(pyridin-2-yl)ethyl]amino)methylidene)-3,4-dihydro-2H-1-benzopyran-2,4-dione

(46)

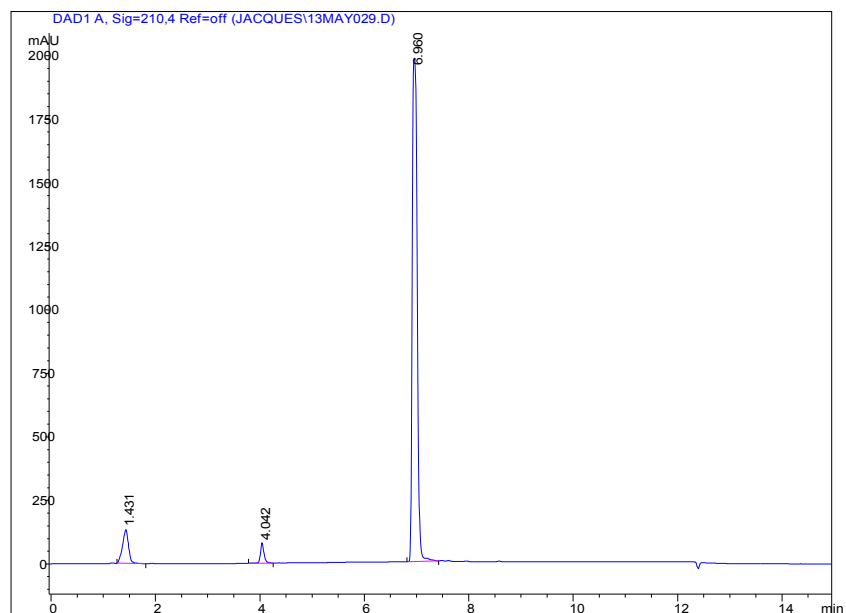


HPLC CHROMATOGRAMS

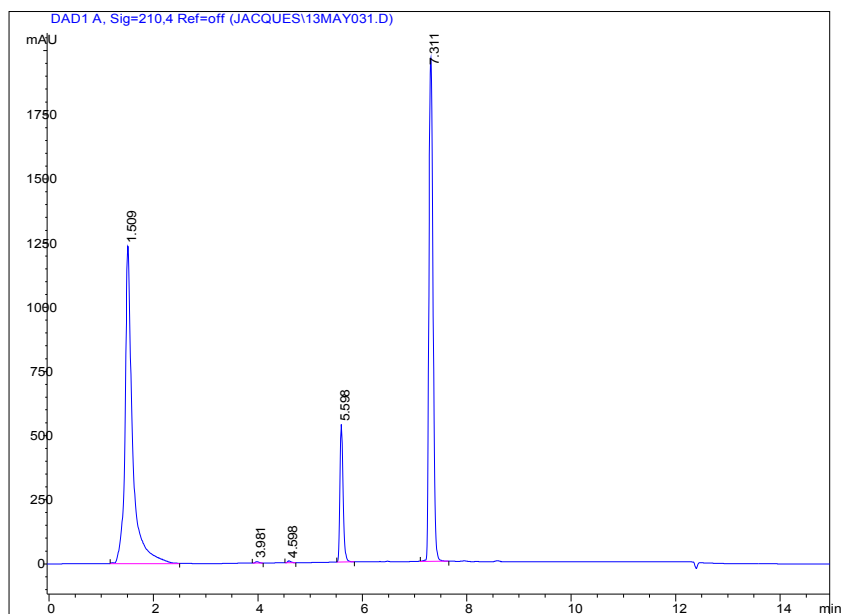
Phenyl 4-oxo-4*H*-chromene-3-carboxylate (31)



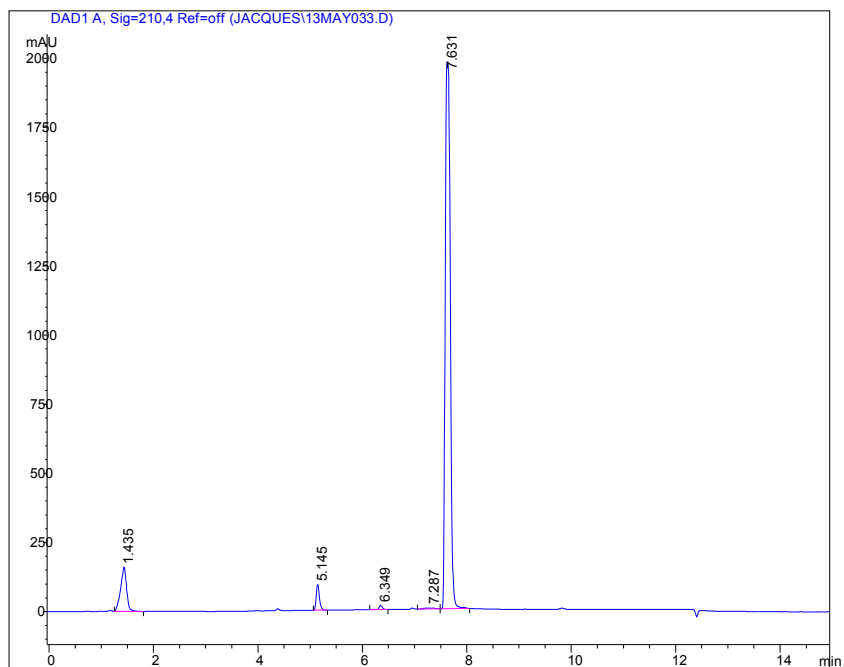
Benzyl 4-oxo-4*H*-chromene-3-carboxylate (32)



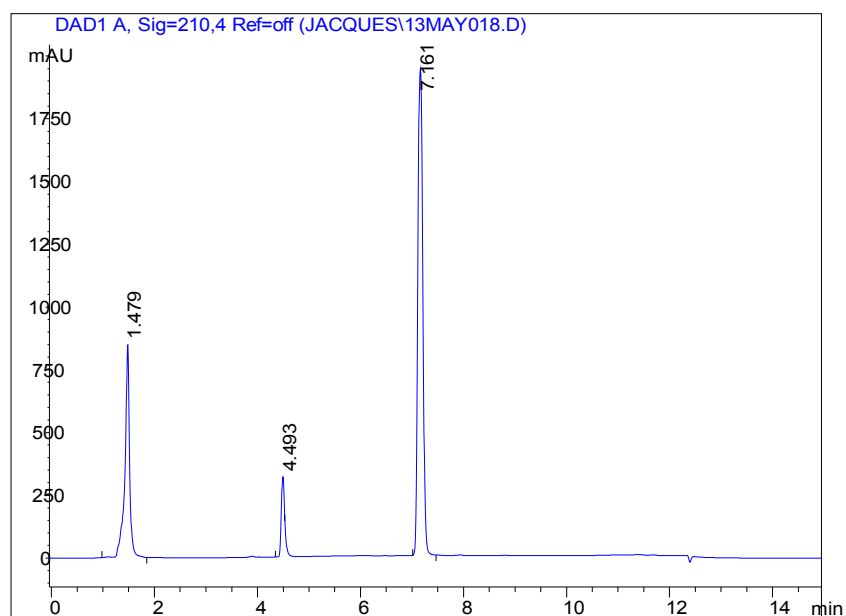
4-chlorophenyl-4-oxo-4H-chromene-3-carboxylate (33)



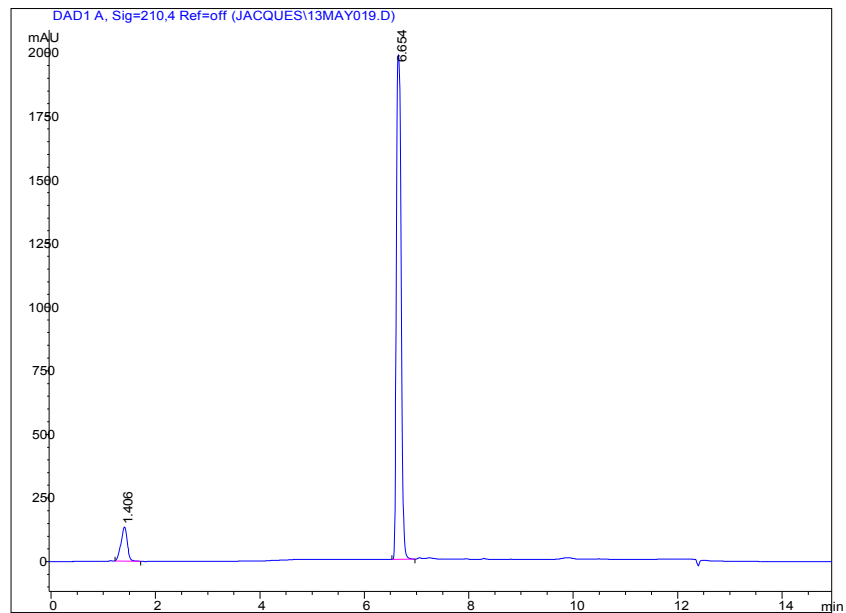
(4-chlorophenyl)methyl-4-oxo-4H-chromene-3-carboxylate (35)



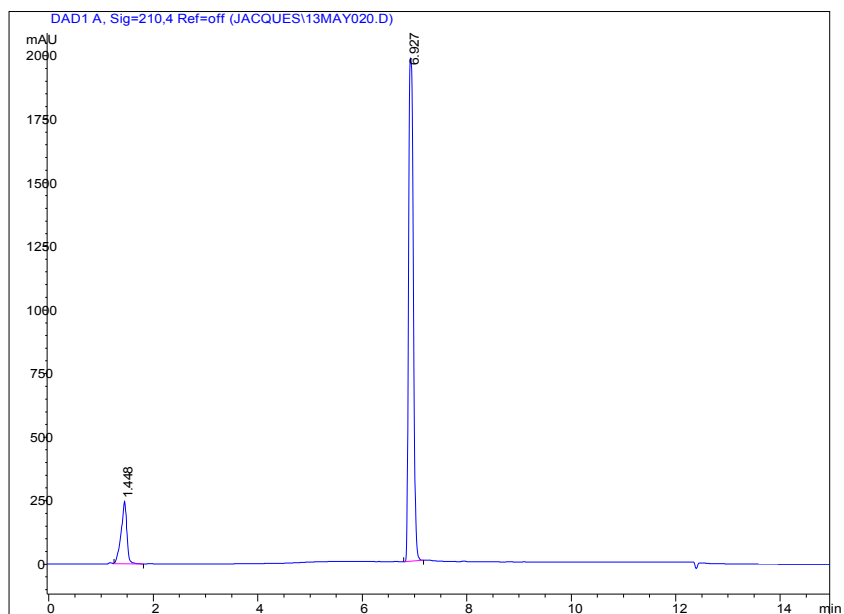
(3E/Z)-3-[(phenylamino)methylidene]-3,4-dihydro-2H-1-benzopyran-2,4-dione (37)



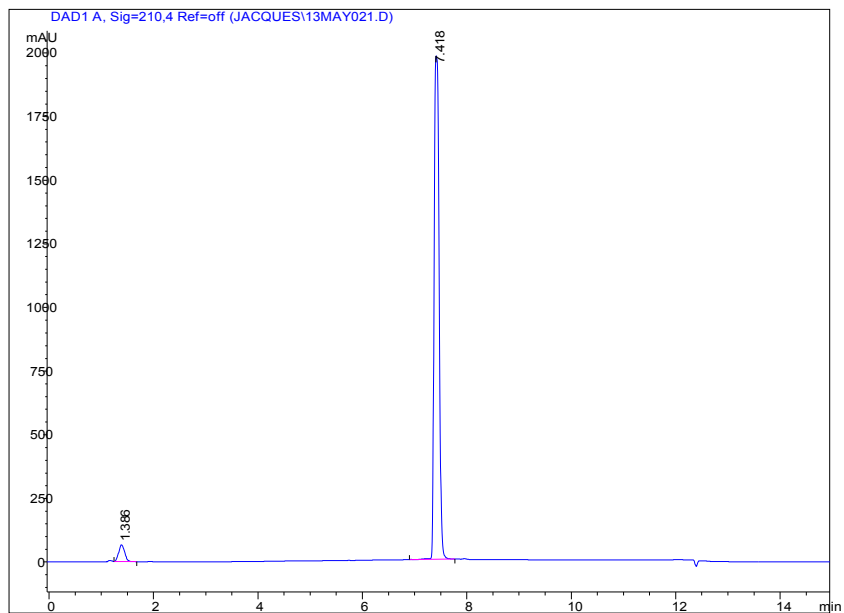
(3E/Z)-3-[(benzylamino)methylidene]-3,4-dihydro-2H-1-benzopyran-2,4-dione (38)



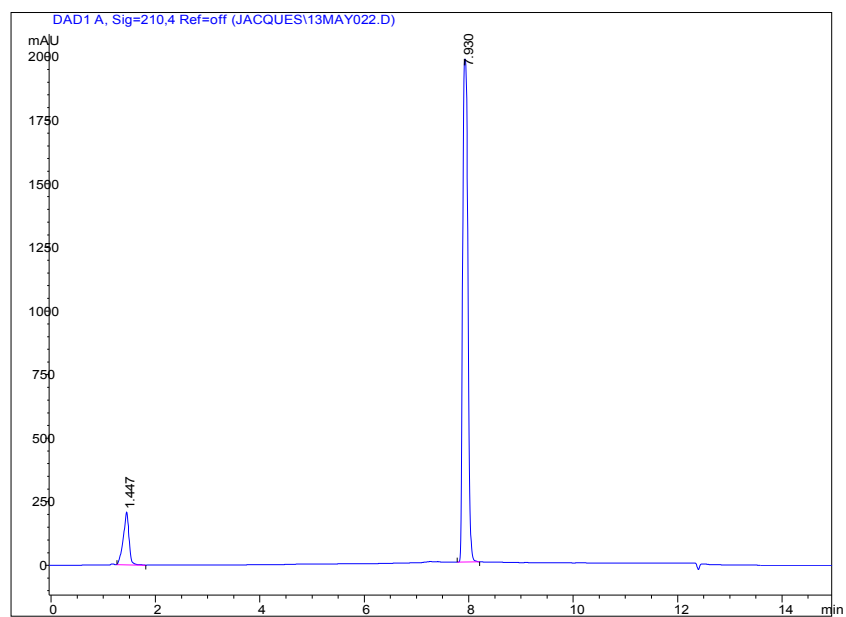
(3E/Z)-3-[(2-phenylethyl)amino]methylidene}-3,4-dihydro-2H-1-benzopyran-2,4-dione (39)



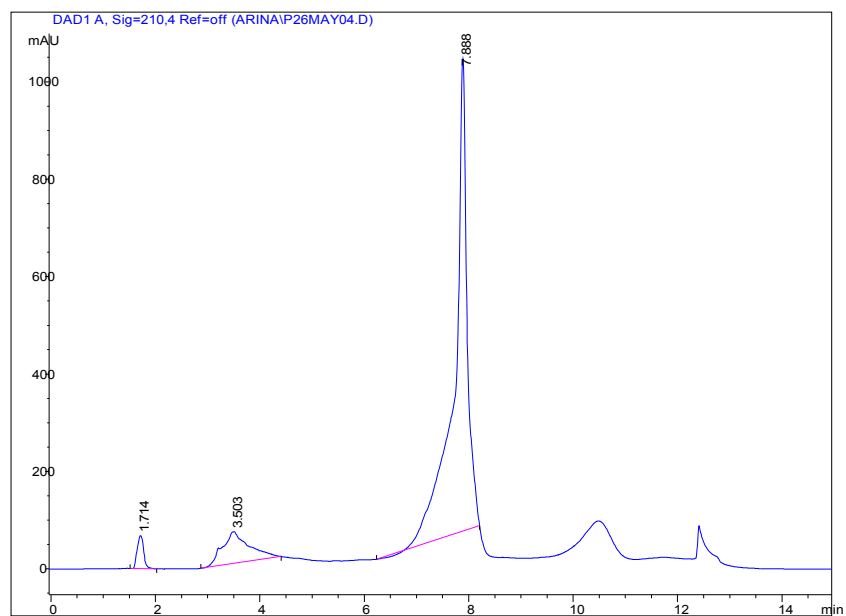
(3E/Z)-3-[(3-phenylpropyl)amino]methylidene}-3,4-dihydro-2H-1-benzopyran-2,4-dione (40)



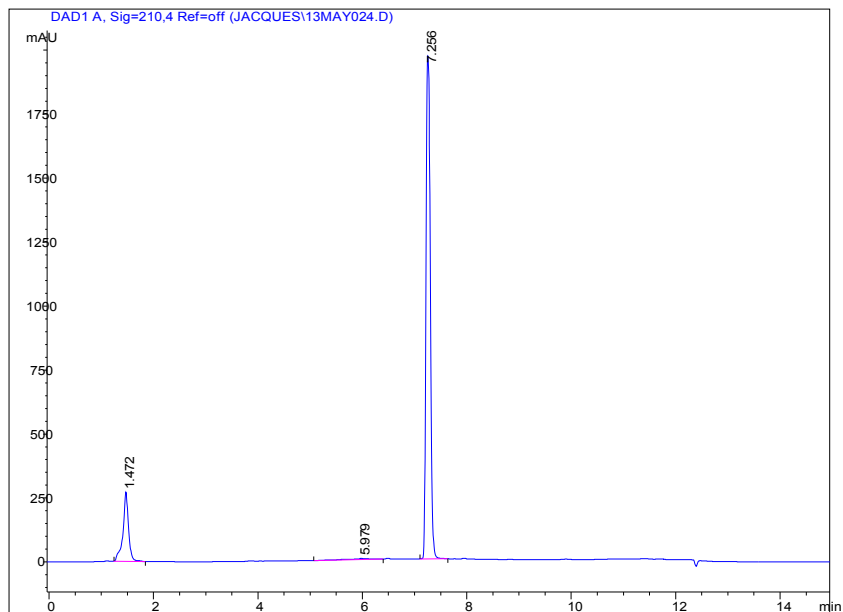
3(E/Z)-3-[(4-phenylbutyl)amino]methylidene}-3,4-dihydro-2H-1-benzopyran-2,4-dione (41)



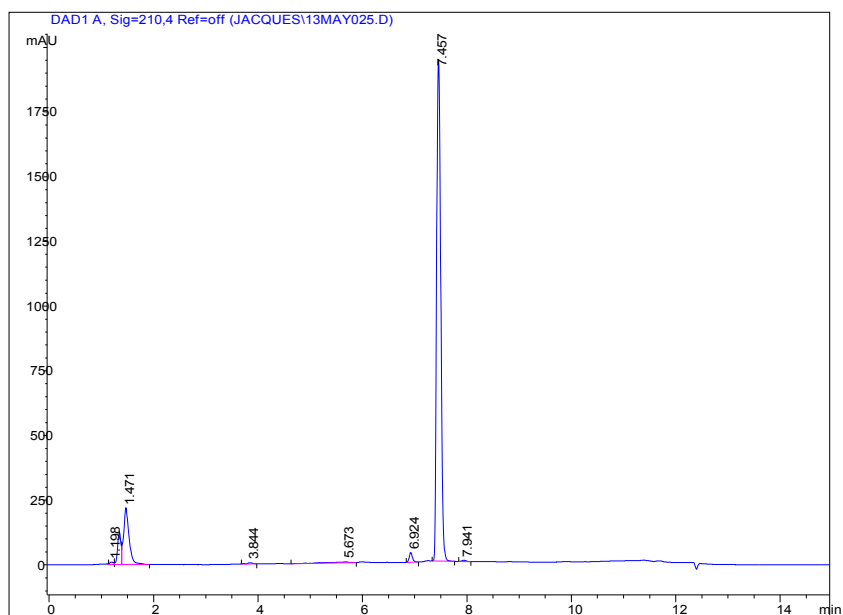
(3E/Z)-3-[(4-chlorophenyl)amino]methylidene}-3,4-dihydro-2H-1-benzopyran-2,4-dione (42)



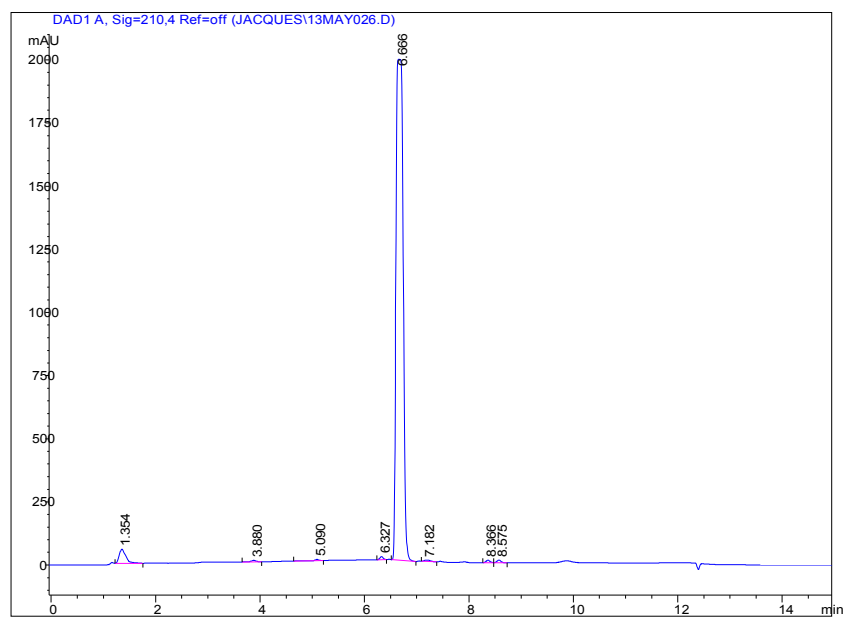
(3E/Z)-3-({[(4-chlorophenyl)methyl]amino}methylidene)-3,4-dihydro-2H-1-benzopyran-2,4-dione (43)



(3E/Z)-3-({[2-(3-chlorophenyl)ethyl]amino}methylidene)-3,4-dihydro-2H-1-benzopyran-2,4-dione (44)



(3E/Z)-3-[[pyridin-2-yl]amino]methylidene}-3,4-dihydro-2H-1-benzopyran-2,4-dione (45)



(3E/Z)-3-[[2-(pyridin-2-yl)ethyl]amino]methylidene}-3,4-dihydro-2H-1-benzopyran-2,4-dione (46)

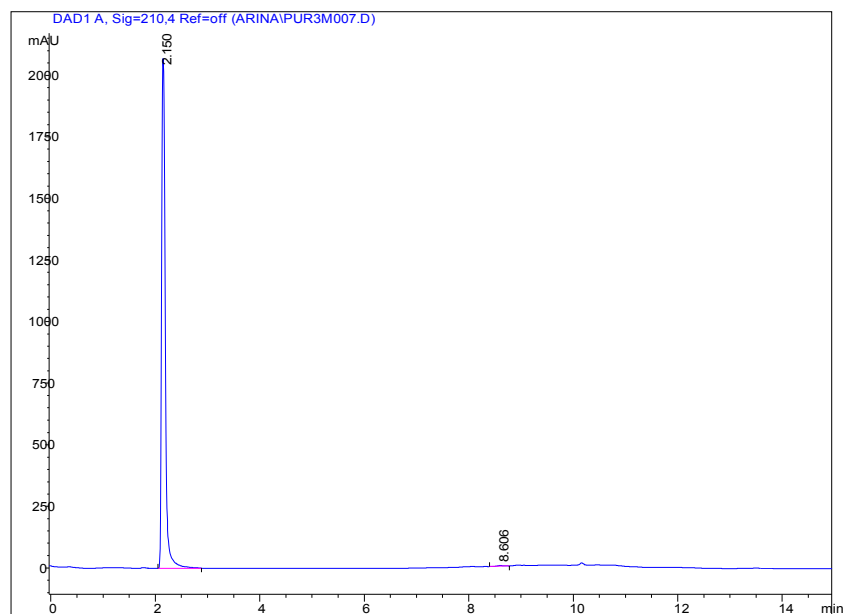


Table 1. Crystal data and structure refinement for compound 46.

Identification code	AMS2_76	
Empirical formula	C ₁₇ H ₁₅ N ₂ O ₃	
Formula weight	295.31	
Temperature	300(2) K	
Wavelength	0.71073 Å	
Crystal system	Monoclinic	
Space group	C 1 2/c 1	
Unit cell dimensions	a = 33.227(3) Å	α = 90°
	b = 4.9978(4) Å	β = 127.927(2)°
	c = 21.7702(18) Å	γ = 90°
Volume	2851.7(4) Å ³	
Z	8	
Density (calculated)	1.376 Mg/cm ³	
Absorption coefficient	0.096 mm ⁻¹	
F(000)	1240	
Crystal size	0.20 x 0.20 x 0.60 mm ³	
Theta range for data collection	1.55 to 25.05°	
Index ranges	-38 ≤ h ≤ 39, -5 ≤ k ≤ 5, -25 ≤ l ≤ 25	
Reflections collected	14094	
Independent reflections	2512 [R(int) = 0.0369]	
Completeness to theta = 25.05°	100.0%	
Absorption correction	Multiscan	
Max. and min. transmission	0.9811 and 0.8642	
Refinement method	Full-matrix least-squares on F ²	
Data / restraints / parameters	2512 / 0 / 199	
Goodness-of-fit on F ²	1.024	
Final R indices [I > 2σ(I)]	R1 = 0.0594, wR2 = 0.1725	
R indices (all data)	R1 = 0.0754, wR2 = 0.1972	
Largest diff. peak and hole	0.362 and -0.380	

Table 2. Atomic coordinates ($\times 10^4$) and equivalent isotropic displacement parameters ($\text{\AA}^2 \times 10^3$) for compound 46.

U(eq) is defined as one third of the trace of the orthogonalized U^{ij} tensor.

	x	y	Z	U(eq)
O1	3405(1)	6599(4)	6221(1)	50(1)
O2	2948(1)	9778(4)	5397(1)	62(1)
O3	2789(1)	7768(4)	7351(1)	53(1)
N1	2213(1)	11773(4)	6283(1)	44(1)
N2	618(1)	15229(6)	5028(1)	64(1)
C1	4118(1)	1576(6)	7718(2)	59(1)
C2	3944(1)	3191(6)	7084(2)	54(1)
C3	3566(1)	5098(5)	6859(1)	41(1)
C4	3040(1)	8547(5)	5946(1)	43(1)
C5	2820(1)	8937(5)	6344(1)	38(1)
C6	2447(1)	10954(5)	6019(1)	42(1)
C7	1815(1)	13845(5)	5881(1)	45(1)
C8	1303(1)	12647(6)	5231(2)	68(1)
C9	892(1)	14725(5)	4788(1)	46(1)
C10	255(1)	17061(8)	4646(2)	77(1)
C11	142(1)	18422(7)	4035(2)	77(1)
C12	2976(1)	7416(5)	7012(1)	39(1)
C13	3379(1)	5369(5)	7272(1)	39(1)
C14	3561(1)	3721(6)	7902(1)	52(1)
C15	3926(1)	1852(6)	8123(2)	61(1)
C16	414(1)	17924(8)	3777(2)	83(1)
C17	807(1)	16040(7)	4170(2)	65(1)

Table 3. Bond lengths (Å) and angles (°) for compound 46

O1-C4	1.372(3)
O1-C3	1.365(3)
O2-C4	1.204(3)
O3-C12	1.236(3)
N1-C6	1.286(3)
N1-C7	1.470(3)
N2-C9	1.323(3)
N2-C10	1.323(4)
C1-C15	1.376(4)
C1-C2	1.382(4)
C2-C3	1.403(4)
C3-C13	1.379(3)
C4-C5	1.450(3)
C5-C6	1.405(3)
C5-C12	1.426(3)
C7-C8	1.516(4)
C8-C9	1.500(4)
C9-C17	1.360(4)
C10-C11	1.325(5)
C11-C16	1.349(6)
C12-C13	1.491(3)
C13-C14	1.381(4)
C14-C15	1.365(4)
C16-C17	1.396(5)
C4-O1-C3	121.57(19)
C6-N1-C7	121.9(2)
C9-N2-C10	117.8(3)
C15-C1-C2	120.4(3)
C1-C2-C3	118.8(3)
O1-C3-C13	123.9(2)

O1-C3-C2	115.8(2)
C13-C3-C2	120.3(2)
O2-C4-O1	114.5(2)
O2-C4-C5	127.6(2)
O1-C4-C5	117.9(2)
C6-C5-C12	123.4(2)
C6-C5-C4	114.1(2)
C12-C5-C4	122.5(2)
N1-C6-C5	126.4(2)
N1-C7-C8	111.1(2)
C9-C8-C7	112.5(2)
N2-C9-C17	121.4(3)
N2-C9-C8	116.9(3)
C17-C9-C8	121.7(3)
N2-C10-C11	125.0(3)
C10-C11-C16	118.2(3)
O3-C12-C5	122.2(2)
O3-C12-C13	122.3(2)
C5-C12-C13	115.6(2)
C3-C13-C14	119.5(2)
C3-C13-C12	118.6(2)
C14-C13-C12	121.9(2)
C15-C14-C13	120.6(3)
C14-C15-C1	120.4(3)
C11-C16-C17	118.8(3)
C9-C17-C16	118.8(3)

Table 4. Anisotropic displacement parameters ($\text{\AA}^2 \times 10^3$) for compound 46.

The anisotropic displacement factor exponent takes the form: $-2\pi^2 [h^2 a^{*2} U^{11} + \dots + 2 h k a^* b^* U^{12}]$

	U^{11}	U^{22}	U^{33}	U^{23}	U^{13}	U^{12}
O1	59(1)	54(1)	53(1)	9(1)	9(1)	9(1)
O2	71(1)	71(1)	55(1)	18(1)	18(1)	11(1)
O3	61(1)	59(1)	50(1)	3(1)	3(1)	1(1)
N1	43(1)	50(1)	38(1)	1(1)	1(1)	0(1)
N2	62(2)	74(2)	64(2)	7(1)	7(1)	13(1)
C1	43(1)	40(2)	62(2)	2(1)	2(1)	8(1)
C2	48(1)	51(2)	64(2)	-8(1)	-8(1)	-1(1)
C3	42(1)	39(1)	39(1)	-1(1)	-1(1)	-4(1)
C4	42(1)	42(1)	43(1)	1(1)	1(1)	-2(1)
C5	35(1)	36(1)	39(1)	-1(1)	-1(1)	-1(1)
C6	40(1)	45(1)	39(1)	-2(1)	-2(1)	-4(1)
C7	39(1)	43(1)	49(1)	-2(1)	-2(1)	4(1)
C8	41(1)	50(2)	85(2)	-8(2)	-8(2)	0(1)
C9	33(1)	49(2)	50(1)	-9(1)	-9(1)	-5(1)
C10	65(2)	77(2)	105(3)	0(2)	0(2)	13(2)
C11	43(2)	62(2)	88(2)	8(2)	8(2)	6(1)
C12	39(1)	38(1)	39(1)	-5(1)	-5(1)	-7(1)
C13	44(1)	35(1)	36(1)	-4(1)	-4(1)	-9(1)
C14	60(2)	49(2)	41(1)	3(1)	3(1)	-4(1)
C15	61(2)	53(2)	47(2)	7(1)	7(1)	-0(1)
C16	88(3)	76(2)	52(2)	10(2)	10(2)	-18(2)
C17	67(2)	72(2)	70(2)	-10(2)	-10(2)	-13(2)

Table 5. Hydrogen coordinates ($\times 10^4$) and isotropic displacement parameters ($\text{\AA}^2 \times 10^3$) for compound 46

	x	y	z	U(eq)
H1	2290	11089	6706	52
H1A	4367	293	7872	70
H2	4075	3018	6812	65
H6	2362	11776	5570	50
H7A	1909	15180	5667	54
H7B	1789	14727	6252	54
H8A	1335	11697	4874	81
H8B	1204	11361	5451	81
H10	66	17421	4819	92
H11	-118	19687	3791	92
H14	3433	3886	8179	63
H15	4047	759	8550	73
H16	341	18820	3344	99
H17	1006	15690	4013	79